DOE/ER/40442-9

STUDIES OF NUCLEAR PROCESSES AT THE TRIANGLE UNIVERSITIES NUCLEAR LABORATORY

Progress Report

1 September 1995–31 August 1996

E. J. LUDWIG
Department of Physics and Astronomy
University of North Carolina
Chapel Hill, North Carolina 27599-3255

1 September 1996

PREPARED FOR THE U. S. DEPARTMENT OF ENERGY
UNDER GRANT NUMBER DE-FG05-88-ER40442

TUNL XXXV

PROGRESS REPORT

1 SEPTEMBER 1995–31 AUGUST 1996

TRIANGLE UNIVERSITIES NUCLEAR LABORATORY

DUKE UNIVERSITY
NORTH CAROLINA STATE UNIVERSITY
UNIVERSITY OF NORTH CAROLINA AT CHAPEL HILL

BOX 90308, DURHAM, NORTH CAROLINA 27708-0308, USA

Work described in this Progress Report is supported by the United States Department of Energy, Office of High Energy and Nuclear Physics, under:

Grant No. DE-FG05-91ER40619 (Duke University),
Grant No. DE-FG05-88ER40441 (North Carolina State University), and
Grant No. DE-FG05-88ER40442 (University of North Carolina).

DISCLAIMER

Contents

Introduction

The Triangle Universities Nuclear Laboratory (TUNL) – a collaboration of Duke University, North Carolina State University, and the University of North Carolina at Chapel Hill – has had a very productive year. The following reports cover parts of the second and third year of a three-year grant between the U.S. Department of Energy and the three collaborating universities.

During the current grant period TUNL physicists have achieved several major successes:

- **Parity nonconservation in the nuclear interaction:**
  We performed measurements at LANSCE with a new large-area and high-polarization proton filter, a new ^{10}B-loaded liquid scintillator system, and a large solid-angle CsI detector for capture studies. New transmission and capture measurements have been carried out on a number of new targets in the A=100 region. The previously observed sign correlation in ^{232}Th is confirmed with greater statistical significance, but the signs of the other parity violations appear to be randomly distributed.

- **Time-reversal invariance tests:**
  We performed the most precise test of parity-even time-reversal invariance in a dynamical process. The measurement used 6 MeV polarized neutrons transmitted through a nuclear spin aligned, single-crystal holmium target. Relative cross sections for spin-up versus spin-down neutrons were found to be equal to within 1.2×10^{-5} (80%), a factor of 400 improvement compared to traditional detailed balance studies. The measurement gives a bound on the T-violating meson coupling $\bar{g}_\rho \leq 5.8\times10^{-2}$ (95%).

- **Chaos in the nucleus:**
  With the new Compton-suppression spectrometer and the excellent beam energy resolution of ~200 eV, we studied 50 resonances in the ^{29}Si(p,γ)^{30}P reaction in order to obtain a complete level scheme of ^{30}P. The measured elastic scattering and capture spectra limit the quantum numbers of both initial (resonant) and final states. The complete level scheme will not only provide a definitive study of the statistical properties of eigenvalues and transition matrix elements in light nuclei, but will also clarify the effect of symmetry breaking on these quantities.

- **Astrophysical S-factors:**
  We found significant p-wave capture in the reactions ^{2}H(p,γ)^{3}He, ^{1}H(d,γ)^{3}He, and ^{7}Li(p,γ)^{8}Be at very low energies. The measured astrophysical S-factors are smaller than the presently adopted values. The ^{7}Li work is closely related to the ^{7}Be(p,γ)^{8}B reaction which is of importance to the solar-neutrino problem. The ^{2}H(p,γ)^{3}He and ^{1}H(d,γ)^{3}He data exhibit large sensitivity to non-nucleonic degrees of freedom.

- **Polarized-ion source and real-time beam polarization measurements:**
  An atomic physics spin filter polarimeter was constructed and installed on the high-voltage frame of our high-intensity atomic-beam polarized ion source. A real-time beam polarization display allows tuning of ion-source parameters to optimize and monitor beam polarization for all users. Routine beam polarization checks with an uncertainty $<2\%$ can be obtained within a few seconds.

- **The tensor force in the nucleon-nucleon interaction:**
  By scattering polarized neutrons from a polarized proton target we measured the spin-dependent neutron-proton total cross-section difference $\Delta\sigma_T$ between 10 and 20 MeV. Our high-accuracy data rule out any low-energy anomaly in the nucleon-nucleon tensor force.

- **0^- state of ^{4}He:**
  By measuring $K_z^{z'}(0°)$ in the ^{3}H($\vec{p}$,$\vec{n}$)^{3}He reaction around E_p=1.5 MeV, we confirmed the existence of a narrow low-lying 0^- state in ^{4}He, which was previously predicted from R-matrix studies of the 4N system. This level is of importance for the study of parity violation in the mass-4 system.

- **Proton-deuteron scattering:**
  We made scattering measurements of protons from deuterons at energies as low as 0.3 MeV. These experiments confirmed the accuracy of recent theoretical calculations that include, for the first time, the Coulomb interaction in rigorous calculations of nuclear systems heavier than A=2.

- **Cryogenic microcalorimeters:**
  We constructed and successfully tested our first prototype cryogenic microcalorimeter. These devices are being developed for measurements of β-spectra in weak-interaction studies.

- **Sonoluminescence:**
  We explained important phenomena surrounding sonoluminescence by observing striking similarities between the light emission processes in high-pressure gas scintillators and single-bubble sonoluminescence.

- **$^{17}O(p,\alpha)^{14}N$ reaction at stellar energies:**
  The results of our measurements of the $^{17}O(p,\alpha)^{14}N$ reaction at stellar energies will enable astronomers to interpret observations of stellar oxygen abundances in terms of the dynamics of stellar interiors.

- **Nuclear data project:**
  We published the review "Energy Levels of Light Nuclei A=18–19". Very recently, a preliminary version for A=20 has been completed and distributed. We also increased our World Wide Web (WWW) service. A short version of the Table of Isotopes which has information about A=1–20 nuclei is now available. We added abridged versions of Fay Ajzenberg-Selove's most recent evaluations of A=5–10, and they are available online. We are currently working to make modified versions of all her compilations available online.

- **Low-Energy Beam Facility:**
  We completed the upgrade of the Low-Energy Beam Facility. The range of energies accessible to this system using the polarized ion source, the mini-tandem accelerator, and the high-voltage chamber is 20–680 keV.

- **Focal-plane detector for Enge split-pole spectrometer:**
  We built a new focal-plane detector that dramatically enhances our capability of high-resolution spectroscopy.

TUNL seeks to be on several of the nuclear physics research frontiers identified in the 1996 NSAC Long Range Plan. The TUNL research program focuses on the following areas:

- Precision test of parity-invariance violation in resonance neutron scattering at LANSCE/LANL.

- Parity violation measurements using charged-particle resonances in A=20–40 targets and the A=4 system at TUNL.

- Chaotic behavior in the nuclei ^{30}P and ^{34}Cl from studies of eigenvalue fluctuations in nuclear level schemes.

- Search for anomalies in the level density (pairing phase transition) in 1f–2p shell nuclei using GEANIE at LANSCE/LANL.

- Parity-conserving time-reversal noninvariance tests using ^{166}Ho resonances at Geel, ORELA, or LANSCE/LANL.

- Nuclear astrophysics, using the refurbished Enge split-pole spectrometer, the Low-Energy Beam Facility, a new 200 keV accelerator for high-intensity unpolarized beams,

and the KN accelerator (all at TUNL); facilities at HRIBF, TRIUMF, and Yale; and the planned HIGS facility at Duke's FELL. Emphasis is placed on the following reactions:

- ^{7}Li(p,γ)^{8}Be, ^{7}Be(p,γ)^{8}B, ^{12}C(α,γ)^{16}O, ^{14}N(p,γ)^{15}O, and ^{16}O(γ,α)^{12}C;

  with specific experiments to address:

  * explosive nucleosynthesis
  * explosive hydrogen burning
  * ^{26}Al nucleosynthesis
  * He burning
  * NeNa cycle
  * galactic chemical evolution
  * rp processes

- Few-body nuclear systems, with specific experiments to address:
  - radiative capture reactions on hydrogen isotopes to investigate non-nucleonic degrees of freedom
  - the role of three-nucleon forces in the 3N and 4N continuum using hadronic and electromagnetic probes
  - the strength of the tensor force in the NN interaction
  - determination of the charged πNN coupling constant
  - determination of the ^{3}P$_{J}$ components of the NN interaction
  - proton-deuteron scattering at a very low energies and the ^{2}S$_{1/2}$ scattering length
  - electron screening
  - reactions on helium isotopes to determine astrophysical S-factors via analytic continuation techniques
  - D-state of ^{6}Li
  - the quark structure of nucleons in experiments at Bates and TJNAF
- Study of double β decay to excited 0^{+} states
- High-spin spectroscopy and superdeformation
- Nuclear Data evaluation for A=3–20 for which TUNL is now the international center. Extensive services are provided through our WWW site and are constantly being improved.

Developments in technology and instrumentation are vital to our research and training program. We continued our innovative work in:

- polarized beam developement
- polarized target development
- designing new cryogenic systems
- designing new detectors
- improving high-resolution beams for the KN and FN accelerators
- development of an unpolarized Low-Energy Beam Facility for radiative capture studies of astrophysical interest.

During the last year we worked on a major new initiative to develop an intense beam of polarized γ-rays. This High-Intensity Gamma-ray Source (HIGS) will utilize the facilities of the Duke Free-Electron Laser Laboratory (DFELL). The DFELL currently includes a 500 MeV LINAC injector, a 1.3 GeV electron storage ring, and the OK-4 undulator. It is possible to tune the electron beam in a manner which allows the FEL photons produced by one electron bunch to backscatter from a second electron bunch, all within the ring. This leads to an intense beam of almost 100% polarized γ-rays whose energy can be readily tuned from about 8 MeV to greater than 200 MeV. Furthermore, beam energy spreads of less than 1% can be obtained by purely geometrical collimation. In order to achieve this, it will be necessary to upgrade the present LINAC to an energy of 1.3 GeV and to make minor modifications in the electron beam optics in the FEL storage ring.

Funds for upgrading the LINAC to 1.1 GeV, which will allow us to produce γ-rays up to about 170 MeV (above the pion threshold), will constitute the major part of a supplemental proposal that will be submitted to DOE this Fall.

TUNL is recognized internationally for its development of polarized ion sources and low-temperature targets and detectors. Another major new initiative developed during the last year is to construct a new, super-intense polarized ion soure for H^- and D^- beams of intensities at least 20 times greater than those currently available. Two options are being considered. 1) Recent technical advances make an old idea, that of obtaining polarized H^-(or D^- ions) from the very low-energy ($\sim$1 keV) charge-exchange reactions

$$D^- + H(pol.) \rightarrow D + H^-(pol.)$$
or
$$H^- + D(pol.) \rightarrow H + D^-(pol.)$$

appear extremely attractive. Projected performance figures for such a scheme, using the best sources for producing the H^-(or D^-) beam and the best polarized H-atom (or D) storage

cell systems reported to date, imply that negative polarized beam currents up to 0.38 mA can be obtained. 2) Optically-pumped polarized sources developed at TRIUMF and KEK are now the technology of choice for producing polarized H^- beams. Currents greater than 300 μA with polarizations above 85% have been obtained for dc beams having emittance appropriate to TUNL's tandem accelerator. However, these sources are not yet capable of producing tensor-polarized deuteron beams, which are used extensively at TUNL. We plan to submit to DOE a supplemental proposal for funding to start design and construction of the new source, using the best of these two technologies.

In the development of polarized targets we plan to convert the dynamically polarized proton target at TUNL into a vector (or tensor) polarized deuteron target. We also plan to explore new ideas about the possibility of building room-temperature polarized proton and deuteron targets.

With respect to innovative detector develpment, we are currently optimizing our rapid-cycle cryogenic microcalorimeter-bolometer, a device that operates in the mK temperature regime to detect incident radiation with superb energy resolution. We are also improving our recently installed focal-plane detector for the Enge spectrometer.

The Nuclear Data Evaluation project for nuclei A=3–20, which was moved to TUNL in 1990, continues not only to benefit our local research, but is also providing an important service to the international nuclear physics community.

As one of the largest university-based nuclear physics laboratories, TUNL has special responsibilities and opportunities. In January of 1995 TUNL hosted the NSAC Town Meeting on Nuclear Structure, Low-Energy Nuclear Reactions, and Radioactive Beams. In October of 1995 the annual Symposium of Northeastern Accelerator Personnel (SNEAP) took place at TUNL.

The TUNL seminar program continues with characteristic vigor, supplemented by 16 in-house lectures on TUNL instrumentation and safety procedures. A related program, the Triangle Nuclear Theory seminars, is also beneficial to TUNL faculty and students.

The talents and enthusiasm of the 18 faculty members, 9 research staff and post-doctoral associates, and 30 graduate students from the three Triangle universities are responsible for the successes of our research program. We also benefit from collaborations with Tennessee Technological University, North Georgia University, North Carolina A&T State University, North Carolina Central University, State University of New York-Geneseo, China Institute of Atomic Energy and Tsinghua University (Beijing), and Jagellonian University (Cracow).

The TUNL Advisory Committee - Drs. David Balamuth (University of Pennsylvania), Baha Balantekin (University of Wisconsin), James Friar (Los Alamos National Laboratory), Gerald Garvey (The White House), and Steven Vigdor (University of Indiana) - continues to provide valuable advice on the research program.

The research summaries presented in this progress report are preliminary. They should not be referenced in other publications. If you wish to know the current status of a project, please contact the person whose name is underlined in the author list.

Triangle Universities Nuclear Laboratory

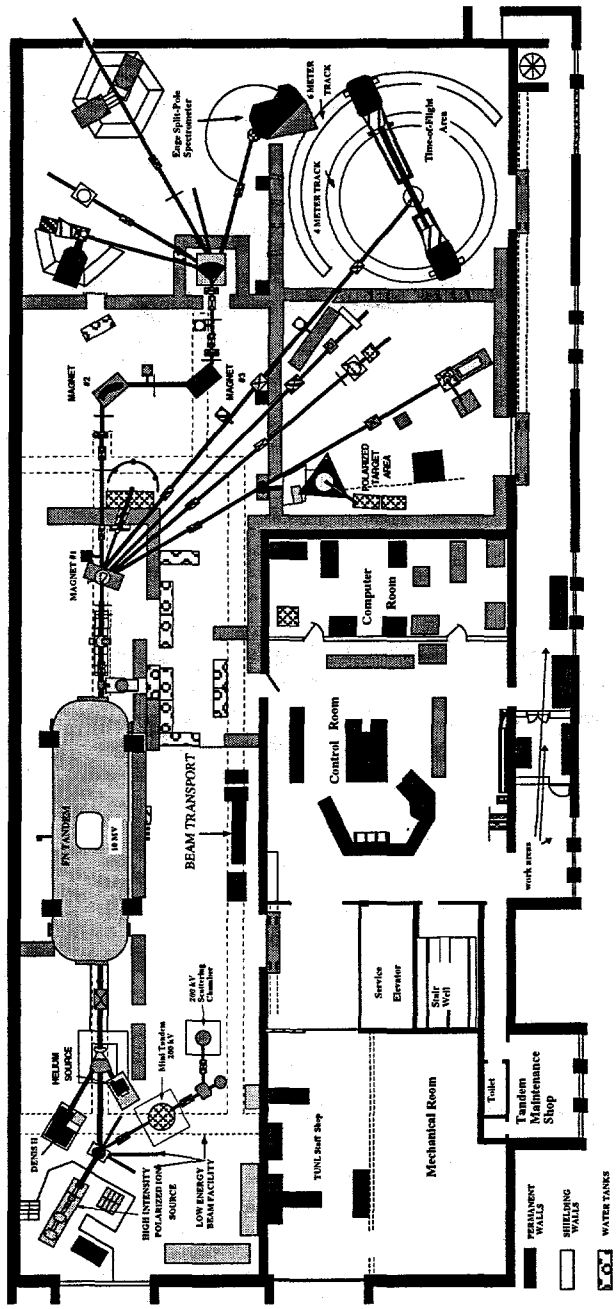

Personnel[1]

Duke University, Box 90308, Durham, NC 27708-0308
Department of Physics, Box 8202, North Carolina State University,
Raleigh, NC 27695-8202
Department of Physics and Astronomy, University of North Carolina,
Chapel Hill, NC 27599-3255

Faculty

Bilpuch, E. G. (Professor)	Duke
Brune, C. R. (Research Assistant Professor)	UNC
Champagne, A. E. (Professor)	UNC
Clegg, T. B. (Professor)	UNC
De Braeckeleer, L.[2] (Assistant Professor)	Duke
Gould, C. R. (Professor)	NCSU
Haase, D. G. (Professor)	NCSU
Howell, C. R. (Associate Professor)	Duke
Iliadis, C.[2] (Assistant Professor)	UNC
Karwowski, H. J. (Professor)	UNC
Ludwig, E. J. (Associate Director, Professor)	UNC
Merzbacher, E. (Professor Emeritus)	UNC
Mitchell, G. E. (Associate Director, Professor)	NCSU
Moore, E. F. (Assistant Professor)	NCSU
Roberson, N. R. (Associate Director, Professor)	Duke
Seagondollar, L. W. (Professor Emeritus)	NCSU
Seely, M. L. (Research Assistant Professor)	NCSU
Tilley, D. R. (Professor)	NCSU
Tornow, W. (Director, Research Professor)	Duke
Walter, R. L. (Professor)	Duke
Weller, H. R. (Professor)	Duke
Wilburn, W. S.[2] (Research Assistant Professor)	Duke

[1] As of August, 1 1996.
[2] As of Fall semester 1996.

TUNL Advisory Committee

Balamuth, D. P.	University of Pennsylvania
Balantekin, A. B.	University of Wisconsin
Friar, J. L.	Los Alamos National Laboratory
Garvey, G. T.	Los Alamos National Laboratory
Vigdor, S. E.	University of Indiana

Associated Faculty

Fletcher, K. A.	State University of New York, Geneseo
Jackson, C. R.	North Carolina A & T State University
Prior, R. M.	North Georgia College
Shriner, J. F.	Tennessee Technological University

Research Staff

Blackmon, J. (Research Associate)	UNC
Crowe, B. (Research Associate)	UNC
Guillemette, J. (Research Associate)	Duke
Hansper, V. (Research Associate)	UNC
Kalbach Walker, C. (Senior Research Scientist)	Duke
Spraker, M. (Research Associate)	Duke
Wallace, P. (Research Associate)	Duke
Westerfeldt, C. (Research Scientist, Radiation Safety Officer)	Duke

Technical Support Staff for TUNL

Carter, E. P.	Accelerator Supervisor
Cheves, C. M.	Staff Specialist
Collins-Perry, B. M.	Research Secretary
Dunham, J. D.	Accelerator Technician
Edwards, S. E.	Computer Maintenance Supervisor
Gibson, P. M.	Staff Assistant
Mulkey, P. H.	Electronics Technician
O'Quinn, R. M.	Accelerator Technician

Graduate Students

Adams, A.	NCSU	Junkin, D.	UNC
Beal, W.	NCSU	McLean, L.	NCSU
Bertone, P.	UNC	Norman, A	Duke
Braun, R.	Duke	Novotny, S.	UNC
Canon, S.	Duke	Powell, D.	UNC
Chen, Q.	Duke	Raichle, B.	NCSU
Crawford, B.	Duke	Rice, B.	Duke
Crowell, A.	Duke	Roper, C.	Duke
Fisher, B.	UNC	Salinas, F.	Duke
Geist, W.	UNC	Schreiber, E.	Duke
Godwin, M.	Duke	Veal, K.	UNC
González Trotter, D.	Duke	Walston, J.	NCSU
Grossman, C.	NCSU	Wood, M.	UNC
Hale, S.	UNC	Wulf, E.	Duke
Holzknecht, K.	NCSU		

Visiting Scientists

Yingtan Chen	8/95	Tsinghua University, Beijing, China
Zemin Chen	1/96–4/96	Tsinghua University, Beijing, China
Antonio Fonseca	6/96–7/96	Centro de Fisica Nuclear, Lisbon, Portugal
Gerry Hale	3/96	LANL, Los Alamos, NM
Hartmut Hofmann	3/96	University of Erlangen, Germany
Ge-Cheng Kiang	8/95–9/95	Academia Sinica, Taipei, Taiwan
Lin Lee Kiang	8/95–9/95	Tsinghua University, Taipei, Taiwan
Alejandro Kievsky	3/96	INFN, Pisa, Italy
Beata Kozlowska	8/95–9/95	University of Silesia, Poland
Ulf-G. Meißner	10/95, 3/96	University of Bonn, Germany
Blaine Norum	3/96, 6/96	University of Virginia
Eduard Sharapov	1/96–3/96	JINR, Dubna, Russia
Joann Shriner	8/95, 5/96–7/96	Tennessee Technological University
Ivo Šlaus	11/95, 4/96	Rudjer Boskovic, Zagreb, Croatia
Michele Viviani	5/96	INFN, Pisa, Italy
Henryk Witała	9/95, 3/96	Jagellonian University, Cracow, Poland

Temporary Student Personnel

Du, Y.	Duke
Nugent, A.	Duke
Jones, B.	Duke
Taalman, L.	Duke

Undergraduates

Burton, A.	NC A & T
Cox, J.	Tennessee Tech. Univ.
Fittje, L.	Tennessee Tech. Univ.
Goldsmith, C.	Duke
Lea, C.	UNC
Rogers, R.	Duke
Weller, A.	UNC
Zeibel, J.	Duke

1 Fundamental Symmetries in the Nucleus

1.1 Parity-Mixing Measurements

1.1.1 Parity Violation with Polarized Epithermal Neutrons – General – The TRIPLE Collaboration

B. E. Crawford, L. Y. Lowie, G. E. Mitchell, N. R. Roberson, S. L. Stephenson and other members of the TRIPLE Collaboration[1]

The nucleon-nucleon force consists of the strong parity conserving (PC) interaction and the weak parity nonconserving (PNC) interaction. The PNC interaction has a strength of order 10^{-7} relative to the PC interaction. The weak interaction can be detected by measurement of pseudo-scalar observables of the type $(\vec{\sigma}\cdot\vec{k})$, where $\vec{k}$ is the momentum and $\vec{\sigma}$ is the spin of the nucleon. Resonances formed with polarized low-energy neutrons show strong PNC effects. The weak interaction causes the mixing of nuclear levels of the same spin and opposite parity. Two mechanisms enhance the size of the parity violation: the levels are very close together in energy, and very strong (s-wave) resonances are mixed into very weak (p-wave) resonances. In heavy nuclei these combined enhancements magnify the PNC effects (by 10^4 to 10^6) in the helicity dependence of the neutron cross-section.

The TRIPLE collaboration uses the high-flux epithermal neutron beam from LANSCE (Los Alamos Neutron Scattering Center) to study the neutron-nucleus weak interaction. The longitudinal asymmetry is measured for neutron energies up to several hundred eV. Our approach treats the PNC matrix elements as random variables. A statistical analysis of our initial results yielded root-mean-squared PNC matrix elements with values M≈1 MeV. This agrees well with the expected estimate $M_{Theory}=M_{sp}/N^{1/2}$, where the single particle weak matrix element is taken as Msp≈0.5 eV, and N≈10^6 is the approximate number of quasiparticle components in the wave function of a typical compound-nuclear (CN) state in a heavy nuclide.

Our first measurements studied the transmission of longitudinally polarized neutrons through ^{238}U and ^{232}Th. These early results are summarized in two review articles [Bow93, Fra93]. The ^{232}Th measurement revealed an unexpected correlation in the sign of the longitudinal asymmetries. All attempts to explain the sign effect as a general feature of the weak neutron-nucleus interaction failed.

[1]Los Alamos National Laboratory, Los Alamos, NM 87545; TRIUMF, Vancouver, BC V6T 2A3; Joint Institute for Nuclear Research, 141980 Dubna, Russia; Kyoto University, Kyoto 606-01, Japan; National Laboratory for High Energy Physics, 1-1 Oho, Tsukuba-shi 305, Japan; University of Technology, P.O. Box 5046, 2600 GA, Delft, The Netherlands.

We have developed improved equipment for this experiment, including a new large-area, high-polarization proton target for polarizing the neutron beam [Pen94], a new neutron detector for transmission experiments with large samples [Yen94], and a large solid angle pure CsI detector for capture experiments with isotopic samples [Fra94]. These three devices are described in a series of papers in the proceedings of a workshop on time-reversal-invariance and parity-violation held at JINR in Dubna.

The polarized proton filter system is based on a 5-Tesla split-coil superconducting magnet operating at 1 K. The microwave dynamic nuclear polarization method is used with electron-beam irradiated solid ammonia. Neutron polarizations of 70% are achieved. The new high count-rate neutron detector is a ^{10}B-loaded liquid scintillator. The scintillator housing is divided into 55 cells, each viewed by a photomultiplier with a high-current base. Pulses are summed to produce a voltage signal whose amplitude is proportional to the total count rate in the detector. This voltage is digitized for each beam burst by a transient digitizer and the results are stored in a summation memory. The neutron-capture γ-ray detectors are pure CsI, 12 inches long and approximately 4 inches by 4 inches in cross-section. The cross-section is a partial wedge, so that 12 detectors form a cylinder around the beam pipe. Two such cylindrical arrays (24 detectors) provide a solid angle of approximately 2.8 sr. The 24-detector array is located in the 56-meter counting house.

During the 1993 run cycle we performed transmission measurements on ^{238}U and ^{232}Th (repeating our initial measurements), obtained new transmission data on natural In (mainly ^{115}In) and natural silver (^{107}Ag and ^{109}Ag), and performed a capture measurement on ^{113}Cd (with a preliminary version of the capture detector). Resonances with parity violations were observed for ^{238}U, ^{232}Th, ^{115}In, ^{107}Ag, ^{109}Ag, and ^{113}Cd. LANSCE was not available to perform experiments in 1994. Another set of experiments was performed in 1995. The focus was on capture experiments and on targets in the mass A$\approx$100 region. The motivation was to experimentally determine the mass dependence of the weak neutron-nucleus interaction. Capture data were obtained on the separated isotopes ^{106}Pd, ^{108}Pd, ^{107}Ag, and ^{121}Sb. Transmission measurements were performed on natural Sb (^{121}Sb and ^{123}Sb), and the monoisotopic targets ^{127}I and ^{133}Cs. In addition, a transmission measurement was performed on a natural liquid xenon target.

The most important result is that the sign correlation in the ^{232}Th longitudinal asymmetries is confirmed – eight of eight statistically significant effects are positive. Excluding ^{232}Th, the new data (combined with a few older measurements) yield longitudinal asymmetries which have approximately 20 positive values and 10 negative values. This suggests that the sign correlation observed in ^{232}Th is specific to that nuclide, and is not a general feature of the weak interaction. This new result has led to a number of new, local doorway state models. The status for each target is summarized in the next section.

We have improved our data processing and analysis in a number of ways. There is a γ-ray component in the neutron beam, and these γ-rays are detected by our detector array. We have developed a procedure that permits the determination of the γ-ray content in

any pulsed neutron beam. For the LANSCE beam the γ-ray content is about 2% at 1 eV neutron energy, and about 10% at 340 eV. Our data have been corrected for this effect.

The parity violating longitudinal asymmetries have been obtained from the data with an empirical single level code. There are a number of difficulties: (1) at times, several p-wave resonances interfere and a multilevel code is needed; (2) the background flux is determined empirically, and the shape can be appreciably distorted from the expected smooth energy dependence by strong neighboring s-wave resonances; (3) for higher energies the observed resonance shape is dominated by the beam energy resolution function, which is asymmetric due to the time structure of the neutron beam; and (4) the effects of Doppler broadening and the beam energy resolution cannot be simulated by one symmetric convolution, as in our empirical code. Therefore we have written a multilevel code that incorporates improvements to address all of these (and other) concerns. This code is now at the final testing stage.

The analysis used to determine the rms parity violating matrix element M from the longitudinal asymmetries has been extended to include targets with spin and to situations where only partial spectroscopic information is available. In practice, the precision with which M can be determined is governed by the status of the relevant nuclear spectroscopic information. In favorable cases with all spectroscopic information available, the uncertainty is determined by the sample size. However, in most cases there is incomplete information available for some or all of the relevant spectroscopic parameters. We have considered the methods of analysis appropriate under various circumstances, corresponding to the wide range of spectroscopic knowledge available for different nuclides. We derived probability density functions when there is complete knowledge, partial knowledge, or no information concerning the spectroscopic parameters. Given the probability density functions, the likelihood method can be used to determine the relevant parameters from the experimental results.

Our conclusion is that given the relevant spectroscopic parameters, one can obtain reliable and reasonably precise values for the rms PV matrix element M from the longitudinal asymmetry data. With partial information M can still be obtained, but with increased uncertainty. Our considerations provide a framework for establishing priorities among the various spectroscopic measurements. A detailed paper on this analysis has recently been published [Bow96].

[Bow93] J. D. Bowman *et al.*, Ann. Rev. Nucl. Part. Sci. **43**, 829 (1993).

[Bow96] J. D. Bowman *et al.*, Phys. Rev. **C53**, 285 (1996).

[Fra93] C. M. Frankle *et al.*, Phys. Part. Nucl. **24**, 401 (1993).

[Fra94] C. M. Frankle *et al.*, *Time Reversal Invariance and Parity Violation in Neutron Reactions*, p. 204, ed. C. R. Gould and J. D. Bowman and Yu. P. Popov, World Scientific, Singapore, 1994.

[Pen94] S. I. Penttilä *et al.*, *Time Reversal Invariance and Parity Violation in Neutron Reactions*, p. 198, ed. C. R. Gould and J. D. Bowman and Yu. P. Popov, World Scientific, Singapore, 1994.

[Yen94] Y.-F. Yen *et al.*, *Time Reversal Invariance and Parity Violation in Neutron Reactions*, p. 210, ed. C. R. Gould and J. D. Bowman and Yu. P. Popov, World Scientific, Singapore, 1994.

1.1.2 Parity Violation with Polarized Epithermal Neutrons – Status of Experiments – The TRIPLE Collaboration

B. E. Crawford, L. Y. Lowie, G. E. Mitchell, N. R. Roberson, S. L. Stephenson and other members of the TRIPLE Collaboration[1]

^{232}Th – The thorium target was studied in transmission in 1991 and with the improved system in 1993. For all practical purposes thorium is monoisotopic. Preliminary analysis of the new data yields the following results: 28 p-wave resonances were analyzed, and the results are qualitatively consistent with the older measurements, but much improved. There are now eight 5σ PNC effects. The sign correlation is confirmed. Reanalysis with the more comprehensive code to determine the longitudinal asymmetries is expected to make only slight differences in the values of M and B determined from the asymmetries with the likelihood analysis.

^{238}U – The uranium target was studied in transmission in 1990 and with the improved system in 1993. Since the target was depleted to 0.2% ^{235}U, the target was essentially ^{238}U. Preliminary analysis of the new data yields the following results: approximately 20 p-wave resonances were analyzed, with five PNC effects observed at the 4σ level. The preliminary value of M is very close to that obtained in the earlier measurement.

^{115}In – A natural indium target was studied in transmission. Natural indium is 95.7% ^{115}In and 4.3% ^{113}In. An enriched ^{115}In sample was studied with the capture detector. The combination of these measurements led to a significant improvement in the neutron spectroscopy for ^{115}In, and a paper was published on these spectroscopic results [Fra93]. Preliminary analysis of 36 p-wave resonances yields five PNC effects at the 5σ level.

^{107}Ag – A natural silver target was studied in transmission. Natural silver is 51.8% ^{107}Ag and 48.2% ^{109}Ag. An enriched ^{107}Ag target was studied with the capture detector. The combination of these measurements led to a significant improvement in the neutron spectroscopy for ^{107}Ag. A paper is in preparation on these spectroscopic results. Preliminary analysis of 16 p-wave resonances yields five PNC effects at the 3σ level.

[1]Los Alamos National Laboratory, Los Alamos, NM 87545; TRIUMF, Vancouver, BC V6T 2A3; Joint Institute for Nuclear Research, 141980 Dubna, Russia; Kyoto University, Kyoto 606-01, Japan; National Laboratory for High Energy Physics, 1-1 Oho, Tsukuba-shi 305, Japan; University of Technology, P.O. Box 5046, 2600 GA, Delft, The Netherlands.

^{109}Ag – The combination of measurements described above identified new resonances in ^{109}Ag. In addition, an enriched ^{109}Ag target is being studied in neutron capture at Geel. Preliminary analysis of 9 p-wave resonances yields two PNC effects at the 3σ level.

^{127}I – A natural iodine target was studied in transmission. Iodine is monoisotopic. Preliminary analysis indicates five PNC effects at the 3σ level.

^{133}Cs – A natural cesium target was studied in transmission. Cesium is monoisotopic. Preliminary analysis indicates one PNC effect at the 3σ level.

^{106}Pd – An enriched ^{106}Pd target was studied with the capture detector. These measurements make a significant improvement in the neutron spectroscopy for ^{106}Pd. Preliminary analysis indicates one PNC effect at the 3σ level.

^{108}Pd – An enriched ^{108}Pd target was studied with the capture detector. Preliminary analysis indicates no PNC effects.

^{113}Cd – An enriched ^{113}Cd target was studied with the capture detector. Preliminary results indicate three PNC effects at the 3σ level. Resonance spin measurements have been performed with the same target at Geel. This is the most extensive analysis (at present) for any target with spin.

^{121}Sb – Natural antimony was studied in transmission. Antimony is 57.25% ^{121}Sb and 42.75% ^{123}Sb. An enriched ^{121}Sb target was studied with the capture detector. Preliminary analysis indicates three PNC effects at the 3σ level.

Xe – Natural xenon was studied in transmission. (This experiment was in collaboration with an Indiana group. Some xenon isotopes can be highly polarized and the polarization maintained extremely well. These properties are now being exploited in medical applications. The interest here was as a possible polarized target for time reversal studies. The first step was to find suitable resonances displaying PNC effects.) One PNC effect was observed, but it was not known which isotope was responsible. Subsequent measurements at JINR (Dubna) have identified the isotope as ^{131}Xe. Two rapid communications have been published in Phys. Rev. C on this work.

[Fra93] C. M. Frankle *et al.*, Phys. Rev. **C48**, 1601 (1993).

1.1.3 Parity Violation in the ^{4}He System

C. R. Gould, C. D. Keith,[1] *N. R. Roberson, W. Tornow and W. S. Wilburn*

The hadronic weak interaction in nuclei can be described by the exchange of mesons which couple weakly at one vertex and strongly at the other. Since the strong couplings are known, the interaction is then completely determined by the values of the weak coupling constants. These coupling constants can be determined by measuring parity-violating

[1]Indiana University Cyclotron Facility.

(PV) observables in nuclear processes. While the most direct approach is to make these measurements in the nucleon-nucleon (NN) system, the effects are very small (10^{-7}) and only limited information has been obtained in this way. Additional measurements in nuclei are required to fully characterize the hadronic weak force.

An advantage of carrying out parity-violation measurements in nuclei arises from the phenomenon of resonance enhancement. For epithermal neutron resonances in heavy nuclei this can enhance parity-violation by up to 10^6 compared to the NN system. Unfortunately, extracting the weak coupling constants from compound nuclear systems relies on statistical arguments and is therefore subject to theoretical uncertainties not present in the NN system, and not as yet fully understood. Intermediate between these approaches is the possibility of studying light mass nuclear systems where some measure of resonance enhancement may survive, but where exact calculations of wave functions are possible.

In particular, recent progress by the Pisa group in exact few-body calculations [Kie93, Kie94] holds the possibility of uniquely relating four-nucleon PV observables to the weak coupling meson-exchange parameters. The ^{4}He system is especially interesting because the first two excited states are closely spaced isoscalar 0^+ and 0^- levels. Parity mixing is primarily sensitive to just one weak coupling constant h^0_ρ, and the isovector coupling h^1_π does not contribute.

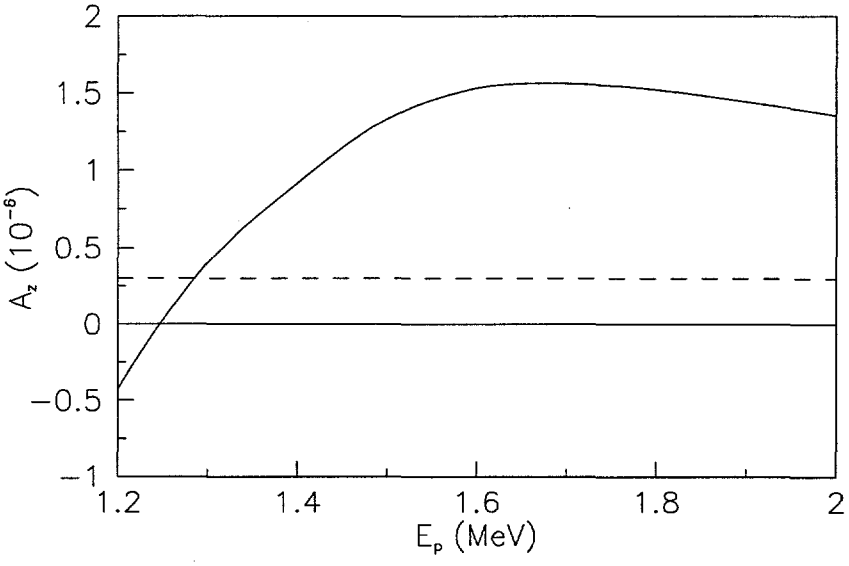

Figure 1.1–1: Predicted value of $A_z(\theta)$ for the ^{3}H($\vec{p}$,n)^{3}He reaction from R-matrix theory. The experimental value for $\vec{p}$-$\vec{p}$ scattering is shown as a dashed line.

Progress has been made toward planning an experiment to measure the longitudinal analyzing power $A_z(\theta)$ for the reaction ^{3}H($\vec{p}$,n)^{3}He at 1.6 MeV. This corresponds to the peak of the 0^- strength. The existence of this level has recently been confirmed at TUNL via a polarization transfer measurement (see Section 3.1.2). Because the levels are spin zero, the analyzing power $A_z(\theta)$ is isotropic. The analyzing power will be determined by observing the asymmetry in the total flux of outgoing neutrons. The target will consist of a permanently sealed tritium gas cell and the neutrons will be detected in a large solid-angle array of plastic scintillators.

We have made a preliminary estimate of $A_z(\theta)$ from R-matrix theory fits to four-nucleon data [Hal88]. This prediction, shown as the solid curve in Figure 1.1–1, gives the size of the effect at $A_z(\theta) \approx 2 \times 10^{-6}$. As can be seen in the figure, a substantial enhancement over the value obtained from $\vec{p}$-$\vec{p}$ scattering (dashed line) is expected. In addition, the effect is seen to be very broad in energy, allowing a thick target to be used without causing unacceptable energy loss to the incident beam. A more accurate estimate from exact four-nucleon calculations is being made by the Pisa group. A statistical precision of 1×10^{-7} can be obtained in approximately 30 days. Systematic effects will also need to be reduced to this level. Many of the techniques required are being developed for the other charged-particle symmetry violation experiments planned at TUNL.

[Hal88] G. Hale, D. Dodder, and K. Witte, 1988, private communication.

[Kie93] A. Kievsky, M. Viviani, and S. Rosati, Nucl. Phys. **A551**, 241 (1993).

[Kie94] A. Kievsky, M. Viviani, and S. Rosati, Nucl. Phys. **A577**, 511 (1994).

1.2 Time-Reversal Invariance Measurements

1.2.1 Test of Parity-Conserving Time-Reversal Invariance Using Polarized Neutrons and Nuclear Spin Aligned Holmium

C. R. Gould, D. G. Haase, P. R. Huffman [1], C. D. Keith[2], B. W. Raichle, N. R. Roberson, M. L. Seely, J. R. Walston and W. S. Wilburn

Parity-conserving time-reversal non-invariance (PC TRNI) arises only through second-order weak effects within the Standard Model. As such, observables from these interactions are expected to be extremely small [Her88]. Nevertheless, experimental bounds are much less stringent. Previously, the most precise dynamical bound came from the detailed balance studies of the reaction ^{24}Mg$(\alpha,\mathrm{p})^{27}$Al and its inverse [Bla83], where relative differential cross-sections were found to be equal to within 5.1×10^{-3} (80% confidence).

We recently carried out an improved search for PC TRNI, using polarized neutron transmission through a rotating cryogenically aligned ^{165}Ho target [Huf96]. The measurement tests reciprocity, or more colloquially, "running the movie backwards." If reciprocity holds, the total cross-sections will be equal for vertically polarized spin-up and spin-down neutrons transmitted through a tensor polarized target whose alignment axis lies in the horizontal plane at 45 degrees with respect to the beam direction. We find the relative cross-sections for 5.9 MeV neutrons to be equal to within 1.2×10^{-5} (80%), which, compared to detailed balance studies, is a factor of four hundred improvement in a measurement of PC TRNI relative cross-sections.

The present measurement consists of a search for the five-fold correlation (FC) term $\vec{s}\cdot(\vec{I}\times\vec{k})(\vec{I}\cdot\vec{k})$ in the neutron-nucleus forward scattering amplitude. Here, $\vec{s}$ is the spin of the neutron, $\vec{k}$ is the momentum of the neutron, and $\vec{I}$ is the spin of the holmium target. The total cross-section for neutrons polarized parallel/anti-parallel $(+/-)$ to the direction $\vec{I}\times\vec{k}$ is [Hni94]

$$\sigma_T^{\pm}(\theta) = \sigma_0(1+\tilde{t}_{20}(I)\,\sigma_2\,P_2(\cos\theta)\pm\tilde{t}_{10}(s)\,\tilde{t}_{20}(I)\,A_5\,\sin 2\theta),$$

where $\tilde{t}_{10}(s)$ is the polarization of the neutron beam, $\tilde{t}_{20}(I)$ is the tensor alignment of the holmium target with respect to its crystal symmetry axis, σ_0 is the unpolarized cross-section, σ_2 is the deformation effect cross-section, A_5 is the PC TRNI spin-correlation coefficient, and θ is the angle between the alignment axis of the holmium crystal and the beam direction. The FC term is isolated by reversing the spin of the neutron beam, and simultaneously rotating the holmium alignment axis.

The count rate and accuracy improvement compared to our previous work result from using the ^{2}H$(\vec{d},\vec{n})^3$He reaction instead of the ^{3}H$(\vec{p},\vec{n})^3$He reaction, using a cryogenically

[1]Present address: Department of Physics, Harvard University, Cambridge, MA.
[2]Present address: IUCF, 2401 Milo B. Sampson Lane, Bloomington, IN.

cooled deuterium gas cell, moving source and detectors into a close, unshielded geometry, and longer run times.

The data were accumulated over a period of one week, and correspond to a total of $\sim 10^{12}$ neutrons detected. The run-by-run asymmetries are fit to the form $a_0 + a_2 \sin 2\theta$ using least squares. A value of $a_2 = (1.1 \pm 1.0) \times 10^{-6}$ is extracted from the data. The chi-square per degree of freedom is 0.9994, indicating no significant random errors other than those associated with counting statistics. Using the measured polarizations ($\tilde{t}_{10}(s) = 0.67 \pm 0.05$, $\tilde{t}_{20}(I)$=0.62±0.05), the asymmetry is converted to the spin-correlation coefficient A_5, yielding

$$A_5 = (8.6 \pm 7.7) \times 10^{-6}, \tag{1.1}$$

consistent with time-reversal invariance. At 45°, the relative spin-up versus spin-down cross-section difference is less than 1.2×10^{-5} (80% confidence).

The most natural parameter for describing PC TRNI is $\bar{g}_\rho$, the ratio of T-violating to T-conserving coupling constants for ρ exchange. Using a recent theoretical analysis by Engel *et al.* [Eng94], A_5 can be directly converted into $\bar{g}_\rho$. In this analysis, the Simonius potential is used in a folding-model calculation to generate an optical potential for ^{165}Ho. This optical potential is then used in a coupled-channels calculation to extract A_5 as a function of $\bar{g}_\rho$. Using our value of A_5, we obtain $\bar{g}_\rho = (2.3 \pm 2.1) \times 10^{-2}$.

The FC term arises only from the valence proton in holmium, and therefore the aligned target PC TRNI experiments suffer from a 1/A suppression compared to one body nuclear effects such as parity violation. Nevertheless, we see that an experiment with MeV neutrons is able to probe TRNI in the ρ-exchange part of the NN potential at the level of a few percent. Further improvement in this PC TRNI bound will likely come either from resonance tests exploiting compound nucleus enhancements, or from storage-ring experiments exploiting increased sensitivity at few GeV energies.

[Bla83] E. Blanke *et al.*, Phys. Rev. Lett. **51**, 355 (1983).

[Eng94] J. Engel *et al.*, Phys. Rev. Lett. **73**, 3508 (1994).

[Her88] P. Herczeg, Hyperfine Interact. **43**, 77 (1988).

[Hni94] V. Hnizdo and C. R. Gould, Phys. Rev. **C49**, R612 (1994).

[Huf96] P. R. Huffman *et al.*, Phys. Rev. Lett. **77**, 4681 (1996).

1.2.2 Neutron Resonances in ^{166}Ho

C. M. Frankle[1], C. R. Gould, D. G. Haase, J. A. Harvey[2] P. R. Huffman[3], N. R. Roberson and L. W. Weston[2]

The nucleus ^{165}Ho (J^{π}=7/2$^-$) offers a number of advantages for the fivefold correlation test of parity-conserving time-reversal non-invariance (PC TRNI): it is monoisotopic with a high level density (D_0=4.2 eV), guaranteeing close proximity of the levels; the spins of many of the strong s-wave resonances are already known from previous work [Mug84]; and finally, large single crystals are available in which the nuclei can be readily aligned cryogenically. While ^{166}Ho is a well studied system, it is possible that a number of weak resonances have either been misidentified or not identified at all. Accordingly, we recently completed [Huf96a] a high sensitivity study of resonances below 500 eV, an energy region in which intense epithermal neutron fluxes are available at several facilities.

The Oak Ridge Electron Linear Accelerator (ORELA) was used to produce a pulsed source of epithermal neutrons. Neutron transmission spectra and neutron capture γ-ray spectra were accumulated in separate experiments. The ^{165}Ho samples were obtained in the form of solid metal. The transmission sample had a thickness of 0.10 atoms/b and mass of 560 g. A chemical assay was provided for the ^{165}Ho and indicated that the only significant impurity was 0.03% of ^{181}Ta. The capture sample had a thickness of 3.35×10^{-3} atoms/b and a mass of 13.01 g, with impurities less than 0.01%. The primary analysis was made on the transmission data set using the neutron resonance analysis code SAMMY [Lar89]. The capture data were used to confirm that resonances were from ^{166}Ho and not from an impurity.

From the fits, typical statistical errors in the widths are of order 2% or less. However, in the vicinity of large s-wave resonances, the fits are not exact and we increase the error to take into account systematic uncertainties. Based on the deviations of the fits off resonance, we estimate systematic uncertainties to be typically 5%, approaching 20% at the higher energies near the largest s-wave resonances.

The majority of the resonance energies and parameters were consistent with the assignments in Mughabghab [Mug84]. However, nine new resonances were observed at energies 24.79, 75.08, 119.98, 187.94, 210.86, 227.87, 235.94, 248.60, and 264.98 eV. Eight of the nine were observed in the capture data. The 24.8 eV resonance was not observed in capture due to a high background of γ rays from room scattered neutrons at long flight times. A systematic check of strong s-wave resonances from a number of nuclei verified that the new resonances in ^{166}Ho did not arise from beam line components or unexpected target impurities.

[1]Los Alamos National Laboratory, Los Alamos, NM.
[2]Oak Ridge National Laboratory, Oak Ridge, TN.
[3]Present address: Department of Physics, Harvard University, Cambridge, MA.

The 10.32 eV resonance previously given in Mughabghab [Mug84] was found to be from ^{181}Ta and eliminated as a holmium resonance. The 375 eV resonance was not observed and removed from the analysis.

Since the new resonances are weak, we consider the possibility that they are positive parity, formed by p-wave capture. Following Bollinger and Thomas [Bol68], the probability is

$$P(p) = \frac{1}{(1+\frac{z}{2})} \tag{1.2}$$

where

$$z = \sqrt{\frac{3S_1P_1}{2S_0P_0}} \exp\left[\frac{-g\Gamma_n}{2\sqrt{E_n}D_0}\left(\frac{1}{S_0P_0} - \frac{2}{3S_1P_1}\right)\right]. \tag{1.3}$$

Here, S_0, S_1 are the s- and p-wave strength functions, and $P_0=1$, $P_1=kR$ are the penetrabilities.

Using $R=1.35A^{1/3}$ fm, we find $P(p)<10^{-4}$ in all cases. Hence, we conclude that the newly located resonances are all negative parity, formed predominately by s-wave capture.

A paper summarizing the experimental findings and tabulating the resonance parameters has been accepted for publication [Huf96b]. In addition, a second paper outlining a technique for identifying d-wave admixtures, and estimating the sensitivity to PC TRNI has been submitted to Nuclear Instruments and Methods.

[Bol68] L. M. Bollinger and G. E. Thomas, Phys. Rev. **171**, 1293 (1968).

[Huf96a] P. R. Huffman *et al.*, Phys. Rev. Lett. **77**, 4681 (1996).

[Huf96b] P. R. Huffman *et al.*, to be published, 1996.

[Lar89] N. Larson, *Oak Ridge National Laboratory Report TM-9179/R2*, 1989.

[Mug84] S. F. Mughabghab, *Neutron Cross Sections, vol. 1*, 1984.

1.3 Quantum Chaos in Nuclei

1.3.1 A Complete Level Scheme for ^{30}P

E. G. Bilpuch, C. A. Grossmann, G. E. Mitchell, E. F. Moore, J. D. Shriner, J. F. Shriner, Jr.[1], *G. A. Vavrina, P. M. Wallace and C. R. Westerfeldt*

Detailed studies of the ^{29}Si(p,γ) reaction are in progress to establish a complete level scheme for ^{30}P up to $E_x \approx 8$ MeV. The goal is to use these data to study both chaos and isospin breaking in this nucleus by comparing the experimental energy eigenvalue fluctuations with predictions of random matrix theory. Because such comparisions require data of extremely high quality, we are combining the ultrahigh resolution proton beam available from the TUNL High Resolution Laboratory (HRL) [Wes95] with a high-resolution γ-ray detection system to maximize the probabilities of resolving close-lying levels and of detecting weak γ-ray branches.

The work has proceeded in several stages: (1) Excitation functions for the ^{29}Si(p,γ) reactions have been measured using NaI detectors in the energy range E_p=1.0–3.3 MeV [Fra92]. Sixteen previously unknown resonances in p+^{29}Si were identified. Strengths S=(2J+1)$\Gamma_p\Gamma_\gamma/\Gamma$ were measured for all resonances (J is the spin of the compound nuclear state in ^{30}P). If Γ_p is known, then this measurement yields a value of Γ_γ for any possible value of J. (2) A high-resolution γ-ray detection system consisting of two 60% HPGe detectors, one of which has a large BGO Compton supression shield, was designed, built, and installed [Dra94]. (3) For each of the 47 resonances in the range E_p=1.0–2.5 MeV, γ-ray spectra were measured with the suppressed HPGe detector at 55° and the unsuppressed HPGe detector at 90°. From these measurements, branching ratios were determined for each resonance. The branching ratios were then combined with the values of Γ_γ for the resonance state to yield the partial γ-ray widths to the final state of each primary transition.

For γ-ray transitions of pure multipolarity, the partial γ-ray widths can be converted into reduced transition probabilities B(E1), B(M1), etc. Possible values of the spin J, parity π, and isospin T can often be limited by comparing the experimental reduced transition probabilities to recommended upper limits (RULs) in this mass region obtained by Endt [End93]. If a specific transition probability significantly exceeds the RUL for a given choice of J^π; T (either initial or final state), then that choice is rejected. For transitions which can be mixed multipolarity (e.g., M1/E2), the determination of reduced transition probabilities requires additional information, the γ-ray mixing ratio δ_γ for the transition in question. In these cases, the fixed-detector measurements provide only upper limits for each of the two transition probabilities. In some cases, each of the two possibilities are sufficiently large that no value of δ_γ can prevent exceeding one of the RULs. In other cases, specific knowledge of

[1]Tennessee Technological University, Cookeville, TN.

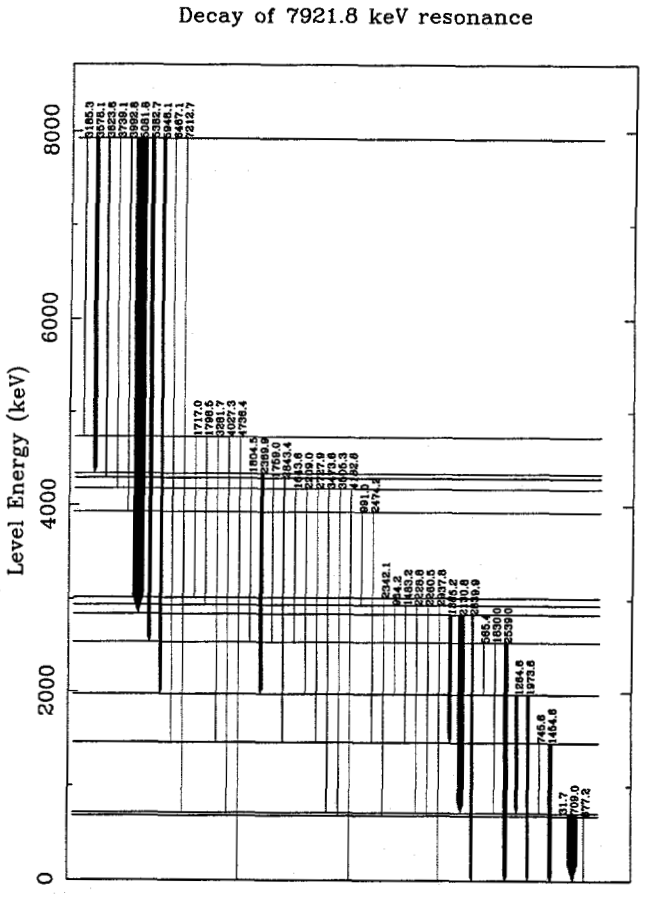

Figure 1.3–1: Decay scheme measured for the E_x=7922 keV level.

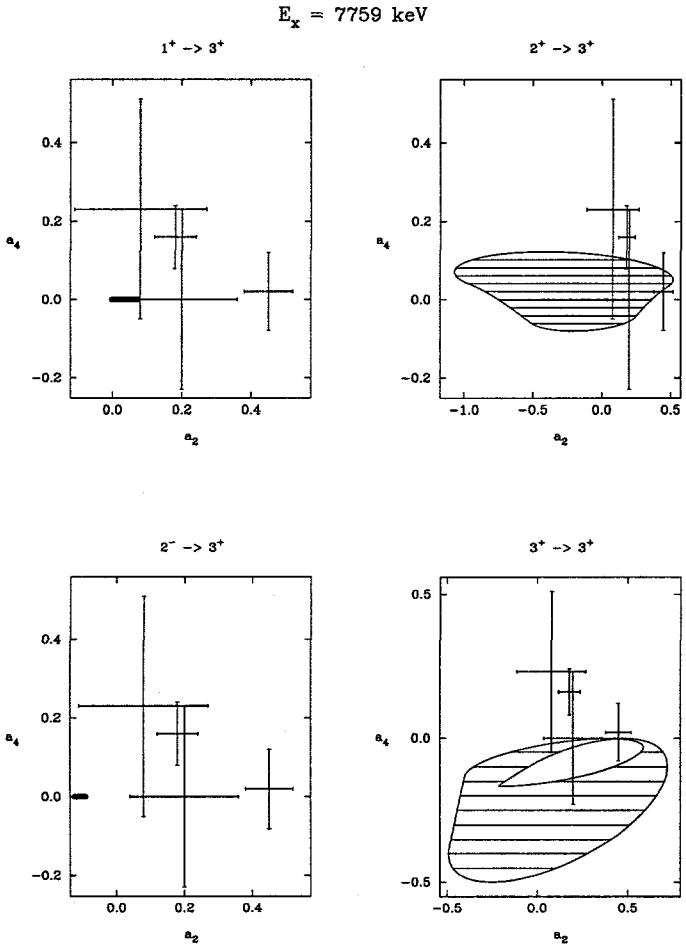

Figure 1.3–2: Allowed regions and measured values of a_2 and a_4 for 4 primary transtions to 3^+ final states from the E_x=7759 keV resonance. The allowed regions are denoted by either a shaded area or by a wide line segment.

δ_γ is required to rule out specific possibilities.

When the results of the fixed-detector measurements are combined with results from other previous experiments [e.g., (p,p_0) or (^{3}He,t)], 9 of the 47 resonances have unique J^π; T assignments. One of these is the resonance at E_x=7922 keV, whose decay scheme is shown in Figure 1.3–1; primary transitions to 10 final states were observed. Prior to these measurements, no information on J^π; T values for this state was known; the fixed detector measurements provide a unique assignment of J^π; T=3$^+$; 0.

For those states which are not uniquely assigned after the fixed-detector measurements, the next step is a measurement of γ-ray angular distributions. Because the ^{29}Si target has J^π=1/2$^+$, there is in general the possibility of ℓ mixing or channel spin mixing in the entrance channel in addition to the possibility of multipole mixing in the exit channel. This complicates the extraction of mixing ratios significantly, since the fitting procedure then requires a simultaneous nonlinear fit of all angular distributions with the number of parameters being approximately twice the number of γ-rays studied. A preliminary way to examine the angular distributions is to extract the coefficients a_2 and a_4 (and a_6 if allowed) and compare them to physically allowed regions of the coefficients for a particular choice of J^π. Coefficients which lie significantly outside the physically allowed range can be used to eliminate possible values. As an example, consider the primary transitions from the E_x=7759 keV state. On the basis of the fixed-detector measurements, assignments of 1$^+$, 2$^+$, 2$^-$, and 3$^+$ were allowed for this state. Figure 1.3–2 shows the experimental a_2 and a_4 coefficients and the allowed regions for each of these J^π possibilities for 4 primary transitions to 3$^+$ final states. It can be seen that the 1$^+$ and 2$^-$ possibilities are eliminated; one of the transitions is outside the allowed region if the resonance state is 3$^+$, but it is not so far outside that we eliminate this assignment without a more detailed analysis. Further analysis on this state is in progress.

Thus far, angular distributions have been measured for six of the resonances. The next step in the experiments is to measure angular distributions for the remainder of the states which do not have unique J^π;T assignments. We expect that this will still leave a few ambiguities because of the quadratic uncertainties. Possible measurements to eliminate these remaining ambiguities include analyzing power measurements for the (p,p_0) and/or (p,γ) reactions or γ-ray linear polarization measurements.

[Dra94] J. M. Drake, Ph.D. thesis, North Carolina State University, 1994.

[End93] P. M. Endt, Atomic Data and Nucl. Data Tables, **55**, 171 (1993).

[Fra92] S. C. Frankle *et al.*, Phys. Rev. **C45**, 2746 (1992).

[Wes95] C. R. Westerfeldt, G. A. Vavrina, and J. J. F. Shriner, *The TUNL High Resolution Laboratory System and Operating Procedures, 3rd Edition*, 1995, Triangle Universities Nuclear Laboratory, Durham, NC.

1.3.2 Reduced Transition Probability Distributions

A. A. Adams, E. G. Bilpuch, G. E. Mitchell, W. E. Ormand[1], *J. D. Shriner and J. F. Shriner, Jr.*[2]

As discussed in the previous section, energy eigenvalue analyses can provide one signature of chaos in a quantum system; however, the data must be of extremely high quality. An alternative signature of chaos without such stringent requirements would be most beneficial. We are studying the distribution of reduced transition probabilities to see if these can provide an alternate signature.

Several previous theoretical studies have studied transition strengths in this context. Alhassid and Novoselsky [Alh92] and Meredith [Mer93] have studied statistical distributions in the context of the interacting boson model and a schematic shell model, respectively. They suggest that the strengths follow a χ^2 ($\nu=1$) distribution if the system is chaotic and a χ^2 ($\nu<1$) distribution if the system is regular.

We started our study by calculating over 74,000 B(M1) and B(E2) values in ^{22}Na using the shell model code OXBASH. The first 25 positive parity states were calculated for each spin J from 0 to 8 and for isospins T=0 and 1. The reduced transition probabilities B(M1) and B(E2) were calculated for each pair of states for which they were allowed. This large data set enabled us to develop an appropriate analysis technique without the concerns of experimental uncertainties or limited statistics. Later we will apply the same techniques to experimental data.

To compare different subsets of data, we needed to ensure that all sets were normalized. We used the method of Alhassid and Novoselsky in which each strength is divided by the local average for that group of transitions, and the local average is generated by using a pair of Gaussian weighting factors centered on the initial and final states of the transition. We find that the normalized transition strengths show no dependence on spin, electromagnetic character, isospin character, or excitation energy. The shell-model calculations are all consistent with $\nu=1$, suggesting that the shell model shows ^{22}Na to be chaotic. The distributions for the M1, E2, isoscalar (IS), and isovector (IV) decays are shown in Figure 1.3–3.

Our next step is to apply this technique to experimental data from ^{26}Al [End88a, End88b]. A nearly complete level scheme is known for ^{26}Al up to $E_x \approx 8$ MeV, and extensive γ-ray measurements have been performed to measure branching ratios and quantum numbers. We have found that for these data the transition strength histogram is distorted during the normalization process due to missing small values of the strengths. We are currently studying how to appropriately unfold this effect to determine the underlying distribution.

[1]University of Tennessee, Knoxville, TN and Oak Ridge National Laboratory, Oak Ridge, TN.
[2]Tennessee Technological University, Cookeville, TN.

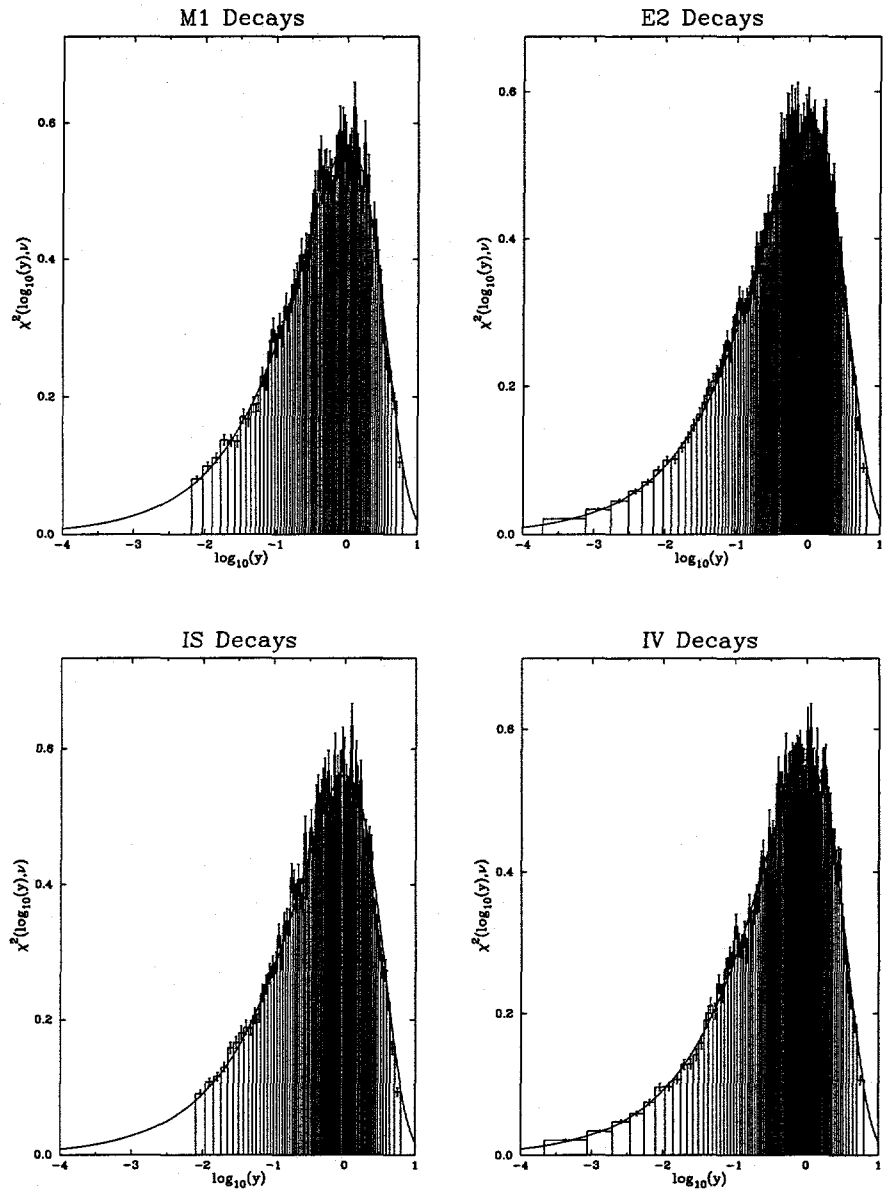

Figure 1.3–3: Distributions of reduced transition probabilities calculated in ^{22}Na for M1 decays, E2 decays, isoscalar (IS) decays, and isovector (IV) decays. The smooth lines represent the fitted $\chi^2(\nu)$ functions with ν=1.03 ± 0.04, 0.99 ± 0.03, 1.01 ± 0.04, and 1.00 ± 0.02, respectively.

[Alh92] Y. Alhassid and A. Novoselsky, Phys. Rev. C, **45** (1992).

[End88a] P. M. Endt, P. de Wit, and C. Alderliesten, Nucl. Phys., **A476**, 333 (1988).

[End88b] P. M. Endt, P. de Wit, and C. Alderliesten, Nucl. Phys., **A476**, 221 (1988).

[Mer93] D. C. Meredith, Phys. Rev. E, **47**, 2405 (1993).

2 Internucleon Reactions

2.1 Neutron-Proton Interaction

2.1.1 Measurements of the Spin Dependent Total $\vec{n}$-$\vec{p}$ Cross-Section Difference

B. E. Crawford, D. S. Junkin, C. R. Gould, D. G. Haase, B. W. Raichle, M. L. Seely, W. Tornow, J. R. Walston and W. S. Wilburn

Determination of the nucleon-nucleon (NN) tensor force below 35 MeV is the goal of an ongoing series of experiments at TUNL. The measurements are made by observing the transmission asymmetry for polarized neutrons on a polarized proton target. The neutrons and protons are polarized transverse to the beam momentum, yielding the transverse spin-dependent total cross-section difference $\Delta\sigma_T$, or polarized longitudinally, yielding $\Delta\sigma_L$. These observables are primarily sensitive to the phase-shift parameter ϵ_1, which parameterizes the NN tensor force at low energies. In addition, they are also sensitive to the singlet and triplet s-wave phase shifts $^1S_0$ and $^3S_1$. Measurements of both $\Delta\sigma_T$ and $\Delta\sigma_L$, when combined with the known n-p total cross-section, allow the extraction of all three phase-shift parameters.

Before our efforts began, ϵ_1 was poorly determined at low energies, with substantial discrepancy between theory and experiment, as demonstrated by the open symbols in Figure 2.1–1 (see [Wil95] for references). The most striking disagreement occured below 20 MeV, where very low values of ϵ_1 are reported by two separate experiments. In contrast, above 20 MeV the data indicate that ϵ_1 is higher than theoretical predictions. Measurements of $\Delta\sigma_T$ in the energy range 4–12 MeV have already been made at TUNL (solid triangles [Wil95]). These measurements show no evidence for a small value of ϵ_1 at low energies. The addition of accurate $\Delta\sigma_T$ and $\Delta\sigma_L$ data presently in progress or beginning in the near future will complete the data set below 20 MeV and remove the remaining ambiguity.

The experimental setup for the measurement of the neutron transmission asymmetry is as follows. As shown in 2.1–2, neutrons are produced at the end of the beamline via the $^2\mathrm{H}(\vec{d},\vec{n})^3\mathrm{He}$ reaction, transmitted through the polarized target, and detected at 0°. The spins of the neutrons are reversed at a rate of 10 Hz, removing the effects of detector and electronic gain drifts. The neutron flux is monitored by a small scintillator placed in front of the neutron production cell. Compared to the previous polarized proton target [Wil95], the product of polarization and target thickness of the new dynamically polarized proton target 6.6 is improved by a factor of 6. In addition, the spin of the dynamically polarized target can be reversed every three hours, reducing the influence of systematic effects. Twenty-four

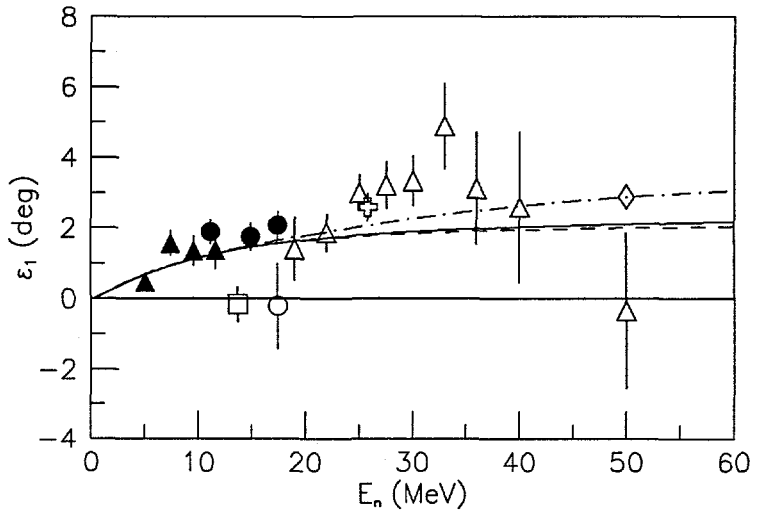

Figure 2.1–1: Values of the phase-shift parameter ϵ_1 from experimental measurements and theoretical predictions.

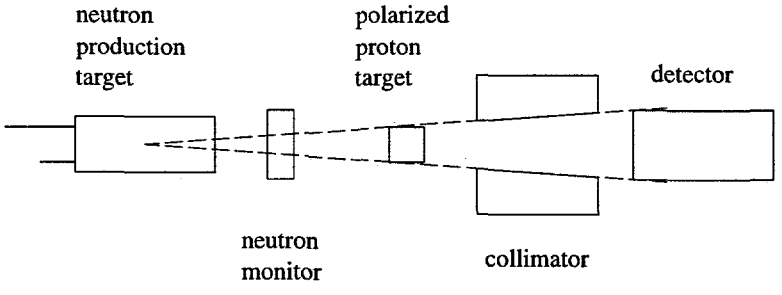

Figure 2.1–2: Experimental layout for measurement of $\Delta\sigma_T$.

hours of data were taken at each energy.

Recently, we have measured $\Delta\sigma_T$ at E_n=11.13, 14.97, and 17.37 MeV. The measurements extend our data to higher energies with improved uncertainties. Preliminary data are shown as closed circles in Figure 2.1–1. These data show good agreement with predictions and present no evidence for a low energy anomaly in ϵ_1.

Future efforts will focus on measuring $\Delta\sigma_L$ in order to remove the sensitivity to s-waves, and on measuring both $\Delta\sigma_T$ and $\Delta\sigma_L$ at 35 MeV. The measurements at a higher energy will help to resolve both the discrepancies between experiment and theory and between competing phase-shift analyses.

[Wil95] W. S. Wilburn *et al.*, Phys. Rev. **C52**, 2351 (1995).

2.1.2 Neutron-Proton Analyzing Power Measurements at E_n=12 and 7.6 MeV

R. T. Braun, C. D. Roper, D. E. Gonzalez, C. R. Howell, F. Salinas, H. R. Setze, W. Tornow and R. L. Walter

Since 1987 there has been some controversy as to the accurate determination of the πNN coupling constants. Before this time they were believed to be well known, with values of $g_c^2/4\pi$=14.47 fm for the charged pion and $g_o^2/4\pi$=14.54 fm for the neutral pion. But in 1987 a reanalysis of all p-p scattering data by the Nijmegen group resulted in a significantly lower value for the neutral pion coupling constant. Subsequent reanalysis by the Nijmegen group also determined a lower coupling constant for the charged pion. Their current values are $g_c^2/4\pi$=13.52 $\pm$ 0.05 fm and $g_o^2/4\pi$=13.56 $\pm$ 0.09 fm [Sto93]. Independent analyses by Arndt [Arn95] and Bugg [Bug95] have determined supporting, though slightly larger values. However, a recent work by Ericson *et al.* [Eri95] studying the n-p elastic cross-section at E_n=162 MeV supports the older, larger value for the charged coupling constant. Clearly more information is needed. As Machleidt [Mac95] and Ericson *et al.* [Eri95] have pointed out, this lower value for the πNN coupling constant has profound consequences for nuclear physics.

One gauge to the πNN coupling constant appears to be the low-energy n-p $A_y(\theta)$. At low energies the n-p $A_y(\theta)$ is completely determined by the ^3P_J waves. These waves probe the long-range tail of the nuclear force and therefore should be sensitive to the dominant meson exchange process in this range, the one-pion exchange. The extent of this sensitivity can be seen from the curves in Figure 2.1–3. The curves are the calculated observables from three NN potentials based on the Bonn B potential [Mac95], and the only major difference between each of the models is the value used for the πNN coupling constant. Model A (dotted curve) has $g^2/4\pi$=13.6 fm, model B (solid curve) has $g^2/4\pi$=14.0 fm, and model C (dashed curve) has $g^2/4\pi$=14.4 fm.

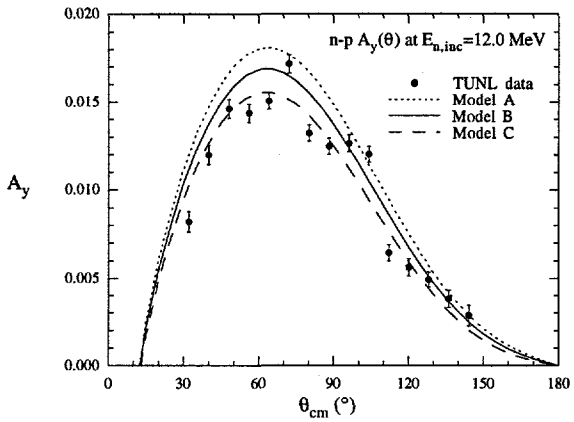

Figure 2.1–3: TUNL n-p $A_y(\theta)$ data at 12 MeV. The data are corrected for instrumental effects; some of the corrections are still preliminary. The curves shown are based on the Bonn B NN potential with modified values for $g_c^2/4\pi$. Model A (dots) uses 13.6, model B (solid) 14.0, and model C (dashes) 14.4. Observables were calculated using the code SAID.

At TUNL we have measured the n-p $A_y(\theta)$ at E_n=12.0 MeV and 7.6 MeV to a statistical accuracy of ±0.0005 or better. This is the most accurate measurement ever obtained below E_n=180 MeV. At each energy a 15-point angular distribution, from θ_{lab}=16–72°, was measured. Due to the small size of the analyzing power, it is crucial to correct the data for the effects of additional scattering processes and for finite geometry effects. One of the most important corrections comes from multiple scattering within the neutron detector. In this process a neutron scattered from the proton target enters the detector and is scattered first from ^{12}C and finally from ^{1}H. However, due to large resonances in the n-^{12}C analyzing power over certain energy ranges, additional asymmetry can be introduced. These resonances cause the n-^{12}C to swing from large negative to large positive values over an energy range of a few hundered keV, within the energy range accepted by a single neutron detector at a given angle. A detector covering the range of such a resonance would have an increased/decreased efficiency, depending on the neutron spin, and this efficiency effect does not cancel when the spin of the incident neutron beam is flipped.

In order to correct for this effect, accurate Monte-Carlo simulations of the experiment have been performed using phase-shift calculations to model the n-^{12}C cross-sections and analyzing powers. The regions most affected by the n-^{12}C scattering can be seen in Figure 2.1–3, near θ_{cm}=75° and 110°. However, the phase shifts at these energies are not well known, so the accuracy of our corrections, as seen in the lack of smoothness in the data, causes uncertainty in the determination of $g_c^2/4\pi$.

Currently experiments are underway at TUNL to measure the n-^{12}C $A_y(\theta)$ at the ener-

gies where the resonances are most pronounced. This data can then be incorporated into the n-p Monte-Carlo simulations to provide more accurate corrections to the data. Section 5.3.1 shows preliminary data from the n-^{12}C; in particular note the data at 6.95 MeV which corresponds to the data in Figure 2.1–3 at θ_{cm}=75°.

[Arn95] R. A. Arndt *et al.*, Phys. Rev. Lett. **52**, 2246 (1995).

[Bug95] D. Bugg and R. Machleidt, Phys. Rev. Lett. **52**, 1203 (1995).

[Eri95] T. E. O. Ericson *et al.*, Phys. Rev. Lett. **75**, 1046 (1995).

[Mac95] R. Machleidt, 1995, private communication.

[Sto93] V. Stoks *et al.*, Phys. Rev. Lett. **47**, 512 (1993).

2.1.3 The TUNL Neutron-Proton Scattering Length Experiment – A Status Report

F. Salinas, T. S. Carman, Q. Chen, A. S. Crowell, D. E. González Trotter, C. R. Howell, C. D. Roper, H. Tang, W. Tornow and R. L. Walter

We have completed data taking for the measurement of the $^1S_0$ neutron-proton (n-p) scattering length (a_{np}) in a kinematically complete n+d→n+n+p breakup experiment at E_n=13.0 MeV. The goal of this experiment is to study the influence of possible three-nucleon force (3NF) effects on the extracted value for a_{np}, which is very well known from n-p elastic scattering. We have accumulated 2900 hours of data. According to estimates based on the analysis of about 30% of our data [Sal95], this should result in about 830 counts at the peak of the main enhancement in the n-p final-state interaction (FSI) spectrum for the Θ_{n1}=43.0°, Θ_{n2}=55.7°, ϕ_{12}=180° configuration. Since the background due to accidental coincidences is small for the n-p FSI configuration, less than 10% of the accumulated counts, our goal of achieving a statistical accuracy of ±3.5% in 0.5 MeV bins at the FSI peak was reached. The other configurations have a higher number of counts at the peak of interest.

To study 3NF effects and to extract a_{np} we measure the absolute cross-section of the n-p FSI peak at four production angles and compare our experimental results to exact n-d calculations performed with different values for a_{np} (see [Sal94]). In the comparison, the calculations are smeared over the experimental resolution and finite geometry of our experimental setup using Monte-Carlo techniques.

The experimental setup is shown in Figure 2.1–4. It is the same setup used for the a_{nn} measurements, with detectors D9 through D12 added to detect the second neutron in the four n-p FSI configurations. In fact, this experiment took place simultaneously with the

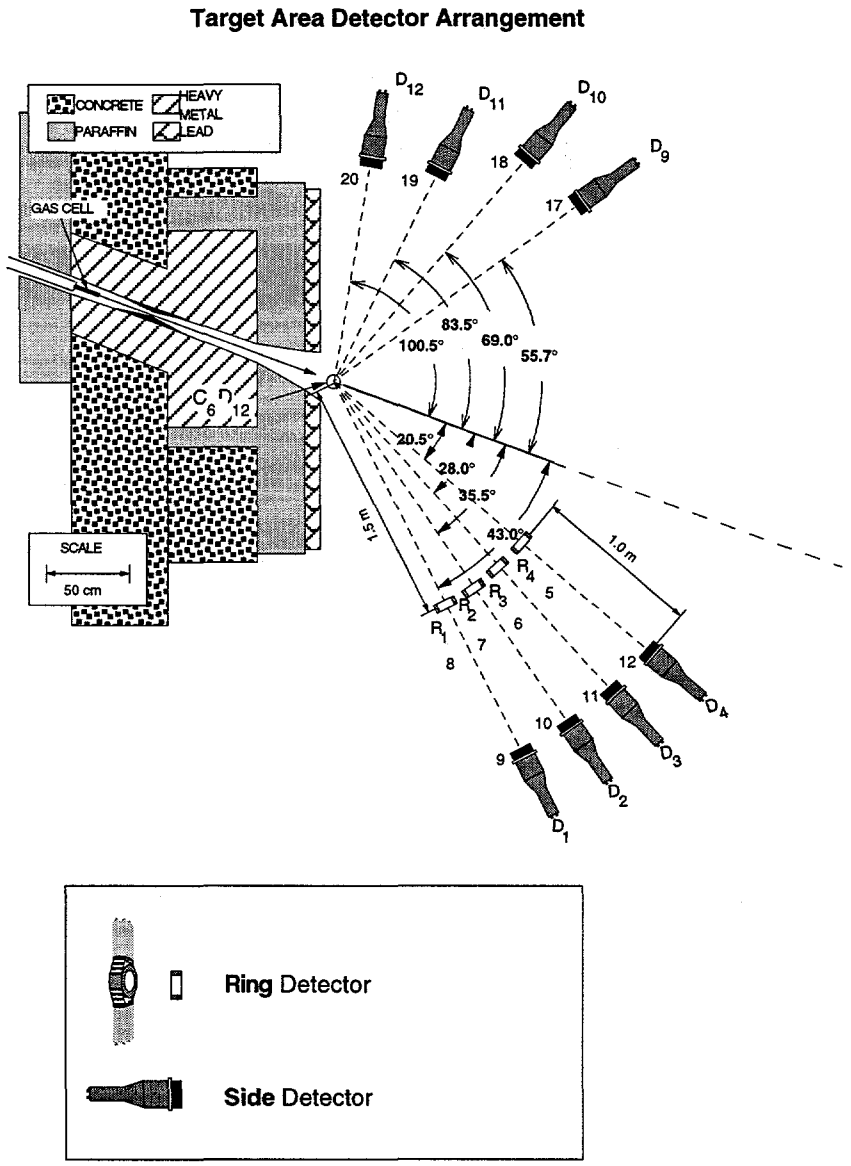

Figure 2.1–4: Experimental setup.

TUNL a_{nn} experiment. The angles of the four detected neutron pairs in the a_{np} determination are: Θ_{n1}=20.5°,Θ_{n2}=100.5°; Θ_{n1}=28.0°,Θ_{n2}=83.5°; Θ_{n1}=35.5°,Θ_{n2}=69.9°; and Θ_{n1}=43.0°,Θ_{n2}=55.7°. In all configurations the azimuthal angle between the two neutrons is ϕ_{12}=180°. The neutron that forms the final-state interaction (FSI) with the proton is labeled as n1.

About 830 hours of data have been analyzed using the methods described in the previous progress report [Sal95]. Cross-section data have been extracted from the resulting E_{n1} vs. E_{n2} spectra by projecting the events onto the point geometry kinematic locus. Our preliminary results are in fair agreement with point-geometry calculations using the Bonn-B OBEPQ with the standard value of a_{np}=–23.7 fm. Final values for a_{np} should be available by the end of 1996.

[Sal94] F. Salinas, In *TUNL Progress Report*, volume XXXIII, p. 31, 1993-1994.

[Sal95] F. Salinas, In *TUNL Progress Report*, volume XXXIV, p. 36, 1994-1995.

2.2 Neutron-Neutron Interaction

2.2.1 Measurement of the $^1S_0$ Neutron-Neutron Scattering Length Using the $^2H(\pi^-,nn\gamma)$ Reaction: LAMPF E1286

T. S. Carman [1], *Q. Chen, C. R. Howell, A. Hussein* [2], *G. Mertens* [3], *C. F. Moore* [4], *C. Morris* [5], *A. Obst* [5], *E. Pasyuk* [6], *C. D. Roper, F. Salinas, H. R. Setze, I. Slaus* [7], *S. Sterbenz* [5], *W. Tornow, R. L. Walter, C. R. Whiteley* [4], *M. Whitton* [5] *and B. F. Gibson* [5]

The nucleon-nucleon (NN) scattering lengths are measures of the NN forces at zero energy. Their relative magnitudes are constrained by charge symmetry and charge independence of the strong nuclear force. Charge dependence is well understood in items of the meson-exchange model of the NN force. The additional exchange of charged mesons makes the n-p force stronger than the n-n and p-p forces. The differences in the n-n and p-p nuclear forces have been attributed to the mass difference of the up and down quarks [Hen69]. The p-p and n-p scattering lengths, a_{pp} and a_{np}, can be determined to an accuracy of ± 0.3 fm and <0.1 fm, respectively, from free two-nucleon scattering data. However, measuring the neutron-neutron scattering length a_{nn} to the accuracy needed to address charge-symmetry issues is difficult. The standard technique for determining a_{nn} is to use a reaction that emits two neutrons with low relative momentum and to measure the cross-section for the final-state interaction (FSI) enhancement. We summarize the current status of the value for the $^1S_0$ a_{nn} below.

A suggested average value of a_{nn} from the ^{2}H(n,nn)p reaction is -16.8 ± 0.4 fm [Sch87], but values from different measurements range from about -16 fm to -23 fm. Other reactions, such as ^{3}H(d,2n)^{3}He and ^{3}H(t,2n)^{4}He, yield results ranging from -16 to -17 fm [Sch87]. Measurements of a_{nn} using $^2H(\pi^-,nn\gamma)$ have also been published. A value of -18.7 ± 0.6 fm [Gab84, Sch87] was obtained in a recent measurement. An earlier study had obtained a value of -16.7 ± 1.3 fm [Sal75].

We have made new measurements of neutron-γ coincidence spectra for stopped pions in a liquid deuterium target. The measurements were conducted in the LEP cave at LAMPF. Neutrons were detected by an array of 24 liquid scintillators, and one arm of the neutral meson spectrometer (NMS) was used to detect the associated γ-rays. The large solid angle, high efficiency, and high x-y position resolution of the NMS were critical ingredients in

[1]Lawrence Livermore National Laboratory, Livermore, CA.
[2]University of Northern British Columbia, Canada.
[3]University of Tübingen, Tübingen, Germany.
[4]University of Texas, Austin, TX.
[5]Los Alamos National Laboratory, Los Alamos, NM.
[6]Joint Institute of Nuclear Research, Dubna, Russia.
[7]Rudjer Boskovic Institute, Zagreb, Croatia.

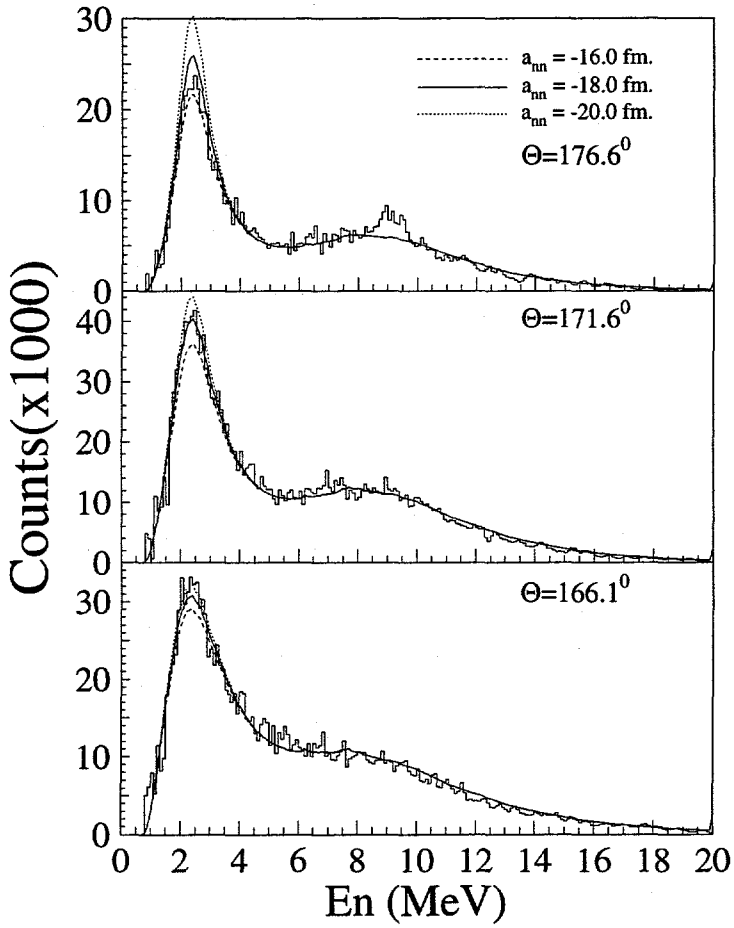

Figure 2.2–1: Neutron yields for the ^{2}H(π^-,nγ) reaction as a function of the neutron energy for three mean values of θ, the angle between the momentum vectors of the detected neutron and γ-ray. The curves are point-geometry calculations made by Gibson [Gib95].

the design of E1286. Each neutron detector was a 12 cm diameter cylindrical cell with a thickness of about 5 cm or 2 cm. Liquid scintillators were preferred over plastics because they enabled γ-ray rejection by pulse-shape techniques. The γ-ray suppression was about 1:20 with our neutron-energy threshold setting of about 1 MeV. The experimental setup was shown in last year's Progress Report [How95]. Data were accumulated over a period of two weeks, with liquid hydrogen and empty target runs included for detector resolution, energy calibrations, and background measurements.

Data analysis is underway. Values for a_{nn} will be extracted from two classes of events: those involving only one neutron and a γ (kinematically complete), and those involving two neutrons and a γ (kinematically over-determined). The first pass analysis is complete. All calibrations, pedestal corrections, and time offsets have been applied to the raw data, and data summary tapes with 16-parameter events have been made for use in the final analysis. A value of a_{nn} will be extracted from our π^-d capture data for several opening angles between the emitted γ-ray and one of the emitted neutrons by comparing calculations by Gibson [Gib95, Gib75] to the neutron energy spectrum of that neutron. The calculations will be smeared over the finite geometry and energy resolution (energy and position) of our experimental arrangement using Monte-Carlo methods. A chi-square analysis will be used to determine the optimum value of a_{nn} in the calculations to describe each experimental spectrum. Several milestones were achieved this year. Work on the π^-p simulation code was completed and used to determine crucial calibration and resolution information of our system. The time-of-flight resolution of the system and the position resolution of the NMS, both of which are critical for this type of analysis, have been determined using the π^-p capture data. The code to simulate the π^-d capture experiment is in the final stage of development and testing and should be ready by early Fall 1996. The neutron detection efficiency for two of each of the four detector types used in our experiment has been determined. The efficiency curves of detectors of the same design have identical shapes and nearly the same absolute magnitudes. All are well predicted by the neutron-detector simulation code of the PTB group.

In our preliminary analysis, a value of a_{nn} was extracted from the neutron energy spectra of our γ-n coincidence data using the point-geometry calculations of Gibson [Gib95]. The calculations were corrected for the average detection efficiency of our neutron detector array, the mean neutron attenuation in the liquid deuterium target, and the neutron attenuation in the iron containment vessel of the cryostat and in the approximately 2.5 m of air between the cryostat and the neutron detectors. The experimental data were summed over 0.1 radians in θ, the opening angle between the detected γ-ray and neutron. The neutron energy spectra for three mean values of θ are shown in Fig. 2.2–1 in comparison to point-geometry calculations for three values of a_{nn} made at the mean angle. In all calculations a value of 2.8 fm is used for the effective range parameter r_{nn}. The enhancement centered around 2.5 MeV is the n-n FSI peak, and the broad mound centered around 8.5 MeV is due to quasi-elastic π^- capture on a bound nucleon in deuterium. The narrow peak in the 176.6°

spectrum at 9 MeV is due to π^-p capture on a hydrogen contaminant in the deuterium target. Kinematic constraints disallow γ-n coincidence events for the two-body π^-p capture reaction at the smaller angles shown in Fig. 2.2–1. The average value extracted from these spectra is a_{nn}=18.2±1.4 fm. The uncertainty represents the deviation in the three values and is not the result of a full chi-square analysis as will be used in the final analysis, which should be completed during the first quarter of 1997.

[Gab84] B. Gabioud *et al.*, Nucl. Phys. **A420**, 496 (1984).

[Gib75] W. Gibbs, B. F. Gibson and G. J. Stephenson, Jr., Phys. Rev. **C11**, 90 (1975).

[Gib95] B. F. Gibson, 1995, private communications.

[Hen69] E. M. Henley, *Isospin in Nuclear Physics*, North Holland, Amsterdam, 1969, ed. D. H. Wilkinson.

[How95] C. R. Howell *et al.*, Nucl. Instr. and Meth., **B99**, 316 (1995).

[Sal75] R. W. Salter *et al.*, Nucl. Phys. **A245**, 241 (1975).

[Sch87] O. Schori *et al.*, Phys. Rev. **C35**, 2252 (1987).

2.2.2 The TUNL Neutron-Neutron Scattering Length (a_{nn}) Experiment and Analysis

D. E. González Trotter, Q. Chen, A. S. Crowell, C. R. Howell, F. Salinas, C. D. Roper, H. Tang, W. Tornow, R. L. Walter and H. Witała[1]

The TUNL a_{nn} experiment[2] is designed to extract the absolute cross-section for several neutron-neutron final-state interaction (n-n FSI) configurations (θ_{lab}=20.5°, 28°, 35.5°, and 43°) through a kinematically complete analysis of the ^{2}H(n,nnp) reaction. From these data it is possible to extract a_{nn} for each of these n-n FSI configurations. A systematic dependence of a_{nn} on θ_{lab} would indicate that a significant three-body force is present in the ^{2}H(n,nnp) reaction [Tor95]. Over 2500 net hours of data have been accumulated during eight runs over a period of a year and a half. We estimate that this is enough to achieve the 3% statistical precision we seek for the smallest (~4.5 mb/(sr^{2}MeV)) of the four cross-sections measured in the present work.

Experimental n-d elastic data from several detectors are analyzed independently for every run (four out of eight have been analyzed so far). The n-d elastic yields are related

[1] Jagellonian University, Cracow, Poland.

[2] For experimental setup and other aspects refer to TUNL Progress Reports XXXIII 93–94, p.29 and XXXIV 1994–95, p.33.

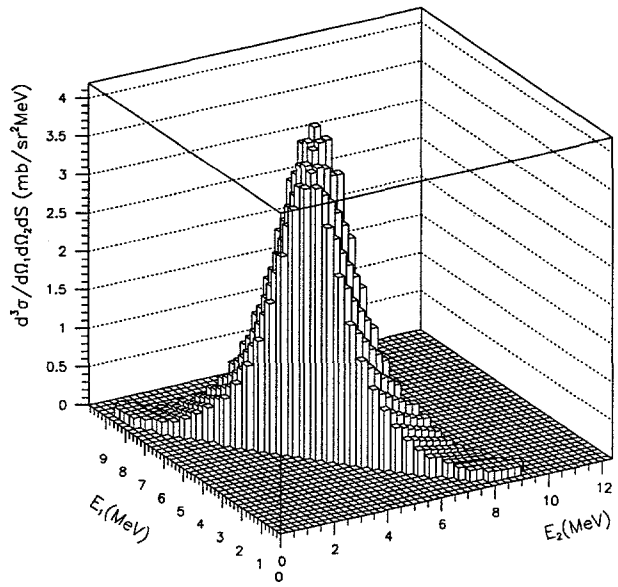

Figure 2.2–2: Monte-Carlo simulation of n-n FSI at θ_{lab}=20.5°. Shown is the product of the cross-section and the proton energy weight distribution as a function of the energy of the two outgoing neutrons.

to their corresponding cross-sections and used to normalize the experimental n-n FSI yields to obtain breakup cross-sections. The latter are compared to Monte-Carlo (MC) generated data treated in the same way as the experimental data. The MC codes take into account attenuation, detector efficiency, detector energy resolution, and finite-geometry effects due to detector size and shape (see Figure 2.2–2) for all experimental n-n FSI configurations. These MC codes make use of extensive cross-section libraries spanning the finite geometry space of our experimental n-n FSI configurations. Libraries were generated by a program written by the Bochum-Cracow group and executed on a Cray T90 supercomputer located at MCNC[3]. The library generating program calculates 3N amplitudes using a modified version of the Bonn-B nucleon-nucleon potential. Cross-sections based on values of a_{nn} ranging from −19 fm to −15 fm in steps of 1 fm have been calculated. New libraries based on other modern potentials will be calculated for a more comprehensive analysis of the experimental data.

[Tor95] W. Tornow, In *TUNL Progress Report*, volume XXXIV, p. 39, 1995.

[3]MCNC, North Carolina Supercomputing Center, Research Triangle Park, NC 27709.

2.3 Neutron-Deuteron Reactions

2.3.1 D-P Elastic Scattering at Low Energies

T. C. Black, C. R. Brune, H. J. Karwowski, E. J. Ludwig, S. Novotny and M. Wood

There is currently a great deal of experimental and theoretical interest in three-nucleon systems. There has been substantial progress in the computational techniques utilizing modern nucleon-nucleon (NN) and three-nucleon (3N) forces. However, significant discrepancies still exist between measured nucleon-deuteron scattering observables and rigorous calculations. The extracted scattering lengths for p-d scattering from Huttel *et al.* [Hut83] differ considerably from calculations [Kie95]. In addition, the same calculations underestimate the measured vector analyzing powers at $E_{\rm c.m.}$=2 MeV, just below the deuteron breakup threshold.

The analysis of p-d elastic scattering angular distributions at $E_{\rm p}$=314 and 250 keV is now complete. These measurements are particularly relevant for determinig the p-d scattering lengths. The angular distribution measured at $E_{\rm p}$=314 keV is shown in Fig. 2.3–1, along with the calculation of Kievsky, Viviani, and Rosati, using the AV18 NN potential and the UR 3N interaction and the techniques described in Kievsky, *et al.* [Kie95]. The data appear to be well described by these calculations which include the Coulomb interaction exactly. A paper describing this work is in preparation.

An energy-dependent phase-shift analysis would be very useful for determining the origin of the analyzing power discrepancies. It would also allow for the determination of the energy dependence of the $^2S_{1/2}$ phase shift, which is predicted to have an anomalous behavior due to the presence of a pole in the effective-range function. A considerable amount of high-quality p-d analyzing power data exists at $E_{\rm c.m.}$=2 MeV, but there is very little data at lower energies. We have begun a series of analyzing power measurements at $E_{\rm c.m.}$=0.43 and 0.21 MeV. These data will provide the basis for an energy-dependent phase shift analysis. The required proton or deuteron beams can be supplied by the LEBF or FN tandem accelerators. To date, we have measured $T_{20}(\theta)$ and $iT_{11}(\theta)$ with a 1.3-MeV deuteron beam (yielding $E_{\rm c.m.}$=0.43 MeV) provided by the FN tandem. In Fig. 2.3–2 the $T_{20}(\theta)$ results from a preliminary analysis of the data are shown with the calculations of Kievsky, Viviani, and Rosati, using the AV18 NN potential and the UR 3N interaction and the techniques described in Kievsky, *et al.* [Kie95].

[Hut83] E. Huttel *et al.*, Nucl. Phys. **A406**, 443 (1983).

[Kie95] A. Kievsky, M. Viviani, and S. Rosati, Phys. Rev. **C52**, R15 (1995).

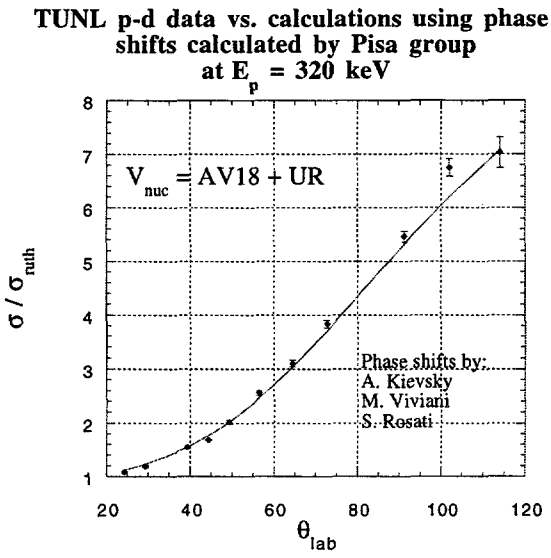

Figure 2.3–1: The angular distribution for p-d scattering measured at $E_{\rm p}$=314 keV, compared to the calculations of Kievsky, Viviani, and Rosati.

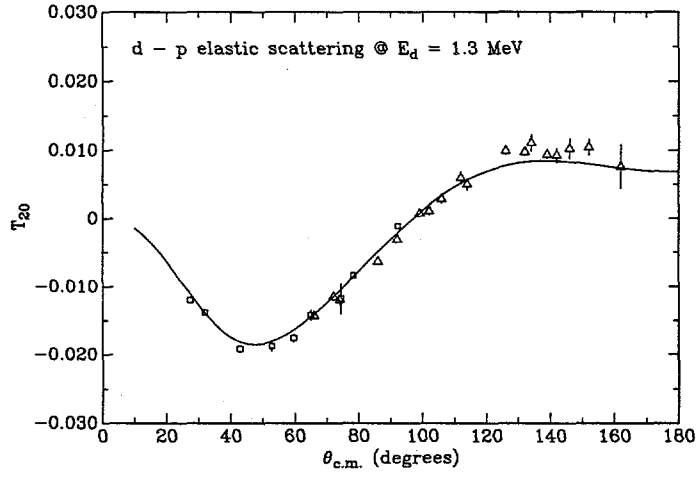

Figure 2.3–2: A preliminary analysis of the $T_{20}(\theta)$ angular distribution measured at $E_{\rm c.m.}$=0.43 MeV. The data points from detected deuterons and protons are given by squares and triangles, respectively. The solid curve is the theoretical prediction of Kievsky, Viviani, and Rosati, carried out at the energy of the experimental data.

2.3.2 Toward a Solution of the Neutron-Deuteron $A_y(\theta)$ Puzzle

W. Tornow, A. Kievsky[1] and H. Witała[2]

Since its discovery some ten years ago, the neutron-deuteron (n-d) analyzing power $A_y(\theta)$ puzzle [Wit94] remains the most elusive problem in low-energy three-nucleon (3N) elastic scattering. Although various groups have performed intensive studies with state-of-the-art nucleon-nucleon (NN) potential models, including various types of three-nucleon forces (3NF), it turned out to be impossible to account for the 25–30% discrepancy between rigorous 3N calculations and experimental data (see Figure 2.3–3 a and b). Sensitivity studies have clearly demonstrated that $A_y(\theta)$ in n-d elastic scattering is governed by a complicated interplay between the $^3P_0$, $^3P_1$, and $^3P_2$ NN interactions.

After more than thirty years of intensive work by various mathematicians and theoretical physicists, the 3N scattering problem is now tractable with the Coulomb interaction taken into account in a rigorous way [Kie94]. Unfortunately, the solution of the charged 3N scattering problem is restricted to energies below the deuteron breakup threshold (i.e., E_p=3.3 MeV in the case of p-d scattering or E_d=6.6 MeV in the case of d-p scattering). Nevertheless, this new development not only has the potential of solving the $A_y(\theta)$ puzzle, but it has also provided some important additional information. First, it confirmed speculations that an $A_y(\theta)$ puzzle also exists for p-d elastic scattering [Kie95] (see Figure 2.3–3 c). Second, it showed that a similiar problem exists with respect to $iT_{11}(\theta)$ in d-p scattering [Kie96] (see Figure 2.3–3 d).

For p-d and d-p scattering a complete set of observables, $\sigma(\theta)$, $A_y(\theta)$, $iT_{11}(\theta)$, $T_{20}(\theta)$, $T_{21}(\theta)$, and $T_{22}(\theta)$, exists at E_p=3.0 MeV, E_d=6.0 MeV ($E_{c.m.}$=2.0 MeV) [Shi95]. Starting from the Pisa phase-shift calculations [Kie95] at $E_{c.m.}$=2.0 MeV based on the Argonne AV18 [Wir95] NN potential+Urbana 3NF [Pud95], a phase-shift search was performed. It turned out that an appropriate search on the p-d $^4P_{1/2}$, $^4P_{3/2}$, and $^4P_{5/2}$ phase shifts, the mixing parameter $\epsilon_{3/2-}$, and leaving all other phase shifts as calculated from AV18+3NF, gives a reasonable fit to the p-d data (see Figure 2.3–3 c and d). From the relation established by the Bochum-Cracow group [Hüb95] for n-d scattering between $^4P_{1/2}$ and $^3P_0$, $^4P_{3/2}$ and $^3P_1$, and $^4P_{5/2}$ and $^3P_2$, new experimental $^3P_0$, $^3P_1$, and $^3P_2$ n-p and p-p phase shifts were obtained. The ^3P_J NN phase shifts are still preliminary and somewhat uncertain due to various assumptions used in their determination. Nevertheless, we replaced the original ^3P_J phase shifts in the Nijmegen phase-shift analysis by our new experimental ^3P_J phase shifts and calculated $A_y(\theta)$ for n-p and p-p scattering at E_N=3.0 MeV. We obtained good agreement with the original Nijmegen result for n-p and fair agreement for p-p. We also calculated all other NN observables and found in all cases good agreement with the predictions of the Nijmegen phase-shift analysis.

[1]INFN, Pisa, Italy.
[2]Jagellonian University, Cracow, Poland.

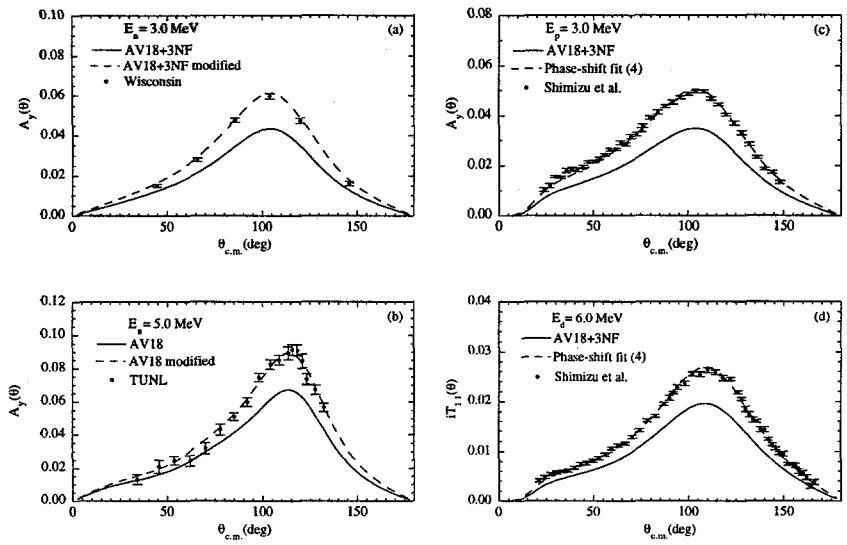

Figure 2.3–3: Comparison of n-d $A_y(\theta)$, p-d $A_y(\theta)$, and $iT_{11}(\theta)$ data to rigorous calculations and phase-shift predictions. In panel (a) the $A_y(\theta)$ data [McA93] at E_n=3.0 MeV are compared to the calculation (solid curve) of the Pisa group [Kie95] using the AV18+3NF potential. In panel (b) the $A_y(\theta)$ data [Tor91] at E_n=5.0 MeV are compared to the calculation (solid curve) of the Bochum group using the AV18 potential [Wir95]. In panel (c) and (d) the p-d $A_y(\theta)$ and $iT_{11}(\theta)$ data of [Shi95] are compared to calculation by the Pisa group (solid curve). In panels (a) to (d) the dashed curves were obtained using our modified $^4P_{1/2}$, $^4P_{3/2}$, $^4P_{5/2}$, and $\epsilon_{3/2-}$ phase-shift parameters.

To further test our findings, we investigated n-d scattering at E_n=3.0 MeV. We multiplied the AV18 n-d ^4P_J phase shifts by the ratios $R_J = (^4P_J)^{AV18+3NF}_{p-d} / (^4P_J)^{experimental}_{p-d}$ and calculated the n-d $A_y(\theta)$. As can be seen from Figure 2.3–3 a, a very good description of the experimental data of the Wisconsin group [McA93] was obtained. This observation shows that our approach does not require any large charge symmetry breaking (CSB). In fact, it confirms the CSB used in the AV18 potential for the ^3P_J interactions. As can be seen from Figure 2.3–3 b, our approach also works very well at E_n=5.0 MeV, where the modified ^4P_J phase shifts give an excellent description of the TUNL n-d data [Tor91]. However, starting at E_n=6.5 MeV small deviations begin to emerge at the maximum of $A_y(\theta)$ which are clearly established at E_n=8.5 MeV. We conclude from this study that our ^3P_J modification

factors must be slightly energy dependent.

Since rigorous p-d 3N calculations are not yet available above the deuteron breakup threshold, our approach cannot be extended to higher energies. Of course, rigorous n-d calculations giving n-d phase shifts [Hüb95] are available above the n-d breakup threshold and could be used as starting values in n-d phase-shift analyses. However, our p-d phase-shift analyses clearly showed that $\sigma(\theta)$ and $A_y(\theta)$ data alone do not permit an accurate determination of the ^4P_J phase shifts. Data for the vector analyzing power $iT_{11}(\theta)$ or for one of the two tensor analyzing powers $T_{20}(\theta)$ or $T_{21}(\theta)$ in d-n scattering are required. Unfortunately, no such data exist.

[Hüb95] D. Hüber *et al.*, Few-Body Syst. **19**, 175 (1995).

[Kie94] A. Kievsky, M. Viviani, and S. Rosati, Nucl. Phys. **A577**, 511 (1994).

[Kie95] A. Kievsky, M. Viviani, and S. Rosati, Phys. Rev. **C52**, R15 (1995).

[Kie96] A. Kievsky *et al.*, 1996, Nucl. Phys. A. in press.

[McA93] J. E. McAninch *et al.*, Phys. Lett. **B307**, 13 (1993).

[Pud95] B. S. Pudliner *et al.*, Phys. Rev. Lett. **74**, 4396 (1995).

[Shi95] S. Shimizu *et al.*, Phys. Rev. **C52**, 1193 (1995).

[Tor91] W. Tornow *et al.*, Phys. Lett. **B257**, 273 (1991).

[Wir95] R. B. Wiringa, V. G. J. Stoks, and R. Schiavilla, Phys. Rev. **C51**, 38 (1995).

[Wit94] H. Witała, D. Hüber, and W. Glöckle, Phys. Rev. **C49**, R14 (1994), and references therein.

2.3.3 No Evidence for Large Charge-Symmetry Breaking Effects in the ^3P_J Nucleon-Nucleon Interactions

A. Kievsky and W. Tornow

Experimental progress over the last 15 years has made it possible to definitely establish small differences between proton-deuteron (p-d) and neutron-deuteron (n-d) analyzing power $A_y(\theta)$ data in the incident nucleon (N) energy range from 3 to 14 MeV. These differences occur both at forward angles and in the region of the maximum in the $A_y(\theta)$ angular distribution, around $\theta_{c.m.}$=90–120°. Except for electromagnetic effects (i.e., Rutherford scattering, Mott-Schwinger interaction, etc.), which are known to be important at forward

scattering angles, p-d scattering is governed by p-p and n-p nuclear forces while n-d scattering is governed by n-n and n-p nuclear forces. Therefore, the comparison of p-d and n-d data in the angular region of the maximum of $A_y(\theta)$ (in the following referred to as "A_y^{max}") can provide estimates of posssible charge-symmetry breaking (CSB) effects in the underlying NN interaction. Since $A_y(\theta)$ in N-d scattering has been shown to be extremely sensitive to the ^3P_J NN interactions, it is not surprising that attempts have been made to extract information about CSB in these interactions [Wit91, Tak91]. However, these theoretical studies were hampered by two shortcomings. First, rigorous 3N calculations of the n-d $A_y(\theta)$ using realistic NN potential models fail to describe the magnitude of $A_y(\theta)$ by more than 25%. Second, rigorous 3N p-d calculations that include the Coulomb interaction exactly were not available.

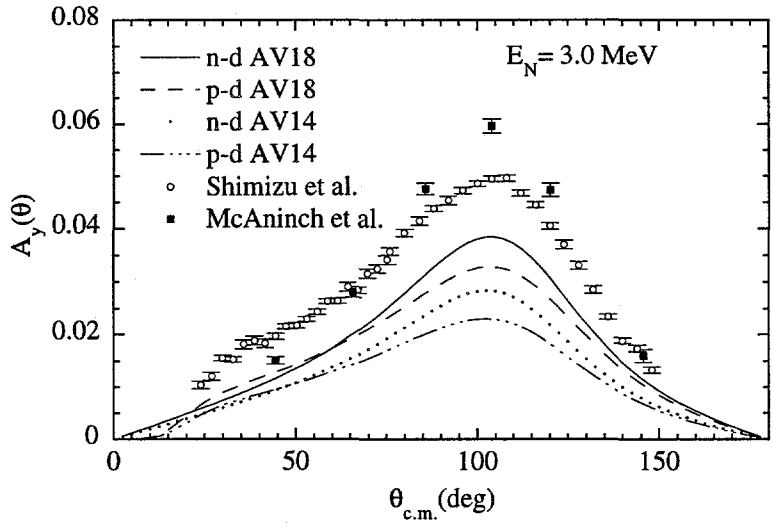

Figure 2.3–4: Comparison of n-d [McA94] and p-d [Shi95] analyzing power $A_y(\theta)$ data and rigorous calculations at E_N=3.0 MeV.

In the meantime, using the Pair Correlated Hyperspherical Harmonic method [Kie94] and the Argonne AV14 [Wir84] and AV18 [Wir95] NN potentials, the Pisa group can treat the Coulomb interaction in p-d scattering in a rigorous way. This approach is currently limited to energies below the deuteron breakup threshold (i.e., to incident nucleon energies E_N <3.33 MeV). Fortunately, accurate p-d and n-d $A_y(\theta)$ data are available at E_N=3 MeV [Shi95, McA94]. Similiar to the situation for n-d scattering below and above the deuteron breakup threshold, the p-d calculations underestimate the p-d $A_y(\theta)$ data considerably. Figure 2.3–4 shows calculated $A_y(\theta)$ angular distributions at E_N=3 MeV for n-d (solid and dotted curves) and p-d (dashed and dashed-dotted curves) scattering in comparison to n-d

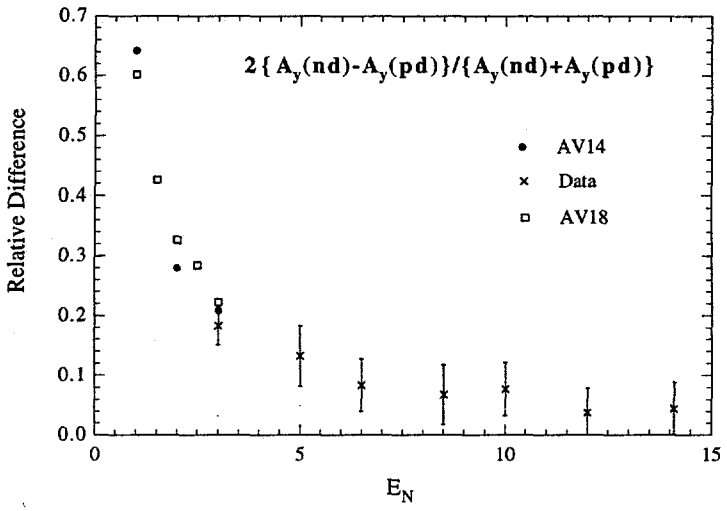

Figure 2.3–5: Calculated (solid dots and open squares) and measured (crosses with error bars) energy dependence of the relative difference between the n-d and p-d analyzing power $A_y(\theta)$ obtained at the maximum in the $A_y(\theta)$ angular distribution. The experimental results at E_N=5.0 MeV and above were taken from Ref. [Tor92].

(solid squares [McA94]) and p-d (open dots [Shi95]) data. The differences between the solid and dashed curves (AV18) and between the dotted and dashed-dotted curves (AV14) clearly document the A_y^{max} difference referred to above. The AV14 potential does not contain any charge dependence in the ^3P_J interactions. Therefore, the difference between the dotted and dashed-dotted curves is caused solely by the Coulomb interaction. The "old" AV14 potential does not provide an optimal description of the NN $A_y(\theta)$ data. Therefore, it is not too surprising that the predictions calculated with AV14 deviate even further from the experimental N-d data than the calculations using the new AV18 potential. The latter includes charge dependence in the ^3P_J phase shifts, i.e., ^3P_J(n-p)$\neq$$^3P_J$(p-p)$\neq$$^3P_J$(n-n). The relative difference between the n-d and p-d $A_y(\theta)$ at the maximum of $A_y(\theta)$ is given in Figure 2.3–5 as a function of E_N. The crosses with error bars represent the experimentally observed relative differences. As expected from simple Coulomb-force arguments [Tor92], the relative difference increases dramatically with decreasing E_N. At E_N=3 MeV, the only energy where a comparison can be made, the calculated and the experimentally observed relative differences agree rather well. In addition, at this energy the AV14 and AV18 potential models give almost identical results.

We conclude that the Coulomb interaction, and not CSB, is responsible for the vast majority of the sizeable A_y^{max} difference observed at low incident nucleon energies. This observation confirms the conclusion of Ref. [Tor92] and makes the strategy ["scenario (ii)"] devoloped recently in Soldi *et al.* [Sol96] for establishing CSB effects in the ^3P_J NN interactions unnecessary.

[Kie94] A. Kievsky, M. Viviani, and S. Rosati, Nucl. Phys. **A577**, 511 (1994).

[McA94] J. E. McAninch, L. O. Lamm, and W. Haeberli, Phys. Rev. **C50**, 589 (1994).

[Shi95] S. Shimizu *et al.*, Phys. Rev. **C52**, 1193 (1995).

[Sol96] A. Soldi *et al.*, J. Phys. G: Nucl. Part. Phys., **22**, LG5 (1996).

[Tak91] T. Takemiya, Prog. Theor. Phys. **86**, 975 (1991).

[Tor92] W. Tornow *et al.*, Phys. Rev. **C45**, 459 (1992).

[Wir84] R. B. Wiringa *et al.*, Phys. Rev. **C29**, 1207 (1984).

[Wir95] R. B. Wiringa, V. G. J. Stoks, and R. Schiavilla, Phys. Rev. **C51**, 38 (1995).

[Wit91] H. Witała and W. Glöckle, Nucl. Phys. **A528**, 48 (1991).

2.3.4 Neutron-Induced Deuteron Breakup Cross-Section Measurements at 13.0 MeV

H. R. Setze, C. R. Howell, W. Tornow, H. Witala [1], *R. T. Braun, D. E. González Trotter, A. Hussein* [2], *J. M. Lambert* [3], *G. Mertens* [4], *C. D. Roper, F. Salinas, I. Slaus* [5], *R. L. Walter and B. Vlahovic* [5]

The analysis of the 13 MeV neutron-deuteron (n-d) breakup cross-section data is proceeding on schedule. The cross-section data for the star and collinear configurations which motivated the experiment are finalized, and a manuscript reporting our results for the space-star, the coplanar-star, and one of the collinear configurations has been submitted for publication. Our data for these configurations are shown in Figure 2.3–6 (left side) in comparison to n-d calculations and n-d [Str89] and p-d [Rau91] data. The analyses of four more configurations, two of which were neutron-proton (n-p) final-state interactions

[1]Jagellonian University, Cracow, Poland.
[2]University of Northern British Columbia, Canada.
[3]Georgetown University, Washington, DC 20057.
[4]University of Tübingen, Tübingen, Germany.
[5]Rudjer Boskovic Institute, Zagreb, Croatia.

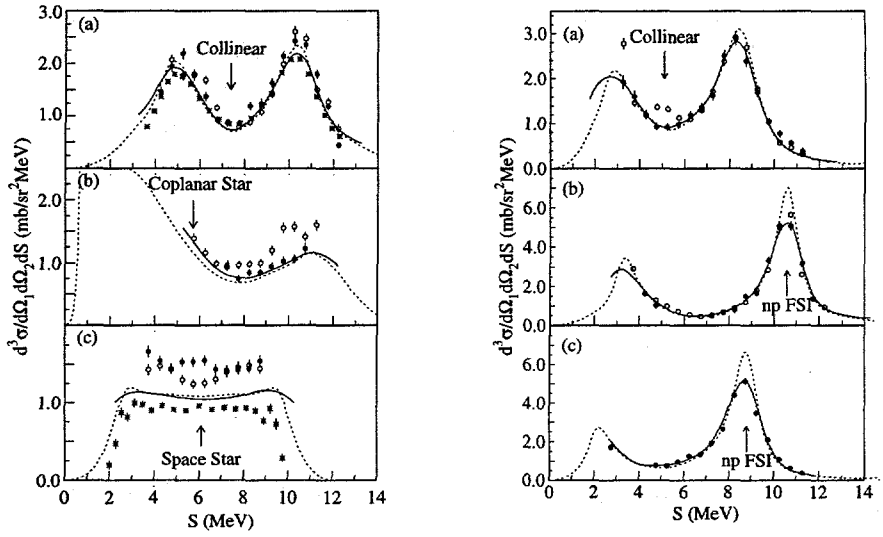

Figure 2.3–6: Cross-section as a function of arc-length along the point-geometry S-curve for collinear, star, and n-p FSI configurations. The solid circles are the present data, the open circles are previous n-d data [Str89], and the crosses are p-d data [Rau91]. The dashed curves are point-geometry calculations with the Bonn-B NN potential, and the solid curves result when the Bonn-B potential predictions are smeared over the finite geometry and resolution of the TUNL experiment. Left: (a) Collinear configuration: θ_{n1}=50.5°, θ_{n2}=62.5°, ϕ_{12}=180.0°. (b) Coplanar-star configuration: θ_{n1}=17.0°, θ_{n2}=50.5°, ϕ_{12}=180.0°. (c) Space-star configuration: θ_{n1}=50.5°, θ_{n2}=50.5°, ϕ_{12}=120.0°. Right: (a) Collinear configuration: θ_{n1}=39.0°, θ_{n2}=75.5°, ϕ_{12}=180.0°. (b) n-p FSI configuration: θ_{n1}=39.0°, θ_{n2}=62.5°, ϕ_{12}=180.0°. (c) n-p FSI configuration: θ_{n1}=32.0°, θ_{n2}=75.5°, ϕ_{12}=180.0°.

(FSI), are completed. Six of the seven configurations analyzed were at the same angles as measured by Strate *et al.* [Str89]. Our data for four configurations are in good agreement with those of Strate *et al.* [Str89]. The two discrepant configurations were the coplanar-star and the configuration with θ_{n1}=17.0°, θ_{n2}=50.5°, and ϕ_{12}=120° (not shown). In both cases the cross-sections of Strate *et al.* were higher than our data by about three standard deviations beyond the reported systematic uncertainties in the experiments. The differences between the two data sets were found to be attributable mainly to uncertainties in the data of Strate *et al.* due to approximations made in their background subtraction, whereas in our measurements the backgrounds were empirically determined. The data for five of the seven configurations analyzed were described well by the n-d calculations. The agreement between data and theory was particularly good for the n-p FSI configurations as shown in Fig. 2.3–6 on the right side. Curiously, the n-d data for both configurations with ϕ_{12}=120° were about 20% higher than the predicted cross-sections.

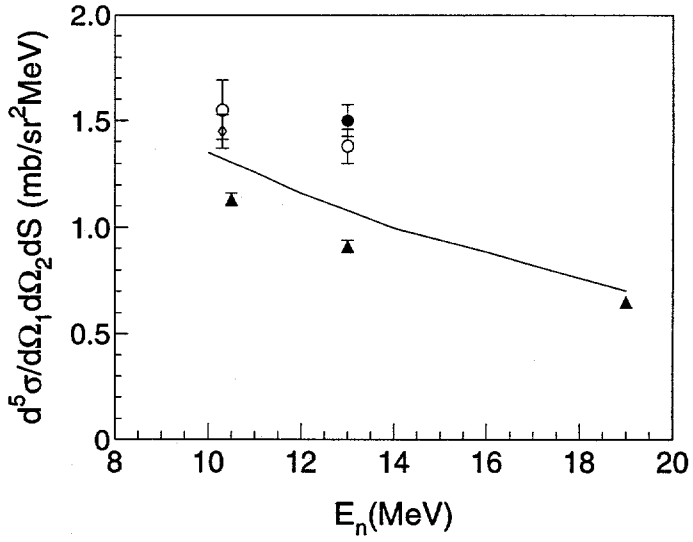

Figure 2.3–7: Average cross-section in the region of the space-star point. The solid circle represents the new TUNL n-d datum, the open circles are the Erlangen n-d data [Str89, Geb93], the open diamond is the Bochum n-d datum [Ste89], and the solid triangles are the Cologne p-d data [Gro94, Rau91, Pat96]. The curve is a point-geometry calculation with the Bonn-B NN potential at the kinematics for the space-star point.

The space-star anomaly, first reported by Strate *et al.* [Str89], is confirmed by the new data and clearly illustrated in Figure 2.3–7 where statistical uncertainties in the n-d measurements have been greatly reduced by averaging. The cause of the space-star anomaly is unclear. Unlike the n-d $A_y(\theta)$ problem which is related to the NN p-wave forces [How87],

the space-star discrepancy seems to be associated with the s-wave forces as is the triton binding energy defect. However, unlike the triton binding energy, the space-star anomaly cannot be fixed by the inclusion of a traditional three-nucleon force (3NF). The addition of the Tucson-Melbourne [Coo93] 3NF changes the predicted cross-section by less than 3% and in the opposite direction required to describe the data. In addition, off-shell effects do not seem to be the answer. The theoretical predictions of the star cross-section are very stable with respect to the choice of NN potential, less than 2% dispersion between modern potentials which have somewhat different off-shell characteristics. A more detailed theoretical study of off-shell effects in the space-star configuration is underway [Ple96]. It is puzzling that theory correctly predicts the cross-section for the coplanar-star but fails in the case when the star plane is rotated by 90° to form the space-star. It would be interesting to compare theory to data for the star configuration as a function of the plane orientation between the two extremes of the coplanar- and space-stars.

[Coo93] S. A. Coon and M. T. Pena, Phys. Rev. **C48**, 2559 (1993).

[Geb93] K. Gebhardt *et al.*, Nucl. Phys. **A561**, 232 (1993).

[Gro94] R. Großmann *et al.*, In F. Gross, editor, *14th International IUPAP Conference on Few-Body Problems in Physics*, p. 66, Williamsburg, VA, 1994.

[How87] C. R. Howell *et al.*, Few-Body Syst. **2**, 19 (1987).

[Pat96] H. Patberg *et al.*, Phys. Rev. **C53**, 1497 (1996).

[Ple96] W. Plessas and H. Witała, 1996, private communications.

[Rau91] G. Rauprich *et al.*, Nucl. Phys. **A535**, 313 (1991).

[Ste89] M. Stephan *et al.*, Phys. Rev. **C39**, 2133 (1989).

[Str89] J. Strate *et al.*, Nucl. Phys. **A501**, 51 (1989).

2.4 Sub-Nucleonic Degrees of Freedom

2.4.1 Measurement of Electric and Magnetic Form Factors of the Neutron and Hall-A Collaboration Experiments

A. S. Crowell, C. R. Howell, W. Tornow, R. L. Walter and the G_E^n-G_M^n Collaboration

Our group is collaborating on measurements of the electric and magnetic form factors of the neutron, G_E^n and G_M^n, respectively, at four Q^2 points: 0.30, 0.50, 1.00 and 1.73 $(GeV/c)^2$. The measurements at Q^2=0.30 and 0.50 $(GeV/c)^2$ will run at the MIT-Bates Linear Accelerator Centers in the South Hall during the first or second quarter of 1997, depending on when polarized beam will be available. Beam time for the 1.00 and 1.73 $(GeV/c)^2$ points has been approved to run in Hall C at CEBAF (E93-038). We anticipate that beam time at CEBAF for the G_E^n and G_M^n measurements will start during the Summer 1997. The G_E^n measurement will use the polarization transfer technique D($\vec{e}$,e$\vec{n}$)p suggested by Arnold, Carlson and Gross [Arn81]. Polarized electrons will be used to electrodisintegrate deuterons in an unpolarized liquid deuterium target. The scattered electrons and outgoing neutrons will be detected in coincidence at angles in the kinematic region of electron-nucleon quasi-free scattering. The longitudinal-sideways and longitudinal-normal polarization transfer coefficients $D_{LS'}$ and $D_{LN'}$ will be measured using the Kent State large neutron polarimeter [Mad89]. Calculations by Arenhövel [Are87] show that $D_{LS'}$ in the quasi-free region in e-d scattering is sensitive to the electric form factor of the struck nucleon and insensitive to details of the deuteron wave function. By measuring both $D_{LS'}$ and $D_{LN'}$ in the same experiment, the dependence of the ratio of g$\equiv G_E^n/G_M^n$ on the helicity of the incident electrons and the analyzing power of the polarimeter analyzer can be eliminated. Since g is directly proportional to the ratio of $D_{LN'}$ to $D_{LS'}$, the helicity dependence in g cancels in the ratio. To measure $D_{LN'}$ a magnet will be placed in front of the polarimeter to precess the neutron spin through 90°. The spin orientation magnet for both measurements will be the H-shaped dipole Charybdis, currently being refurbished at Bates. The TUNL group is responsible for mapping the fields of this magnet.

The G_M^n determination requires an absolute measurement of the electron-neutron coincidence cross-section. For these measurements an accurate calibration of the neutron detector efficiency is needed at the energies of the recoil neutron (T_n=161, 266, 533 and 922 MeV) for the four Q^2 points listed above. Our plan is to use the γ+p$\rightarrow \pi^+$+n reaction initiated with virtual photons from the electron beam for the efficiency calibration. The π^+ associated with the emitted neutron will be detected in a magnetic spectrometer. The G_M^n measurements at Bates and CEBAF will use a new neutron detector array designed by the Hampton University group. Ten detectors will be arranged to form a 1m x 1m x 10cm detector array which is mean timed. This new design will improve the neutron detection efficiency by about a factor of two over the previous design which used the analyzer plane

of the neutron polarimeter. The G_M^n measurement at Q^2=1.00 $(GeV/c)^2$ will be the thesis project of TUNL student Alex Crowell.

The collaboration calibrated the polarimeter at IUCF for neutron energies of 124 and 160 MeV in Summer 1994. In May 1996 we conducted a 7 day run at Saturne to calibrate the polarimeter at 7 neutron energies between 161 and 1057 MeV, covering the Q^2 range of the proposed G_E^n measurements.

As part of our preparation for the measurements at Bates and CEBAF, we have begun to look at the impact of edge effect losses in the neutron detection system. By far, the largest source of systematic uncertainty in the determination of G_M^n comes from uncertainty in the neutron detection efficiency. Preliminary results from Monte-Carlo simulations indicate that approximately 1–2% of the incident neutrons will scatter out of the sides of the detectors before depositing sufficient energy to produce pulse heights above threshold. Further studies will look at methods for minimizing these edge losses and on how they differ between the G_M^n measurements and the efficiency calibration using the γ+p$\rightarrow \pi^+$+n reaction.

In May 1996 the first beam was delivered to target in Hall A at CEBAF. Electron scattering from a carbon target at an incident electron energy of 0.845 GeV was used to make the initial resolution evaluation of one of the two 4 GeV/c spectrometers and the associated detectors in Hall A. The beam had a remarkably low emmittance and was impressively stable (position and intensity). All worked well from the beginning. The hardware resolution of the system was $\delta p/p$=10^{-3}, and after minor second-order corrections for aberrations in the field the resolution was improved to 4×10^{-4}. Corrections for finite target thickness, straggling in vacuum chamber windows, and third-order field corrections should easily bring the resolution to the 10^{-4} design specifications. As part of the Hall A collaboration we will participate in the commissioning of the two spectrometers and associated detector packages through Fall 1996 and Spring 1997. Starting in 1997 we will participate in several collaboration experiments over the next three to four years.

[Are87] H. Arenhövel, Phys. Lett. **B199**, 13 (1987).

[Arn81] R. G. Arnold, C. E. Carlson, and F. Gross, Phys. Rev. **C23**, 363 (1981).

[Mad89] R. Madey *et al.*, IEEE Trans. Nucl. Sci. **36**, 231 (1989).

3 Dynamics of Very Light Nuclei

3.1 Four and Five Nucleon Reactions

3.1.1 Measurements of the Total Cross-Section for the Scattering of Polarized Neutrons from Polarized ^{3}He

C. D. Keith[1], *C. R. Gould, D. G. Haase, P. R. Huffman*[2], *N. R. Roberson, M. L. Seely, W. Tornow and W. S. Wilburn*

Recent computational advances in the field of few-nucleon dynamics have fueled renewed interest in the three-nucleon and four-nucleon systems [Glö95]. Exact bound-state calculations utilizing realistic, meson-exchange forces are now possible for both the 3N and 4N systems. Similar calculations are currently available for the 3N continuum, and extension to the 4N continuum is under active investigation.

We recently completed the first measurements of longitudinal and transverse neutron total cross-section differences $\Delta\sigma_L$ and $\Delta\sigma_T$ in n-^{3}He scattering [Kei96]. These two spin observables are directly related to the forward elastic-scattering amplitude through the optical theorem [Kei94]. As such, they allow for a simple interpretation in terms of the properties of the scattering states. The measurements were performed at energies corresponding to excitations 22–27 MeV above the ^{4}He ground state, where a number of broad, negative-parity levels are believed to exist.

The measurements were performed with a solid polarized ^{3}He target, described in greater detail in Ref. [Kei95]. A ^{3}He-^{4}He dilution refrigerator was used to cool the ^{3}He sample in an externally applied magnetic field of 7 T. The magnet was physically rotated to provide fields either parallel (longitudinal) or perpendicular (transverse) to the incident beam direction. The lowest target temperature obtained during these measurements was 11.9±0.2 mK, corresponding to 38.7±0.6% polarization.

Polarized neutrons were produced as secondary beams from either the ^{3}H($\vec{p}$,$\vec{n}$)^{3}He or ^{2}H($\vec{d}$,$\vec{n}$)^{3}He polarization-transfer reaction at 0°. Transmission asymmetries were measured for the transverse spin geometry at neutron energies of 1.94, 3.65, 4.95, and 7.46 MeV. Transmission asymmetries for the longitudinal geometry were measured at neutron energies 3.65, 4.95, and 7.46 MeV. A measurement at 1.94 MeV was not attempted because the longitudinal polarization-transfer coefficient for the ^{3}H($\vec{p}$,$\vec{n}$)^{3}He reaction was expected to be too small to produce a useful asymmetry result.

[1]Present address: Indiana University Cyclotron Facility, Bloomington, IN.
[2]Present address: Physics Department, Harvard University, Cambridge, MA.

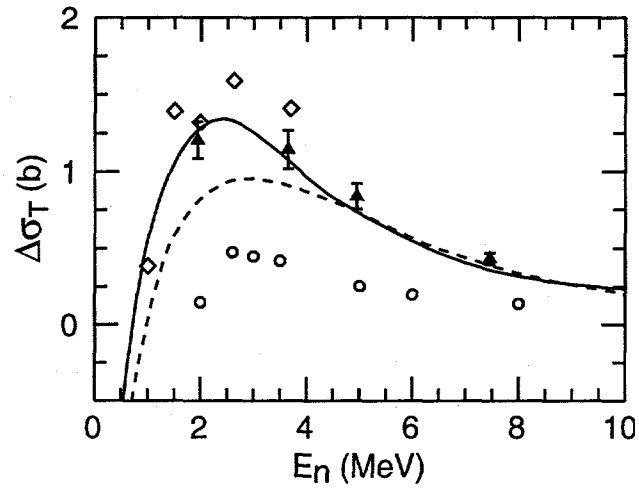

Figure 3.1–1: Measured values of $\Delta\sigma_T$ (triangles). Also shown are phase-shift predictions of $\Delta\sigma_T$: R matrix (solid line), MCRGM (dashed line), Jany PWA (diamonds), and Lisowski PWA (circles).

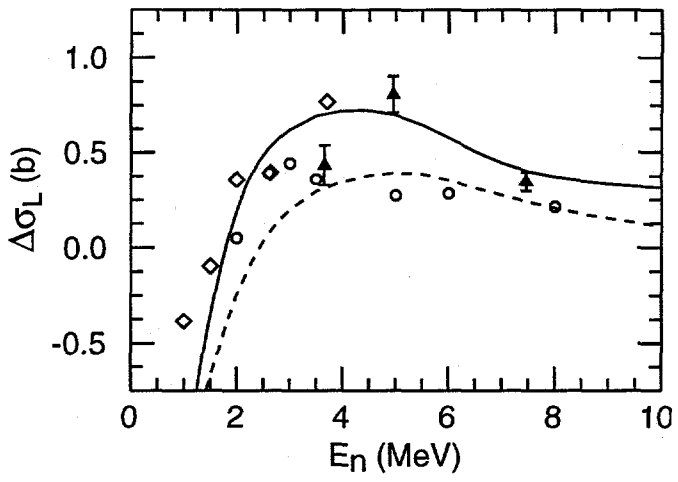

Figure 3.1–2: Measured values of $\Delta\sigma_L$. Symbols same as Fig. 3.1–1.

The $\Delta\sigma_T$ and $\Delta\sigma_L$ results are plotted in Figures 3.1–1 and 3.1–2, respectively. The error bars were obtained by adding the systematic and statistical uncertainties in quadrature. Also shown are phase-shift predictions from four previous analyses of scattering data. The R-matrix phase shifts reproduce $\Delta\sigma_T$ at all four energies and come closest to reproducing the $\Delta\sigma_L$ except at 3.65 MeV. This may possibly be due to the $^3P_1$ partial wave which, in the R-matrix analysis, is much larger at 3.65 MeV than in the other three phase-shift analyses.

[Glö95] W. Glöckle *et al.*, *Proceedings of the XIV International Conference on Few Body Problems in Physics, Williamsburg, VA.*, p. 45, American Institute of Physics, New York, 1995.

[Kei94] C. D. Keith *et al.*, Phys. Rev. **C50**, 237 (1994).

[Kei95] C. D. Keith *et al.*, Nucl. Instr. and Meth. **A357**, 34 (1995).

[Kei96] C. D. Keith *et al.*, to be published, 1996.

3.1.2 Measurement of Longitudinal Polarization-Transfer in the T($\vec{p},\vec{n}$) Reaction

C. R. Gould, D. G. Haase, C. D. Keith [1], *B. W. Raichle, M. L. Seely, W. Tornow, J. R. Walston and W. S. Wilburn*

In our investigations of the cross-section differences $\Delta\sigma_T$ and $\Delta\sigma_L$, and the ϵ_1 mixing parameter for $\vec{n}$-$\vec{p}$ scattering, we use the T($\vec{p},\vec{n}$) reaction to produce beams of polarized neutrons. The polarization-transfer coefficient, $K_y^{y'}(0°)$, for the T($\vec{p},\vec{n}$) reaction, involving a transversely polarized incident proton beam and a transversely polarized resultant neutron beam, has been previously measured at TUNL [Wil]. However, data for the corresponding longitudinal polarization-transfer coefficient, $K_z^{z'}(0°)$, do not extend below 4 MeV proton energy [Jar74].

As seen in Figure 3.1–3, calculations based on recent R-matrix analyses show resonance structure in $K_z^{z'}(0°)$. The structure is related to the 0^- resonance in ^{4}He. The calculations indicate that the T($\vec{p},\vec{n}$) reaction, with a Q=−0.764 MeV, is potentially an intense source of longitudinally polarized neutrons below 1 MeV.

To verify these predictions, we have recently measured the longitudinal polarization-transfer coefficient in the T($\vec{p},\vec{n}$) reaction from 1.3 to 2.7 MeV proton energy. A beam of polarized protons from the TUNL atomic beam polarized ion source was used to bombard a tritiated titanium target. The polarization of the protons was monitored both with the

[1] Present address: Indiana University Cyclotron Facility, Bloomington, IN.

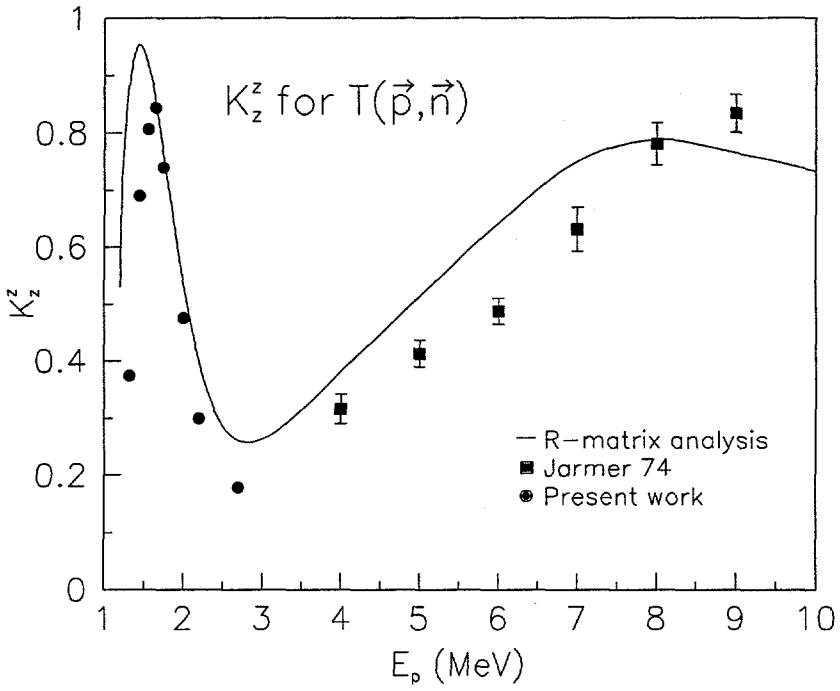

Figure 3.1–3: Theoretical predictions and experimental data for $K_z^{z'}(0°)$ in the $T(\vec{p},\vec{n})$ reaction.

Lamb-shift spin-filter polarimeter as well as with a high-energy elastic scattering polarimeter located on the target beam leg. A proton polarization greater than 80% was achieved.

The neutron beam polarization was determined by transmitting the neutrons through our newly developed dynamically polarized proton target (See Section 2.1). Because the longitudinal $\vec{n}$-$\vec{p}$ cross-section difference $\Delta\sigma_L$ is large and well known at the energies of interest, $K_z^{z'}(0°)$ could be determined from transmission-asymmetry measurements to high statistical accuracy in only a few hours. The superconducting magnet in the target was oriented so that the polarization of the proton target was aligned parallel to the neutron beam direction and polarization axis. The neutron polarization direction was reversed at 10 Hz, and to reduce systematic errors the proton target polarization was reversed once during each measurement. Assuming 65% polarization for the proton target, we obtained the $K_z^{z'}(0°)$ values plotted in Figure 3.1–3. The data have not been corrected for the energy spread in the neutron beam, nor have they been normalized to an absolute measurement of $K_z^{z'}(0°)$. The results indicate that the $T(\vec{p},\vec{n})$ reaction is an excellent source of low-energy longitudinally polarized neutrons.

[Jar74] J. J. Jarmer *et al.*, Phys. Lett., **48B**, 215 (1974).

[Wil] W. S. Wilburn, to be published.

3.1.3 Polarization Measurements in D($\vec{d}$,d)D Scattering

B. J. Crowe III, C. R. Brune, K. A. Fletcher[1]*, W. H. Geist, H. J. Karwowski, E. J. Ludwig and K. D. Veal*

We have completed our investigation of the D($\vec{d}$,d)D reaction at energies below the deuteron breakup threshold and are in the process of writing a paper for publication. This data set is the lowest energy analyzing power data yet obtained for this scattering process. This work has been described more fully in previous Progress Reports [Lud94, Cro95]. Therefore, only a brief summary of the motivation, experimental setup, and results will be given below.

Recent comparisons of resonating group model (RGM) calculations [Hof93] with previous polarization data at 6–10 MeV [Gru72] have been inconclusive as to the amount of tensor force needed to describe the data. To test further predictions of R-matrix, RGM, and 4-body theories, we have recently measured the tensor analyzing powers $T_{20}(\theta)$ and $T_{22}(\theta)$ at incident deuteron energies of 1.5, 3, and 4.75 MeV. These data were taken at lab angles of 20–50 degrees using the TUNL FN tandem accelerator. Thin, durable, deuterated-carbon targets with thicknesses of $\approx 4.5 \mu g/cm^2$ were bombarded by polarized deuteron beams produced by the TUNL polarized-ion source. Scattered particles were viewed by symmetrically placed detector telescopes containing ΔE detectors of 6 and 16 μm for 3 and 4.75 MeV, and 5 and 8 μm for 1.5 MeV.

Our results for $T_{20}(\theta)$ and $T_{22}(\theta)$ at 4.75 MeV are shown in Figure 3.1–4 along with predictions from RGM [Hof96], R-matrix [Hal96], and 4-body [Fon96] theories. The RGM calculations were adjusted to provide best agreement with the data. An interesting point is how sensitive the model is to changes in the matrix element $\langle {}^5D_0 \,|V_{dd}|^1 S_0\rangle$. The size of this matrix element is dependent on the choice of the tensor potential. The agreement of the 4-body calculation with the experimental data is striking since there were no adjustments made to improve this agreement. Theoretical predictions using the 4-body calculation are underway for 3 MeV. The results will be compared to the 3 MeV data.

[Cro95] B. J. Crowe, In *TUNL Progress Report*, volume XXXIV, p. 63, 1994-1995.

[Fon96] A. C. Fonseca, 1996, private communication.

[1]State University of New York at Geneseo.

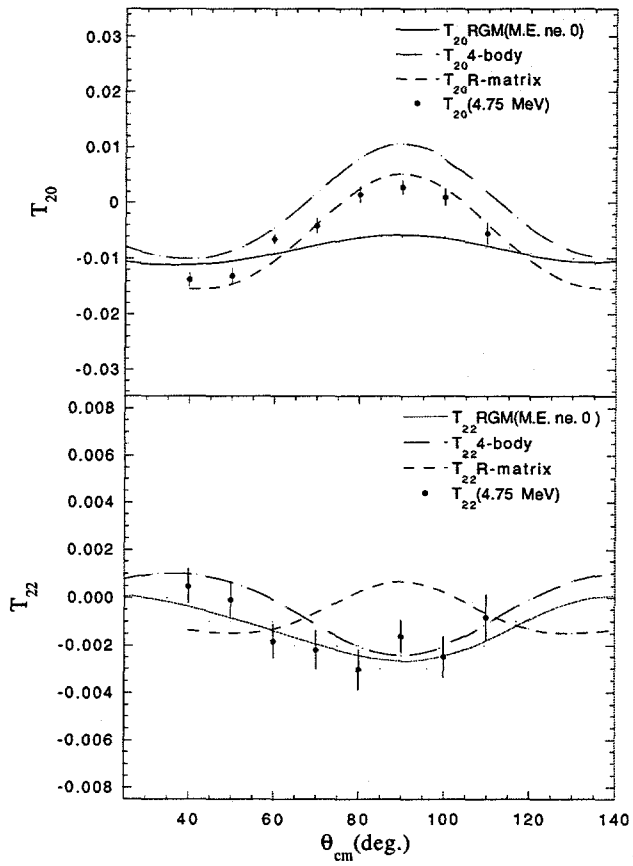

Figure 3.1–4: Comparison of $T_{20}(\theta)$ and $T_{22}(\theta)$ data with theoretical predictions from RGM, R-Matrix, and 4-body calculations at 4.75 MeV.

[Gru72] W. Grubler *et al.*, Nucl. Phys. **A197**, 259 (1972).

[Hal96] G. M. Hale, 1996, private communication.

[Hof93] H. Hofmann, 1993, private communication.

[Hof96] H. Hofmann, 1996, private communication.

[Lud94] E. J. Ludwig, In *TUNL Progress Report*, volume XXXIII, p. 63, 1993-1994.

3.1.4 The ^{4}He(γ,d)^{2}H Reaction at E_γ=150–250 MeV

B. J. Rice, E. A. Wulf, G. Feldman[1], N. R. Kolb[1], R. E. Pywell[1], G. A. Retzlaff[1], D. M. Skopik[1], D. E. Tiller[1] and H. R. Weller

The four-nucleon system serves as a critical testing ground for much of the theory of few-body systems. Recent advances in few-body calculation techniques, which require accurate data to test the theory, have illuminated the paucity and/or inconsistency of data in certain systems at or above pion threshold. The ^{4}He(γ,d)^{2}H reaction with E_γ=150–250 MeV exemplifies this lack of high-quality data. In the past thirty years, five separate measurements have yielded an uncertainty of a factor of 100 in the (γ,dd) cross-section [Sil84, O'R95] in this energy region.

We propose to perform a (hopefully) definitive measurement of this cross-section at the Saskatchewan Accelerator Laboratory (SAL). With this goal in mind, we have designed, constructed, and tested an experimental setup at SAL. For details of the experimental setup, see Section 3.3.2 of *TUNL Progress Report, Volume XXXIV*. The test run was completed in July 1995. The smallness of the cross-section (less than 1 nb/sr) and the presence of many competing channels with much higher cross-sections made the choice between running untagged and tagged (modes in which the incoming γ-ray energy is either unknown or known, respectively) a difficult one. As a compromise we ran in both modes, allotting the bulk of the beam time to untagged operation with its high count rate. The tagged data, with its lower count rate but additional kinematics information, was taken to provide background estimates for the competing channels.

Preliminary results from the test run indicate reasonably low background as well as good particle identification. A typical spectrum from an E-ΔE telescope is shown in Figure 3.1–5. These preliminary data indicate an angular distribution of the cross-section suggestive of $\sin^2 2\theta$, as expected for an E2 process. Rough count rate estimates are in line with peak differential cross-sections less than 1 nb/sr. The production run, tentatively planned for late in the Summer of 1996, should yield sufficient data to resolve firmly the discrepancy in the measured value of the cross-section. These data will be combined with the analyzing

[1]Saskatchewan Accelerator Laboratory, Saskatoon, SK, Canada.

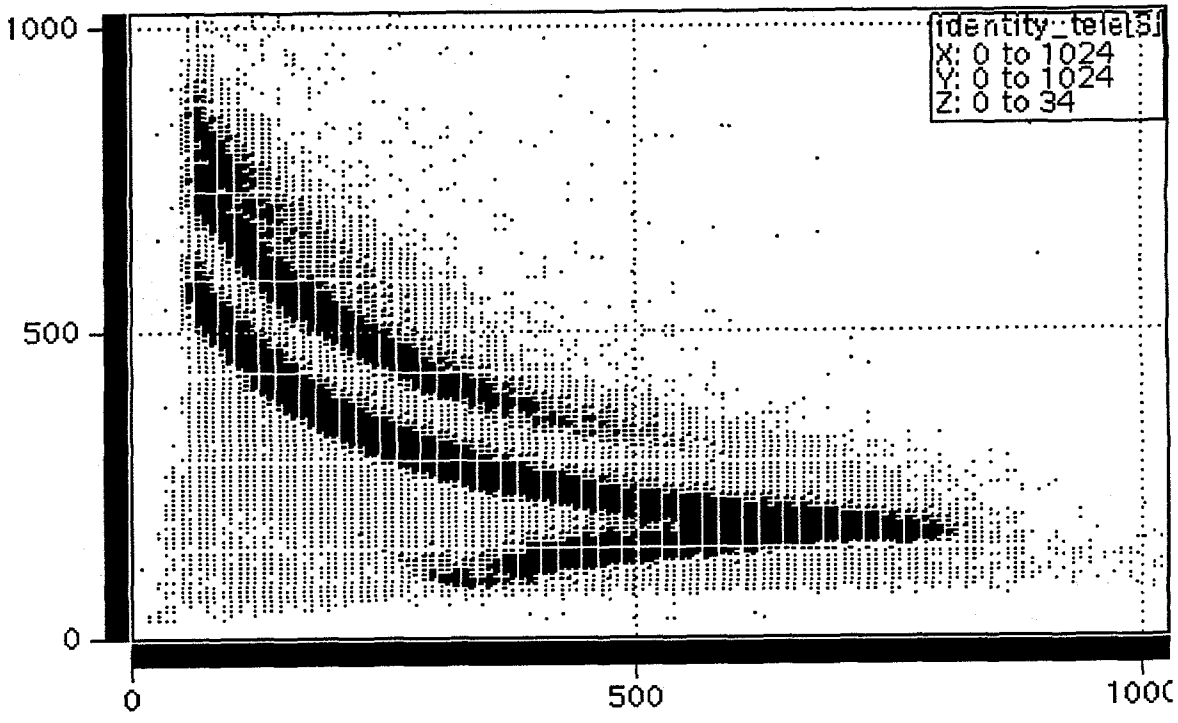

Figure 3.1–5: A typical spectrum from an E-ΔE telescope detector. The bands indicate, from top to bottom, tritons, deuterons, and a proton band folding back. Axes are labeled in ADC channels.

power data from an experiment performed at LEGS in order to extract the multipolarites of the contributing capture amplitudes.

[O'R95] G. V. O'Rielly, Ph.D. thesis, SAL, 1995.

[Sil84] B. H. Silverman *et al.*, Phys. Rev. **C29**, 35 (1984).

3.1.5 Measurement of the ^{3}He($\vec{d}$,p)^{4}He Analyzing Powers at Low Energies

W. H. Geist, H. J. Karwowski and E. J. Ludwig

The ^{3}He(d,p)^{4}He reaction proceeds through a broad $\frac{3}{2}^+$ s-wave resonance at a deuteron energy of 430 keV. For a $\frac{3}{2}^+$ s-wave reaction amplitude the analyzing powers follow certain relationships, namely the tensor analyzing powers $A_{yy}(\theta)=\frac{1}{2}$, $A_{zz}(\theta)=(1-3cos^2\theta)/2$, and

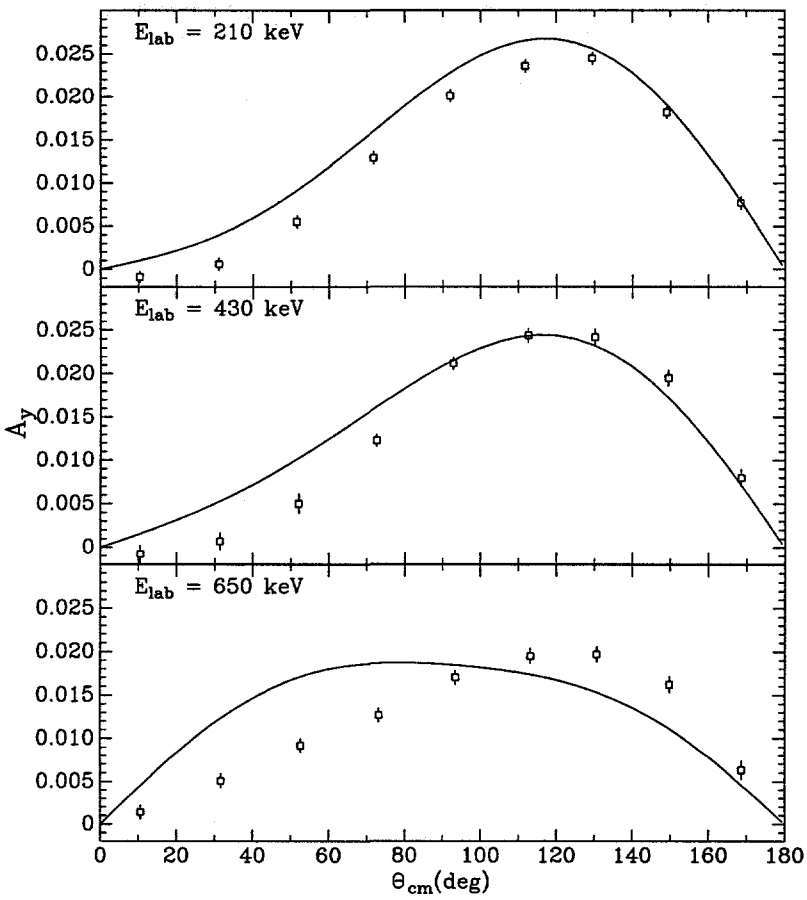

Figure 3.1–6: The vector analyzing power $A_y(\theta)$ at E_d =210, 430, and 650 KeV. The solid curve is a theoretical prediction from an R-Matrix parameterization [Hal96].

$A_{xz}(\theta)=-\frac{3}{2}cos\theta sin\theta$; and the vector analyzing power $A_y(\theta)$ will be zero. Measurements of these analyzing powers around the resonance will enable us to understand the reaction mechanism and determine if other reaction amplitudes are important in the low-energy regime.

We have measured full angular distributions of $\sigma, A_y(\theta), A_{yy}(\theta), A_{xz}(\theta)$, and $A_{zz}(\theta)$ for the ^{3}He($\vec{d}$,p)^{4}He reaction at E_d=210, 430, and 650 keV. These measurements were made by accelerating a polarized deuteron beam through the low-energy beam facility and into a ^{3}He ion-implanted target. Three pairs of silicon detectors were placed on rotating plates inside the high-voltage chamber. The analyzing powers were determined using fast spin flip and placing the detectors symmetrically about the beam direction. An excitation function of the cross-section from 80 to 680 keV was also measured.

The analyzing powers and cross-section measurements will be used in an R-Matrix parameterization of the A=5 system. This analysis is useful for determining the bare nuclear cross-section at very low energies to better understand electron screening effects. The current R-Matrix parameterization [Hal96], which does not include our data, can be refined at low energies as shown by the discrepancy with the $A_y(\theta)$ data, Figure 3.1–6. We also plan to measure a complete set of analyzing powers at E_d=80 keV.

[Hal96] G. M. Hale, 1996, private communication.

3.2 Measurements of D-States of Very Light Nuclei Using Transfer Reactions

3.2.1 Analyzing Powers of the ^{58}Ni($^{6}\vec{\text{Li}}$,d)^{62}Zn Reaction at E(^{6}Li)=34 MeV

K. D. Veal, E. E. Bartosz [1], C. R. Brune, P. D. Cathers [1], T. L. Drummer [1], A. M. Eiró [2], H. J. Karwowski, K. W. Kemper [1], B. Kozlowska [3], E. J. Ludwig, A. J. Mendez, F. D. Santos [2] and I. J. Thompson [4]

There is considerable theoretical and experimental interest in investigating the structure of the ^{6}Li nucleus [Kuk95, San90]. A recent article [Eir95] summarizes existing information about the D-state component of the ^{6}Li wave function via the obvservable $\eta(^{6}\text{Li})$, the asymptotic D- to S-state ratio. Estimates of the D-state wave function are so widely varying that even the sign of $\eta(^{6}\text{Li})$ is uncertain. Following our successes in determining the D- to S-state ratios for the triton [Koz94] and ^{3}He [Aye95], we continue the D-state studies with ^{6}Li. The goal of this study is to learn more about the α-d cluster structure of the ^{6}Li nucleus.

Calculations of Eiró *et al.* [Eir95] have shown that tensor analyzing powers of transfer reactions induced by polarized ^{6}Li ions show considerable sensitivity to the ^{6}Li D-state. Thus, analogous to our previous D-state analyses, we will attempt to extract $\eta(^{6}\text{Li})$ by a comparison of DWBA calculations of polarization observables with experimental data, treating $\eta(^{6}\text{Li})$ as the only adjustable parameter.

In the present work, these transfer reactions take place with both the incoming and outgoing particles having energies well above the Coulomb barrier. To simplify the analysis and reduce theoretical uncertainties, we have chosen to measure the ^{58}Ni($^{6}\vec{\text{Li}}$,d)^{62}Zn reaction. This reaction proceeds via L=0 transfer to the ground state and has a well separated ground state and first excited state in the residual nucleus. We measured this reaction at E(^{6}Li)=34 MeV where effects of compound-nucleus formation and multi-step processes are expected to be small. To date, we have completed measurements of $A_y(\theta)$ and $A_{zz}(\theta)$ for this reaction.

The experiment was performed using the Optically Pumped Polarized Lithium Ion Source at the Florida State University Superconducting Linear Accelerator Laboratory. The detectors used were Si ΔE-E telescopes, each with a solid angle of 4.7 msr. The targets were isotopically enriched rolled foils of ^{58}Ni with thicknesses of either 0.75 or 1.5 mg/cm^2. The energy spectrum of the detected deuterons at θ_{lab}=15° is shown in Figure 3.2–1. The angular distrubutions of σ, $A_y(\theta)$, and $A_{zz}(\theta)$ for transfers to the ground state of ^{62}Zn are

[1]Florida State University, Tallahassee, Florida.
[2]University of Lisbon, Lisbon, Portugal.
[3]University of Silesia, Katowice, Poland.
[4]University of Surrey, Surrey, England.

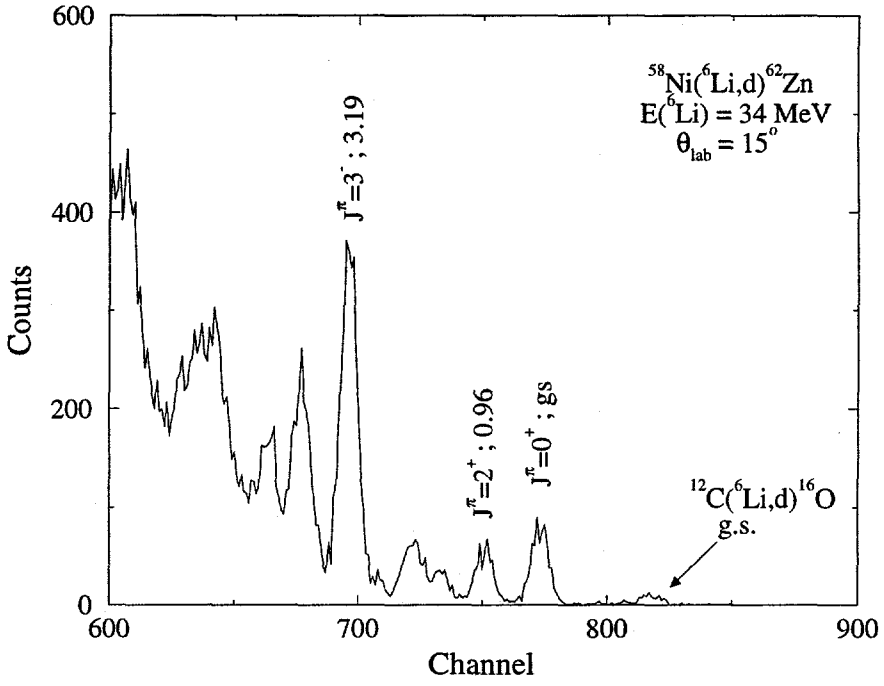

Figure 3.2–1: Spectrum for the ^{58}Ni(^{6}Li,d)^{62}Zn reaction at E(^{6}Li)=34 MeV. Excitation energies are in MeV.

shown in Figure 3.2–2. The cross-section, extracted as a relative yield and normalized to data in the literature [Bet78], has an interference pattern indicative of direct α transfer. The $A_y(\theta)$ data oscillate about zero and $A_{zz}(\theta)$ is small and mostly negative.

The curves in Figure 3.2–2 were calculated by an exact, finite-range DWBA code, PTOLEMY, for $\eta(^{6}\mathrm{Li})$=0, +0.0145, and −0.0145. The optical-model parameters for the entrance channel are those which fit ^{6}Li+^{58}Ni elastic scattering. Global optical-model parameters appropriate for d+^{62}Zn elastic scattering were used for the exit channel, with a 12% decrease of the deuteron real well radius to better fit the reaction data. Sensitivity of the calculations to the optical-model parameters shows that a 16% decrease of the deuteron real well *depth* also provides a good description of the data. The calculations of Figure 3.2–1 reproduce the cross-section and vector analyzing power well. A comparison with the $A_{zz}(\theta)$ data suggests that $|\ \eta(^{6}\mathrm{Li})|$<0.0145, though the sign is still undetermined.

Further experiments in this study include a measurement of $A_{xz}(\theta)$ for the ^{58}Ni($^{6}\vec{\mathrm{Li}}$,d)^{62}Zn

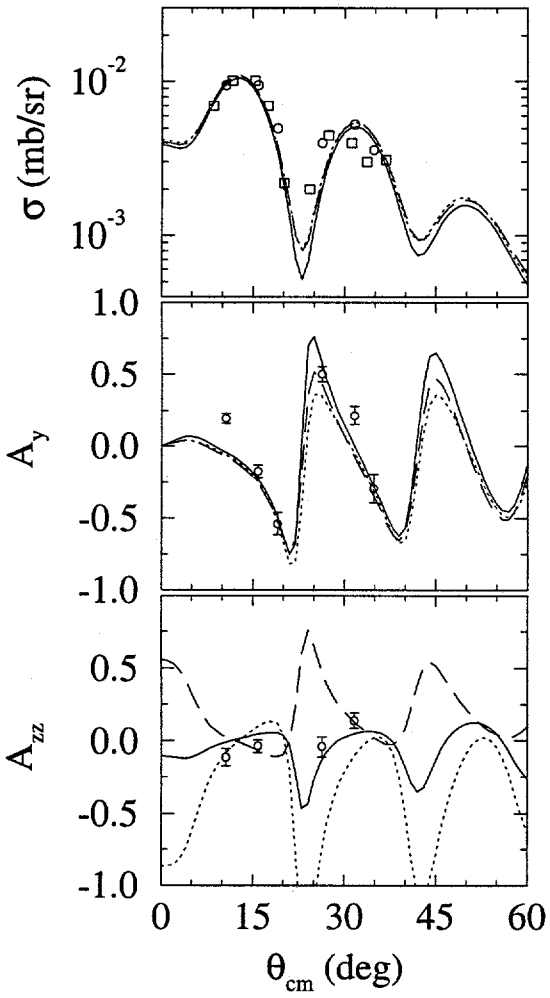

Figure 3.2–2: A comparison of DWBA calculations with $\sigma(\theta)$, $A_y(\theta)$, and $A_{zz}(\theta)$ for the ^{58}Ni(^{6}Li,d)^{62}Zn (0^+ gs) reaction at E(^{6}Li)=34 MeV. The squares are existing data [Bet78] and the circles are our experimental data. The solid curve is calculated assuming $\eta(^6\text{Li})=0$. The dashed and dotted curves are for $\eta(^6\text{Li})=+0.0145$ and $\eta(^6\text{Li})=-0.0145$, respectively.

reaction at E(^{6}Li)=34 MeV. Future plans also include measurements of the tensor analyzing powers of the ^{28}Si($^6\vec{\text{Li}}$,α)^{30}P reaction at E(^{6}Li)=34 MeV and measurements of the analyzing powers for these reactions at E(^{6}Li)=50 MeV.

[Aye95] Z. Ayer *et al.*, Phys. Rev. **C52**, 2851 (1995).

[Bet78] R. R. Betts *et al.*, Phys. Lett. **76B**, 47 (1978).

[Eir95] A. M. Eiró *et al.*, Few-Body Systems, **Suppl. 8**, 369 (1995).

[Koz94] B. Kozlowska *et al.*, Phys. Rev. **C50**, 2695 (1994).

[Kuk95] V. I. Kukulin *et al.*, Nucl. Phys. **A586**, 151 (1995).

[San90] F. D. Santos *et al.*, Colloque de Physique Suppl. n 22, Colloque C6, **51**, 443 (1990).

3.2.2 Analyzing Powers of the ^{12}C($^6\vec{\text{Li}}$,d)^{16}O Reaction at E(^{6}Li)=34 MeV

A. J. Mendez, E. E. Bartosz [1], *C. R. Brune, P. D. Cathers* [1], *T. L. Drummer* [1], *H. J. Karwowski, K. W. Kemper* [1], *B. Kozlowska* [2], *E. J. Ludwig and K. D. Veal*

As mentioned in the discussion of the ^{58}Ni($^6\vec{\text{Li}}$,d)^{62}Zn reaction (see Section 3.2.1), present models of the ^{6}Li nucleus are in disagreement [Leh90, Eir95] as to the sign of the asymptotic D- to S-state ratio, η. Transfer reactions induced by polarized ^{6}Li have been predicted [Eir95] to be sensitive to η, and recent measurements [Men95] have shown a sensitivity to the presence of the D-state in ^{6}Li. As with the ^{58}Ni($^6\vec{\text{Li}}$,d)^{62}Zn reaction study, we are attempting to extract η(^{6}Li) information from exact, finite-range DWBA calculations by comparing calculated analyzing power angular distributions with the experimental data.

To date, we have measured a cross section, and $A_y(\theta)$ and $A_{zz}(\theta)$ angular distributions for this reaction at 34 MeV over the laboratory angular range 6.5°–60°. Experimental details are similar to those for the ^{58}Ni work, and a typical spectrum is shown in Figure 3.2–3. As in the ^{58}Ni study, the ground state transition is an L=0 transfer to a 0^+ state which is well separated from the nearest excited states. The next two peaks in the energy spectrum, although well resolved from each other, are actually each unresolved doublets, a 0^+, 3^- doublet at about 6.1 MeV; and a 2^+, 1^- doublet at about 7 MeV. Angular distributions for some of the data are shown in Figure 3.2–4. Preliminary calculations, assuming a one-step reaction mechanism, are underway. Calculations including multi-step processes, such as a coupling to the 3^+ state in ^{6}Li, are also planned.

[1]Florida State University, Tallahassee, Florida.
[2]University of Silesia, Katowice, Poland.

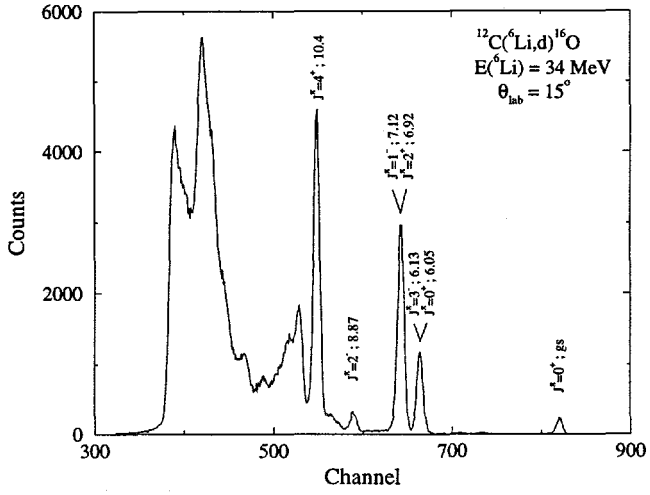

Figure 3.2–3: Spectrum for the $^{12}C(^6Li,d)^{16}O$ reaction at $E(^6Li)$=34 MeV. Excitation energies are in MeV.

[Cun78] A. Cunsolo *et al.*, Phys. Rev. **C18**, 856 (1978).

[Eir95] A. M. Eiró *et al.*, Few-Body Systems, **Suppl. 8**, 369 (1995).

[Leh90] D. R. Lehman, Colloque de Physique Suppl. n 22, Colloque C6, **51**, 47 (1990).

[Men95] A. J. Mendez *et al.*, Phys. Rev. **C51**, 651 (1995).

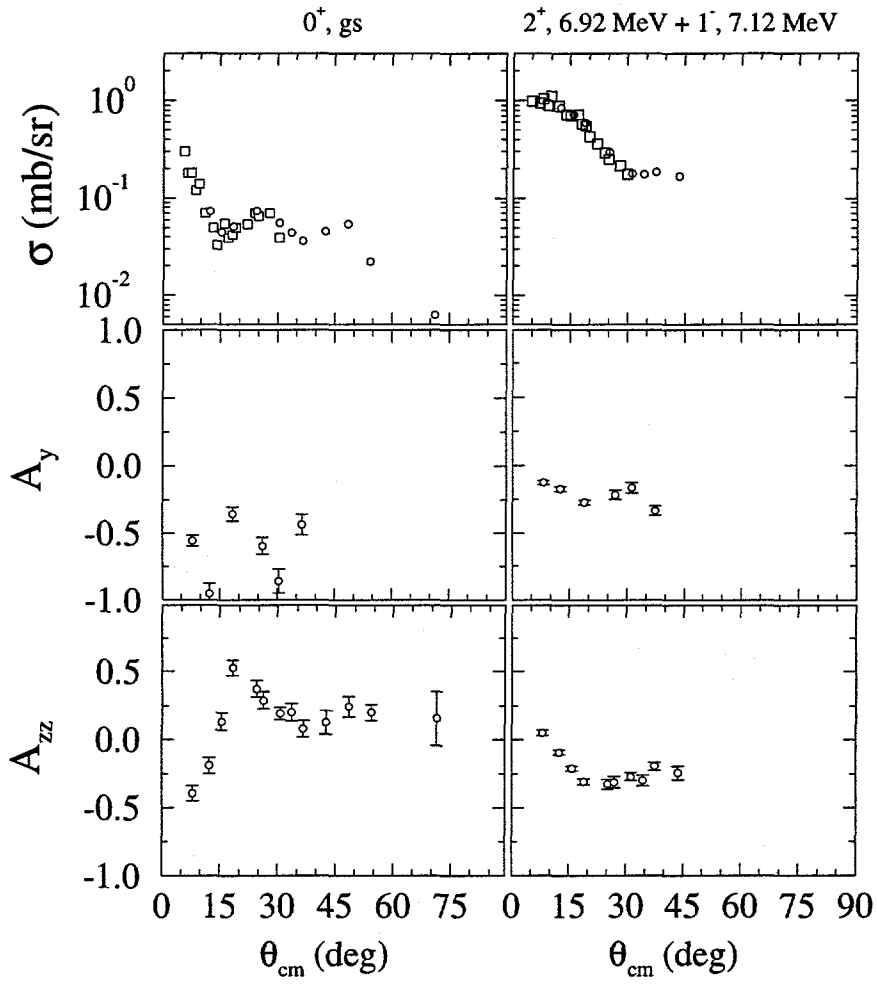

Figure 3.2–4: The squares are the data of Cunsolo *et al.* [Cun78]. The circles are our experimental data. The data in the left column are for transitions to ^{16}O(0^+,gs). On the right are data for transitions to the ^{16}O(2^+, 6.92 MeV+1^-, 7.12 MeV) doublet.

3.3 Radiative-Capture Reactions and Few-Nucleon Systems

3.3.1 Effects of Non–Nucleonic Degrees of Freedom in the $D(\vec{p},\gamma)^3He$ and $p(\vec{d},\gamma)^3He$ Reactions Below $E_{p,d}$=80 keV

G. J. Schmid[1], M. Viviani[2], B. J. Rice, R. M. Chasteler, M. A. Godwin, G. C. Kiang[3], L. L. Kiang[4], A. Kievsky[2], C. M. Laymon, R. M. Prior, R. Schiavilla[5,6], D. R. Tilley and H. R. Weller

Significant results from this experiment have been published in the April 1996 issue of Physical Review Letters [Sch96]. The letter summarizes results from both experimental and theoretical investigations of the p-d system. On the experimental side, details of the physical setup are given, followed by a presentation of the measured data for the cross-section, vector and tensor analyzing powers, and γ-ray polarization. On the theoretical side, a technique for treating the p-d system using pair correlated hyperspherical harmonic (PCHH) wave functions is discussed. This technique, which includes Coulomb distortions and both one- and two-body currents in the nuclear current operator (meson-exchange currents), produces values for a variety of trinucleon properties in good agreement with recent Faddeev calculations. The experimental results are then compared with these *ab initio* PCHH calculations, highlighting the importance of meson-exchange currents (MEC's) to this reaction at low energies. The vector and tensor analyzing powers are shown to be particularly sensitive to the presence of MEC's. The extrapolation to zero energy of the present data leads to a value for the S-factor of S(E=0)=0.165 $\pm$ 0.014 eV·b, in reasonable agreement with theory.

[Sch96] G. J. Schmid *et al.*, Phys. Rev. Lett. **76**, 3088 (1996).

3.3.2 A Formalism for Gamma-Ray Linear Polarization in Photonuclear Reactions

J. F. Guillemette, H. R. Weller, B. J. Rice and R. G. Seyler [7]

During the past year we have expanded our investigation of photonuclear reactions to include γ-ray polarization in radiative-capture reactions with polarized particle beams. This

[1]Lawrence Berkeley Laboratory, Berkeley, CA.
[2]INFN, Sezione di Pisa, 56100 Pisa, Italy.
[3]Academia Sinica, Taipei, Taiwan.
[4]National Tsing-Hua University, Taipei, Taiwan.
[5]CEBAF Theory Group, Newport News, VA.
[6]Department of Physics, Old Dominion University, Norfolk, VA.
[7]The Ohio State University, Columbus, OH 43210-1106.

particular phase of the study has already revealed a number of interesting results, including a new experimental observable we have termed the *"Polarization Analyzing Power."* Previous work on γ-ray-in particle-out reactions involved linearly and circularly polarized photons incident upon polarized targets [Wel92, Wel94], and was based on a formalism for polarization and scattering in nuclear reactions developed by T. A. Welton [Mar63]. This same formalism is used to derive angular momentum coupling coefficients (B-coefficients) for particle-capture, γ-ray-out reactions. The B-coefficients are used in conjunction with the rotation matrix, $D(\phi, \theta, 0)$, to express experimental observables, such as the γ-ray linear polarization and the new observable, *polarization analyzing power*, in terms of the transition matrix elements (TME's). Expressions for the γ-ray linear polarization are easily obtained with the aid of a new FORTRAN program that calculates these B-coefficients. Although at present this code is restricted to reactions involving spin-1/2 particles, work is under way on a more complete version that will also calculate B-coefficients for incident beams of integral spin.

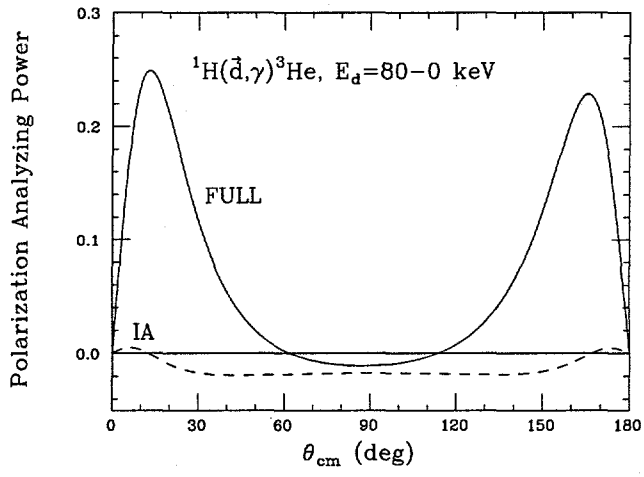

Figure 3.3–1: Polarization analyzing power calculations for the ^{1}H($\vec{d}$,γ)^{3}He reaction.

Initial results indicate that the γ-ray linear polarization obtained with polarized proton beams is sensitive to the phase difference between contributing TME's. We have also discovered that this sensitivity is enhanced in polarization analyzing power measurements. The latter is defined as the difference between the γ-ray linear polarization with spin "up" and spin "down" incident beams. The extreme sensitivity of the polarization analyzing power can be best demonstrated by examining the results of state-of the-art, 3-body calculations

for the ^{1}H($\vec{d}$,γ)^{3}He reaction [Viv], in Figure 3.3–1. The curve labeled *"IA"* was generated from the theoretical matrix elements for the case when only nucleon-nucleon forces are considered, while the *"FULL"* curve was generated from the matrix elements when meson-exchange currents and delta effects were included. We therefore expect this new observable to provide significant guidance to theorists and experimentalists alike. Plans to measure this new observable are underway.

[Mar63] J. B. Marion and J. L. Fowler, *Fast Neutron Physics*, volume 157, p. 1317, Interscience, New York, 1963.

[Viv] M. Viviani *et al.*, private communication.

[Wel92] H. R. Weller *et al.*, Atomic Data and Nucl. Data Tables, **50**, 29 (1992).

[Wel94] H. R. Weller *et al.*, Atomic Data and Nucl. Data Tables, **58**, 219 (1994).

3.3.3 A Determination of the Asymptotic D- to S-state ratio for ^{3}He from the Reaction ^{1}H($\vec{d}$,γ)^{3}He at E_d =80–0 keV

B. J. Rice and H. R. Weller

Over the past three years, the Radiative Capture Group at TUNL has been studying the reactions ^{2}H($\vec{p}$,γ)^{3}He and ^{1}H($\vec{d}$,γ)^{3}He at E_p, E_d=80–0 keV (described in Section 3.3.1 of this report). One parameter which provides information about the internal dynamics of the ^{3}He wave function and which may be determined via ^{1}H($\vec{p}$,γ)^{3}He is the asymptotic D- to S-state ratio, η. Specifically, we have measured the tensor analyzing power $T_{20}(\theta_{lab}$=90°) and have performed direct-capture calculations of $T_{20}(\theta)$ while varying the choice of η to determine a best-fit value for η. Such a radiative capture-based determination of η has been attempted previously [Vet85b] with E_d=19.8 MeV, but the result was found to be highly dependent upon the choice of ^{3}He wave function. At energies below 80 keV, however, we have found the value of η to be nearly independent of the choice of ^{3}He wave function.

Any choice of bound-state wave function for the innermost few fermis of p-d separation is subject to debate. Beyond three to five fermis, however, the behavior of the wave function is, to a good approximation, an exponentially decreasing function of the p-d separation energy [Fri82]. If one can show that the bulk of the reaction strength occurs in the asymptotic region of the wave function, then the model-independent choice of the asymptotic form is justified. We performed direct-capture calculations of the contribution to the total cross-section as a function of p-d separation at E_d=19.8 MeV [Vet85a] and E_d=80 keV and found that at 80 keV$\sim$93% of the reaction strength occurs beyond three fermis, compared with $\sim$65% at 19.8 MeV.

η	r_{cut} (fermis)					
E_d (MeV)	1.0	1.5	2.0	2.5	3.0	4.0
19.8	(-0.012)	-0.022	-0.032	-0.042	(-0.052)	
0.080	-0.0353		-0.0379		-0.0402	-0.0428

Table 3.3–1: Extracted values of η that result from varying r_{cut} in a purely asymptotic ^{3}He wave function at E_d=19.8 MeV and at E_d=80 keV (present). At the higher energy, η changes by 0.01 for every change in r_{cut} of 0.5 fermis. At 80 keV, η changes by roughly 0.001 for every 0.5 fermis.

One problem with using the asymptotic (Whittaker function) wave functions, however, is that they diverge at a p-d separation distance of zero, and consequently direct-capture calculations overpredict the contributions of the innermost few fermis. One technique for handling this is to choose a cutoff radius, r_{cut}, truncating the asymptotic wave function from r=0 fermis to r=r_{cut}. The results of the best-fit process for η while varying r_{cut} are shown in Table 3.3–1, which includes the results of a similar analysis from Vetterli [Vet85a]. We see that the present work is approximately ten times less sensitive to the choice of r_{cut} than in the case of Vetterli *et al.*

In order to extract a reasonable value for η we have constructed a wave function, $\psi_{matched}$, that is composed of a realistic wave function inside approximately four fermis and the asymptotic form beyond four fermis. The choice for the realistic wave function comes from Lehman and Friar [Fri82] and matches the experimentally observed p-d separation energy. Use of this matched wave function yields a best-fit value of $\eta = -0.0399 \pm 0.0091$, where the error arises primarily from the statistical error of the $T_{20}(90°)$ measurement and uncertainty in the beam polarization. Rough limits on the model dependence of this have been established by creating two other "matched" wave functions that are representative of choices for ^{3}He wave functions with less strength in the internal region of the wave function and more in the asymptotic region, and vice versa. The final result we obtain is then η=$-0.0399 \pm 0.0091^{+0.0012}_{-0.0019}$, where the second uncertainties represent rough upper and lower limits on η due to dependence upon our (arbitrary) choice of ^{3}He wave function. The results of this work have been submitted to *Physical Review C.*

[Fri82] J. L. Friar *et al.*, Phys. Rev. **C25**, 1616 (1982).

[Vet85a] M. C. Vetterli, Ph.D. thesis, McMaster University, 1985.

[Vet85b] M. C. Vetterli *et al.*, Phys. Rev. Lett. **54**, 1129 (1985).

4 Nuclear Astrophysics

4.1 Radiative Capture Reactions

4.1.1 Measurement of the ^{7}Li(n,γ)^{8}Li Cross-Section at E_n=1–1000 eV.

J. C. Blackmon[1], *A. E. Champagne, J. K. Dickens*[1], *M. A. Hofstee, D. C. Larson*[1], *D. C. Powell, S. Raman*[1] *and M. S. Smith*[1]

The flux of high-energy solar neutrinos is directly proportional to the low-energy ^{7}Be(p,γ) ^{8}B cross-section, which is the most uncertain cross-section in the proton-proton chain. The rate for this reaction is determined from an extrapolation of existing ^{7}Be(p,γ)^{8}B cross-section data (E_p>100 keV) to solar energies.

A recent measurement of the analyzing power in the ^{7}Li(p,γ)^{8}Be reaction and its interpretation in terms of a substantial p-wave contribution may have implications for this extrapolation procedure [Cha94]. A similar p-wave contribution to the ^{7}Be(p,γ)^{8}B cross-section would imply a substantial reduction in the predicted flux of ^{8}B neutrinos. Unfortunately, a similar analyzing power measurement using a ^{7}Be target is not feasible owing to the high flux of gamma radiation produced in the decay of ^{7}Be. Consequently, we have measured the analog reaction, ^{7}Li(n,γ)^{8}Li, where p-wave capture would manifest itself as a deviation from the well-known $1/v$ behavior of the cross-section at low energies. Experimental details and preliminary interpretations were summarized in last year's progress report.

No deviation from $1/v$ capture is observed and so clearly the mechanism that enhances p-wave capture for protons does not play a significant role for neutrons. Given that the respective capture processes take place at very different radii, it is easy to make some general speculations concerning the origin of the p-wave strength. However, a quantitative explanation will now have to account for both the proton- and neutron-capture results. A paper describing this work has recently been published [Bla96].

[Bla96] J. Blackmon *et al.*, Phys. Rev. **C54**, 383 (1996).

[Cha94] R. M. Chasteler *et al.*, Phys. Rev. Lett. **72**, 3949 (1994).

[1]Oak Ridge National Laboratory, P.O. Box 2008, Oak Ridge, TN.

4.1.2 Search for p-Waves in Low-Energy Proton Capture Reactions Relevant to the Solar Neutrino Problem

M. A. Godwin, R. M. Chasteler, C. M. Laymon, R. M. Prior, D. R. Tilley and H. R. Weller

The initial stages of a study of the ^{7}Li($\vec{p}$,γ)^{8}Be reaction have been completed. A previous study of the ground state transition of the ^{7}Li($\vec{p}$,γ)^{8}Be reaction at energies of E_p(lab)=80–0 keV indicated the possibility of a large p-wave capture amplitude in this reaction. A similar p-wave component in the ^{7}Be(p,γ)^{8}B reaction could seriously affect the extrapolation used to obtain the astrophysical S-factor. The present work examines this possibility by observing the closely related ^{7}Li($\vec{p}$,$\gamma_{16.6}$)^{8}Be* (2^+, T=0+1) reaction with polarized protons. In short, we have measured the analyzing power and relative cross-section for polarized proton capture to the third excited state of ^{8}Be at energies of E_p=80–0 keV. This state has the same spin and parity as the ground state of ^{8}B, and is completely isospin mixed (T=0+1) with the fourth excited state. Collectively, the T=1 portion of these states is the isobar analog to the ^{8}B ground state. The data show an isotropic cross-section and analyzing powers consistent with zero. A transition matrix element (TME) analysis of the data yields two solutions. One consists of 99.9% E1 strength, (s-wave capture) and the other 99.9% M1 strength (p-wave capture). Direct capture calculations favor the E1 predominant solution. Based on this result, we conclude that p-waves are unlikely to be important in the ^{7}Be(p,γ)^{8}B reaction. However, a definitive experimental proof requires showing that the s-wave capture E1 solution is indeed the physical one. This can be done by measuring the linear polarization of the outgoing γ-rays. An experiment which will use our new Compton Polarimeter in order to perform this measurement is being developed.

4.1.3 Cross-Section Studies of the ^{7}Li(p,γ)^{8}Be Reaction at Low Energies

M. Spraker, J. Guillemette, M. A. Godwin, R. M. Prior, B. J. Rice, D. R. Tilley, H. R. Weller, C. Westerfeldt and E. A. Wulf

Over the last few years, we have been studying the ^{7}Li(p,γ)^{8}Be reaction at energies E_p=80–0 keV. Of particular interest for this experiment is the capture to the ground state and the first excited state of ^{8}Be. Due to the proton's very low incident energy, the beam is stopped within the target and the cross-sections previously measured have been for the full energy range from 80 to 0 keV. Evidence for p-wave effects in this energy range ([Cha94, God96] for example) has led us to pursue measurement of the reaction cross-section for smaller energy bins. Previously, we have taken the full energy range data and deconvoluted it using the detector response function or binned it allowing for the extraction of information for smaller energy bins [Sch95, Sch96]. This method requires detectors with excellent energy

resolution and reactions with a high count rate to achieve reasonable statistics for the lowest energy points. For this purpose, intrinsic, high-purity Ge detectors have been used in the past. Unfortunately, the efficiency of Ge detectors for the 17 MeV gammas produced in the ^{7}Li(p,γ)^{8}Be reaction is very small, making them of limited use for the study of this reaction.

In May, 1996 we began test runs with a system using two 10″x10″ NaI detectors. Although the energy resolution is poor ($\sim$3%), the efficiency for 17 MeV gammas is about 25 times higher than that of the available Ge detectors. Two 20 kV power supplies of opposite polarity were connected to the target chamber. The supplies are computer controlled and provide voltages from 0 to $\pm$20 kV with an accuracy of better than 1 kV. The 80 keV incident proton beam can then be accelerated by the target bias to energies between 60 and 100 keV. We incremented the voltages in 5 kV steps and stored data for each incident proton energy from 60 to 100 keV in 5 keV steps. The times spent at each energy were set so that nearly equal statistical accuracies were obtained in each energy bin. Furthermore, the cycle time over the full voltage range was limited to about 20 minutes, so that each energy was sampled about 70 times per day. This is important since it should average out systematic errors such as those which arise from changes in the beam energy, beam profile, target thickness, or contamination effects. By subtracting spectra, the cross-sections for each 5 keV energy bin from 60 to 100 keV can then be determined. The result should be a reliable measurement of the energy dependence of the cross-section and, therefore, of the astrophysical S-factor. Preliminary results indicate a significantly different slope for capture to the ground and first excited states of ^{8}Be, contradicting the usual pure, direct S-wave capture assumption. A detailed analysis of these data is currently underway and additional runs are planned.

During the past run, we also spent some time studying the effect of the target voltage on the incident beam profile. There was no apparent effect. In addition to the capture data, the ^{7}Li(p,α)^{4}He reaction was studied and will be used as a normalization reaction so that cross-sections can be calculated. We also hope to use the data already taken with this reaction to look for any effects of the target bias voltage on the incident beam current. Also, consistency checks are planned where the incident beam energy will be changed from 80 keV to 60 keV and the data will then be taken from 40 to 80 keV. The 60 to 80 keV data will then be measured both by "ramping up" from 60 keV and by "ramping down" from 80 keV.

These measurements should allow for a direct observation of the slope of the S-factor which should answer the question of the role, if any, of p-wave capture in extrapolating data from 100 keV and above down to the astrophysical region.

[Cha94] R. M. Chasteler *et al.*, Phys. Rev. Lett. **72**, 3949 (1994).

[God96] M. A. Godwin *et al.*, Phys. Rev. **C53**, R1 (1996).

[Sch95] G. J. Schmid *et al.*, Phys. Rev. **C52**, R1732 (1995).

[Sch96] G. J. Schmid *et al.*, Phys. Rev. Lett. **76**, 3088 (1996).

4.1.4 ^{7}Li(p,γ)^{8}Be Absolute Cross-Section Measurement

M. A. Godwin, J. F. Guillemette, C. M. Laymon, R. M. Prior, B. J. Rice, M. C. Spraker, D. R. Tilley, H. R. Weller and E. A. Wulf

Our previous analysis of the ^{7}Li($\vec{p}$,γ)^{8}Be reaction [God96] provided detailed information about the relative cross-section and analyzing power for capture to the third excited state of ^{8}Be. During the course of performing that experiment, it was determined that an accurate evaluation of the absolute cross-section could not be obtained from the data. In order to perform this measurement a new setup was developed. The details of this setup are described below.

Recall that the solar neutrinos detected in ^{37}Cl based detectors mostly come from the decay of ^{8}B and that ^{8}B is created in the sun from the ^{7}Be(p,γ)^{8}B reaction. An accurate measurement of the cross-section at low energies for this reaction would be most useful, especially in light of another recent low-energy experiment [Cha94], which has found evidence of substantial p-wave strength. Unfortunately, a direct γ-ray measurement would be quite difficult, since the (radioactive) target emits $\approx$400 keV γ-rays, yet the capture γ-ray is at $\approx$200 keV. In fact, in a typical experiment setup we would expect the ratio of these to be approximately one million to one. The third and fourth excited states of ^{8}Be are completely isospin mixed (T=0+1) and collectively the T=1 component is the isobar analog to the ^{8}B ground state. Marion *et al.* [Mar67] has shown that these isospin mixed states can be represented as:

$$\begin{aligned} |16.63\rangle &= \ 0.772\ |T=0\rangle \ + \ 0.636\ |T=1\rangle, \\ |16.92\rangle &= \ 0.636\ |T=0\rangle \ - \ 0.772\ |T=1\rangle. \end{aligned} \tag{4.1}$$

Both of these states have the same spin-parity as the ^{8}B ground state and are approximately at the same energy [Ajz88]. The isospin of the ^{8}B ground state is T=1 and both the third and fourth excited states of ^{8}Be are partially T=1, as shown above. By examining the ^{7}Li(p,γ_3)^{8}Be* reaction we hope to gain insight into the ^{7}Be(p,γ_0)^{8}B reaction. Of course, items such as isospin selection rules, isospin mixing, and Coulomb force effects will need to be considered.

Our previous studies showed that in order to extract information about the third excited state we must perform a coincidence experiment, detecting the γ-rays and one of the two alpha particles from the decay of ^{8}Be. We have used a large high-purity germanium (HPGe) detector to measure the γ-rays. The target was made by the evaporation of lithium metal (isotopically enriched to 99.99%) onto a 1/16$''$ thick Al disc. Since the alpha particles

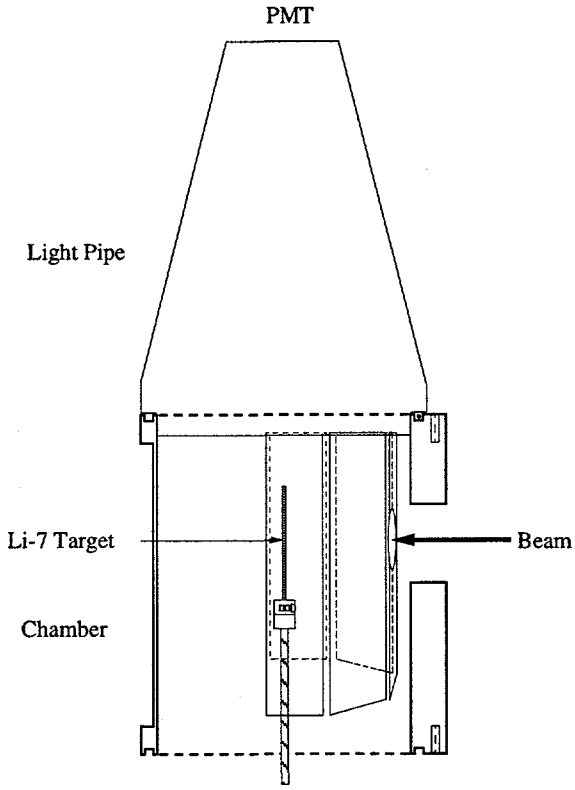

Figure 4.1–1: Conceptual diagram of chamber.

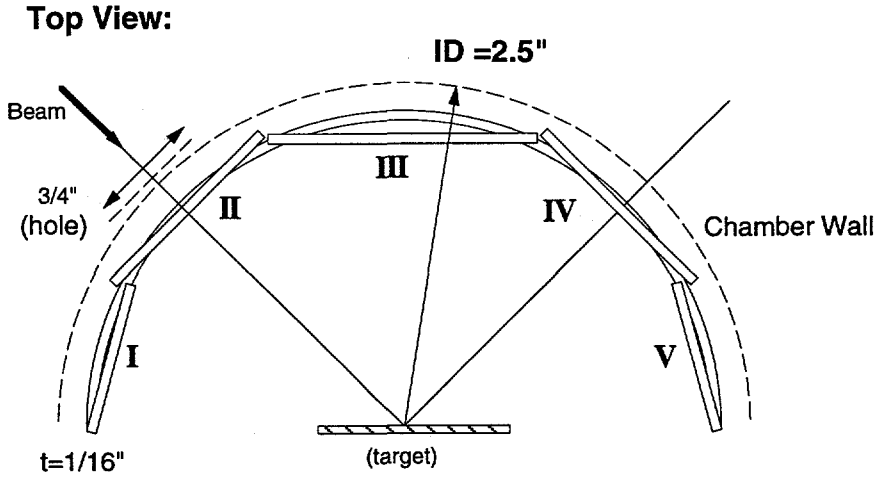

Figure 4.1–2: Top view of the experimental setup.

emerge 180° apart, one will be directed towards the target and will be stopped in the Al backing. To detect the other alpha particle we used plastic scintillators placed in front of the target. Figure 4.1–1 shows a conceptual diagram of this and Figure 4.1–2 is a top view. The alpha distribution is relatively isotropic at these energies so we need to cover as much of 2π steradians as possible, yet still keep the design relatively simple. The plan shown in these figures was easy to implement, inexpensive, and yet still covers approximately 60% of the alpha decays. An additional and equally important benefit of this technique is that the energy distribution of the coincident alpha particles is not "smeared out" from 8.5 to 0 MeV (like our previous measurements), but is a Gaussian-like distribution and so an energy cut off can be established and reproduced.

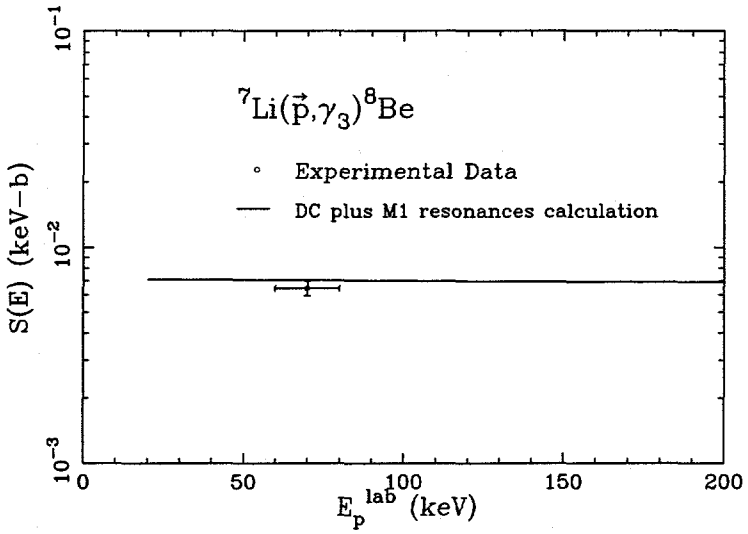

Figure 4.1–3: Preliminary data for the γ_3 astrophysical S-factor shown with a direct-capture calculation. The vertical error bars represent statistical uncertainty only.

Some preliminary data have been obtained and data analysis is currently underway. The work of Zahnow *et al.* [Zah95] presents a detailed evaluation of the cross-section for capture to the ground state. By using direct capture and adding in M1 resonances (at E_p=441 and 1030 keV) we fit his data fairly well. We are extending these calculations to treat the third excited state and the related ^{7}Be(p,γ)^{8}B reaction. Preliminary results indicate good agreement between the calculated and measured values of the absolute cross-section for capture to the third excited state of ^{8}Be. This is shown in Figure 4.1–3.

[Ajz88] F. Ajzenberg-Selove, Nucl. Phys. **A490**, 1 (1988).

[Cha94] R. M. Chasteler *et al.*, Phys. Rev. Lett. **72**, 3949 (1994).

[God96] M. A. Godwin *et al.*, Phys. Rev. **C53**, R1 (1996).

[Mar67] J. B. Marion *et al.*, Phys. Rev. **157**, 847 (1967).

[Zah95] D. Zahnow *et al.*, Z. Phys. **A351**, 229 (1995).

4.1.5 Direct Capture Calculations for the ^{7}Li(p,γ)^{8}Be Reaction

M. A. Godwin and H. R. Weller

A previous study [Cha94] has shown evidence for significant p-wave capture strength of 18–95% in the ^{7}Li(p,γ)^{8}Be reaction at E_p=80–0 keV. This remains unexplained, although some have argued [Bar96] that sufficient p-wave strength can be obtained from the tails of the M1 resonances (at E_p=441 and 1030 keV) to explain the data. The observation of large p-wave capture is interesting because it could lower the astrophysical S-factor (previously extracted by extrapolation assuming pure E1 capture) by 7–38%. Of more significance, however, are the implications on the closely related ^{7}Be(p,γ)^{8}B reaction. As explained (see Section 4.1.4) this reaction is producing ^{8}B and in turn a large portion of the solar neutrinos detected by the Homestake experiment.

In order to better understand the effects of the M1 resonances and the source of the large p-wave capture strength we are performing a series of direct capture calculations. Here we use the computer code HIKARI to calculate the contributions from direct E1, M1, and E2 capture, and we add the known [Ajz88] M1 resonances at E_p=441 and 1030 keV. Our first goal is to reproduce the extensive ground state data of Zahnow *et al.* [Zah95]. Using resonance parameters from the A=5–20 data compilations [Ajz88] and adjusting the strengths of the resonances allow us to fit the data fairly well. Note that we require the two resonances to add constructively in the region between the two levels. Barker [Bar95] has come to the same conclusion and points out that this contradicts findings from shell-model calculations. The data and our fits are shown in Figure 4.1–4.

In a recent paper [Bar96] Barker attempts to account for the data of Zahnow *et al.* [Zah95] and Chasteler *et al.* [Cha94] simultaneously. Contrary to his earlier work [Bar95], these recent fits (using an R-matrix approach and an E1 direct capture calculation) have signs in agreement with shell-model calculations (destructive interference between the two levels). However, we believe that there are some problems with these solutions. The R-matrix fit does agree with the 80 keV analyzing power data, but underpredicts the cross section, at least as measured by Zahnow *et al.* [Zah95]. On the other hand, the direct

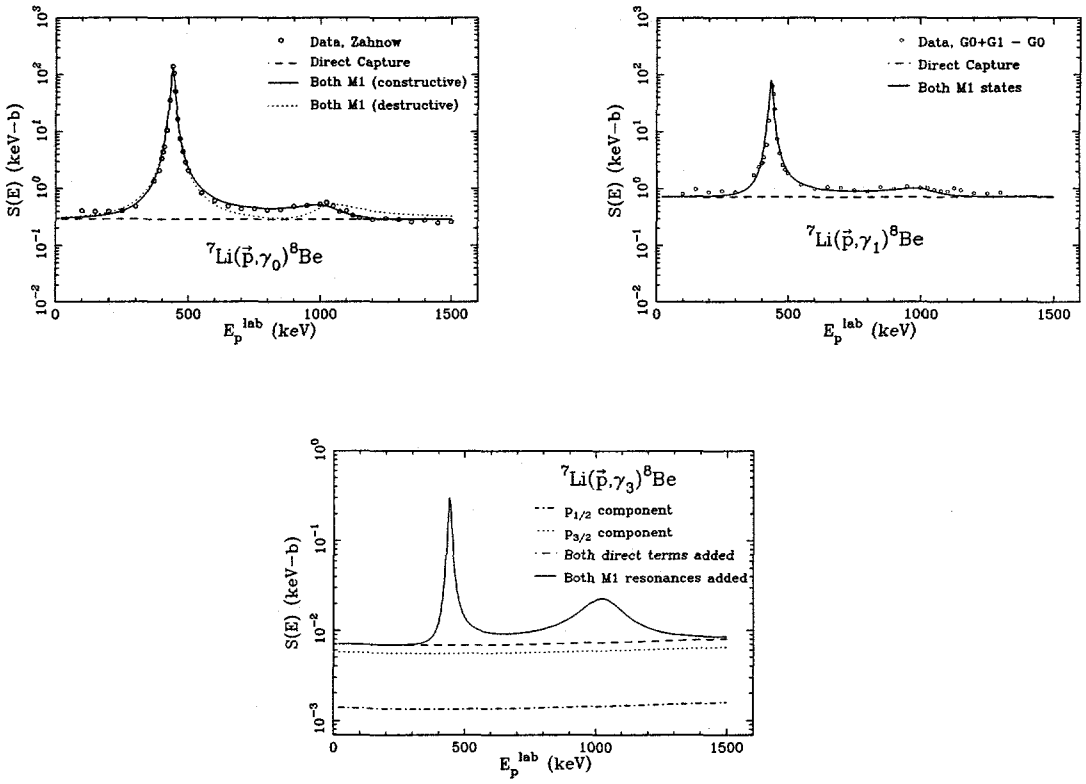

Figure 4.1–4: Direct capture plus M1 resonance calculations for the ^{7}Li(p,γ)^{8}Be astrophysical S-factor for the γ_0, γ_1, and γ_3 transition. The data of Zahnow *et al.* is is shown for capture to the ground and first excited states.

capture calculation, although fitting the low-energy cross-section data, underpredicts the analyzing power.

The data we have gathered are for proton energies of 80–0 keV. Since over 80% of the yield arises from 80–60 keV, we have performed calculations of the relative cross section and analyzing power at 70 keV as a function of angle. These results are shown in Figure 4.1–5.

Following the same procedure we have examined proton capture to the first and third excited states of ^{8}Be. Unlike the ground state, both of these levels are considered to be a mixture of $p_{\frac{3}{2}}$ and $p_{\frac{1}{2}}$ single particles.

The cross section for the first excited state has also been studied by Zahnow *et al.*

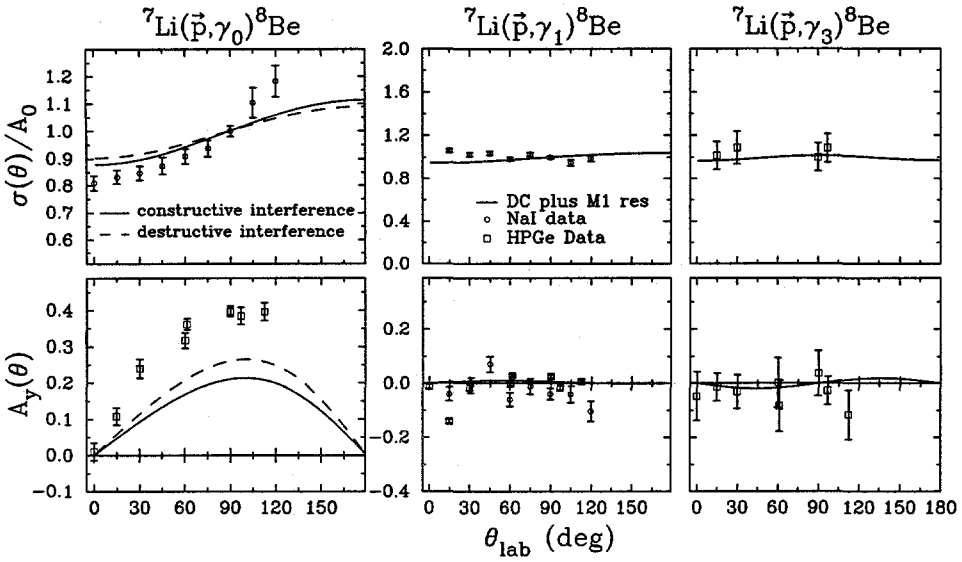

Figure 4.1–5: Relative cross section and analyzing powers at E_p=70 keV for both the γ_0 and γ_1 transitions. The data represent integrated yields from 80 to 0 keV.

They report astrophysical S-factor values for $(\gamma_0 + \gamma_1)$ capture over a large energy range. Once again, we have adjusted the resonance strengths to fit this data. The S-factor (or equivalently cross section) for capture to the first excited state is shown in Figure 4.1–4. The relative cross section and analyzing power (E_p=70 keV) are shown in Figure 4.1–5.

For the γ_3 transition, we have used the data of Sweeney [Swe69] to estimate the strength of the M1 resonance. In this paper, the differential cross section for ^{7}Li(p,γ_3)^{8}Be at θ=120° is given for proton energies of 441 and 1030 keV. Assuming an isotropic cross section we can calculate the S-factor, and adjust the strength of the two M1 resonances to match this value. The calculations for S(E) are shown in Figure 4.1–4. Running these calculations at E_p=70 keV gives the relative cross-section and analyzing powers curves displayed in Figure 4.1–5. Also plotted here are the data of Godwin *et al.* [God96].

The work above shows that the γ_0 absolute cross section is well accounted for when both M1 resonances are added to the direct capture calculation. However, the measured vector analyzing power (≈0.4) is about a factor of two greater than the calculations predict. Thus the M1 amplitude needs to be doubled, and (since $\sigma \approx$ amplitude^2) we need four times as much M1 strength. On the other hand, the γ_1 and γ_3 calculations reproduce the measured cross-section and analyzing power data reasonably well.

[Ajz88] F. Ajzenberg-Selove, Nucl. Phys. **A490**, 1 (1988).

[Bar95] F. C. Barker, Aust. J. Phys. **48**, 813 (1995).

[Bar96] F. C. Barker, submitted to Aust. J. Phys. 1996.

[Cha94] R. M. Chasteler *et al.*, Phys. Rev. Lett. **72**, 3949 (1994).

[God96] M. A. Godwin *et al.*, Phys. Rev. **C53**, R1 (1996).

[Swe69] W. E. Sweeney and J. B. Marion, Phys. Rev., **182**, 1007 (1969).

[Zah95] D. Zahnow *et al.*, Z. Phys. **A351**, 229 (1995).

4.1.6 The ^{7}Be(p,γ)^{8}B Reaction

E. A. Wulf, A. E. Champagne, V. Y. Hansper, M. A. Hofstee[1], D. M. Moltz[2], J. Powell[2], D. Powell, B. J. Rice, M. Spraker and H. R. Weller

The Nuclear Astrophysics and Radiative Capture Groups at TUNL are preparing to measure ^{7}Be(p,γ)^{8}B at energies from 75 to 800 keV. Previous measurements of the cross-section for ^{7}Be(p,γ)^{8}B differ by 30% and do not extend below E_p=130 keV [Kav69, Fil83]. The goal of the current experiment is to measure the cross section at energies down to E_p=75 keV and resolve the discrepancy in the previous data by reducing systematic and statistical errors. This reaction is of particular interest because of its role in the production of solar neutrinos from the decay of ^{8}B. Earth-based measurements of the neutrinos released from this reaction have shown large discrepancies with respect to the predictions of the standard solar-model. The current belief is that the uncertainty in the rate of the ^{7}Be(p,γ)^{8}B reaction is no longer a viable explanation for the solar-neutrino problem. However, an accurate measurement of this cross-section will play a role in a quantitative resolution of the problem.

For the low-energy part of this measurement, a high-current accelerator capable of producing beams with energies up to 220 keV is needed. Unfortunately, none of the accelerators currently at TUNL fulfill that need in their current configuration. To rectify this situation the Direct Extraction Negative Ion Source (DENIS) at TUNL will be used as a positive ion source. In this configuration it can produce proton beams with currents in excess of 100 μA and energies of up to 75 keV. We have recently acquired a high voltage table, power supply, and accelerator tube, which will enable the entire target chamber and associated electronics to be biased up to 200 kV. This table, connected to DENIS by a new beam line, will provide us with sufficient beam current and an energy range of 50–275 keV. Assembly of this new facility will begin this Summer with tests of beam intensity, spot size, and uniformity following. Ramping techniques, similar to those described in 4.1.3, are being investigated

[1]Colorado School of Mines, Golden, CO.
[2]Lawrence Berkeley National Lab, Berkeley, CA.

as a means of reducing systematic errors in measurements of the energy dependence of the cross-section, and thereby, the S-factor.

In the interest of better statistics, a 1 Curie ^{7}Be target will be produced by collaborators at LBNL. This target will produce a high flux of 477 keV γ-rays from the decay of ^{7}Be to ^{7}Li. This will make it impossible to measure the γ-rays from ^{7}Be(p,γ)^{8}B directly because at E_p=200 keV the 477 keV γ-rays will be 11 orders of magnitude more prevalent than the capture γ-rays. Therefore, the reaction yield will be measured by detecting the α-particles from ^{7}Be(p,γ)^{8}B$\rightarrow^8$Be$^*\rightarrow 2\alpha$, the method of past experiments [Kav69, Fil83]. Unlike the previous experiments, a surface barrier detector with a gas proportional counter will be used to detect the α-particles. This detector has been constructed by collaborators at LBNL, can distinguish between α-particles and other background, and has been shown to be capable of detecting protons down to 250 keV [Mol94].

A full calibration and test of the α-detector and beam current integration is required and will be done at the 3 MeV laboratory at TUNL this August. This run will use a 0.1 Curie target and the measurement will map the ^{8}B resonance at 780 keV. The experimental setup includes a surface barrier detector at 160° to monitor backscattered protons, a Cu beam wiper, a collimator, and an electron suppression ring. Initial testing of the beam current integration (BCI) components of the system has been planned for early July.

Even more important than the BCI and α-detector is the determination of the composition, uniformity, and surface contamination of the target, as this was a significant source of systematic error in past experiments. Measurements of the composition of ^{9}Be targets that were created using the same chemistry as for the ^{7}Be target have been completed. These results were obtained with a 2 MeV deuteron beam where the observation of the (d,nγ) and (d,pγ) reactions enabled relative amounts of ^{16}O, ^{9}Be, ^{12}C, and ^{14}N to be determined. Destructive tests to confirm the target composition have also been planned. The strong 477 keV γ-ray from the actual target will enable the measurement of the areal density and distribution of the ^{7}Be. This will be achieved by scanning across the target with a Pb collimator and γ-ray detector. To keep this carefully measured composition from changing due to carbon buildup during the run, the vacuum system will use a turbomolecular pump, a cryo pump, and a long cold trap. Techniques for monitoring the status of the target and beam energy during the experiment are being developed since the cross-section at very low energies is a strong function of the beam-on-target energy.

The final low-energy cross-section measurements of ^{7}Be(p,γ)^{8}B should begin in the Spring of 1997.

[Fil83] B. W. Filippone *et al.*, Phys. Rev. C, **28**, 2222 (1983).

[Kav69] R. W. Kavanaugh *et al.*, Bull. Am. Phys. Soc. **14**, 1209 (1969).

[Mol94] D. M. Moltz *et al.*, Nucl. Instr. and Meth. A, **349**, 210 (1994).

4.1.7 The ^{9}Be($\vec{p}$,γ)^{10}B Reaction at 100–0 keV

E. A. Wulf, M. A. Godwin, J. F. Guillemette, C. M. Laymon, R. M. Prior, B. J. Rice, M. Spraker, D. R. Tilley and H. R. Weller

As part of an ongoing effort to understand the dynamics of proton capture reactions at low-energies, we have measured ^{9}Be($\vec{p}$,γ)^{10}B using the TUNL Intense Polarized Ion Source (IPIS). Studies of other light nuclei at these energies have revealed substantial analyzing powers at 90° in some cases, while others have been consistent with zero. A non-zero $A_y(90°)$ implies that two amplitudes of opposite parity are interfering, which means that there is p-wave (M1) as well as s-wave (E1) strength for this reaction. This contradicts the standard assumption of pure s-wave capture used in extrapolating (p,γ) cross-sections to obtain S-factors.

The cross-section for the ^{9}Be($\vec{p}$,γ)^{10}B reaction is too low at 80 keV, the maximum energy of the IPIS, to be measurable in a reasonable amount of time. Therefore, the target was biased by –20 kV to increase the beam energy to 100 keV, which increased the count rate by a factor of 5. Studies of changes in the beam profile as a function of target bias have shown that bias voltages from +20 to –20 kV do not change the optics of the system. To further increase the total count rate the energy integrated yield of this reaction was obtained from the ^{9}Be target which stopped a 100 keV beam completely.

The integrated current on target could only be measured indirectly with the target biased. A bleed off resistor could be used for this purpose, but has not been implemented as of this writing. For the data obtained to date, a silicon surface barrier detector viewed the ^{9}Be(p,d)^{8}Be and ^{9}Be(p,α)^{6}Li reactions. These two reactions have large cross-sections at 100 keV and can be used to measure the beam current and carbon buildup on the target. The detector was first placed inside the target chamber, but it attracted secondary electrons because it was the closest object to the target. This problem was finally solved by placing it at the end of a long snout coming out of the top of the target chamber at a 55° angle. The detector was also shielded from elastically scattered protons by a thin Ni foil.

The γ-ray spectra were acquired using two large (130%) and three small (60%) high-purity germanium detectors (HPGe). The small HPGe detectors have thin ^{9}Be windows and can detect 20 keV X-rays which were produced in profusion by the secondary electrons from the biased target. A 1 mm sheet of Pb was placed between the small detectors and the target chamber to attenuate the X-rays. One of the large detectors was kept at 90° and the other was moved between 60° and 120°. The three small detectors were arranged at 0°, 40°, and 50°.

Analysis of the data has shown that $A_y(90°)$=0.25±0.05, implying that there is some p-wave strength. Future analysis will determine the cross-section and analyzing power as a function of angle. From this the total amount of p-wave strength will be determined. The $A_y(90°)\neq 0$ in ^{7}Li($\vec{p}$,γ)^{8}Be has been shown to be partly due to resonance tails. This could

also be the case in ^{9}Be($\vec{p}$,γ)^{10}B, but the contributions of both direct and resonance capture have not yet been calculated.

4.2 Nucleon Induced Reactions

4.2.1 The ^{9}Be($\vec{p}$,d)^{8}Be and ^{9}Be($\vec{p}$,α)^{6}Li Reactions at Low Energies

C. R. Brune, H. J. Karwowski and E. J. Ludwig

The Be abundance in low-metallicity stars is an important probe of cosmic-ray and Big-Bang nucleosynthesis, as well as stellar evolution models [Boe93]. In particular, significant Be depletion is observed in some stars. This depletion presumably results from the mixing of material from the stellar surface with material from the interior where the temperature is sufficient for the ^{9}Be(p,d) and ^{9}Be(p,α) reactions to be effective. A previous measurement [Sie73] found the low-energy cross-section in both reaction channels to be dominated by a broad ($\Gamma_{\rm tot}\approx$120 keV) s-wave 1^- resonance at $E_{\rm p}$=330 keV. At lower energies, a significant but very uncertain contribution was attributed to an opposite-parity subthreshold state. This uncertainty is reflected in the estimated $S(0)$ value (summed over both reaction channels) of 35^{+45}_{-15} MeV-b. The $S(0)$ value essentially determines the reaction rate, as the effective energy for this reaction at stellar temperatures is $\sim$7 keV. The existence of a state at 6.57 MeV excitation in ^{10}B (20 keV below the ^{9}Be+p threshold) has been established by many experiments, but spin and parity assignments are not definitive. For example, an analysis of ^{9}Be(^{3}He,d) angular distributions [Bla80] favors negative parity for this state.

During the last year we have made additional angular distribution measurements with unpolarized beam at the energies where we have already taken analyzing power data.

The analyzing power data are particularly sensitive to the presence of the subthreshold state. The analyzing power predicted by previously reported R-matrix parameters is shown in Figure 4.2–1. The large analyzing power predicted in (p,d) channel results from the subthreshold state. Our data clearly indicate that these parameters do not adequately describe the reaction mechanism. Further analysis is in progress.

[Bla80] L. Bland and H. T. Fortune, Phys. Rev. **C21**, 11 (1980).

[Boe93] A. M. Boesgaard and J. R. King, Astron. J. **106**, 2309 (1993).

[Sie73] A. J. Sierk and T. A. Tombrello, Nucl. Phys. **A210**, 341 (1973).

4.2.2 A Comparison of K- and R-Matrix Parameterizations of s-Wave ^{16}O+p Elastic Scattering

C. R. Brune

Low-energy nuclear reaction data are often parameterized in terms of K- or R-matrix representations [Hum90, Lan58]. This type of analysis is particularly useful in astrophysi-

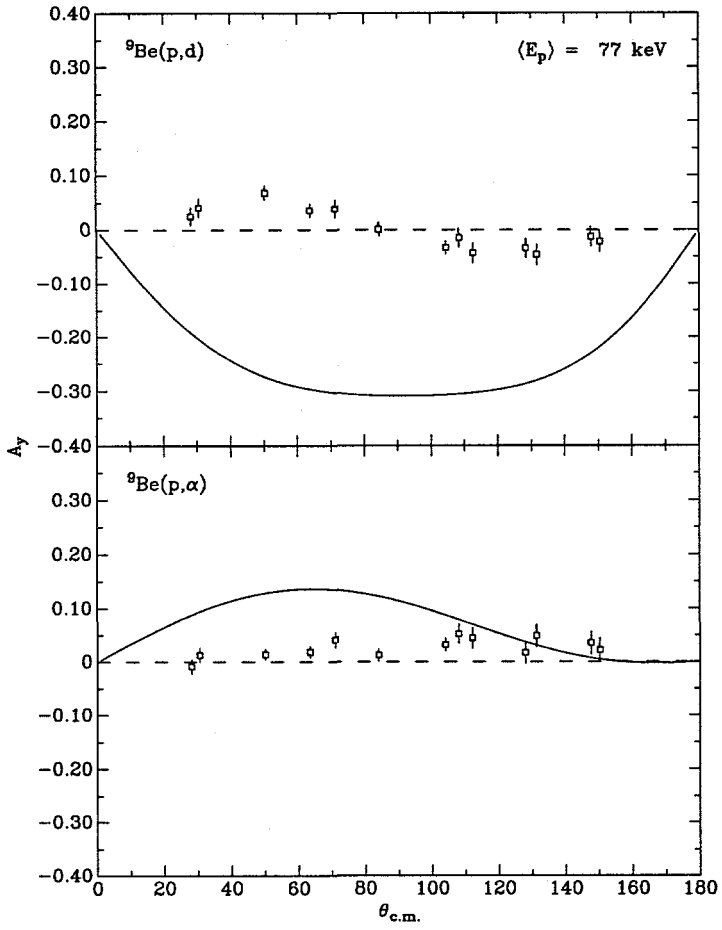

Figure 4.2–1: Analyzing powers measured at a mean proton energy of 77 keV. The anayzing powers predicted by the R-matrix parameters of Sierk and Tombrelllo [Sie73] are given by the solid curves.

cal applications, where the parameterizations are used for extrapolating cross-section data to the needed energies, often well below the range of laboratory measurements. A particularly important case is the $^{12}C(\alpha,\gamma)^{16}O$ reaction, whose rate is essential for understanding the evolution and nucleosynthesis of massive stars. The cross-section for this reaction at the needed energies is still uncertain, due to the presence of bound states just below the $^{12}C+\alpha$ threshold. A recent example of K- and R-matrix fits to this reaction are given in Azuma *et al.* [Azu94]. While these analyses yield consistent results for the low-energy extrapolation, there have been no systematic comparisons of the two techniques. There are significant differences in the two methods, particularly in the way that the background (i.e., nonresonant) amplitude is parameterized.

The elastic scattering of s-wave protons by ^{16}O provides a good test for these reaction theories. Like the p- and d-wave $^{12}C+\alpha$ reactions, this system also has a barely bound state, at $E_{c.m.}$=–0.105 MeV. It also provides an excellent opportunity to investigate the background terms, as ^{17}F has no other $\frac{1}{2}^+$ states up to E=5.96 MeV. In addition, the reduced proton width of the subthreshold state is well-constrained by the direct capture cross-section into this state.

K- and R-matrix fits to the experimental phase shifts were carried out. These results were compared to a potential-model calculation which reproduced the experimental phase shifts and the $^{16}O(p,\gamma)$ cross-section into the $\frac{1}{2}^+$ state. The value of the reduced proton width of the bound state obtained from the K-matrix fit disagreed with the value found with the R-matrix fit, and also with the value inferred from the capture cross-section into this state. A K-matrix analysis of the potential-model calculation revealed that the background contribution to the K-matrix is significantly more complicated than previously assumed. It thus appears that the nature of the K-matrix background in other cases, such as the $^{12}C+\alpha$ reactions, warrants further study. A paper describing this work has been published in Nuclear Physics A.

[Azu94] R. E. Azuma *et al.*, Phys. Rev. C, **50**, 1194 (1994).

[Hum90] J. Humblet, Phys. Rev. C, **42**, 1582 (1990).

[Lan58] A. M. Lane and R. G. Thomas, Rev. Mod. Phys. **30**, 257 (1958).

4.3 Radioactive Beams

4.3.1 Nuclear Astrophysics at HRIBF

J. C. Blackmon and A. E. Champagne for the RIBENS collaboration[1]

Reactions involving radioactive nuclei play an important role in stellar explosions, such as novae, supernovae, and X-ray bursts. Under the extreme temperatures and densities of these events, nuclear reactions occur on time scales as short as seconds. Thus, the radioactive products of one nuclear reaction may undergo a consecutive reaction before they have time to decay. Reactions involving radioactive isotopes may provide much of the energy generation in these events and produce elements not commonly produced in other astrophysical environments. Our understanding of such astrophysical phenomenon depends upon detailed knowledge of certain nuclear reactions involving radioactive isotopes. The work of the RIBENS collaboration at the Holifield Radioactive Ion Beam Facility (HRIBF) is centered on absolute cross-section measurements of these reactions using radioactive ion beams.

The Daresbury Recoil Separator (DRS) has been installed at HRIBF as the primary endstation for nuclear astrophysics experiments. Because these experiments are to be conducted in inverse kinematics, the scattered beam and recoiling reaction products emerge at small angles with nearly equal momentum. The DRS separates the reaction products from the incident beam in two long (1.2 m) crossed-field velocity filters. In addition, there are 12 other magnetic elements which provide a q/m focus of the recoil particles. The physical installation of the separator is complete, including two new diagnostic chambers (constructed at TUNL) which have been installed to assist in the determination of the optimal operating parameters. The computer control system for the separator is currently being developed.

The two elements of the focal-plane detector system which will be used in commissioning, a carbon-foil microchannel plate detector and a ΔE-E gas ionization counter, have been tested in experiments at Yale University. Two target chambers, one for use with large Si detectors and one for use with arrays of BaF detectors, are currently under construction at TUNL. The focal plane detectors and target chamber will be installed in late Summer 1996, and stable beam commissioning of the separator is scheduled for early Fall 1996.

The first beams at HRIBF will be proton-rich beams produced by particle transfer reactions. The radioactive atoms are produced in a high temperature target and diffuse into an ion source where they can be ionized and extracted. Beams of ^{17}F and ^{18}F, important nuclei in the hot-CNO cycle, are currently under development. We have performed a series of activation/release measurements on various refractory oxides to determine a possible target for production of fluorine beams. This is a particularly crucial test owing to the extreme

[1]Involving TUNL, Oak Ridge National Laboratory, Yale Univ., Colorado School of Mines, Notre Dame, Lousiana State Univ., Univ. of Bombay, Indian Inst. of Tech., and Univ. of Liverpool.

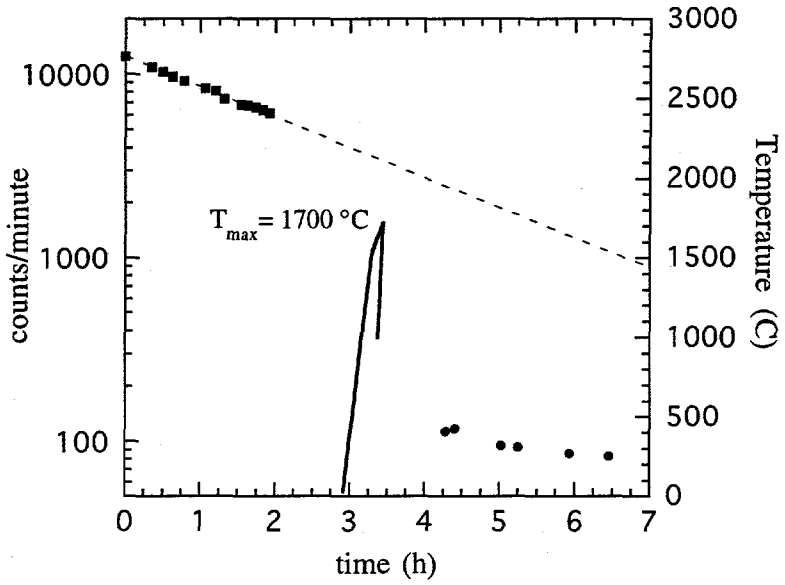

Figure 4.3–1: Activity of a mesh Al_2O_3 pellet before and after heating to 1700° C. The solid curve is the temperature of the sample. The dashed curve is the expected activity assuming no ^{18}F release from the sample.

reactivity of fluorine. The samples were first activated via the $^{18}O(p,n)^{18}F$ reaction. The activity was then measured, the samples heated, and the activity remeasured to determine the activity released. We have observed near total release of ^{18}F from a fibrous Al_2O_3 mesh when heated to temperatures greater than 1400° C. An example of the data from a release measurement where the sample was heated to 1700° C is shown in Figure 4.3–1. While these results are encouraging, "online" testing is required to determine if the release times are fast enough to allow for release of ^{17}F.

5 The Many-Nucleon Problem

5.1 High-Spin Spectroscopy and Superdeformation

As finite condensed-matter systems with strong short-range interactions, nuclei exhibit a tremendous variety of properties that depend on a number of factors including nucleon number, angular momentum, and excitation energy. One manifestation of the dependence on nucleon number is the existence of spherical and deformed gaps in the single-particle energy levels, leading to strong variations in nuclear shape. Our research program focuses on two major areas: (1) studies of nuclear properties associated with very elongated nuclear shapes, the superdeformed (SD) shapes, and (2) investigations of the evolution of nuclear collectivity as a function of particle number and also as a function of angular momentum and excitation energy. Among the collective modes investigated are the rotational excitations of prolate and oblate deformed nuclei, and octupole vibrational states in spherical nuclei.

With the near completion of the GammaSphere detection system at Lawrence Berkeley Laboratory, the experimental sensitivity for the study of nuclear collectivity has increased by orders of magnitude. We have now performed several experiments at this facility and many fascinating new results have come from these studies, perhaps the most exciting of which is the identification of discrete decay paths out of SD bands in ^{194}Hg.

5.1.1 Decay of Superdeformed Bands in ^{194}Hg

T. L. Khoo[1], *M. P. Carpenter*[1], *T. Lauritsen*[1], *E. F. Moore*, *R. V. F. Janssens*[1] *and the ANL-LBL-Orsay collaboration*[2]

Superdeformation has long been a central focus in nuclear structure studies. During the past decade, in excess of 100 SD bands have been identified in the A$\sim$150 and 190 regions. However, despite many attempts, there are no bands for which definite assignments of spin, parity, and excitation energy have been made. Recent calculations of the statistical decay from SD states by Døssing *et al.* [Døs95] suggest that one-step decay from SD bands may have a branching ratio of up to $\sim$5% and may be detectable.

Motivated by these expectations, we performed an experiment at GammaSphere to search for very high-energy γ-rays coincident with transitions in the SD bands of ^{194}Hg. The SD bands were populated using the ^{150}Nd(^{48}Ca,4n) reaction. The beam, delivered from the 88″ Cyclotron at LBNL, had a mid-target energy of 195 MeV. The γ-rays were

[1]Argonne National Laboratory, Argonne, Illinois 60439.
[2]Lawrence Berkeley Laboratory, Berkeley, CA 94720, CSNSM-Orsay, IPN-Orsay.

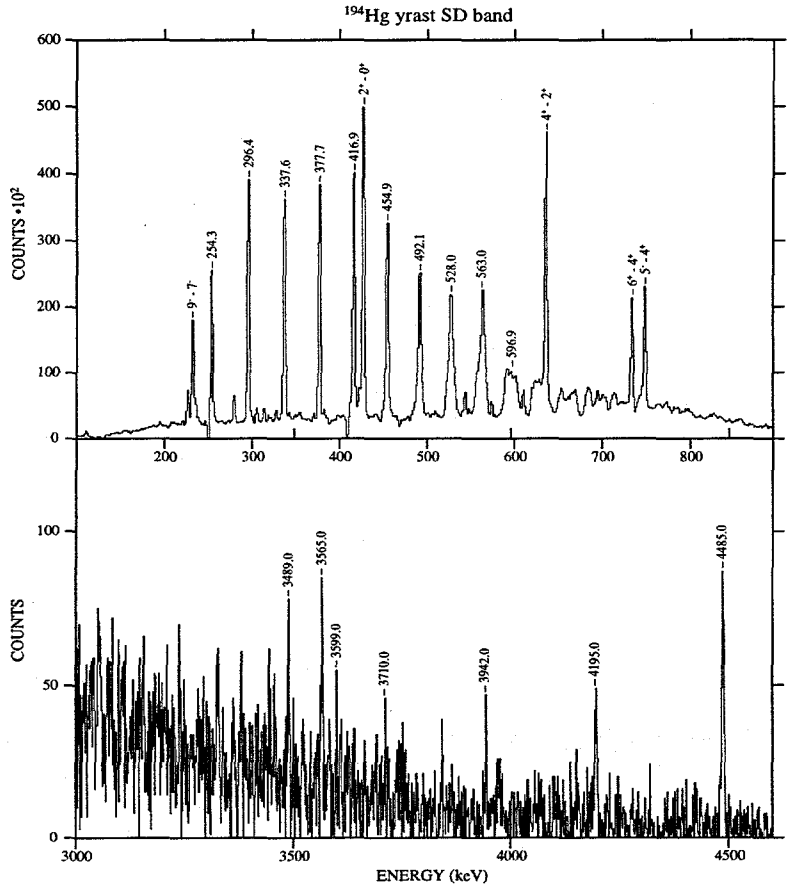

Figure 5.1–1: Low and high energy portions of the spectrum produced by combinations of double gates on members of the yrast SD band in ^{194}Hg. The γ-rays associated with single-step decays of the SD band are indicated on the lower panel of the figure.

detected using GammaSphere, which at the time consisted of 55 Compton Suppressed Ge detectors. The target consisted of 1.0 mg/cm^2 Nd evaporated on a thick Au backing.

In the data analysis, pairwise gates were placed on lines from the three known SD bands to produce one-dimensional spectra extending up to a γ-ray energy of 5.5 MeV. Several distinct peaks in the energy region from 3.4 to 4.5 MeV were found to be in coincidence with members of the yrast SD band of ^{194}Hg (see Figure 5.1–1). The highest energy γ-ray is at 4.485 MeV. We propose that these γ-rays represent one-step decays from members of the SD band to the "normal" states in ^{194}Hg. Further investigation of the coincidence relationships between these high-energy γ-rays and the low-lying transitions in ^{194}Hg has established the excitation energy to the 10^+ state in the SD band at 6.6285 MeV. This is the *first case* for which the excitation energies and spins have been assigned to states in a SD band in either the A$\sim$190 or 150 regions.

Following this first discovery, we have performed additional experiments at GammaSphere using the same reaction to further study ^{194}Hg, and have used similar reactions to populate SD states in ^{192}Hg and ^{193}Hg. To date, we have identified decay-out γ-rays in coincidence with SD band 3 of ^{194}Hg and are investigating possible two-step decays associated with the yrast SD band of ^{192}Hg.

[Døs95] T. Døssing *et al.*, Phys. Rev. Lett., **75**, 1276 (1995).

5.1.2 Lifetime Measurements in Identical Superdeformed Bands in ^{151,152}Dy

E. F. Moore, R. V. F. Janssens[1], *D. Nisius*[1,2] *and the ANL-LBL-LLNL collaboration*[3]

The phenomenon of the so-called "identical" superdeformed (SD) bands (i.e., bands with transition energies or moments of inertia identical to those in neighboring nuclei) has been one of the most surprising and inexplicable results in nuclear structure physics to date. A large number of cases are now known to exist in both the A$\sim$150 and A$\sim$190 regions of superdeformed nuclei [Bak95], but a satisfactory understanding of these observations is still lacking. Theoretical suggestions range from the possible presence of a new symmetry to subtle cancellation effects, from the continuous readjustment of the mean field with increasing angular momentum to new terms in the collective Hamiltonian. Our approach to this problem is to perform Doppler Shift Attenuation Method lifetime measurements to determine the deformation associated with pairs of identical SD bands. We have carried out experiments using Phase I of GammaSphere, consisting of 55 Compton suppressed Ge detectors, on identical SD bands in ^{151,152}Dy.

[1]Argonne National Laboratory, Argonne, Illinois 60439.
[2]Purdue University, West Lafayette, Indiana 47907.
[3]Lawrence Berkeley Laboratory, Berkeley, CA 94720, Lawrence Livermore National Laboratory National Laboratory, Livermore CA 94551.

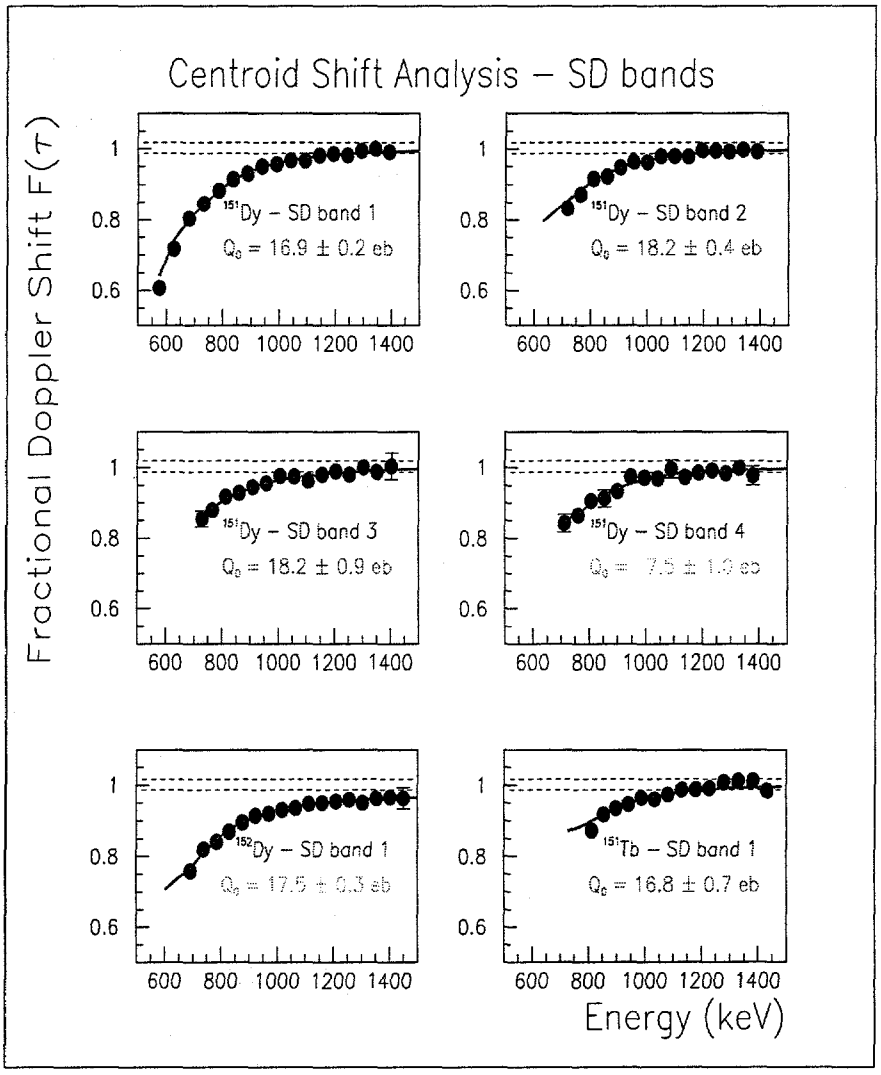

Figure 5.1–2: Fraction of full Doppler shift, F(τ), for transitions in the SD bands of ^{151,152}Dy and ^{151}Tb. Fits to the F(τ) values are represented by the solid curves and the best-fit quadrupole moment (Q_0) values are indicated on each panel.

In this measurement, we used the reactions ^{122}Sn(^{34}S,xn)$^{156-x}$Dy with 175 MeV beams provided by the 88″ cyclotron at LBL. The target consisted of 1.0 mg/cm^2 ^{122}Sn on a thick Au backing. Since SD bands in both Dy isotopes are populated at this beam energy and the recoiling nuclei slow down and stop in the same target/backing combination, our experiment amounts to a "differential" lifetime measurement; i.e., it is free from the systematic uncertainties associated with stopping power formulations. Therefore, we are able to make a direct comparison of the deformation in the two nuclei.

Some five SD bands are now known [Nis95] to exist in the nucleus ^{151}Dy. One of these, band 4 in the notation of Nisius *et al.* [Nis95], has transition energies corresponding to the mid-point of the transition energies of the yrast SD band of ^{152}Dy and is proposed [Nis95] to be the identical band of the ^{152}Dy yrast band. We have extracted the fraction of the full Doppler shift, F(τ), for transitions in the SD bands of ^{151}Dy and the yrast SD band of ^{152}Dy. We have performed fits to the centroid shift data, as shown in Figure 5.1–2. The fits were performed under the assumption of a constant intrinsic quadrupole moment (Q_0) within the band, and the side-feeding into each SD state was approximated by a rotational cascade consisting of 5 transitions, with the same moment of inertia as the main band and controlled by a single side-feeding quadrupole moment Q_{sf}.

As can be seen in Figure 5.1–2, within the experimental errors, the fits to the fractional Doppler shifts indicate that the "identical" SD bands have the same intrinsic quadrupole moment as well. It is also worth noting that there are significant differences in the Q_0 values for the various SD bands of ^{151}Dy. This result is consistent with the expectation that SD bands based on different intrinsic configurations, in particular the so-called "intruder" orbitals, have different deformations. Theoretical calculations of the deformation driving properties of the various configurations thought to be present in the SD bands of ^{151,152}Dy are in progress.

[Bak95] C. Baktash, B. Haas, and W. Nazarewicz, Annu. Rev. Nucl. Part. Sci. **45**, 485 (1995).

[Nis95] D. Nisius *et al.*, Phys. Lett. **B 346**, 15 (1995).

5.1.3 Lifetime Measurements in Identical Superdeformed Bands in ^{192,194}Hg

E. F. Moore, T. L. Khoo[1], T. Lauritsen[1], R. V. F. Janssens[1] and the ANL-LBL-Orsay collaboration[2]

For the Hg measurements, we used the reactions ^{148}Nd(^{48}Ca,4n)^{192}Hg and ^{150}Nd(^{48}Ca,4n) ^{194}Hg at 205 and 202 MeV, respectively. The beams were provided by the 88″ cyclotron

[1]Argonne National Laboratory, Argonne, Illinois 60439.
[2]Lawrence Berkeley Laboratory, Berkeley, CA 94720, CSNSM-Orsay, IPN-Orsay.

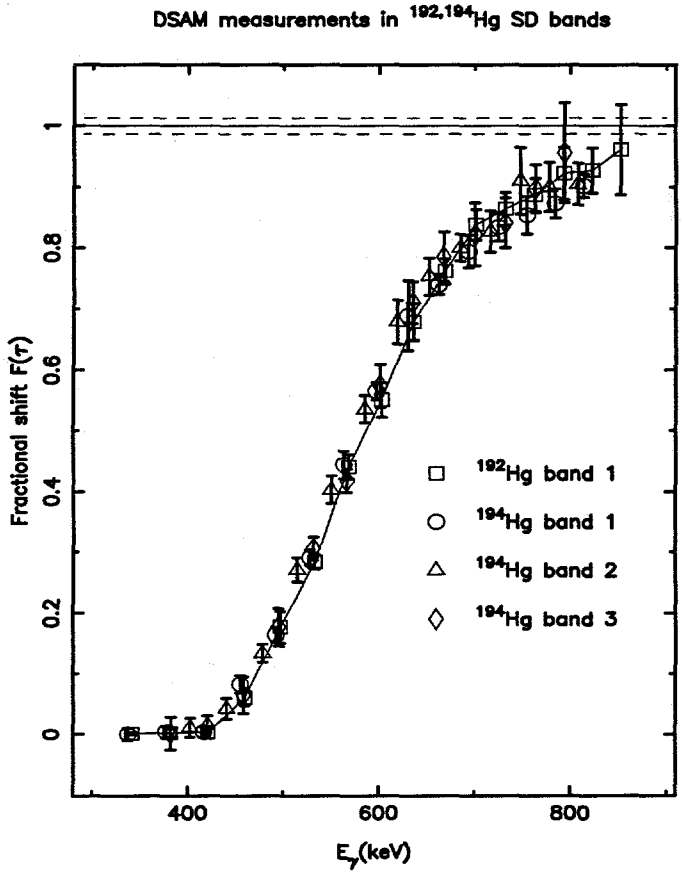

Figure 5.1–3: Fraction of the full Doppler shift extracted for bands 1–3 in ^{194}Hg and band 1 of ^{192}Hg. The dashed horizontal lines represent the spread in recoil velocities due to the slowing down of the beam through the target.

at LBL. The targets consisted of 1.0 mg/cm^2 Nd on thick Au backings. The similarities in target composition and reactions used to populate states in ^{192}Hg and ^{194}Hg will again allow for a nearly direct comparison of the deformations associated with the identical SD bands [Bak95] of the two Hg isotopes. The centroid shifts extracted for the three known SD bands in ^{194}Hg and for the yrast SD band of ^{192}Hg are presented in Figure 5.1–3.

We are in the process of extracting in-band quadrupole moments from fits to the fractional Doppler shifts in the SD spectra. In addition to the F(τ) information, we are performing detailed lineshape analyses of the SD bands. Using a model similar to that described above for ^{151,152}Dy, we have extracted intrinsic quadrupole moments for the Hg SD bands. In particular, preliminary results indicate that the quadrupole moments associated with the

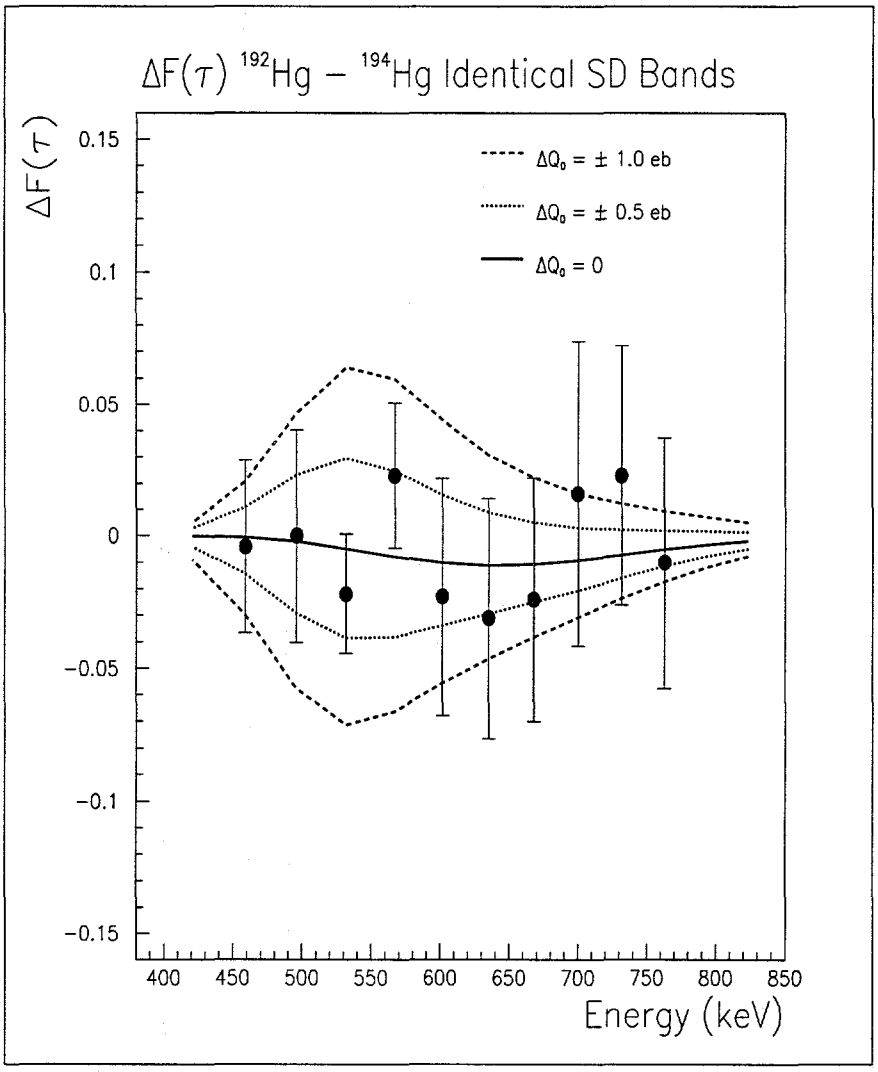

Figure 5.1–4: Difference in the fraction of the full Doppler shift F(τ) for transitions in the identical SD bands of ^{192,194}Hg. Calculated F(τ) differences corresponding to differences in the Q_0 values of the two bands are indicated by the lines.

identical SD bands in ^{192,194}Hg are the same within experimental errors (see Figure 5.1–4).

[Bak95] C. Baktash, B. Haas, and W. Nazarewicz, Annu. Rev. Nucl. Part. Sci. **45**, 485 (1995).

5.2 Phenomenology of Preequilibrium Nuclear Reactions

The exciton model of preequilibrium nuclear reactions provides a simple way to describe the continuum energy and angular distributions of particles emitted during energy equilibration in light particle induced reactions at incident energies of about 14 to 200 MeV. Over the years the model has proven to be quite adaptable to the inclusion of additional physics as well as remarkably successful at describing experimental results. Because of its simplicity, its physical transparency, its utility, and its adaptability, the exciton model continues to be used in spite of the development of more microscopic and quantum mechanical models.

The TUNL exciton model code PRECO-E and its predecessors have been used around the world (either alone or as modules in Hauser-Feshbach codes) in applied projects, in support of Radioactive Ion Beam studies, and in other basic physics research. Model and code development has progressed by using relatively simple physical concepts appealing to available data to direct choices between alternative formulations, and by providing values for key model parameters that cannot be obtained from independent sources.

Current work is aimed toward a revised version of the code with a set of global model inputs that will allow reliable calculation of unmeasured or unmeasureable reaction cross-sections without the use of adjustable parameters. Work is now directed almost exclusively at improving the calculation of the energy spectra, concentrating first on nucleon-nucleon (NN) reactions, which are the most straightforward to address.

5.2.1 Information from 14 MeV Data

C. Kalbach Walker

Most of the general input needed for exciton model calculations for NN reactions is well specified [Kal95a]. Recent work [Kal95a, Kal95b] also indicates preliminary global values for model-specific parameters for systems at incident energies of 18 to 25 MeV and confirms that isospin is conserved in the preequilibrium phase of the reaction, though it appears to be substantially mixed at equilibrium. At 90 MeV isospin appears to be mixed, though other model input is unchanged. Since most of the spectra for these studies were from proton induced reactions, the model has since been applied at incident energies of 14 to 15 MeV where neutron projectile information abounds.

A set of energy spectra were gathered from the literature for study: 15 from (n,xn), 3 from (p,xp), and 21 from (n,xp) reactions. Many of the (n,xn) and a few of the (n,xp) spectra are supported by multiple measurements from different laboratories. Target masses range from 24 to 209. As at higher energies, the ability to reproduce the relative yields in the inelastic and exchange channels of a reaction is an important test of the calculations.

One of the main factors influencing these calculated relative yields is the ratio of the mean square matrix elements for the residual interactions between like and unlike nucleons.

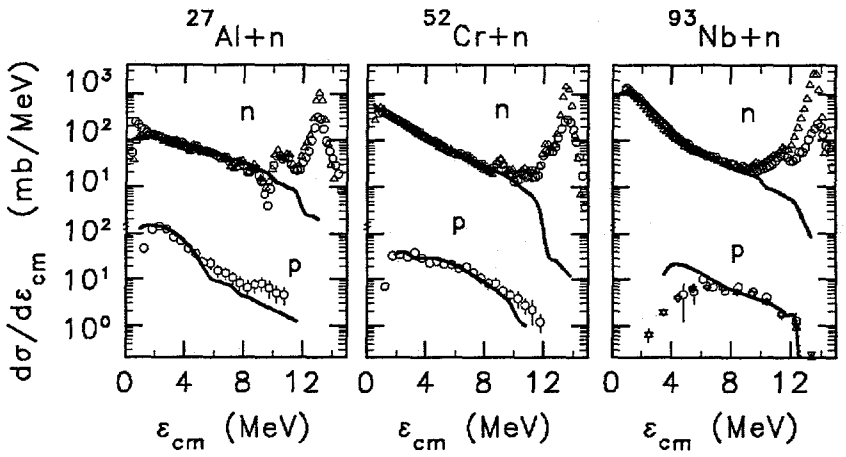

Figure 5.2–1: Comparison between calculated and experimental energy spectra for sample systems at 14 to 15 MeV. The points show the data, while the curves show the results obtained from PRECO-E.

In earlier work it was determined that $(M_{pp})^2$=1.67$(M_{np})^2$. Since the data were not sensitive to $(M_{nn})^2$, it was provisionally assumed that $(M_{nn})^2$=$(M_{pp})^2$. Calculations for the 14–15 MeV systems were run with these assumptions and the results were compared with the experimental spectra. This showed the calculations consistently underestimating the intensity of the (n,xp) channel relative to the (n,xn) channel; a situation that was significantly improved simply by setting $(M_{nn})^2$=$(M_{np})^2$. At the same time, the normalization of the matrix elements had to be adjusted so as to maintain the sum $(M_{nn})^2$+$(M_{pp})^2$+2$(M_{np})^2$ constant, thus leaving the previous results for proton induced reactions essentially unchanged.

Because the evaporation components are much more important at 14 to 15 MeV than they are at higher energies, especially for light targets, much greater attention needs to be paid to the equilibrium state densities used in the calculations. Previously PRECO-E used Fermi gas state densities. At 14 MeV, this produces an unphysical turn up at very low values of the excitation energy in the residual nuclei. Thus the code was modified to go over to a constant temperature state density at low E. This also allows the evaporation components to extend up to the physical ground state energy in the residual nucleus rather than being cut off by the pairing and/or shell corrections. This is essential to the prediction of an adequate amount of secondary particle emission.

Finally, two small changes were made in the neutron reaction cross-sections which are obtained from a simple parameterization [Cha81] of the reaction cross-sections from the optical potential of Mani *et al.* [Man63]. First the arbitrary "barrier" of 2.4 MeV was re-

duced to 0.5 MeV. Second, based on comparisons between calculated reaction cross-sections and experimental total and non-elastic cross-sections [McL88], the calculated values were reduced by a factor of 0.7+0.3A/40 for A<40. A similar reduction for A<100 was already in place for protons.

With these changes, the level of agreement seen with literature energy spectra at incident energies of 14 to 15 MeV is comparable to that found in earlier comparisons at higher incident energies. Those earlier results remain virtually unchanged. Sample comparisons are shown in Fig. 5.2–1 where the (n,xn) data are from Osaka (Takahashi *et al.*) and Sendai (Baba *et al.*), and the (n,xp) data are from Livermore (Grimes *et al.*), Vienna (Fischer, Uhl and Vonach), and Kyushu (Koori, Ohsawa and Kumabe). The main difficulties seen in the calculations are with evaporation intensities for minor channels.

[Cha81] A. Chatterjee, K. H. N. Murthy, and S. K. Gupta, Pramana, **16**, 391 (1981).

[Kal95a] C. Kalbach, J. Phys. **G21**, 1519 (1995).

[Kal95b] C. Kalbach, Acta Phys. Slov. **45**, 685 (1995).

[Man63] G. S. Mani, M. A. Melkanoff, and I. Iori, *Neutron penetrabilities using an optical model potential*, Technical Report CEA 2380, Centre d'Études Nucléaires de Saclay, 1963.

[McL88] V. McLane, C. L. Dunford, and P. F. Rose, *Neutron Cross Sections, Vol. 2 Neutron Cross Section Curves*, Academic Press, Harcourt Brace Jovanovich, 1988.

5.2.2 Exploring the Low-A, Low-E Limit

C. Kalbach Walker

The exciton model implemented in PRECO-E is a statistical model using average state density expressions and phase space arguments in calculating both emission rates and internal interaction rates. The model should thus be applicable only where a statistical number of states is accessible to the system. Typically, statistical models are applied to reactions on nuclei of around mass 40 to 50 or higher. Yet in various applications it is sometimes necessary to estimate cross-sections on nuclei as light as ^{12}C. Thus, a small investigation is underway to determine the range of incident energies at which the code PRECO-E becomes a useful tool for such light nuclei.

The work in the previous section shows that at 14 MeV, the model already does very well for ^{24}Mg and ^{27}Al. On the other hand, the (n,xn) spectrum on ^{12}C is dominated by just a few discrete peaks and cannot be reproduced by a model which yields a smooth spectrum.

As additional data become available, we plan to seek a rough criterion for the applicability of the exciton model and the code PRECO-E based on the target mass and the excitation energy of the system. Preliminary work has been carried out on the 14.1 MeV (n,xn) data for ^{12}C, ^{14}N, and ^{16}O. The ^{14}N spectrum is best reproduced because of the odd-odd nature of (and thus the higher state density in) the residual nucleus. The spectrum for ^{16}O is better reproduced than that for ^{12}C, though both experimental spectra show significant structure. Additional (n,xn) data on ^{19}F at 14 MeV and on ^{12}C and ^{16}O at 18 MeV will also be analyzed, and additional data will be sought in the literature.

5.2.3 Calculations Supporting Radioactive Ion Beam Projects

C. Kalbach Walker

The U.S. Nuclear Reaction Data Network has set up a working group to coordinate with the Radioactive Ion Beam (RIB) community to help meet their needs for reaction data. Much of the resulting work in support of those needs has been and will be done using comprehensive reaction codes such as the Hauser-Feshbach model code GNASH from Los Alamos National Laboratory and ALICE from Lawrence Livermore National Laboratory. GNASH contains an earlier version of PRECO.

Because of important differences between the current version of PRECO-E and the older version contained in GNASH, PRECO-E calculations have been performed covering the emission of the first and second particles in important reactions for ISOL-type RIB facilities. The reactions ^{64}Zn(p,xn) and ^{70}Ge(p,xn) were considered at a set of twelve incident energies from 15 to 100 MeV. Calculations were run assuming isospin to be conserved during the equilibration phase of the reaction at all incident energies. For energies greater than 50 MeV, the calculations were repeated assuming isospin to be fully mixed, as it is known to be at 90 and 100 MeV. The duplicate calculations show that the importance of this choice is greatest (a factor of 1.5 in the preequilibrium part of the spectra) at 100 MeV, decreasing to about a 20% effect at 50 MeV.

Once several open questions, including the transition in isospin behavior with incident energy, are resolved, the new version of PRECO-E will be incorporated into GNASH.

5.3 Neutron Scattering

5.3.1 Analyzing Power Measurements for ^{12}C(n,n)^{12}C from 2 to 8 MeV

C. D. Roper, R. L. Walter, R. T. Braun, Q. Chen, Z. Chen, A. S. Crowell, D. E. González Trotter, C. R. Howell, F. Salinas, H. R. Setze and W. Tornow

In the Spring of 1995 we initiated a set of measurements of $A_y(\theta)$ for neutrons elastically scattered from ^{12}C for energies ranging from 2 to 8 MeV. In order to perform these measurements, the Neutron Time-of-Flight facility (NTOF) was upgraded to include a neutron polarimeter and a charged-particle polarimeter. Using the ^{2}H(d,n)^{3}He reaction we made measurements of $A_y(\theta)$ for 28 neutron energies from 3.92 to 8.47 MeV at angles from 25° to 145° in 10° or 20° steps.

The polarimetry requirements of the 1995 measurments called for the installation of a neutron polarimeter and a deuteron polarimeter. The main purpose of the deuteron polarimeter was to monitor and tune the Atomic Beam Polarized Ion Source (ABPIS) for maximum beam polarization. Therefore, a charged-particle polarimeter was installed in the NTOF beam leg 1.6 m upstream from the neutron production gas cell. The polarimeter chamber was designed to handle both gas and solid targets for various proton and deuteron polarimetry reactions. The detectors in this chamber can be mounted in and out of the horizontal plane for determination of the vector as well as the tensor components of the polarization. Because of the problems involved in extracting the deuteron tensor polarization components of both spin states accurately, we switched to the spin-filter polarimeter which became operational in October of 1995.

Since we are just now becoming familiar with the spin-filter polarimeter, we continue to measure the neutron beam polarization directly using the ^{4}He(n,n)^{4}He scattering reaction. The polarimeter consists of a ^{4}He high-pressure (100 atm) gas cell with a ten percent admixture of xenon to provide proper scintillation. This ^{4}He/Xe mixture is contained in a thin-walled, cylindrical cell with photomultiplier tubes mounted on the top and bottom to detect the scintillations. This gas scintillator is mounted 70 cm downstream from the neutron source. The neutron flux is collimated to minimize scattering from the flanges and frame of the cell. The two neutron side detectors are shielded from the neutron source by copper shadow bars. With the neutron polarimeter in place, the angular range of the main NTOF side detectors that view the carbon scatterer is restricted to angles 45° or greater. Therefore, the neutron polarimeter was removed for the ^{12}C(n,n)^{12}C $A_y(\theta)$ measurements at lab angles of 25° and 35°, and the spin-filter polarimeter was used to monitor the deuteron polarization.

A new data acquisition system was developed to replace the older NTOF system because of the addition of the neutron polarimeter, the charged-particle polarimeter, and the spin-filter polarimeter. The electronics modules used in the older NTOF system were replaced by

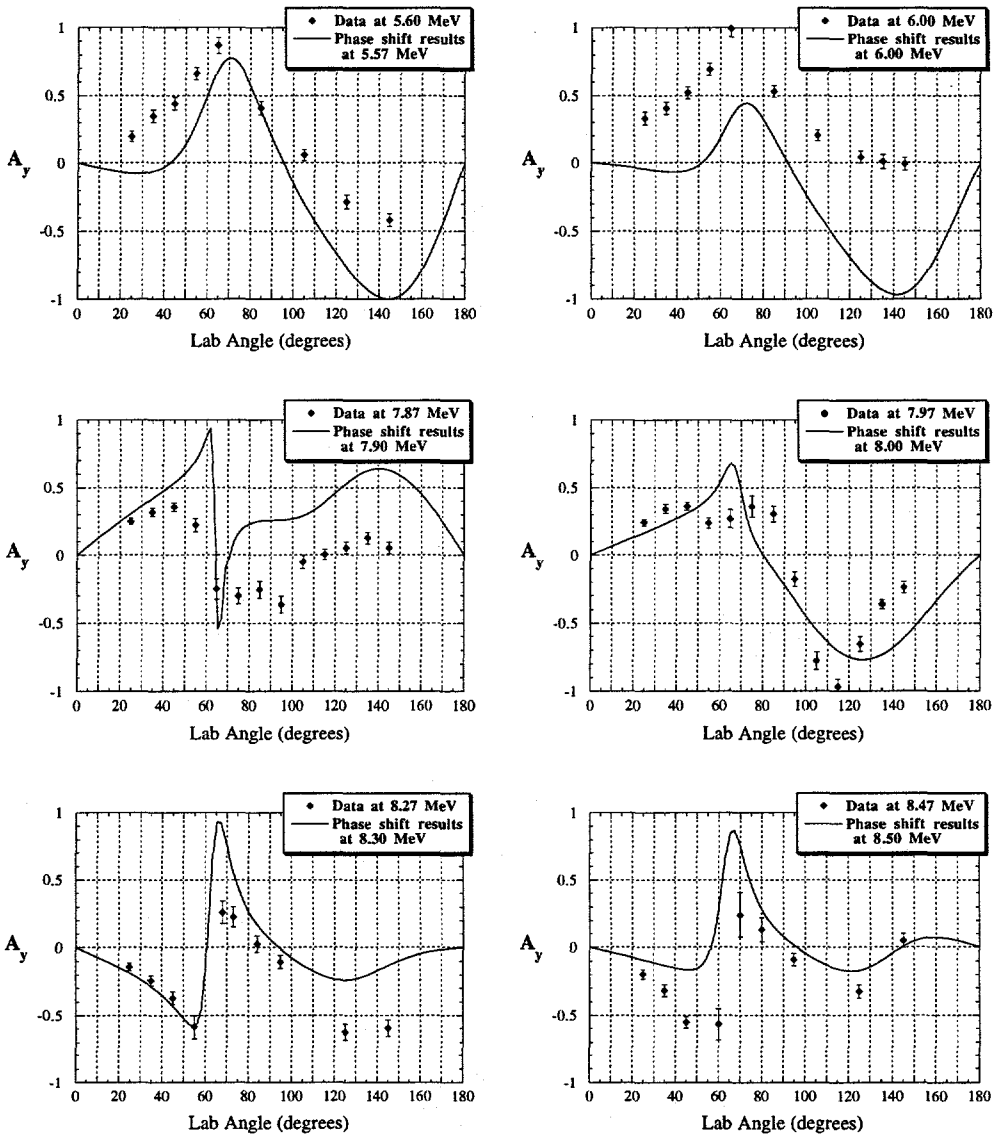

Figure 5.3–1: On-line $A_y(\theta)$ data for the ^{12}C(n,n)^{12}C reaction compared to the results from the phase-shift library used by Braun *et al.* The $A_y(\theta)$ data shown have not been corrected for finite size of the ^{12}C scatterer or multiple-scattering effects.

the LeCroy CAMAC 2249 12-channel charge-integrating ADC for pulse-height spectroscopy and pulse-shape discrimination, and the Phillips CAMAC 7186 16-channel TDC for time-of-flight analysis. The new pulse-shape discrimination method requires both a wide gate and a narrow gate to be supplied to the ADC for the linear signal from each neutron detector. Using the digitized pulse height from the wide gate and narrow gate, a 2-D histogram was produced which revealed a distinct separation between neutrons and gamma rays. The best pulse-shape discrimination was obtained using a 50 ns narrow gate and a 400 ns wide gate. Along with the new data acquisition electronics, the data acquisition software was rewritten and an on-line analysis package was developed.

One of the primary motivations for measuring $A_y(\theta)$ for ^{12}C(n,n)^{12}C elastic scattering was the discovery that the analyzing power predicted by the current phase-shift library compiled at TUNL was producing questionable values for the polarization dependent detector efficiency corrections applied to the high-accuracy n-p $A_y(\theta)$ data of Braun *et al.*, see Section 2.1.2. Shown in Figure 5.3–1 are on-line results for $A_y(\theta)$ from our measurements at six energies compared to values produced by the current phase-shift library. The data have not been corrected for multiple scattering or finite-geometry effects. The energies shown in Figure 5.3–1 were selected because $A_y(\theta)$ is predicted to be fairly constant as function of energy in these energy regions. For this reason, we believe that the clear inconsistencies between our preliminary data and the phase-shift results are not due to the neutron energy spread or slight differences in energy calibrations. Furthermore, multiple scattering or finite geometry corrections do not account for the discrepancies, especially in the regions were the signs of the calculated and measured analyzing powers differ. These $A_y(\theta)$ data will be employed in a new phase-shift analysis for n-^{12}C scattering to provide a more reliable description of this interaction and to provide accurate corrections for the n-p experiment of Braun *et al.*

5.3.2 The Nuclear Mean Field: Dispersion Relations and Nucleon Scattering

R. L. Walter, C. R. Howell, W. Tornow, R. T. Braun, C. D. Roper and Z. M. Chen[1]

For the past five years the Neutron Time-of-Flight (NTOF) group has been involved in measurements and analyses related to the nuclear mean field in the energy range from −50 to +80 MeV. The basis of the analyses are neutron-scattering differential cross-section $\sigma(\theta)$, analyzing power $A_y(\theta)$, and neutron total cross-section σ_T data. Nine nuclei were investigated, ranging in mass from ^{27}Al to ^{209}Bi. The manner in which the mean field is parameterized uses the dispersive optical model (DOM). With this model, it is possible to connect the scattering regime (positive nucleon energies) with the negative energy region

[1]Exchange visitor from Tsinghua University, Beijing, PRC.

for the purpose of studying or predicting bound-state properties, such as binding energies, spectroscopic factors, spectral functions, and occupation probabilities. The power of this model is that it accounts for the energy dependence of the strength and the radius parameter of the central real potential in a natural way, and it allows one to use the wealth of nucleon-nucleus scattering data that is available in the literature to characterize the extension of the nuclear mean field into the shell-model region in a consistent manner. It also assists in determining the formulation of the energy dependence of the absorptive potential in relation to the Fermi energy as a reference point.

For the analyses we use a version of the global optical model search code GENOA into which several modifications have been inserted to allow for the most recent suggestions of Mahaux and Sartor [Mah91] for the DOM potentials. We have also added relativistic kinematics and relativistic corrections to the potentials for the Schrödinger equation.

In constructing the DOM, one must parameterize the absorptive potentials for a large energy range beyond that of the analyses. To do this we rely on extrapolation via energy-dependent formulation of the surface and volume absorptive potentials. Until now, we have relied on differential cross-section data below either 26 or 40 MeV, depending on the nucleus, and total cross-sections up to 100 MeV. For some of the nuclei, there are now σ_T measurements with $\pm 1\%$ accuracy available [Fin93]. Our major problem is that the signature for the relative strengths of the volume and surface absorptions is weak in the current data. To improve the sensitivity, we decided to obtain more $\sigma(\theta)$ data in the 40 MeV region.

For this purpose we combined efforts with the NTOF group (H. Tang, Z. Zhou, B. Qi, Y. Du and others) at the China Institute of Atomic Energy (CIAE) in Beijing. The effort has been supported in part by the U.S. and Chinese National Science Foundations. (One facet of this collaboration is to allow scientists from the CIAE to visit TUNL for extended periods to analyze our CIAE data and to participate in the TUNL few-nucleon program of the neutron group. Since the inception of this collaboration, five scientists have visited TUNL for 4–6 month terms under this exchange program.) At the CIAE we have initiated a program with a beam of "monoenergetic" neutrons having an energy up to 40 MeV. The neutrons are produced via the ^{3}H(d,n) reaction. This neutron source is to be used in high-energy scattering experiments and in few-nucleon reaction studies.

By June of 1996 we completed four measurements over a period of four beam times: calibration of the efficiency of the three-detector cluster of the NTOF system as a function of neutron energy and detector bias; determination of $\sigma(\theta)$ for the ^{3}H(d,n) reaction at 12, 16, and 19 MeV; determination of $\sigma(\theta)$ for ^{12}C(n,n) at 37 MeV from 14° to 155°; and determination of $\sigma(\theta)$ for ^{209}Bi(n,n) at 37 MeV from 14° to 160°. The ^{12}C data will be used in continuing our study of the n+^{12}C interaction as a function of energy. The ^{209}Bi data relate to our analysis recently submitted to Phys. Rev. where our dispersive optical model for ^{209}Bi is compared to our model for ^{208}Pb, which, for the most part, verified the conclusions of Mahaux and Sartor [Mah91] regarding the occupation probabilities for

neutron-particle and neutron-hole states in ^{208}Pb. Preliminary analysis of the new ^{209}Bi data shows it to be consistent with data taken earlier at MSU at 40 MeV for ^{208}Pb; however, the new data extend the angular range and should be more sensitive to the absorption. It now appears that the surface absorption of the DOM model is too large in this higher energy region. Before final conclusions can be drawn, the multiple scattering corrections to the scattering data must be carefully calculated and applied.

The DOM potentials for describing bound and scattering states for n+^{120}Sn and n+^{93}Nb in the –20 to +80 MeV range have been restudied (by Z.M. Chen) with the inclusion of the relativistic corrections and the alterations to the absorptive potential suggested in the work of Mahaux and Sartor [Mah91]. The analysis used the improved (in speed) code of TUNL for the DOM. For both of these systems, all elastic scattering data for $\sigma(\theta)$, $A_y(\theta)$, and the new high-accuracy σ_T data of Finlay *et al.* [Fin93] out to 80 MeV were well described with models having straightforward energy dependences; i.e., similar to those simple forms that have worked well for us for other nuclei. However, for these two nuclei we were able to force the surface absorption to smaller values at the higher energies by only slightly altering the good quality of the fits to the data across the entire energy range. Single-particle properties were calculated and compared to available information for neutron-particle and neutron-hole states in ^{120}Sn. In many cases, the calculated binding energies and the spectroscopic factors are in reasonable agreement with the reported values.

[Fin93] R. W. Finlay *et al.*, Phys. Rev. **C47**, 237 (1993).

[Mah91] C. Mahaux and R. Sartor, Adv. in Nucl. Phys. **20**, 1 (1991), and refs. therein; see also Nucl. Phys., **A528**, 253 (1991).

5.3.3 Energy and Orientation Dependence of Neutron Depolarization in a Large Single Crystal of Ferromagnetic Holmium

C. R. Gould, D. G. Haase, N. R. Roberson, and V. P. Alfimenkov[1] *, A. N. Chernikov*[1]*, L. Lason*[1]*, Yu. D. Mareev*[1]*, V. V. Novitsky*[1]*, L. B. Pikelner*[1]*, V. R. Skoy*[1] *and M. I. Tsulaya*[1]

We have measured the depolarization of epithermal neutrons (1.7 to 59 eV) in magnetic domains of a single 2.0 cm diameter cylindrical crystal of ferromagnetic holmium. The experiment was carried out at the Frank Laboratory, JINR, using a holmium crystal prepared at the Materials Preparation Center in Ames, Iowa. The crystal was originally prepared for tests of time-reversal symmetry in polarized neutron transmission through an aligned

[1]Frank Laboratory of Neutron Physics, JINR, Dubna, Russia.

holmium target. Depolarization of the neutron beam dilutes any time-reversal violating signal and is a special concern in experiments at resonance energies using epithermal neutrons.

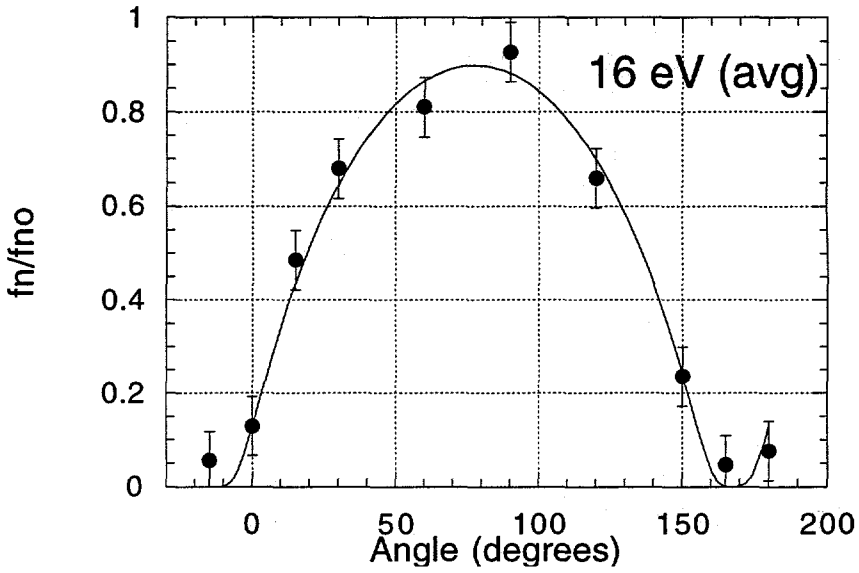

Figure 5.3–2: The measured neutron polarization transmission f_n/f_{no} as a function of the crystal orientation at different energies for the transverse geometry. The 16 eV (avg) data are the average of data from neutron energies of 14, 16, and 18 eV. The dotted lines indicate f_n/f_{no} calculated from the model.

For our experiments the neutrons were polarized by a dynamically polarized proton target and polarization-analyzed using a statically polarized rare earth spin filter. Neutrons from the IBR-30 pulsed source were polarized by passage through a cryogenic dynamically polarized proton target. The neutrons then entered a drift tube in which there was a guide field of 400 gauss. The holmium target was located in a cryostat at 4.2 Kelvin in the neutron guide field. The cylindrical axis of the crystal was oriented perpendicular to the neutron beam and could be rotated by a shaft into the cryostat. Upon exiting the holmium target the neutron beam was guided to a cryogenic statically polarized natural Dy target. Resonances in Dy at 1.7, 2.7, 14, 16, 18, 36, and 59 eV have spin dependent neutron transmission and act as analyzers for neutrons with these energies. The neutrons passing through the Dy analyzer were then counted by a ^{3}He ionization detector. The neutron energies were determined by the time-of-flight technique.

The neutron depolarization was measured in two different arrangements. In each case

the neutron momentum, the neutron spin, and the c axis of the holmium crystal were in the same plane. In the transverse geometry, the neutron spin was perpendicular to the neutron momentum; whereas in the longitudinal geometry, the spin was parallel to the neutron momentum. The polarization transmission f_n/f_{no} was measured in the transverse geometry at ten orientations, θ=–15^o to 180^o.

We have found that the salient characteristics of the depolarization results can be explained by a model in which the ferromagnetic domains are laminar or needle-like with an average thickness of 60 microns and length of 900 microns. The model and the data are compared in Figure 5.3–2. A complete report of the work has been submitted to the Journal of Applied Physics. The measurements are not only the most complete characterization to date of bulk domains in a ferromagnet, but they also show that it is possible to transmit polarized epithermal neutrons (E_n >16 eV) through such a crystal for time-reversal tests.

5.4 High Resolution Resonance Studies at Münster and Bochum

G. E. Mitchell, M. Berheide[1], C. Rolfs[1] and W. H. Schulte[1]

Significant improvements have been made to the energy resolution characteristics of the 400-kV Münster accelerator [Sch92]. The HV terminal ripple is usually less than 12 V. The stability and reproducibility of the ion beam energy were less than 3 eV. For many of these experiments windowless gas targets were used. The target thickness could be varied from less than a monolayer of target material to relatively thick targets. Recent results include measurements with neon targets that directly measure the difference in Doppler broadening for solid and gas targets. The German group has moved to Ruhr-Universität Bochum, where there is a Tandem Dynamitron accelerator. A new large volume 4π γ-ray detector has been developed. This high efficiency summing crystal is ideal for determining resonance strengths and widths.

5.4.1 Vibrations of Solid Neon

A cyrogenic target UHV system has been built to study narrow nuclear resonances [Ber95]. A differential pumping unit reduces the pressure near the target to $\approx 1 \times 10^{-10}$ Torr. The target chamber allows for close geometry for the γ-ray and charged-particle detectors in order to obtain a large solid angle. The crucial part of the system is a liquid-helium cooled sample holder mounted on a goniometer. Samples can be cooled below 10 K even at a beam power of about 1 W. Alternatively, a copper tube with a gas inlet can be attached to the cryostat in order to perform measurements on thin windowless gas targets at low temperatures. First measurements were performed with thin ^{21}Ne gas targets. The neon gas was cooled near its freezing point, which is about 11 K under the experimental conditions. The 272 keV resonance in ^{21}Ne(p,γ)^{22}Na was studied. Under similar conditions (except that the target temperature was about 8 K) a measurement of the 272 keV resonance in the ^{21}Ne(p,γ)^{22}Na reaction was performed with a solid neon target. An extremely large Lewis effect is observed (peak to plateau of 2.5 to 1) for the solid target. The shape of the Lewis peak is affected by both electronic stopping and motion of the target atoms. The gas target (under similar low temperature conditions) gives the largest Lewis peak ever observed. We used the information from these energy-loss spectra in fitting the observed Lewis peak for the solid target. The resulting experimental value for the Doppler width [Ber96] agrees with estimates using an effective temperature calculated from the standard Debye temperature for bulk solid neon. These results also provide the first direct measurement of the difference in the (low) temperature dependence of the Doppler broadening for solid and gas targets.

[1]Ruhr-Universtät Bochum, Germany.

5.4.2 Precision Determination of Resonance Strengths and Widths

A large volume 4π γ-ray detector with a 12″x12″ NaI crystal has been developed. The detector has a large efficiency that is precisely determined, the summing properties make analysis of the γ-ray spectra straightforward, and the 4π geometry integrates over angular distributions. This detector is ideal for the study of low-energy resonances of relevance to astrophysics. However, the availability of a 450-kV electrostatic accelerator and a 4-MV tandem accelerator make it possible to measure a complete and consistent set of resonance parameters over a wide energy range. The very high stopping power at projectile energies of a few hundred keV makes low-energy resonances attractive for depth profiling measurements. However, the relevant resonance parameters have not been well determined. To achieve the full potential, determination of the parameters of these low energy resonances, as well as precise determination of the higher-energy (few MeV) resonances is required. Our goal is a precise and consistent measurement of the resonance parameters for resonances in ^{28,29,30}Si in the relevant energy range. Most of these measurements have now been performed and the analysis of these data is in progress.

[Ber95] M. Berheide *et al.*, Nucl. Instr. and Meth., **B99**, 289 (1995).

[Ber96] M. Berheide *et al.*, to be published, 1996.

[Sch92] W. H. Schulte *et al.*, Nucl. Instr. and Meth., **B71**, 291 (1992).

5.5 Nuclear Data Evaluation for A=3–20

C. M. Cheves, J. F. Guillemette, D. R. Tilley, H. R. Weller and J. G. Zeibel

TUNL efforts in nuclear data evaluation and dissemination are summarized as follows:

5.5.1 Data Evaluation Activities

A=3,4: Reviews for the A=3 and 4 systems were carried out at TUNL and published respectively as "Energy Levels of Light Nuclei A=3," *Nuclear Physics* **A474** (1987), and "Energy Levels of Light Nuclei A=4," *Nuclear Physics* **A541** (1992). (The A=4 review was done in collaboration with G. M. Hale of Los Alamos National Laboratory). TUNL continues to survey the literature and compile references for A=3 and 4 on a regular basis and occasionally carries out literature searches for few-nucleon information in response to requests from researchers.

A=5–20: TUNL now carries on literature coverage for this mass region on a continuing basis, compiling bibliographical listing for relevant experimental and theoretical work, utilizing several resources including Monthly Updates from the National Nuclear Data Center (NNDC), Current Contents on Diskette with Abstracts, and Physics Abstracts. The review of A=16–17 was completed in late 1993 and published as "Energy Levels of Light Nuclei A=16–17," *Nuclear Physics* **A564** (1993). The review for A=18–19 was completed in 1995 and published as "Energy Levels of Light Nuclei A=18–19," *Nuclear Physics* **A595** (1995). A preliminary version of A=20, in collaboration with S. Raman of Oak Ridge National Laboratory is being issued in July 1996. Work has begun on a review of the A=5–10 nuclides in collaboration with G. M. Hale of Los Alamos National Laboratory and H. M. Hofmann of the Universität Erlangen-Nürnberg.

5.5.2 ENSDF

One part of the task that TUNL accepted in 1989 was the entry of A=3–20 data into the Evaluated Nuclear Structure Data Files (ENSDF) which is maintained at the National Nuclear Data Center at Brookhaven National Laboratories. ENSDF files of adopted levels, decay data, and reaction data for A=18–19 were prepared at TUNL by R. M. Chasteler and submitted to NNDC in mid-1995. Adopted level, gamma- and beta-decay diagrams produced by the ENSDAT program from the ENSDF files were included in mailings with the A=18–19 reprints. New A=20 material is currently being entered into ENSDF by J. F. Guillemette.

5.5.3 World-Wide Web Services

In November of 1994, the TUNL A=3–20 Nuclear Data Evaluation Group began setting up its World Wide Web site (accessible at "http://www.tunl.duke.edu/NuclData"). We were encouraged by the response to demonstrations at the NSAC/DNP Long-Range-Planning Town Meeting (January, 1995) and Ion Beam Analysis Conference (May, 1995), and have continued to develop new services for the nuclear science and applications communities. Currently, the following items are available:

- Energy Level Diagrams in the style of Fay Ajzenberg-Selove for A=4–20.
- Abridged versions of TUNL's published evaluations for A=16, 17, 18, 19, and A=20 (preliminary).
- An abridged version of Fay Ajzenberg-Selove's A=5–10 compilation. (We have received permission from *Nuclear Physics A* to put her old compilations on the Web, altered to use NNDC key numbers where possible. We hope to have the most recent evaluation of each mass chain online by the end of 1996.).
- Postscript ENSDAT output of the A=3–20 ENSDF files.
- A short version (A=1–20) of the Table of Isotopes, recently made available by the Berkeley Isotopes Project.
- Information about the status of the project and our publications.

The TUNL Nuclear Data Evaluation Group's WWW services have been very well received; several thousand hits have been logged by the web server since its inception. Our stated goal is to provide through this medium all available forms of evaluated nuclear data for the light nuclei, A=3–20. This should include not only all of the most recently published nuclear data evaluations, but also most of the earlier very-useful-but-hard-to-obtain evaluations, as well as added features to enhance the value of these materials to the nuclear astrophysics community.

5.5.4 Additions to the TUNL Nuclear Data Evaluation Group

In order to address the increased work load created by the TUNL group's WWW committments, a proposal requesting a part-time assistant publications specialist was prepared by TUNL and funded by DOE. TUNL is presently trying to fill this position.

6 Nuclear Instruments and Methods

6.1 FN Tandem Accelerator Operation

C. R. Westerfeldt, E. P. Carter and R. M. O'Quinn

6.1.1 Tandem Operation

The TUNL FN tandem accelerator operated a total of 3129 hours during the period September 1, 1995 through July 10, 1996. The accelerator operated at terminal potentials ranging from 0.524 MV to 8.6 MV during this period. Beams accelerated during this period include polarized and unpolarized protons and deuterons, and also ^{3}He. The terminal operating potential during the reporting period is shown graphically in Figure 6.1–1.

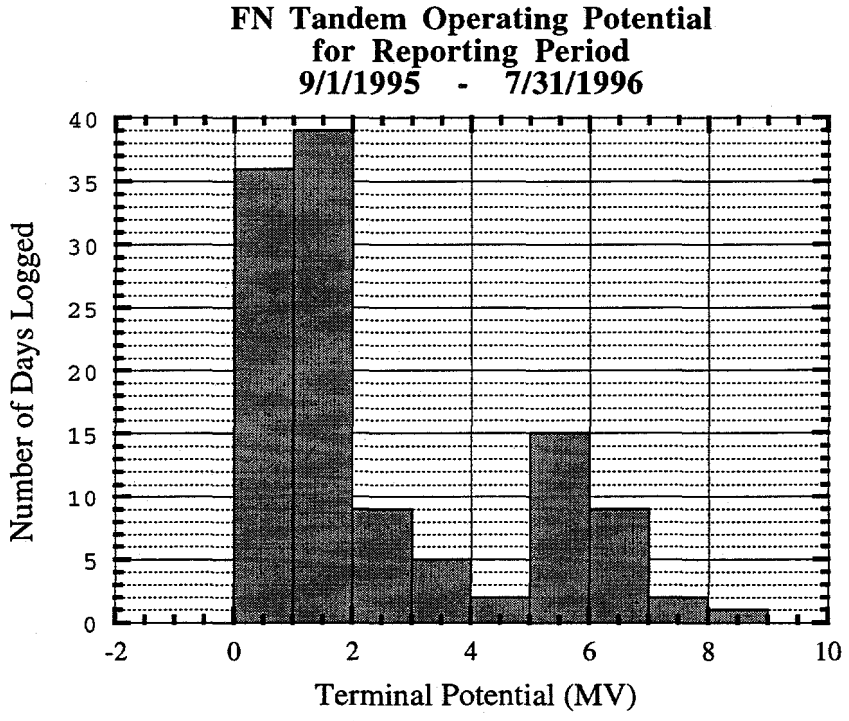

Figure 6.1–1: TUNL FN Tandem operation potential for reporting period 9/1/96–7/31/96.

The three periods with zero terminal voltage indicated represent the three accelerator maintenance periods during this reporting period. Other gaps in the data show periods when the tandem was not operated. However, the low-energy beam facilities were in use and did not allow any simultaneous tandem operation. A histogram showing the fraction of experimental time spent at various terminal potentials is given in Figure 6.1–2.

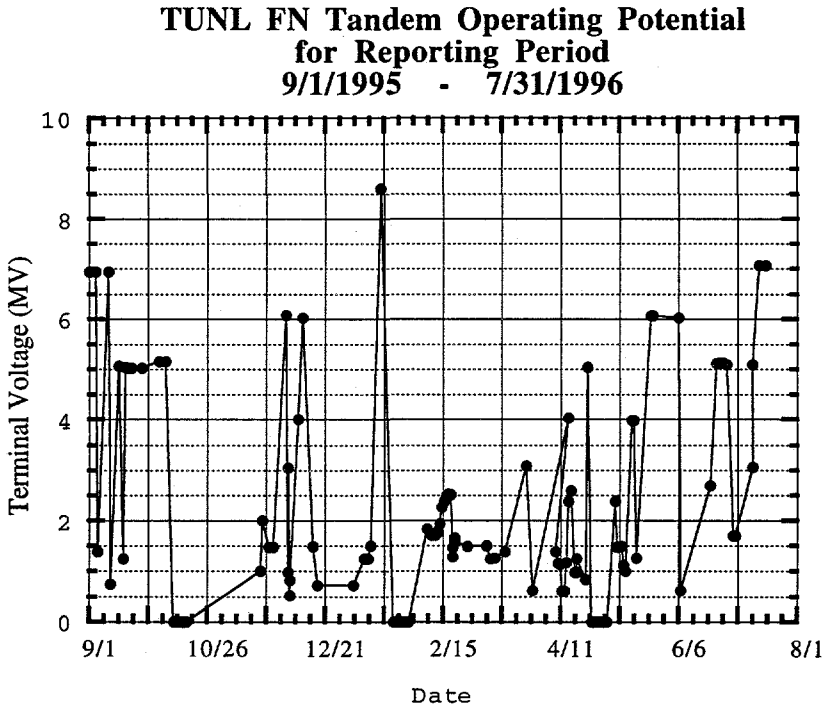

Figure 6.1–2: FN Tandem operating potential for reporting period 9/1/96–7/31/96.

The tandem was opened for maintenance in October 1995 after 21,650 hours of post upgrade operation, and again in February and April of this year for repairs to the new terminal amplifier and some routine maintenance. The Pelletron chains were inspected in October and fret corrosion was discovered in six links of the low-energy chain and 2 links of the high-energy chain. These failing links were replaced, and the chain is currently operating normally. During this tank opening, a bad terminal charge-pickoff pulley in the Pelletron charging system was discovered and replaced. Several failed column resistors were located during a check of the resistor grading strings in February and were also replaced. The terminal amplifier installed last year has suffered repeated failures in the ac line circuit and after several attempts to improve the protection against tank sparks, we have now operated for three months without a failure.

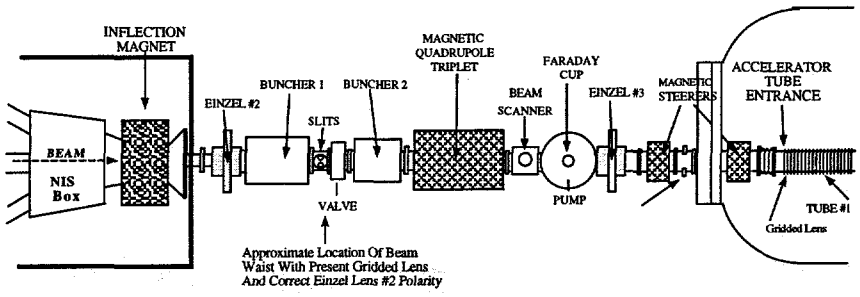

Figure 6.1–3: TUNL Low-energy injection optics.

6.1.2 Vacuum System Improvements

A grant was received for "Beam Transport Improvements" last Spring and a portion of these funds was used to replace the failing cryo-pumps on the tandem accelerator tubes. These pumps were replaced during the April maintenance period and are working well. The next project will be to improve the vacuum in the low-energy experimental area and the transfer line between the Atomic Beam Polarized Ion Source and the tandem. We are investigating the feasibility of installing two additional cryo-pumps in this area to greatly improve the vacuum in these areas. This is important because beam energies are low (80 keV) and transport distances are large 10–15 meters, and thus beam loss and depolarization from scattering with residual gases is a problem.

6.1.3 Beam Transport Improvement

We have investigated improvements to the low-energy beam transport system with the goal of substantially increasing the transmission of polarized beams through the tandem. A breakthrough was made this Spring when we discovered that one of the Einzel lenses (#2) on the low-energy end was biased at the wrong polarity, making it an accel/decel lens rather than the stronger decel/accel lens. This had the effect of moving the low-energy object position much closer to the tandem than is desirable. To compensate, we had to use an additional magnetic quadrupole triplet and another Einzel lens (#3) at the tank base (see Figure 6.1–3).

After replacing the power supply with one of the correct polarity, the transmission was dramatically improved. In addition, the magnetic quadrupole triplet and the third Einzel are not required. We are running calculations to determine whether we should remove these latter two lenses and move the second Einzel to a more optimal position. Removing the quadrupole triplet – which was originally installed for the injector cyclotron's 15 MeV beam – would free up valuable beamline space for needed instrumentation (e.g.: dual slits at the correct object position for the tandem).

6.2 KN Accelerator Operation

C. R. Westerfeldt, W. Beal, E. G. Bilpuch, E. P. Carter, C. Grossmann, L. McClean, G. E. Mitchell, J. F. Shriner, G. A. Vavrina and P. M. Wallace

6.2.1 KN Accelerator

The TUNL KN high energy-resolution accelerator operated a total of 360 hours during the period September 1, 1995 through July 19, 1996 at terminal potentials ranging from 0.99 MV to 2.85 MV. After completing data acquisition for two dissertation projects last Summer, the accelerator has been lightly used until this Summer. A histogram showing the number of days of operation at the logged terminal potentials is shown in Figure 6.2–1.

The accelerator was opened 4 times during this period for maintenance and repairs. Repairs included three repairs to the rf ion source oscillator, cleaning the charging belt, and shorting one failed gap in the accelerator tube.

6.2.2 Computer Control System

The precision energy control system for the analyzing magnet and electrostatic analyzer are in the process of being upgraded. This system, which is based on a PC running National Instruments LabView data acquisition and control system, was installed in 1992 and is being upgraded by installing a newer, faster CPU (100 MHz Pentium) and a fiber-optic based distributed control network based on the Group-3 Control Net system. A drawing illustrating this new system is presented in Figure 6.2–2.

This new plastic fiber based system will integrate with the already existing LabView control program and should require minimal modifications to the existing software. As all nodes in the Control Net system are electrically isolated from each other by the plastic fiber, ground loop noise and transients due to tank sparks are virtually eliminated. Tank sparks have been a serious problem for the existing system which utilizes twisted pair and coaxial cable to read and control devices distributed about the laboratory. We have frequently experienced computer and other instrument lock-up and failures following tank sparks.

This upgrade is being accomplished in two stages. The first, which is underway, involves upgrading an old 386 based PC with a new Pentium motherboard to develop and test the new hardware and software off-line, permitting operation of the accelerator to continue uninterrupted with the existing PC and hardware. We have purchased and have on hand the hardware and software to implement the magnet control portion of the system depicted in Figure 6.2–2. The second stage to this upgrade will entail purchasing the hardware to interface the electrostatic analyzer subsystem to Control Net. The cost for stage two is estimated to be under $2500 and we hope to be able to proceed with it this Fall.

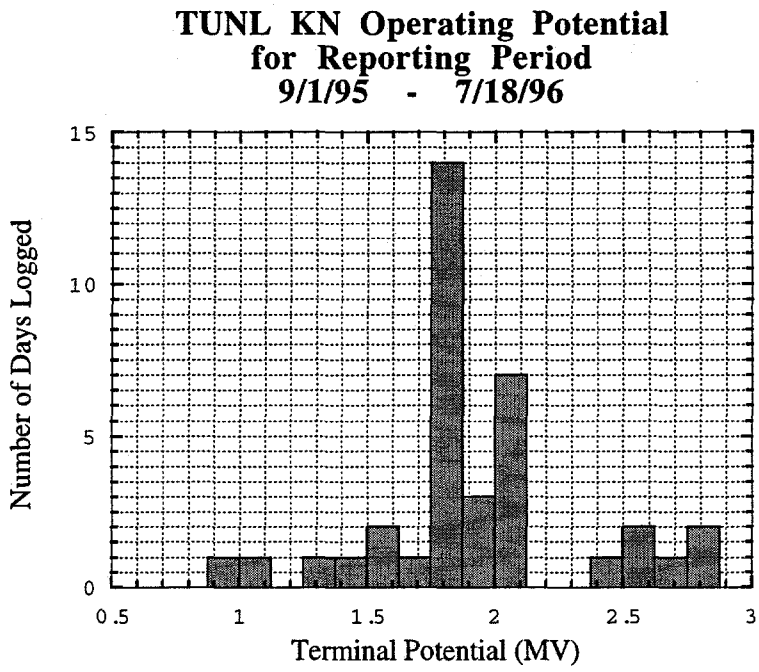

Figure 6.2–1: TUNL KN Operating Potential for Reporting Period 9/1/95–7/18/96.

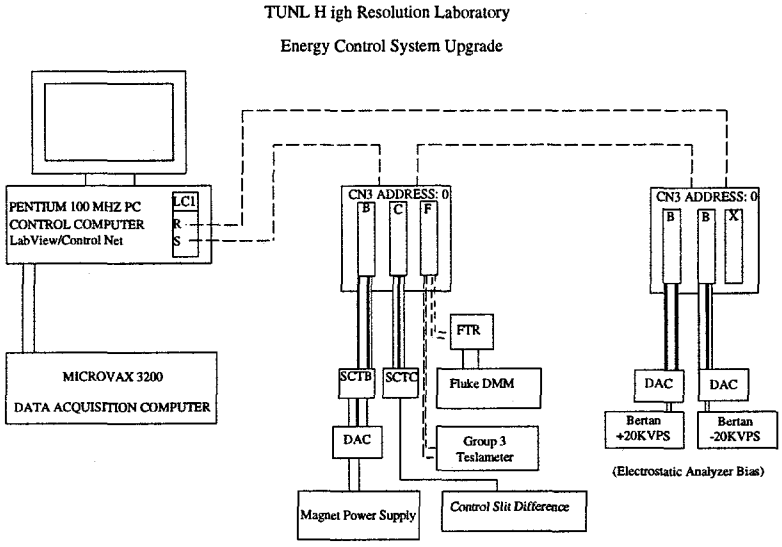

Figure 6.2–2: TUNL High Resolution Laboratory Energy Control System Upgrade.

6.3 Atomic Beam Polarized Ion Source

T. B. Clegg, A. J. Mendez, C. D. Roper and J. D. Dunham

6.3.1 Routine Operation and Maintenance

The TUNL intense atomic beam polarized ion source has been used for experiments during 52% of the calendar days during the past year; 47% of the days for production of polarized ions (69 days for polarized $H^{\pm}$ and 102 days for polarized D^{-}), and 5% for unpolarized H and D ion beams. The use of these beams was divided as follows: 18% for experiments solely in the low-enery target areas, 30% in the high-energy target areas, and 7% for experiments which utilized beams accelerated into both areas. There were also 3 days of scheduled running with a $^{3}He^{-}$ beam. In addition, 46 and 41 days were scheduled, respectively, for source modifications/testing and for routine maintenance.

Overall, the source has operated extremely well during the entire year. The installation of the spin-filter polarimeter (SFP), completed in September 1995, initially caused a reduction of as much as 50% in output beam intensities. Experience with source operation since that time has led to improvements in source output so that it is now operating at levels comparable to its former performance.

As a result of the source modifications required for the SFP installation, a number of routine maintenance procedures have become more difficult and time-consuming. However, the SFP has greatly reduced the time required to tune the rf transition units for maximum beam polarization, and in fact has become an invaluable diagnostic tool, allowing users to distinguish between problems with the transition units and problems with downstream spin handling and measurement. Users have also come to rely on the SFP in some cases as their sole means of polarimetry. This use is reflected in the drastic reduction of scheduled use of combined low-energy and tandem measurements, 7% of total scheduled source use as compared with the 24% reported last year.

A manuscript describing the SFP system, its installation and experience with its operation will be published this year in Review of Scientific Instruments (RSI) [Men96]. The abstract of this paper appears in the SFP section below and in the proceedings of last September's ICIS95 conference in Whistler, British Columbia [Men96].

6.3.2 Spin-Filter Polarimeter

6.3.2.1 Abstract of RSI manuscript

An atomic beam polarized ion source, used heavily since 1989 for producing polarized $H^{\pm}$ and $D^{\pm}$ beams for experiments between 25 keV and 20 MeV, has been modified to accept a Lamb-shift spin-filter polarimeter. In this source, polarized ground-state H or D atoms enter

an ECR ionizer where they are stripped to produce an outgoing positive polarized ion beam. When negative ions are desired, cesium vapor is introduced into a downstream charge-exchange canal. The polarimeter, based on an atomic physics concept first developed to produce nuclear-spin-polarized beams at Los Alamos, is designed to monitor the polarization of $2S_{1/2}$ metastable H or D atoms emerging from this cesium canal. Metastable $2S_{1/2}$ atoms created by electron pickup in a collision with cesium are "filtered" by the polarimeter according to magnetic substate, as the magnetic field imposed on the polarimeter cavity is tuned between 53 and 61 mT. Photons produced by subsequent quenching of these "filtered" atoms to their ground state are monitored downstream by a photomultiplier tube to reveal the magnetic substate population of the incident positive beam. To install the polarimeter cavity and photomultiplier tube assembly, the existing polarized ion source was lengthened by 30 cm. Installation is complete, and comparisons with calibrated nuclear polarimeters have shown agreement to better than 0.023. Principles of operation, a description of the hardware, measurements for cross calibration, and impressions gained from its use are all presented.

6.3.2.2 Recent upgrades and operating experience

Several concerns with SFP operation have been addressed since the submission of the RSI manuscript. The first of these is the problem of signal to noise ratio in SFP spectra. The signal strength is directly proportional to the number of metastable atoms passing through the spin-filter cavity. The metastable production rate is strongly dependent on the Cs-oven temperature, and at temperatures where ion production is maximal the metastable production rate is far below maximum, especially in the case where negative ions are being extracted. Thus, acquisition of high-quality scans often required users to change Cs-oven temperature prior to making a SFP measurement and then to return it to proper ion-production temperature. This process effectively made the SFP data acquisition time 10–15 minutes. The addition of a photomultiplier tube signal-averaging feature to the data acquisition software has alleviated this problem to some degree. The user sets the number of times the systems reads the photomultiplier signal for each B-field point, and the software then does an on-the-fly average, resulting in a much cleaner spectrum as shown in Figure 6.3–1. Using this technique, it is possible to get spectra of adequate quality without changing the Cs-oven temperature.

One other noteworthy upgrade is the inclusion of SFP system control and monitoring of the status of the rf transition units. Prior to the implementation of this feature, a user was required to go out to the source cage and manually switch the transition units in the source HV rack to perform a SFP measurement for each polarization state. This resulted on several occasions in the transition units not being returned to their proper state prior to resuming ion beam use for the ongoing experiment. Now, the SFP measurements can be made completely from the control room. The experimenter simply clicks a button on the

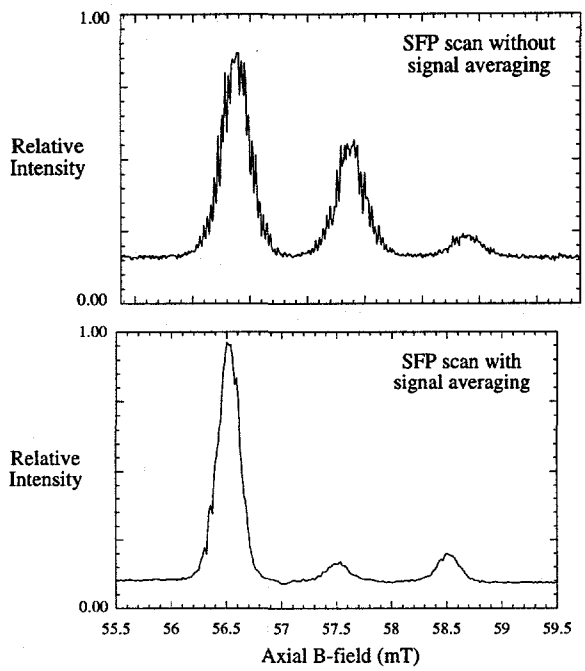

Figure 6.3–1: Spin-filter polarimeter spectra of relative photomulitplier tube signal intensity plotted as a function of axial B-field. Note that the bottom spectrum taken with photomultiplier tube signal averaging is considerably cleaner than the top spectrum taken without signal averaging. (The fact that the spectra are not of the same polarization state is not significant).

PC SFP window to enable PC control of the transition units. Then by clicking the knife switch buttons the user can turn on or off the desired units while making the measurement. A click of the "enable/disable" button subsequently returns control of the units to the experimenter's data acquisition system. Further, by clicking a "monitor transition units" button, the user has real-time monitoring of the status of the units. When this mode is chosen, the transition units' on/off knife switches disappear and are replaced by light bulbs which turn on and off with the corresponding transition units.

[Men96] A. J. Mendez *et al.*, Review of Scientific Instruments, (1996), Accepted for publication.

6.4 Polarimeters

6.4.1 Determination of Low-Energy Proton Polarization via the ^{6}Li($\vec{p}$,^{3}He)^{4}He reaction

C. R. Brune, H. J. Karwowski and E. J. Ludwig

The ^{6}Li($\vec{p}$,^{3}He)^{4}He reaction appears to be the best proton polarimeter for $200 \leq E_p \leq 1000$ keV, which includes most of the energy range of the LEBF facility. The polarimeter described in last year's progress report [Bru95] has now been calibrated for $250 \leq E_p \leq 460$ keV. This energy range is sufficient for doing polarimetry for any envisioned LEBF experiment. Lower-energy beams, including +80-keV protons without any acceleration in the minitandem, can be brought into this range by biasing the high-voltage scattering chamber.

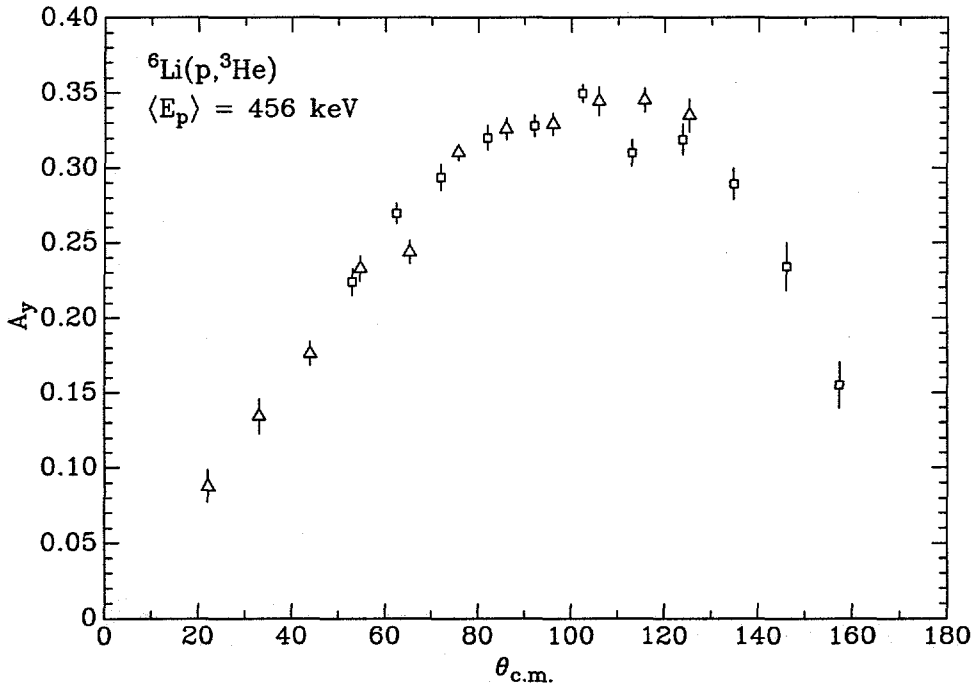

Figure 6.4–1: Angular distribution of vector analyzing power for the ^{6}Li($\vec{p}$,^{3}He)^{4}He reaction. The data points resulting from detected ^{3}He and ^{4}He nuclei are given by triangles and squares, respectively.

In addition, we have measured $A_y(\theta)$ for ^{6}Li($\vec{p}$,^{3}He)^{4}He at mean proton energies of 255, 321, and 456 keV in the high-voltage scattering chamber. There were previously no

measurements in this energy range. The angular distribution obtained at a mean proton energy of 456 keV is shown in Figure 6.4–1.

[Bru95] C. R. Brune *et al*, In *TUNL Progress Report*, volume XXXIV, p. 131, 1994-1995.

6.4.2 TJNAF Hall B Moeller Polarimeter

M. Spraker, R. M. Chasteler, C. M. Laymon and H. R. Weller

As a part of the ongoing physics program at the Thomas Jefferson National Accelerator Facility (TJNAF), the Hall B collaboration is in the process of completing and commissioning the beamline and detector system. Since a longitudinally polarized electron beam is central to many of the experiments planned in that hall, a reliable polarimeter system is required. The TUNL group is responsible for designing, constructing, and commissioning this polarimeter.

The longitudinal polarization of the electron beam will be measured using Moeller scattering. Moeller scattering is an electron-electron scattering process where both the incident and target electrons are polarized. The polarized electron target is created using a thin ferromagnetic foil in a small external magnetic field. The magnetic field aligns the spins of the valence electrons and produces a polarized target. The foil is then tilted to an angle of 20° with respect to the beam direction to produce a longitudinally polarized electron target. Due to the large number of non-valence electrons and quantum effects, typical target polarizations are ~8%. Coils and pickup coils have been wound and preliminary tests to determine the polarization and the accuracy of the polarization have been performed using available foils. An integrating voltmeter is required for the final tests. This will be supplied by TJNAF from their available equipment within the next few months.

During the last few months, a complete design and price list has been assembled for the polarimeter. The Hall B polarimeter will use Permendur (49% Co, 49% Fe, and 2% V) foils which polarize in an external field of ~100 Gauss. Two foils will be used which will be tilted at +20° and –20° with respect to the incident beam direction. Switching between the targets is equivalent to flipping the target's transverse polarization. This is useful because the effect of the vector component of the beam's polarization can be measured. Changing the targets will flip the sign of the vector analyzing power, but not the longitudinal analyzing power.

The Moeller scattered electrons exit the target with roughly half the incident beam energy. They will be separated from the residual beam using a two-quad magnetic filtering system that will defocus the scattered electrons horizontally onto two Pb-scintillating fiber detectors. The detector blocks have not yet been cut or polished, but the light guides have been designed. These detectors will be run in coincidence to minimize the background from the Mott (electron-nuclear scattering) scattered electrons. Given the capacity of the power

supplies being proposed for use for the two quadrupoles, the polarimeter will be able to measure the polarization of incident beams ranging in energy from 400 MeV to 6 GeV. In the current design, the acceptance of the system is .23 sr at 800 MeV and .18 sr at 6 GeV. A 3% measurement of the polarization can be made in 1 to 10 minutes depending on the incident energy.

Currently, designs are complete for the target chamber and necessary beamlines. The two quads are in place with power supplies in the Hall B beamline. Power supplies for the magnetic coils used to polarize the target have to be purchased along with the foils themselves. Due to funding constraints at TJNAF, the parts for the polarimeter will not be machined or purchased until after September, 1996. The polarimeter should be constructed and placed *in situ* in the Hall B beamline by late December, 1996. Polarized beam is not expected until the middle of 1998. Unpolarized commissioning of the polarimeter is tentatively scheduled for the middle of 1997 using a 2 GeV electron beam. Software will be developed and tested during the commissioning. The polarimeter will be in regular use starting in mid to late 1998.

6.5 TUNL/DFELL High Intensity Gamma Source

6.5.1 Shielding Calculations for the HIGS Inverse Compton Scattering Facility at DFELL

E. C. Schreiber, R. S. Canon, M. Spraker and H. R. Weller

The high intensity of γ-rays that will be produced by the HIGS facility could potentially produce high levels of background radiation. Simulations using the EGS4 Monte-Carlo code have estimated this background and facilitated the design of appropriate shielding.

The most intense radiation levels lie directly along the beam path. A beam dump placed outside the DFELL building wall will prevent the beam from leaving the experimental area. This beam dump will consist of a nickel core, a lead shield around the core, and a surrounding layer of concrete. The nickel core, chosen (following LEGS at BNL) for its low photonuclear cross-section, will account for the majority of the γ-ray attenuation. This attenuation will produce scattered photons, electrons, positrons, and neutrons. Scattered photons, electrons, and positrons will be strongly forward peaked and will be attenuated by the lead shield. Neutrons produced by the ^{58}Ni(γ,n) reaction will be scattered nearly isotropically and will be absorbed by the concrete. A schematic diagram of the beam dump is shown in Figure 6.5–1. An EGS4 simulation of this design assuming 10^9 photons/sec with energy of 28 MeV indicates that all scattered photons, electrons, and positrons are attenuated in this beam dump. The neutron attenuation of the concrete is such that the maximum neutron intensity 2 meters from the center of the beam dump is predicted to be 0.2 neutrons/cm^2/sec. Photons of energy 28 MeV were chosen as a worst case scenario, since the photon absorption cross-section is lowest in this energy region.

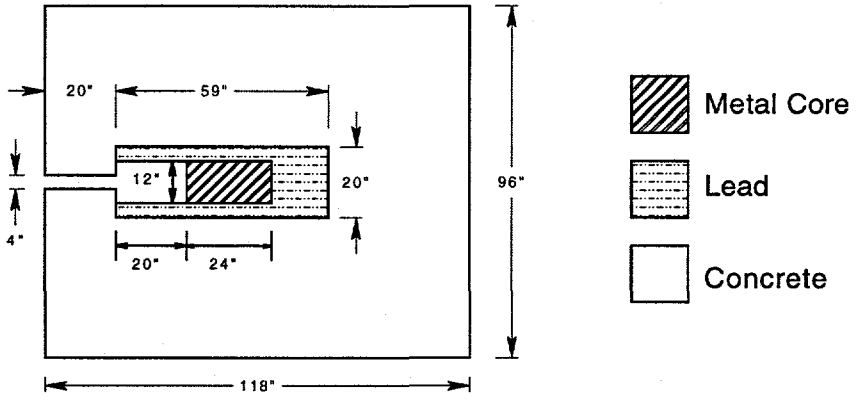

Figure 6.5–1: Schematic for the proposed beam dump. Construction is expected to begin in August 1996.

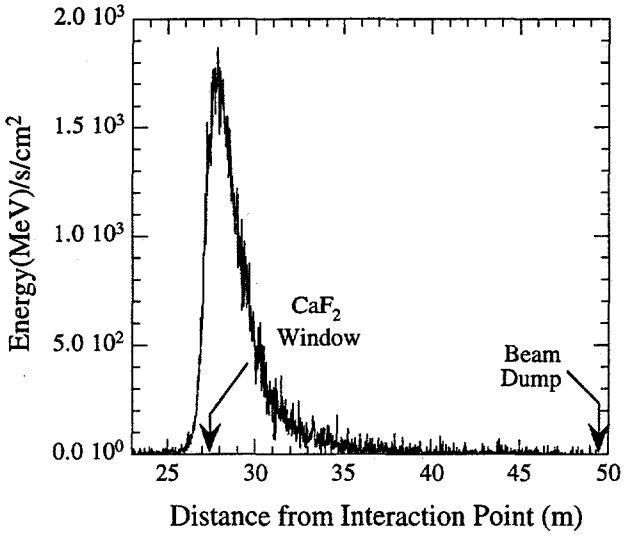

Figure 6.5–2: Photon intensity 50 cm from the beamline axis. An initial γ-ray flux of 10^8 photons/sec with a maximum energy of 28 MeV is assumed. All other configurations should provide lower levels of radiation.

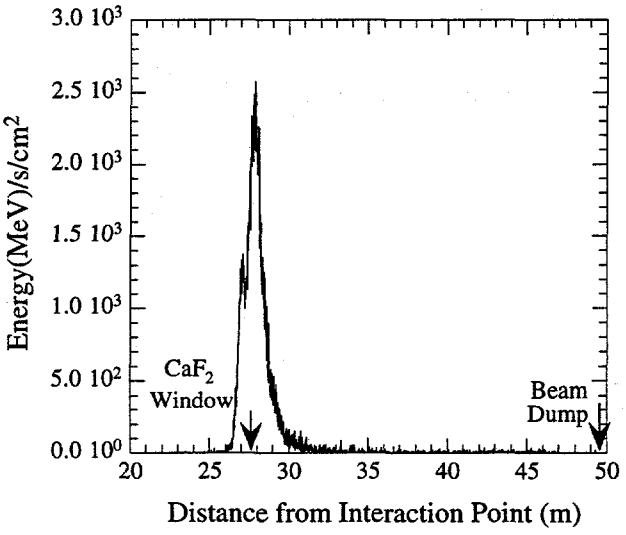

Figure 6.5–3: Energy intensity 50 cm from the beamline axis from electrons produced in and scattered from the beamline. A γ-ray flux of 10^8 photons/sec with a maximum energy of 28 MeV is assumed. All other configurations should provide lower levels of radiation.

Although the majority of the γ-rays will be directed into the beam dump, a small percentage will interact with other elements of the beam line. These interactions will produce radiation outside the beam dump. EGS4 simulations reveal that the majority of the radiation is scattered from elements directly in the beam line, specifically the cavity mirror and the CaF_2 window at the end of the vacuum chamber. The results of this simulation are shown in Figures 6.5–2 and 6.5–3. It has been determined that 2 inches of lead will be sufficient to reduce the dose rate to around 0.1 mrem/hr in the problem regions. These same regions are also the main source of neutron background, with each region producing on the order of 10^6 neutrons/sec. Local concrete shielding, in conjunction with a concrete wall around the optical cavity room, will be used to attenuate these neutrons to safe levels.

6.5.2 Bremsstrahlung Measurements at the DFELL Storage Ring

E. C. Schreiber, R. S. Canon, M. Spraker and H. R. Weller

All electron beam facilities inevitably produce some bremsstrahlung background as electrons interact with the residual vacuum. Prior to the installation of the OK-4 undulator, this background was measured at the DFELL storage ring and found to be negligible in comparison with the expected γ-ray fluxes [Car96] which will be produced via Compton backscattering in the optical cavity. The installation of the OK-4 undulator required modifications to the beam line, so the bremsstrahlung count rates were remeasured in December 1995 and January 1996. These measurements were taken using a 10″x10″ NaI crystal.

These new measurements revealed that the background count rate had increased by two to three orders of magnitude to approximately 10^4 photons per second per 10 mA current in the storage ring. An additional factor of three increase was observed when the undulator was turned on. The cause for these increases over previous measurements is believed to be a lower vacuum quality in the undulator region resulting from new beamline components and the lack of a vacuum pump in the center of the OK-4.

While this increased background is still small compared to the expected γ-ray fluxes, the increased bremsstrahlung production causes a large number of electrons to be knocked out of the circulating electron bunches, severely reducing the stored beam lifetime. Because the amount of bremsstrahlung produced is proportional to the current in the storage ring, beam lifetime could be measured by measuring the bremsstrahlung flux with a NaI detector. As shown in Figure 6.5–4, the current was observed to decrease by a factor of two in roughly six minutes of operation. This level of reduction in beam lifetime would substantially increase the time required to perform experiments needing electron beam energies higher than the LINAC injection energy, since lost electrons would have to be reinjected into the storage ring at a lower energy and slowly ramped up to the required energy. No data could be taken during the ramping process.

The DFELL storage ring was shut down for upgrades and modifications in Summer

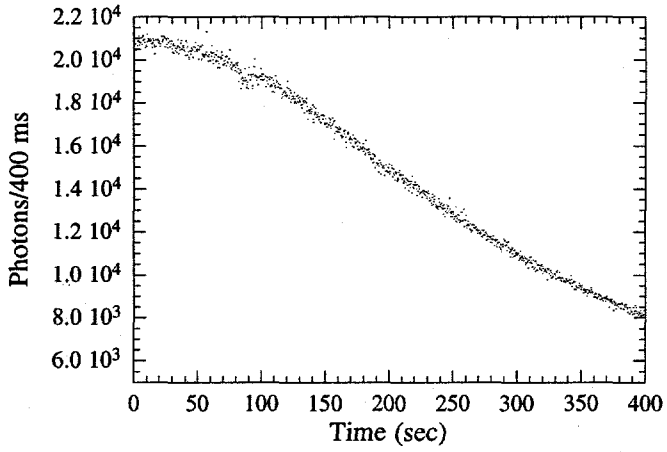

Figure 6.5–4: Bremsstrahlung flux between 4.4 and 10 MeV as a function of time. The initial ring current was 28 mA at 500 MeV.

1996. During this time, all beamline components were reconditioned to improve the vacuum qualities of the system. It is believed that this conditioning will greatly improve the vacuum quality in the undulator region and therefore reduce the bremsstrahlung background to acceptable levels. The new background levels will be measured when the storage ring comes back on-line in September 1996.

[Car96] T. S. Carman *et al.*, expected publication date August 11, 1996.

6.5.3 Initial Design Considerations of a 4π π_o-Spectrometer

R. S. Canon and H. R. Weller

A careful measurement of the photoproduction of π_o near threshold is one of the first experiments planned for the HIGS. Accurately measuring this process will require a detector with good angular resolution. In addition, the detector will need to cover a large solid angle in order to accomplish the experiment in a reasonable time period. Decisions about detector material and geometry must be considered early on so that a reasonable estimate of the construction cost can be determined. These decisions will be based on cost and resolution requirements determined by Monte-Carlo simulations and other calculations.

The primary reason for the demanding detector requirements is the short lifetime of the π_o and its subsequent decay into two photons. As a result, in order to extract information about the pion, the momentum vectors of the two photons must be added to determine the pion production angle. So, the ability to extract precise information about the pion

depends on our ability to measure the kinematics of the photons. Furthermore, the photons are nearly isotropically distributed over 4π, so any reasonable efficiency requires a large solid-angle detector.

Due to the large amount of detector material required to build a 4π-detector, the cost of the material is a driving factor in material selection. For this reason, lead-glass has been chosen. The closest material in cost is NaI, which is approximately five times more expensive per unit volume. The choice of lead-glass might raise concerns due to its poor energy resolution. Although this is undesirable, it will not be detrimental since the angular resolution is the more important factor in this particular experiment.

The detector's angular resolution determines how close to threshold the measurement can be made. At a beam energy of 153 MeV, around 10 MeV above threshold, the photoproduced pion emerges with a momentum as small as 22 MeV/c. As a result, large variations in the production angle of the pions translate into only small variations in the kinematics of the decay photons. For example, keeping the angle of decay fixed for one photon and varying the pion production direction about all possibilities, the second decay photon is restricted to a solid angle of only 0.74 steradians. In order to measure angular distributions accurately, we must be able to segment this small solid angle into enough independent detection cells. Consequently, we must have cells that cover a solid angle on the order 0.06 steradians. Since the angular resolution is mainly determined by the geometry and the amount of segmentation, the angular resolution will be the basis for these aspects of the design.

There are several detectors that can serve as starting point in designing a 4π-detector. Geodesic arrangements offer the best combination of efficiency and accuracy with the least amount of material requirements. These designs incorporate several regular shaped identical pieces that are arranged to fit tightly. Several detectors of this geometry exist which are constructed with more expensive materials (such as NaI, germanium and BGO, and CsI). Examples include the Crystal Ball, GammaSphere, and Euro-ball. Some of these designs are extremely complex and far exceed our requirements. However, these designs, from simple to complex, have similar traits that will be desirable for our design. Their arrangements allow for complete 4π-coverage with the exception of end pieces that would obstruct the beam and target assembly. Also, their arrangements divide the 4π in a way that each segment covers a nearly equal amount of solid angle. Since many of these designs have already been built and applied, we have the benefit of drawing from years of experience in designing the detector geometry and the support structure for our experiment.

The next phase of the design will involve refinement. This includes simulating certain segmentation arrangements to determine the overall resolution and efficiency. Based on preliminary estimates, one possibility is a six-frequency icosahedron with hexagonal facial pattern. This yields 122 faces, including twelve pentagonal faces and one-hundred and ten hexagonal faces, with an average solid angle around a tenth of a steradian. This arrangement should meet the resolution requirements and budgetary constraints.

6.6 Polarized Targets

6.6.1 Development of a Dynamically Polarized Proton Target

C. R. Gould, D. G. Haase, G. W. Hoffmann[1], *S. I. Penttilä*[2], *B. W. Raichle, M. L. Seely, J. R. Walston and W. S. Wilburn*

The Polarized Target group has been involved in a program to study the tensor component of the nucleon-nucleon interaction. Observables which provide such information can only be obtained from experiments where two of the participating particle spins are measured. We have recently developed a dynamically polarized proton target for the study of polarized-neutron, polarized-proton transmission experiments.

Dynamic nuclear polarization (DNP) offers two significant advantages over static polarization techniques. First, better polarization can be achieved at higher temperature and lower magnetic field. Our dynamically polarized target provides a proton polarization of 0.60 at 0.5 K in a 2.5 T magnetic field, whereas the statically polarized target used previously [Wil95] provided a polarization of 0.35 at 0.015 K in a 7.0 T magnetic field. Second, dynamic polarization allows rapid polarization reversal (~30 min), a process excessively long (~24 hr) with static polarization.

During 1994 and 1995 [See95], a dynamically polarized proton target based on the PSI design was completed. The ^{3}He evaporation refrigerator was constructed and has proved highly reliable. LabView software was developed to operate and monitor the target performance, and the nuclear magnetic resonance (NMR) system was characterized.

In August 1995, the target was moved from a setup room to the 59° beamline of the TUNL Polarized Target Facility. The target was cooled several times to verify operation. The target was optically aligned, and alignment was verified by radiography. The product of target polarization and thickness was calibrated by polarized neutron transmission at E_n=2 MeV. The calibration agreed to within 10% with independent measurements of polarization by NMR (0.65) and thickness by volume and packing fraction measurements (0.06 atoms/b). Initially, the target polarization axis was oriented transverse (vertical). In March, 1996, the superconducting magnet which defines this axis was rotated from transverse to longitudinal. The alignment procedure was repeated for this orientation.

This target is presently being used in a polarized-beam, polarized-target transmission experiment to measure the spin dependent total $\vec{n}$–$\vec{p}$ cross-section differences $\Delta\sigma_T$(see Section 2.1) and $\Delta\sigma_L$. During these measurements (10 day runs) the target has run reliably, providing proton polarization of typically 0.65, and having a stability better than 1%.

Our target has also been used as a neutron polarimeter (see Section 3.1.2). At low energy, the spin-dependent cross-section difference is large (3.2 b at E_n=0.84 MeV). This

[1]University of Texas at Austin.
[2]Los Alamos National Laboratory.

behavior has been exploited in a measurement of the longitudinal polarization transfer coefficient, K_z^z, for the $T(\vec{p},\vec{n})$reaction.

[See95] M. L. Seely, In *TUNL Progress Report*, volume XXXIV, p. 148, 1994-1995.

[Wil95] W. S. Wilburn *et al.*, Phys. Rev. **C52**, 2351 (1995).

6.6.2 Calibrating Target Polarization by Polarized Neutron Scattering

M. L. Seely, C. R. Gould, D. G. Haase, B. W. Raichle, J. R. Walston, W. Tornow, W. S. Wilburn and D. S. Junkin

In our polarized-neutron, polarized-proton scattering experiments, two methods of measuring the product of the target polarization and thickness are available. The NMR absorption signal, calibrated with the target at thermal equilibrium, can be used to measure the target polarization. It is also possible to measure the product of target polarization and thickness by measuring the polarized neutron transmission asymmetry at low energies. The purpose of our measurements was to test the agreement between our scattering and NMR measurements to the 5% level.

Our NMR system is a series tuned Q meter based on the Liverpool design. Numerical simulations of the circuit response indicate that the polarization derived from the signal area should differ from the true polarization by approximately 0.3% due to nonlinearity in the circuit response for our operating conditions. Observed NMR signals show an asymmetry which is not presently understood.

In the low-energy limit, the values of spin-dependent cross-section differences are fixed by kinematics (only s-waves contribute to the scattering) and known properties of the deuteron potential. The T(p,n)^{3}He reaction is used to produce polarized neutrons at this energy. The polarization of the proton beam is measured at the source. The transverse polarization transfer coefficient has been measured to 2.6% for the T(p,n)^{3}He reaction at 2 MeV. The neutron beam energy is calibrated against the proton beam energy by observing the 2.075 MeV resonance in carbon.

The results of target polarization measurements during two recent runs are shown in Table 6.6–1. In both cases, the NMR measurement yields a higher target polarization than the low-energy scattering measurement. The difference between the two is approximately twice the combined uncertainty of the measurements. The results of this work were reported at a recent workshop [See96].

[See96] M. L. Seely *et al.*, In *Eighth International Workshop on Polarized Target Materials and Techniques*, 1996.

December 1995 Run	xP_t	P_t
Low-Energy Scattering	0.0393 ± 0.0017 barn^{-1}	67 ± 3 %
NMR	0.0439 ± 0.0010 barn^{-1}	74.8 ± 1.7 %
January 1996 Run		
Low-Energy Scattering	0.0393 ± 0.0017 barn^{-1}	67 ± 3 %
NMR	0.0405 ± 0.0013 barn^{-1}	74.0 ± 1.7 %

Table 6.6–1: Target polarization and the product of polarization and thickness determined by NMR and by low energy scattering.

6.6.3 Microwave Induced Optical Nuclear Polarization

M. L. Seely, C. R. Gould, D. G. Haase, B. W. Raichle, J. R. Walston, N. R. Roberson, W. Tornow and W. S. Wilburn

During the past year, we have carefully studied a promising new technique for producing solid polarized targets, and have proposed experiments intended to make targets based on this technique practical. The use of photoexcited triplet states in dynamic nuclear polarization, known as Microwave Induced Optical Nuclear Polarization (MIONP), could open the way to polarizing nuclei at much higher temperatures and lower magnetic fields than had previously been possible. The KEK-Kyoto-Toyama collaboration recently obtained 20% proton polarization in a single crystal of naphthalene doped with pentacene at 77 Kelvin and 0.3 Tesla [Shi96]. Triplet states of the pentacene molecule were excited by a flash lamp pumped dye laser. Each laser pulse was followed by a pulse of microwave power accompained by a magnetic field sweep to polarize the nuclear spins through the integrated solid effect.

Several difficulties must be overcome before this technique will be able to produce a practical polarized target. Experiments thus far have dealt only with small samples, typically having dimensions on the order of a few millimeters. Also, the aromatic molecules used in these experiments offer only about half the proton density of conventional materials. We believe that the investigation of MIONP in systems other than substitutionally doped single crystals may help to overcome some of these difficulties. Many alternatives to the aromatic single crystal systems would offer a higher density of polarizable protons. Furthermore, the exploration of other systems would allow a broader range of dopant molecules and a broader range of dopant concentrations to be investigated. Substitutionally doped single crystals are used to obtain spatially oriented guest molecules, resulting in a narrow ESR line for the triplet states. Some alternatives to substitutionally doped single crystals might include Shpolskii matrices, polymer films, and hydrocarbon glasses. A Shpolskii matrix is an alkane crystal with the length of the alkane chain selected to match the length of the

guest molecule. Stretched polyethylene films have been used to orient triplet state aromatic molecules for ESR studies. Polyethylene is being investigated as a target material with conventional dopants by several groups. Hydrocarbon glasses offer high proton density and are easy to prepare and to cool in the form of beads. They would offer the widest range of dopant molecules and dopant concentration. However, they provide no orientation of the guest molecules and consequently the ESR line of triplet state molecules in a glassy host would be very broad. The use of polarized incident light would give some selection of guest molecule orientations. Inorganic crystals (NH_3) with fixed paramagnetic centers are widely used in conventional polarized targets. It may be possible to dope an inorganic crystal with an ion having a singlet ground state (such as Cu^+) and an excited triplet state that can be reached through visible or near UV excitation.

MIONP has the potential to produce a totally new type of polarized target: one that is compact, offers a low field at the target, and access to the target over a large solid angle. The freedom from sub-Kelvin cryogenics may reduce the cost and technical complication of polarized targets and broaden the range of polarized target applications. Substitutionally doped aromatic crystals are well suited for MIONP for a number of reasons. Further work is needed to fully understand the factors which limit the proton polarization in these materials. Ultimately, systems other than aromatic mixed crystals may offer certain advantages, particularly in terms of the density of polarizable protons.

[Shi96] H. M. Shimizu, In *Eighth International Workshop on Polarized Target Materials and Techniques*, 1996.

6.7 Detector Developments

6.7.1 Cryogenic Microcalorimeters

D. S. Junkin, A. E. Champagne, D. G. Haase and M. L. Seely

Cryogenic microcalorimeters operate in the milliKelvin temperature regime where specific heats of materials are so small that incident radiation can produce a measurable rise in temperature. In principal, superb energy resolution can be achieved, but at the price of low count rates [Fio93]. Our device is composed of a high-sensitivity thermistor and a radiation absorber, both thermally linked to a dilution refrigerator.

Over the past year, we have concluded our testing of phosphorous doped silicon thermistors (P:Si). Our measurements have shown that commercially implanted P:Si devices have non-uniform doping concentrations which cause thermistors produced from the same wafer to have dramatically different resistance versus temperature curves. We do not consider these implanted devices to be useful thermistors for our experiments.

Since thermistors require reproducible and predictable R vs. T curves with a high sensitivity (which is defined as dlog(R)/dlog(T)), we have decided to use Au_xGe_{1-x} instead of P:Si thermistors. We have measured the resistance versus temperature curves of several Au_xGe_{1-x} thermistors fabricated by a group at Temple University and Rutgers-Camden. These thermistors have reproducible, predictable ($R{=}R_0\ exp\,(T^*/T)^{\frac{1}{2}}$) temperature responses (where T^* is a function of the Au concentration and R_0 is a function of the device geometry) [Wan93]. Since the R vs. T curves are predictable, we can control the sensitivity of the devices in the operating temperature range. We have developed a design for AuGe thermistors that have one fortieth the heat capacity of our current devices. This will increase our signal response size and therefore our overall energy resolution.

The development of these more sensitive thermistors has shown the need to improve the thermal isolation and control of the microcalorimeters. We have improved the thermal anchoring of both the devices and the preamplifier in order to obtain a continuous operating temperature below 130 mK on the cold finger.

Improvements have also been made to the electronics. The single-sided thermistor bias has been replaced by a symmetrical dual biasing system to allow the use of a matched JFET preamplifier to measure the voltage changes across the thermistors. This measurement system helps to remove some of the microphonic noise and electronic pickup between the preamplifier and thermistor.

A differential amplifier system has been designed and built to amplify the signal from the preamplifier such that it can be measured by the data acquisition card in a PC. Extensive effort has been made to remove the extraneous noise and pickup from the electronics. We currently have a system with 5 $nV/\sqrt{Hz}$ input noise over the entire measurement frequency range.

An additional PC has been networked to the data acquisition PC to provide for real time data analysis and storage. The data acquisition software has been modified such that one computer is able to acquire and save data, while the second computer is able to read and process the data.

Our plan for the next year is to improve the energy resolution of our devices by developing smaller and more reliable Au:Ge thermistors. A vibration damping system will be added to the pumping lines of the dilution refrigerator to remove the microphonic effects from the pumps. After optimizing the energy resolution, we plan to measure the beta spectrum of ^{14}C.

[Fio93] E. Fiorini, J. Low Temp. Phys. **93**, 189 (1993).

[Wan93] X. X. Wang, C. J. Martoff, and E. Kaczanowicz, J. Low Temp. Phys., **93**, 349 (1993).

6.7.2 A New Multi-Wire Position Sensitive Proportional Counter for Use with the Enge Split-Pole Spectrometer

S. E. Hale, A. E. Champagne, V. Y. Hansper and D. C. Powell

Several reaction rates in the Neon-Sodium cycle of proton burning still have large uncertainties which impact our understanding of Na signatures in globular clusters. The cross-sections for these reactions, $^{22}Ne(p,\gamma)^{23}Na$, $^{23}Na(p,\gamma)^{24}Mg$, and $^{23}Na(p,\alpha)^{20}Ne$, are too small for direct resonance measurements at the energies of interest. We therefore wish to study them via $(^3He,d)$ spectroscopy using the TUNL split-pole spectrometer. A new detector has been designed and constructed over the past year to achieve the necessary energy reolution.

The device consists of two position sensitive sections, a single-wire energy loss section, and a back scintillator. With the two position measurements, the angle of entry can be determined, allowing corrections to be made for spectrometer aberrations, which in turn permit the use of larger solid angles.

Each of the position sections consists of a ground plane, a wire frame board to carry the high voltage for charge multiplication, and an image pick-up board, all oriented normal to the particle trajectory. The position measurement is achieved using an etched aluminumized mylar foil (0.3 microns thick) on the pick-up board. The foil is stretched taut across a gap cut in G-10 boards (for particle transmission) and affixed with double-sided tape. A pen filled with NaOH, mounted in a computer-controlled milling machine, is then used to remove aluminum from the mylar, resulting in a pattern of vertical, isolated strips [Gra95]. The remaining aluminum strips are 2.54 mm across, separated by a gap of approximately 0.5 mm. Electrical connections are then painted down from each strip to taps on delay lines.

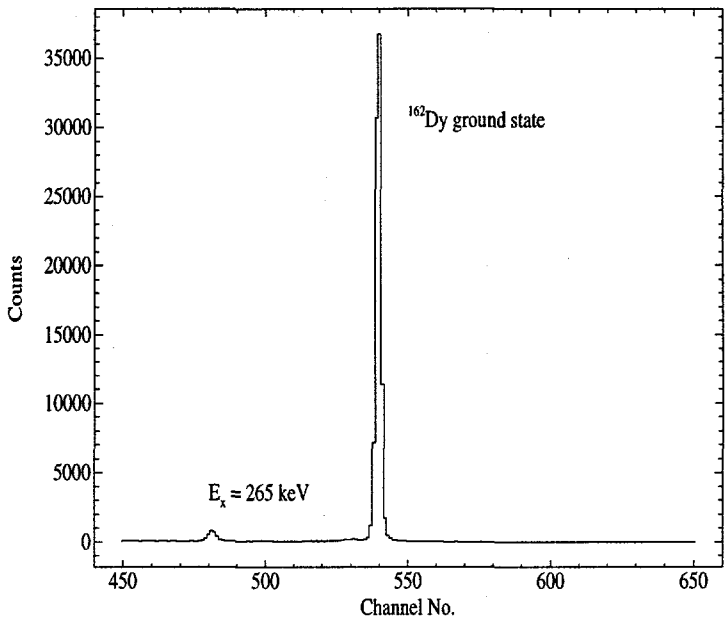

Figure 6.7–1: Back position spectrum from ^{162}Dy(p, p) at 12 MeV.

Particles passing through the propane fill gas create avalanches of charge near the high voltage wires, which induce an image charge on the strips. The charge on the strips will then travel out both ends of the delay lines, resulting in a left and right signal from both the front and back position sections. Lumped constant delay lines are used in the two position sections, the front being a continuous delay line [Mar75] while the back is a series of 20 individual 10-tap delay lines. The overall delay of both lines is 2 μs. They are impedance matched to external electronics using pulse transformers [Bir76]. The right signal of both sections is sent through an additional 2 μs delay box relative to the left signal. Thus, the time difference between the two signals will range from 0 to 4μs, corresponding to an event on the right side and on the left side of the detector, respectively. Timing measurements using the left and right signal as the start and stop of a TAC, respectively, then provide position information.

The detector has been undergoing bench testing since January 1996, and has been used in preliminary elastic scattering experiments in both May and July. A 12 MeV proton beam elastically scattered from a ^{162}Dy target yielded a position resolution of 0.75 mm (8.7 keV) in the back position section. A sample spectrum is shown in Figure 6.7–1.

Several construction flaws have been discovered and remedied. More work remains to be done in eliminating sparking from the high voltage wires in the front position section and interruptions in the painted connections from the delay line taps to the aluminum pick-up strips.

[Bir76] M. Birk, A. Breskin, and N. Trautner, Nucl. Instr. and Meth., **137**, 393 (1976).

[Gra95] G. Graw, private communication, 1995.

[Mar75] R. G. Markham and R. G. H. Robertson, Nucl. Instr. and Meth., **129**, 131 (1975).

6.8 Neutron Detector Efficiency Determinations

6.8.1 Determining Neutron Detection Efficiencies for the TUNL Ring and Transmission Detectors used in the Neutron-Neutron and Neutron-Proton Scattering Length Experiment

D. E. González Trotter, S. Guldbakke[1], H. Klein[1], D. Schmidt[1] and W. Tornow

The TUNL a_{nn}–a_{np} experiment requires unusual detector configurations for which ring (R) and transmission (T) detectors were built by the Neutron Time-of-Flight group. The NRESP7 and NEFF8 Monte-Carlo codes written at PTB are meant for pulse-height analysis and efficiency calculations for detectors of a special cylindrical type only [Die82]. These codes were modified to take into account the unconventional shapes of the active volume, aluminum housing, and lucite light pipes of detectors R and T [Gon94]. Codes NRESPR1 (for R detector) and NRESPT1 (for T detector) were derived from NRESP7. NEFFR1 and NEFFT1 were likewise derived from NEFF8. NRESPR1 and NRESPT1 reproduced very well the experimental pulse-height spectra as well as the fluence of their respective detectors measured using the cyclotron at PTB (see Figure 6.8–1). The aformentioned codes also helped to determine the light output function for protons (L_p) of each detector. L_p is then used in the modified efficiency codes. It contributes to the determination of the shape and magnitude of the calculated efficiency curves in a sensitive way.

Using the modified codes NEFFR1 and NEFFT1 it is now possible to generate efficiency curves for detectors T and R at various thresholds (see Figure 6.8–2). These curves are incorporated as tables in Monte Carlo simulations of the a_{nn}–a_{np} experiment for breakup and n-d elastic events. Presently, we are measuring the efficiency of our T and R detectors using a calibrated ^{252}Cf source purchased from PTB. These measurements will serve for comparison against the present efficiency calculations for the R and T detectors. In addition, it is possible to accumulate pulse-height spectra for E_n<1.2 MeV to further refine the input parameters for the NEFFR1 and NEFFT1 codes in this energy range.

[Die82] G. Dietze and H. Klein, PTB Bericht, **ND-22**, 1 (1982).

[Gon94] D. E. González Trotter, In *TUNL Progress Report*, volume XXXIII, p. 33, 1994.

6.8.2 Determination of Absolute Neutron Detector Efficiencies Using a ^{252}Cf Source

Q. Chen, D. E. González Trotter, C. R. Howell, A. C. Nugent, F. Salinas and W. Tornow

[1]Physikalisch-Technische Bundesanstalt, Braunschweig, Germany.

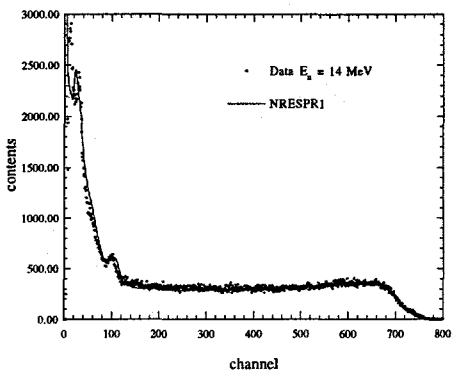

Figure 6.8–1: Experimental R-detector pulse-height spectrum measured at PTB (E_n=14 MeV) and fitted with NRESPR1 calculation.

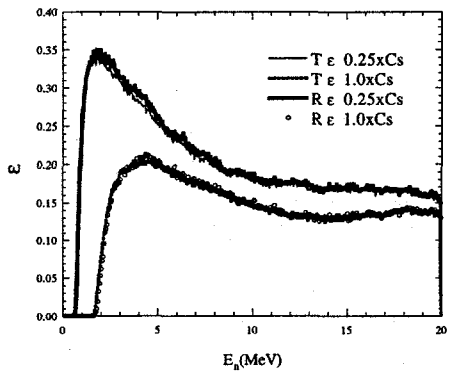

Figure 6.8–2: Efficiency calculations for T and R detectors ($\frac{1}{4}\times$Cs and $1\times$Cs threshold bias).

A ^{252}Cf source constructed and carefully characterized at PTB[1] was purchased by TUNL. The source consists of a smooth platinum disk electroplated with 0.25μg of ^{252}Cf with a fission rate of $(1.54 \pm 0.05) \times 10^5$ s^{-1} (May 1995)[2]. An ionization chamber (25 mm diameter, 0.5 mm thick steel walls) was constructed around the ^{252}Cf-plated disk (see Figure 6.8–3 [Böt90]). The neutron field produced by the complete assembly was investigated at PTB, allowing this source to be used as a secondary world standard for neutron detector efficiency studies.

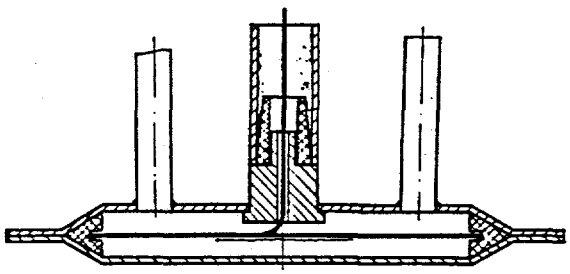

Figure 6.8–3: Cross-section of a ^{252}Cf ionization chamber similar to the one used at TUNL.

The ^{252}Cf source is set up in TUNL's target room 4. The experimental and analytic techniques used to obtain efficiency data are similar to the ones of J. Cub *et al.* [Cub89]. Two neutron detectors are placed 3.0 m away from the source at $\pm 15°$ with respect to the normal of the source's front plate (see Figure 6.8–4). The neutron detectors provide start signals for time-of-flight (TOF) measurements. The source chamber's signal is inverted, integrated, and amplified by an Ortec VT-120 B fast preamplifier in series with a Phillips 771 fast amplifier. A leading-edge discriminator is used to set a hardware threshold on the source's pulse-height signal, minimizing undesired noise and alpha-particle detection. The resulting output pulses from the leading-edge discriminator are used as stop signals for TOF measurements.

Forty-eight hours of foregound+background and twenty-four hours of background measurements are needed to achieve $\pm 2\%$ statistics for each detector's efficiency determination for neutron energies between 2 and 8 MeV. The data collected are written on tape in event mode for later off-line analysis. Detection rates, pulse-height, TOF, pulse-shape discrimination spectra, etc. for all detectors are displayed online to monitor the stability and quality of the incoming data.

[1] Physikalisch-Technische Bundesanstalt, Braunschweig, Germany.
[2] Plating was done at the Radium Institute, St. Petersburg, Russia.

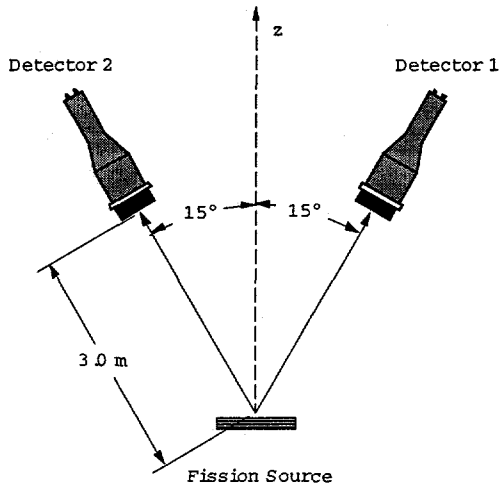

Figure 6.8–4: Experimental setup for the efficiency determination of neutron detectors using a ^{252}Cf source.

The efficiency of twenty neutron detectors used in the a_{nn}-a_{np} n-d breakup experiment will be measured using the ^{252}Cf source. The estimated total running time is 40 days.

[Böt90] R. Böttger *et al.*, Nucl. Sci. and Eng., **106**, 377 (1990).

[Cub89] J. Cub *et al.*, Nucl. Instr. and Meth., **A274**, 217 (1989).

6.9 Data Acquisition Systems

6.9.1 New Data Analysis and Data Acquisition Systems for TUNL

C. R. Howell, S. E. Edwards, R. T. Braun and E. F. Moore

For almost a decade DEC microVAXs have been used for data analysis and real-time data acquisition (DAQ) at TUNL. The growth of the research program at TUNL has clearly surpassed the capabilities of these now obsolete systems. During the last funding period (March 1994-February 1997) TUNL was awarded a special instrumentation grant to build a new data analysis system and new DAQ stations based on modern computers and new interface technologies. The goals of the upgrade included placement of X-window stations (X terminals, PCs, or unix workstations) in all graduate-student and postdoc offices and a switch from the VAX VMS operating system to the more popular unix system. The upgrade is being implemented over a three-year period in three stages. The plan calls for a smooth transition to the new systems with minimal interruption to the TUNL research program and with backwards compatibility for critical software.

The objectives of the first stage were to upgrade the local area network (LAN) hardware, prototype the unix-based data analysis cluster, and install X-window stations in about half the graduate-student and postdoc offices. All were completed in the Spring of 1996. A block diagram of the reconfigured TUNL LAN is shown in Figure 6.9–1. The diagram should be considered a prototype (drawing made in February 1996) rather than a final design, since it is likely to change as experience is gained. An Ethernet switch was installed to divide the network into three segments: the new unix cluster, a MAC working group, and a cluster of DEC VMS workstations. The fourth port on the switch is used to make a fiber link to the Duke backbone. The separation of the LAN into computer working groups (hosts that routinely share data) has significantly improved the network performance. In addition to its segmentation functions, the switch is used to filter undesired traffic and to monitor local network traffic. The connections to the offices in the TUNL building made on the unix branch use 10Base-T hubs and those made on the MAC branch still use the more cumbersome thin-wire loop topology. The plan is to convert fully to star topologies on all branches using 10Base-T hubs in the third phase of the upgrade. The server and two satellites for the unix-based data analysis system have been installed and configured as data analysis stations. The server is a Sun Ultra-1/170 with 128 MBytes of RAM, and the two client nodes are Sun Sparc-4/110 workstations with 64 MBytes of RAM each. The new workstations run the Sun Solaris operating system. Twelve GBytes of disk storage were added to bring the total storage capacity on the unix cluster to about 18 GBytes. For backwards compatibility and to expedite the decommissioning of the DEC microVAX stations, two DEC Alpha-200/233 workstations running OpenVMS have been installed on the DEC network branch. The TUNL XSYS analysis software has been ported to the Alpha

platform, and utilities have been written that enable the analysis of IUCF-XSYS histogram and event data with the TUNL XSYS software. The addition of the new Sun and DEC Alpha workstations increased the aggregate computing speed of the TUNL data analysis facility by a factor of 10. The third milestone of the first stage was to put X-window stations in about 50% of the graduate student and postdoc offices. This was achieved with the purchase of 6 NCD 19 inch monochrome X-terminals, a P5/133 PC, and the relocation of three older Sun workstations. The experience gained in operating and maintaining these three types of stations will drive the choice for the next set of X-window stations.

The goal of the second stage is to build two network based DAQ stations, one for the tandem laboratory and one for the high-resolution laboratory. These will replace the microVAX-MBD stations. The station for the tandem laboratory will be built first and will serve as a prototype for finalizing design decisions and developing software. Because CAMAC performance specifications conservatively meet the requirements of all proposed experiments to be conducted at TUNL over the next five years, and because TUNL heavily invested in CAMAC hardware during the last funding period, the plan is for the initial main digitizer bus to be CAMAC with migration toward running a mixture of CAMAC and VME digitizers from a single controller CPU. A block diagram of the prototype DAQ station is shown in Figure 6.9–2. The event data flow will be controlled by a single board computer (SBC) that resides in a VME crate. The CAMAC modules will be read out by the SBC via a commercially available VME-CAMAC interface. The interface permits up to 7 CAMAC crates to be daisy chained and is rated for a data throughput of 1.1 MBytes/s which will comfortably meet TUNL DAQ needs. The readout code will be compiled on a unix workstation and downloaded onto the SBC over Ethernet. The SBC will run a real-time kernel and be able to respond in real time to hardware interrupts generated in the CAMAC and VME crates. The event data will be buffered in the SBC memory and shipped to the target unix workstation via a network link using standard TCP/IP protocol. Fast Ethernet (100 Mbits/s) will be used for data transfer between the SBC and the DAQ workstation. The DAQ workstation will be equipped with two Ethernet cards (one regular and one fast) to create a firewall between the event data flow and the data-analysis LAN. Perhaps in time both cards will support fast Ethernet. The components for the prototype station were purchased during the Summer of 1996, and assembly and development of the prototype station and data analysis software will start in early Fall. We anticipate all major hardware design decisions to be made and most keystone soft modules to be written by the end of 1996. Two hardware compatible packages, CODA from CEBAF and LUCID from Saskatoon, are being considered as the software engine for DAQ.

In the third stage, which should start in the Spring of 1997, the data analysis system will be completed, the remaining offices will be equipped with X-window stations, and a second network-based DAQ station will be installed in the tandem laboratory. In addition to the local cluster, two standalone workstations will be located in the physics department at NC State University and at the University of NC at Chapel Hill. The computing speed

is expected to be quadrupled by the acquisitions in the third stage. All workstations will be configured for data replay and will have a tape drive and 4 GBytes of disk storage for temporary use. The X-window stations will likely be a mixture of color X-terminals and Pentium-pro PCs with color monitors. The PCs will be configured similar to the unix workstations to facilitate their use as data replay stations. Once the third DAQ station is made operational, the microVAX stations will be decommissioned and the DEC Alphas will be used to complete the analysis of data taken with the microVAX stations.

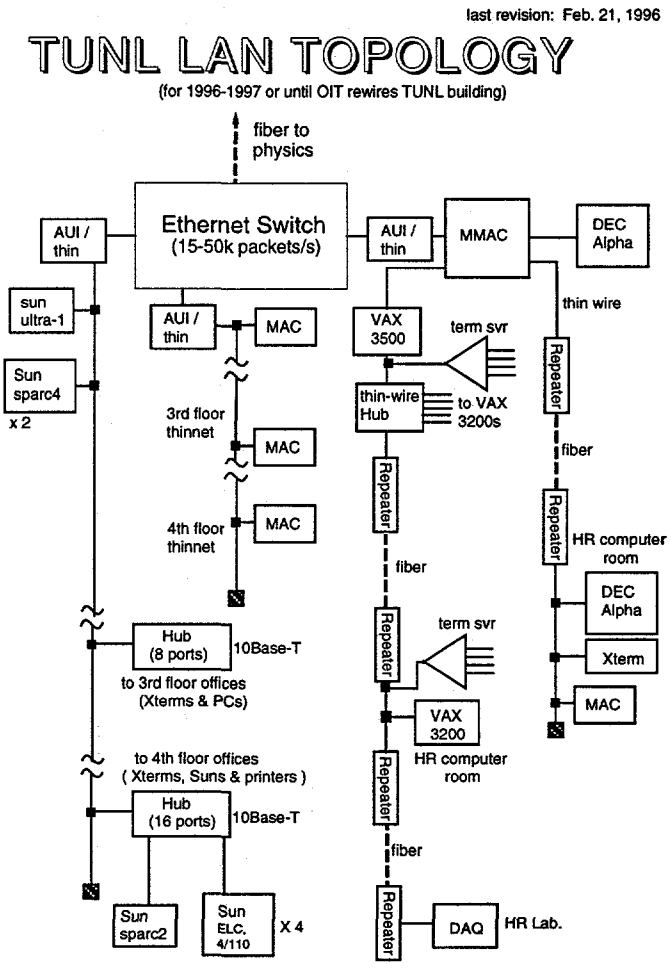

Figure 6.9–1: Block diagram of the TUNL LAN (February 1996).

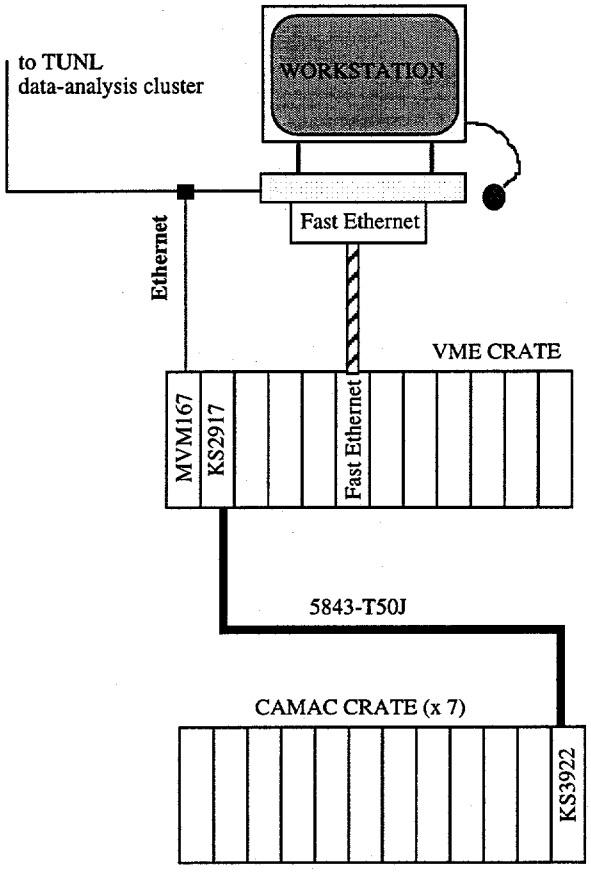

Figure 6.9–2: Block diagram of prototype of network based DAQ station.

7 Interdisciplinary Research

7.1

7.1.1 Comparison of Experimental Data and Theoretical Predictions for the n-d Cross-Section at Low Energies

A. Kievsky[1] *and* *W. Tornow*

The neutron-deuteron (n-d) cross-section at low energies plays an important role in the design and operation of heavy-water moderated nuclear fission reactors. Therefore, we calculated the n-d differential cross-section in the incident neutron energy range from 1 to 3.3 MeV and compared the theorectical results to the available experimental data. The Pair Correlated Hyperspherical Harmonic method developed by the Pisa group was used [Kie93]. The Argonne AV18 nucleon-nucleon interaction [Wir95] was employed and the three-nucleon interaction (TNI) of Urbana (UR) was added. The combination of AV18+TNI [Pud95] correctly describes the ^{3}H binding energy. It has been shown [Kie96] that the rigorous proton-deuteron (p-d) calculations of the Pisa group below the deuteron breakup threshold (E_p=3.33 MeV), again using AV18+TNI, are in excellent agreement (~1% deviation) with experimental p-d cross-section data in this energy range. Therefore, we expect the present n-d calculation to have the same accuracy as well.

Figure 7.1.1 shows our calculations in comparison to the experimental data. Except for the forward angle data at 1.0 MeV (Figure 7.1.1 a), the data of Adair *et al.* [Ada53] (Figure 7.1.1 c, e and j) and Seagrave and Cranberg [Sea57] (Figure 7.1.1 h and n) are in very good agreement with the theorectical predictions. This is very satisfying, considering the fact that these data are some 40 years old. However, the 30 year old data of Vedrenne [Ved66] (Figure 7.1.1 b, d, g, and m) have both the wrong shape and magnitude. The data of Weber [Web81] (Figure 7.1.1 f) and Chatelain *et al.* [Cha79] (Figure 7.1.1 i and o) are too high at backward angles. Finally, (Figure 7.1.1 k and l) the data of Schwarz *et al.* [Sch83] are compared to the theoretical results at E_n=2.5 and 3.0 MeV. These are the most recent data for the n-d differential cross-section in the energy range of interest and the associated experimental uncertainities are rather small. The agreement between data and theorectical predictions is very good.

We conclude that the n-d differential cross-section can now be predicted reliably in the energy range of interest. In fact, the theorectical calculations are probably more accurate than the accuracy of the best experimental data. Therefore, for heavy-water moderated

[1]INFN, Pisa, Italy.

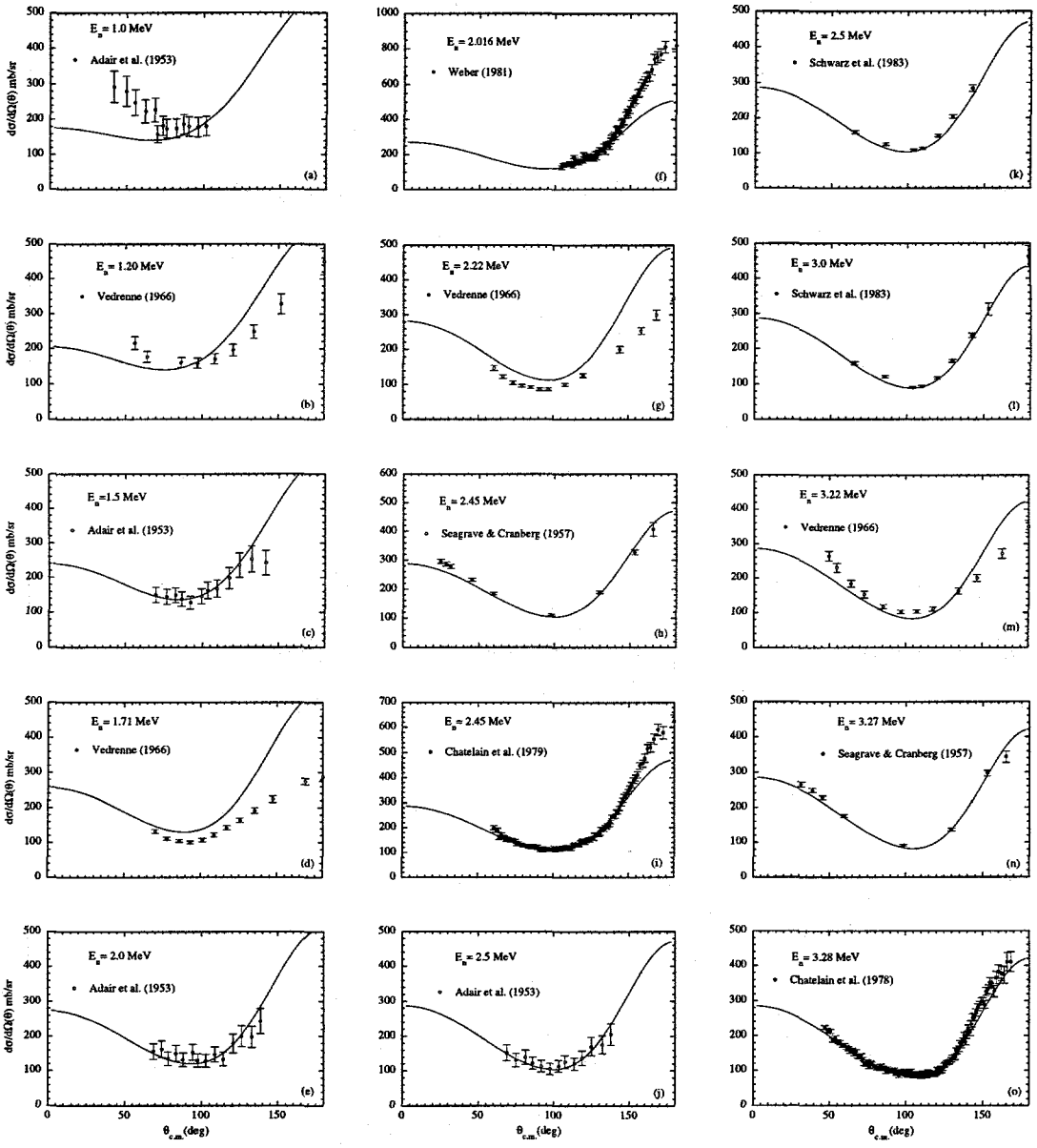

Figure 7.1–1: Comparison of experimental n-d differential cross-section data with theoretical predictions.

fission reactor design studies, n-d cross-sections calculated using AV18+TNI can be used in the energy range of interest without any reservation.

[Ada53] R. K. Adair and A. Okazaki and M. Walk, Phys. Rev. **89**, 1165 (1953).

[Cha79] P. Chatelain, Y. Onel, and J. Weber, Nucl. Phys. **A319**, 71 (1979).

[Kie93] A. Kievsky, M. Viviani, and S. Rosati, Nucl. Phys. **A551**, 241 (1993).

[Kie96] A. Kievsky *et al.*, 1996, Nucl. Phys. A. in press.

[Pud95] B. S. Pudliner *et al.*, Phys. Rev. Lett. **74**, 4396 (1995).

[Sch83] P. Schwarz *et al.*, Nucl. Phys. **A398**, 1 (1983).

[Sea57] J. D. Seagrave and L. Cranberg, Phys. Rev. **105**, 1816 (1957).

[Ved66] W. Vedrenne, Journal de Physique Colloque, **27**, 71 (1966).

[Web81] J. Weber, Helv. Phys. Act. **54**, 547 (1981).

[Wir95] R. B. Wiringa, V. G. J. Stoks, and R. Schiavilla, Phys. Rev. **C51**, 38 (1995).

7.1.2 Sonoluminescence and High-Pressure Gas Scintillators

W. Tornow

Sonoluminescence (SL) is a nonequilibrium phenomenon which occurs when acoustic energy is focused on a bubble of air trapped in water such that the bubble emits light [Bar91]. The light emission is visible to the unaided eye and appears blue. The acoustic energy (10^{-11} eV/atom) enters in a continuum at the macroscopic level and spontaneously focuses down to the molecular, atomic, and electron degrees of freedom, concentrating the ambient energy by more than twelve orders of magnitude.

The experimental arrangement for achieving stable single-bubble SL consists of piezoelectric transducers that excite breathing resonances in a water-filled spherical glass flask to which they are attached [Put95]. Above a certain threshold acoustic amplitude a bubble can be trapped. The water acts like a piston that compresses and decompresses the air periodically and the collapse of a bubble formed by cavitation occurs such that the energy of collapse is delivered to a small number of molecules, which are thus excited or dissociated. Light is emitted in the deexcitation or recombination process. The light emission occurs only during an interval of less than 100 ps or 150 ps within each cycle in the sound field, which has a period of a few tens of microseconds (depending on the diameter of the glass flask). The temperature of 10^5 K required to explain the ultraviolet light emitted by the

bubble suggests that an inward-moving shock wave remains intact to a radius of 2.5×10^{-4} cm from the center of the bubble. If the shock front survives down to 20 nm, the temperature would reach 10^6 K. However, the associated photons (soft X-rays) do not propagate through water and therefore it is not clear what the highest temperature associated with the sonoluminescence really is.

According to Refs. [Put95, Hil94], pure N_2 bubbles produced hardly any light. The same observation was made for O_2, a 80%–20% mixture of N_2 and O_2, and gas from a liquid-air container. It is the 1% presence of Ar in natural air that is responsible for the vast majority of the light emission. Subsequently, it was found that Ar can be replaced by other noble gases like He and Xe. The admixture of Xe (He) produces more (less) light than the admixture of Ar. The observed light emission depends strongly on the nature of the gas inside the bubble. For example, Xe yields a spectral peak at about 300 nm, whereas in the case of other noble gases the peak is located further in the ultraviolet region, which is obscured by the cutoff of water.

The importance of noble gases for observing SL raised our suspicion of a possible relationship between the light emission processes in SL and high-pressure gas scintillators. In the following we will review some of the information necessary to support our conjecture.

High-pressure N_2-Ar and N_2-Xe mixtures were investigated by Engelke [Eng60] and Tornow *et al.* [Tor76]. It was found that the light output is independent of pressure at pressures above a few atmospheres. In Ref. [Tor76], it was reported that a high-pressure N_2-Xe gas scintillator produces about a factor of 7 more light than a N_2-Ar gas scintillator at the same pressure. This observation is in qualitative agreement with the gas doping results of SL bubbles by Hiller *et al.* [Hil94].

The relative scintillation efficiencies of noble gases and their mixtures were investigated by Northrop and Gursky [Nor58]. Of all the noble gases, Xe produces the largest light output. In striking similarity to the work of Ref. [Nor58], Xe produced the largest light intensity in the SL studies of Ref. [Hil94].

Most of the light arising in a noble gas following the passage of a charged particle lies in the ultraviolet. Strickler and Arakawa [Str64] showed that pure Ar bombarded by α-particles emits a continuum which extends from about 110 nm to 280 nm. The decay of the scintillation light has been reported to be as fast as 10^{-9} s with a decay period inversely proportional to pressure. The first excited state of non-ionized and ionized noble gas atoms lies very high (i.e., at about two-thirds the energy required for ionization). Therefore, transitions from excited states to the ground state produce ultraviolet light. The energies of resonance levels of noble gas atoms from which the atoms are able to return directly to the ground state without passing through intermediate excited states are given in Table 7.1–1. According to this table, the statement made in Ref. [Hil92] that the spectral peak of SL appears to be located at photon energies above 6 eV is not surprising. In fact, Table 7.1–1 explains why a spectral peak was observed in Ref. [Hil94] for Xe and not for Ar and He. According to Table 7.1–1, in the latter two cases the spectral peaks are expected to lie at

Table 7.1–1: Energies (in eV) and associated wavelengths λ (in nm)

	para He	ortho He	Ne	Ar	Kr	Xe
1^{st} metastable level	20.7	19.7	16.50	11.5	9.9	8.2
1^{st} resonance level		21.1	16.55	11.59	10.0	8.4
2^{nd} metastable level			16.60	11.61	10.5	9.41
1^{st} ionization level	24.46		21.5	15.7	13.9	12.1
λ of resonance radiation	50.2	58.4	74.5	106.3	117.5	146.0

a much shorter wavelength.

The speed of the scintillation light depends on the speed of its radiative transition and on the probability for reabsorption and subsequent reemittance (resonance radiation trapping). The lifetime of resonance levels of noble gas atoms or ions is $<10^{-9}$ s. It is well known that the effect of pressure broadening reduces the trapping time of resonance radiation at high pressures. In addition, considering the pressure and temperature associated with SL, the lifetime of the metastable levels given in Table 7.1–1 may be reduced by collisions with neutral or excited atoms or ions to the level of that expected for resonance radiation. Therefore, the sub-nanosecond time scale of SL is not too surprising. However, presently unknown mechanisms, most likely related to the high pressure in the bubble, must be responsible for the pico-second SL light pulses.

In Ref. [Hil92], it was found that by lowering the temperature from 20°C to below 10°C the total light emission from a single bubble can be enhanced by over a factor of ten. In a subsequent paper, Barber *et al.* [Bar94] reported that as the water temperature decreased from 40°C to 1°C the intensity of the light emission increased by a factor of over 200.

To establish the connection to gas scintillators we notice that they are very susceptible to poisoning of the light by contaminants, especially to organic substances like hydrocarbons. Therefore, we speculate that the strong increase of light emission observed in SL with decreasing temperature is (similarly to gas scintillators) a direct consequence of the purification process accompanied with the temperature decrease. Not only is the partial vapor pressure of light absorbing contaminants in the bubble and the surrounding driving fluid reduced, but the contaminants are also preferentially absorbed at the inner wall of the glass container where the temperature is lowest.

In summary, the existing experimental information suggests that the light emission processes associated with SL are closely related, if not identical, to the ones known to occur in high-pressure gas scintillators. In fact, we think that the small SL-bubble trapped in water acts like a high-pressure micro gas scintillator.

[Bar91] B. P. Barber and S. J. Putterman, Nature, **352**, 318 (1991), and references therein.

[Bar94] B. P. Barber *et al.*, Phys. Rev. Lett. **72**, 1380 (1994).

[Eng60] C. E. Engelke, I. R. E. Trans. Nucl. Sci. **NS-7**, 32 (1960).

[Hil92] R. Hiller, S. J. Putterman, and B. R. Barber, Phys. Rev. Lett. **69**, 1182 (1992).

[Hil94] R. Hiller *et al.*, Science, **266**, 248 (1994).

[Nor58] J. A. Northrop and J. C. Gursky, Nucl. Instr. and Meth., **3**, 207 (1958).

[Put95] S. J. Putterman, Scientific American, **Feb.**, 46 (1995).

[Str64] T. D. Strickler and E. T. Arakawa, J. Chem. Phys. **41**, 1783 (1964).

[Tor76] W. Tornow *et al.*, Nucl. Instr. and Meth., **133**, 435 (1976).

Appendices

I. Graduate Degrees Awarded

Ph.D. Degrees

1. Paul R. Huffman, "A Measurement of the Parity-Conserving Time-Reversal Violating Cross Section of Polarized Neutrons on Aligned Holmium," Duke University, *Supervisor*: N.R. Roberson.

2. Lijun Ma, "P-D Radiative Capture at Low Energies," University of North Carolina at Chapel Hill, *Supervisor*: H.J. Karwowski.

3. Paul M. Wallace, "A High-Resolution Study of the ^{29}Si(p,γ) Reaction," Duke University, *Supervisor*: E.G. Bilpuch.

4. Sharon L. Stephenson, "Parity Violation in ^{232}Th -A Study of the 'Sign Effect'," North Carolina State University, *Supervisor*: G.E. Mitchell.

5. Gerard A. Vavrina, "Resonance Spectroscopy of the ^{29}Si(p,γ)^{30}P Reaction," North Carolina State University, *Co – Supervisors*: G.E. Mitchell and E.F. Moore.

6. Lisa Y. Lowie, "Parity Nonconservation in Neutron Resonances in A$\cong$100 Nuclei," North Carolina State University, *Supervisor*: G.E. Mitchell.

7. Amzie A. Adams, "Analysis of Transition Strength Distribution in ^{22}Na and ^{26}Al," North Carolina State University, *Co – Supervisors*: G.E. Mitchell and J.F. Shriner, Jr.

Master's Degrees

1. Hugh L. Harrington, "Collectivity of the Dipole Band in ^{196}Pb," M.S. degree, North Carolina State University, *Supervisor*: E.F. Moore.

2. Eric C. Schreiber, "Developing a Gamma-Ray Beam at DFELL for Nuclear Physics and Other Applications," A.M. degree, Duke University, *Supervisor*: H.R. Weller.

3. Alexander S. Crowell, "The Magnetic Form Factor of the Neutron from the d($\vec{e}$,e'$\vec{n}$)p Reaction," A.M. degree, Duke University, *Supervisor*: C.R. Howell.

4. Eric A. Wulf, "Radiative Capture Reactions and the New TUNL Compton Polarimeter," A.M. degree, Duke University, *Supervisor*: H.R. Weller.

5. Denise C. Powell,"A Measurement of the ^{7}Li(n,γ)^{8}Li Cross Section from $E_{\rm n}$=1-1000 eV," M.S. degree, University of North Carolina at Chapel Hill, *Supervisor*: A.E. Champagne.

II. Publications

Articles Published

1. Phase-Shift Analysis of Neutron-^{209}Bi Scattering and its Comparison to Neutron-^{208}Pb Scattering, Z.P. Chen, W. Tornow and R.L. Walter, Phys. Rev. **C52** 1702 (1995).

2. Polarized Proton Capture by Deuterium and the ^{2}H(p,γ)^{3}He Astrophysical S Factor, G.J. Schmid, R.M. Chasteler, C.M. Laymon, H.R. Weller, R.M. Prior and D.R. Tilley, Phys. Rev. **C52** R1732 (1995).

3. Sodium Enrichment in A-F Type Supergiants, M. F. El Eid and A. E. Champagne, Ap. J. **451** 298 (1995).

4. Study of Parity and Time-Reversal Violation in Neutron-Nucleus Interactions, Yi-Fen Yen, J.D. Bowman, B.E. Crawford, P.P.J. Delheij, C.M. Frankle, K. Fukuda, C.R. Gould, A.A. Green, D.G. Haase, M. Iinuma, J.N. Knudson, L.Y. Lowie, A. Masaike, Y. Masuda, Y. Matsuda, G.E. Mitchell, S.I. Penttilae, H. Postma, N.R. Roberson, S.J. Seestrom, E.I. Sharapov, H.M. Shimizu, S.L. Stephenson and V.W. Yuan, Polarization Phenomena in Nuclear Physics, AIP **339** 120 (1995).

5. New Results in Nucleon-Nucleon Scattering at Low Energies, W. Tornow, Polarization Phenomena in Nuclear Physics, AIP **339** 260 (1995).

6. A Constrained Dispersive Optical Model for the Neutron-Nucleus Interaction from -80 to +80 MeV for the Mass Region 26 $\leq$ A $\leq$ 33, M.A. Al-Ohali, C.R. Howell, W. Tornow and R.L. Walter, Polarization Phenomena in Nuclear Physics, AIP **339** 593 (1995).

7. An Experimental Test of Parity-Even Time Reversal Invariance with MeV Neutrons, P.R. Huffman, C.R. Gould, D.G. Haase, C.D. Keith, N.R. Roberson, M.L. Seely and W.S. Wilburn, Polarization Phenomena in Nuclear Physics, AIP **339** 185 (1995).

8. Neutron-Proton Analyzing Power at 12 MeV and Charged πNN Coupling Constant, R.T. Braun, W. Tornow, D.E. Gonzalez Trotter, C.R. Howell, R. Machleidt, C.D. Roper, F. Salinas, H.R. Setze and R.L. Walter, Polarization Phenomena in Nuclear Physics, AIP **339** 290 (1995).

9. Determination of the Asymptotic D- to S-State Ratio for the Triton and ^{3}He via (d,t) and (d,^{3}He) reactions, Z. Ayer, B. Kozlowska, R. K. Das, H. J. Karwowski and E. J. Ludwig, Polarization Phenomena in Nuclear Physics, AIP **339** 337 (1995).

10. Electromagnetic Field Requirements for a Lamb-Shift Spin-Filter Polarimeter, C. D. Roper, T. B. Clegg and A. J. Mendez, High Energy Spin Physics, AIP **343** 132 (1995).

11. Modeling the Hyperfine State Selectivity of a Short Lamb-Shift Spin-Filter Polarimeter, A. J. Mendez, C. D. Roper and T. B. Clegg, High Energy Spin Physics, AIP **343** 137 (1995).

12. The IUCF/TUNL Spin-Filter Polarimeter, V. P. Derenchuk, A. J. Mendez and T. B. Clegg, High Energy Spin Physics, AIP **343** 142 (1995).

13. The Use of the ^{3}He(d,p)^{4}He Reaction for Polarimetry at Low Energies, W. Geist, Z. Ayer, A. C. Hird, K. A. Fletcher, H. J. Karwowski and E. J. Ludwig, High Energy Spin Physics, AIP **343** 177 (1995).

14. A Statically Polarized ^{3}He Target, D.G. Haase, C.D. Keith, C.R. Gould, P.R. Huffman, N.R. Roberson, M.L. Seely and W.S. Wilburn, High Energy Spin Physics, AIP **343** 527 (1995).

15. Shell-Corrected Particle-Hole State Densities for Pre-Equilibrium Reaction Calculations, C. Kalbach, J. Phys. G **21** 1499 (1995).

16. Consistent Exciton Model Calculations with Shell Struture, Pairing and Isospin Effects, C. Kalbach, J. Phys. G **21** 1519 (1995).

17. Measurement of $\Delta\sigma_T$ in Polarized-Neutron-Polarized-Proton Scattering, W.S. Wilburn, C.R. Gould, D.G. Haase, P.R. Huffman, C.D. Keith, N.R. Roberson and W. Tornow, Phys. Rev. **C52** 2351 (1995).

18. Parity Violation in Neutron Resonances: the TRIPLE Collaboration Recent Results, E.I. Sharapov, J.D. Bowman, B.E. Crawford, P.P.J. Delheij, C.M. Frankle, K. Fukuda, C.R. Gould, A.A. Green, D.G. Haase, M.Iinuma, J.N. Knudson, L.Y. Lowie, A. Masaike, Y. Masuda, Y. Matsuda, G.E. Mitchell, S. Penttila, H. Postma, N.R. Roberson, S.J. Seestrom, H.M. Shimizu, S.L. Stephenson and V.W. Yuan, Low Energy Nuclear Dynamics, World Scientific, p.138 (1995).

19. Determination of the Asymptotic D- to S-state Ratio for ^{3}He via ($\vec{d}$,^{3}He) Reactions, Z. Ayer, H. J. Karwowski, B. Kozlowska and E. J. Ludwig, Phys. Rev. **C52** 2851 (1995).

20. Energy Levels of Light Nuclei A = 18-19, D.R. Tilley, H.R. Weller, C.M. Cheves and R.M. Chasteler, Nucl. Phys. **A595** 1 (1995).

21. Tensor Analyzing Power A_{yy} for dp Breakup in the Symmetric Constant Relative Energy Configuration, Phys. Rev. **C52** 2906 (1995), H. Witała, J. Golak, W. Glöckle, D. Hüber, H. Kamada, W. Tornow, E.J. Stephenson and D. A. Low, Phys. Rev. **C52** 2906 (1995).

22. A Deuteron Tensor Polarimeter for Low-Energy Experiments, W. Geist, Z. Ayer, A. C. Hird, H. J. Karwowski and E. J. Ludwig, Nucl. Instum. Meth. Phys. Res. **A365** 36 (1995).

23. Selected Topics of the Few-Nucleon Research Program at TUNL, W. Tornow, C.R. Howell, R.T. Braun, Q. Chen, D.E. Gonzalez Trotter, C.D. Roper, F. Salinas, H.R. Setze, R.L. Walter and H. Witała, Few-Body Systems Suppl. **8** 161 (1995).

24. Measurement of $\Gamma\gamma/\Gamma$ for the E_x = 2.646 MeV State in ^{20}Na, M. A. Hofstee, J. C. Blackmon, A. E. Champagne, N. P. T. Bateman, Y. Butt, P. D. Parker, S. Utku, K. Yildiz, M. S. Smith, R. B. Vogelaar and A. J. Howard, Proc. 3rd Int. Symposium on Nuclear Astrophysics, Nuclei in the Cosmos, AIP **327** 195 (1995).

25. Toward a Global Exciton Model for Light Particle Reactions, C. Kalbach, International Symposium on Pre-Equilibrium Reactions, Smolenice Castle, Slovakia (1995).

26. Search for p Waves in Low-Energy Proton Capture Reactions Relevant to the Solar Neutrino Problem, M.A. Godwin, R.M. Chasteler, C.M. Laymon, R.M. Prior, D.R. Tilley and H.R. Weller, Phys. Rev. **C53** R1 (1996).

27. T_{20} Measurements for ^{1}H($\vec{d}$,γ)^{3}He and the p-Wave Component of the Nucleon- Nucleon Force, G.J. Schmid, R.M. Chasteler, H.R. Weller, D.R. Tilley, A.C. Fonseca and D.R. Lehman, Phys. Rev. **C53** 35 (1996).

28. Analysis of Parity Violation in Neutron Resonances, J.D. Bowman, L.Y. Lowie, G.E. Mitchell, E.I. Sharapov and Yi-Fen Yen, Phys. Rev. **C53** 285 (1996).

29. Unique Determination of the Tensor Spin-Spin Part of the Nucleon-Nucleon Forward Scattering Amplitude, W.S. Wilburn, Phys. Rev. **C53** 518 (1996).

30. A Comparison of K- and R-Matrix Parameterizations of s-Wave ^{16}O+p Elastic Scattering, C.R. Brune, Nucl. Phys. **A596** 122 (1996).

31. Effects of Non-Nucleonic Degrees of Freedom in the D($\vec{p}$,γ)^{3}He and p($\vec{d}$,γ)^{3}He Reactions, G.J. Schmid, M. Viviani, B.J. Rice, R.M. Chasteler, M.A. Godwin, G.C. Kiang, L.L. Kiang, A. Kievsky, C.M. Laymon, R.M. Prior, R. Schiavilla, D.R. Tilley and H.R. Weller, Phys. Rev. Lett. **76** 3088 (1996).

32. Predicting ^{26}Al+p Resonances Using ^{26}Al(^{3}He,d)^{27}Si, R. B. Vogelaar, L. W. Mitchell, R. W. Kavanagh, A. E. Champagne, P. V. Magnus, M. S. Smith, A. J. Howard, P. D. Parker and H. A. O'Brien, Phys. Rev. **C53** 1945 (1996).

33. Low-Energy Polarized-Proton Capture on ^{6}Li, C. M. Laymon, R. M. Prior, D. R. Tilley and H.R. Weller, Phys. Rev. **C53** 1977 (1996).

34. Sonoluminescence and High-Pressure Gas Scintillators, W. Tornow, Phys. Rev. **E53** 5495 (1996).

35. Test of Parity Conserving Time-Reversal Invariance Using Polarized Neutrons and Aligned Holmium, P.R. Huffman, N.R. Roberson, W.S. Wilburn, C.R. Gould, D.G. Haase, C.D. Keith, B.W. Raichle, M.L. Seely and J.R. Walston, Phys. Rev. Lett. **76** 4681 (1996).

36. The Isotopic Identification of the Parity-Violating Neutron p-Wave Resonance at E_0=3.2 eV in Xe, V.R. Skoy, E.I. Sharapov, N.A. Gundorin, Yu. P. Popov, Yu. V. Prokofichev, N.R. Roberson, and G.E. Mitchell, Phys. Rec. **C53** R2573 (1996).

37. Excitation Energies and Spins of a Superdeformed Band in ^{194}Hg from One-Step Discrete Decays to the Yrast Line, T. L. Khoo, M. P. Carpenter, T. Lauritsen, D. Ackerman, I. Ahmad, D. J. Blumenthal, S. M. Fischer, R. V. F. Janssens, D. Nisius, E. F. Moore, A. Lopez-Martens, T. Dossing, R. Kruecken, S. J. Asztalos, J. A. Becker, L. Bernstein, R. M. Clark, M. A. Deleplanque, R. M. Diamond, P. Fallon, L. P. Farris, F. Hannachi, E. A. Henry, A. Korichi, I. Y. Lee, A. O. Macchiavelli and F. S. Stehens, Phys. Rev. Lett. **76** 1583 (1996).

38. Observation of a Large Parity Non-Conserving Effect in Xe, J.J. Szymanski, W.M. Snow, J.D. Bowman, B. Cain, B.E. Crawford, P.P.J. Delheij, R.D. Hartman, T. Haseyama, C.D. Keith, J.N. Knudson, A. Komives, M. Leuschner, L.Y. Lowie, A. Masaike, Y. Matsuda, G.E. Mitchell, S. Penttila, H. Postma, D. Rich, N.R. Roberson, S.J. Seestrom, E.I. Sharapov, S.L. Stephenson, Yi- Fen Yen and V.W. Yuan, Phys. Rev. **C53** R2576 (1996).

39. Atomic Beam Polarized Sources-Recent Progress and Future Possibilities, T. B. Clegg, International Workshop on Polarized Beams and Polarized Gas Targets, World Scientific, p. 155 (1996).

40. Roundtable Discussion on Optically Pumped Ion Sources, M. Tanaka, A. Zelenski and T. B. Clegg, International Workshop on Polarized Beams and Polarized Gas Targets, World Scientific, p. 144 (1996).

41. Roundtable Discussion on Atomic Beam Polarized Ion Sources, P. A. Schmelzbach and T. B. Clegg, International Workshop on Polarized Beams and Polarized Gas Targets, World Scientific, p. 243 (1996).

42. Measurement of the ^{7}Li(n,γ_0)^{8}Li Cross Section at Low Energies, J. C. Blackmon, A. E. Champagne, J. K. Dickens, M. A. Hofstee, D. C. Larson, D. C. Ralston, S. Raman and M. S. Smith, Phys. Rev. **C54** 383 (1996).

43. Ion-Implanted ^{3}He Targets for Very Low-Energy Experiments, W. Geist, Z. Ayer, A. C. Hird, E. J. Ludwig and K. A. Fletcher, Nucl. Instrum. Methods Phys. Res. B **111** 176 (1996).

44. On the Extraction of the Neutron-Neutron Scattering Length a_{nn} from Kinematically Complete nd Breakup Experiments, H. Witała, D. Hüber, W. Glöckle, W. Tornow and D.E. Gonzalez Trotter, Few-Body Syst. **20** 81 (1996).

45. Evidence for Large Discrepancies Between Data and Calculations for the Kinematically Incomplete Neutron-Deuteron Breakup Reaction, W. Tornow, R.T. Braun, H. Witała and N. Koori, Phys. Rev. **C54** 42 (1996).

46. Parity Violation in the Compound Nucleus, E. I. Sharapov, J. D. Bowman, B. E. Crawford, P. P. J. Delheij, C. M. Frankle, K. Fukuda, C. R. Gould, A. A. Green, D. G. Haase, M. Iinuma, J. N. Knudson, L. Y. Lowie, A. Masaike, Y. Masuda, Y. Matsuda, G. E. Mitchell, S. Pentilla, Yu. P. Popov, H. Postma, N. R. Roberson, S. J. Seestrom, H. M. Shimizu, S. L. Stephenson, Yi-Fen Yen, and V. W. Yuan, Proceedings of the Third International Seminar on Neutron- Nucleus Interactions (JINR, Dubna, 1995) p.27.

47. Extraction of Parity Violating Matrix Element from Data on Neutron Resonances, J. D. Bowman, L. Y. Lowie, G. E. Mitchell, E. I. Sharapov and Yi-Fen Yen, Proceedings of the Third International Seminar on Neutron- Nucleus Interactions (JINR, Dubna, 1995) p.57.

48. Parity Violation in Charged-Particle Resonance Reactions, G. E. Mitchell and J. F. Shriner, Phys. Rev. **C54** 371 (1996).

49. Measurement of the Total Cross Section for Scattering of Polarized Neutrons from Polarized ^{3}He, C.D. Keith, C.R. Gould, D.G. Haase, M.L. Seely, P.R. Huffman, N.R. Roberson, W. Tornow and W. S. Wilburn, Phys. Rev. **C54** 477 (1996).

Articles Accepted

1. Structure of ^{18}Ne and the Breakout of the Hot CNO Cycle, K. I. Hahn, N. Bateman, B. Lund, M. S. Smith, S. Utku, A. J. Howard, P. D. Parker, A. Garcia, P. V. Magnus, E. G. Adelberger, D. M. Markoff, K. B. Swartz, G. P. A. Berg, A. D. Bacher, E. J. Stephenson, J. Liu, R. B. Vogelaar, Z. Q. Mao, A. E. Champagne and J. C. Blackmon, Phys. Rev. C.

2. Neutron Resonances in ^{166}Ho, P. R. Huffman, C. M. Frankle, C. R. Gould, D. G. Haase, J. A. Harvey, N. R. Roberson and L. W. Weston, Phys. Rev. C.

3. Correction Factors for Gamma-Ray Relative Intensities in the ^{46}Ca radio-isotope, G. J. Schmid, R. M. Chasteler, C. M. Laymon, H. R. Weller, E. F. Moore, C. R. Bybee, J. M. Drake, D. R. Tilley, G. Vavrina, P. M. Wallace, Nucl. Phys. A.

4. The Physics of Radiative Capture Reactions Below 100 keV, H. R. Weller, in New Perspectives on Problems in Classical and Quantum Physics, Gordon and Breach.

5. The TUNL-FELL Inverse Compton Gamma-Ray Source as a Nuclear Physics Facility, T. S. Carman, V. Litvinenko, J. Madey, C. Neuman, B. Norum, P. O'Shea, N. R. Roberson, C. Y. Scarlett, E. Schreiber and H. R. Weller, Nucl. Inst. Methods.

6. Parity Violation in the Compound Nucleus, J. D. Bowman, C. M. Frankle, A. A. Green, J. N. Knudson, S. I. Penttilla, S. J. Seestrom, Yi-Fen Yen, V. W. Yuan, B. E. Crawford, N. R. Roberson, C. R. Gould, D. G. Haase, L. Y. Lowie, G. E. Mitchell, S. L. Stepenson, P. P. J. Delheij, E. I. Sharapov, H. Postma, Y. Masuda, H. M. Shimizu, M. Iinuma, A. Masaike, Y. Matsuda and K. Fukuda, Proceedings of the First International Symposium on Symmetries in Subatomic Physics.

7. Verification of the Space-Star Anomaly in nd Breakup, H. R. Setze, C. R. Howell, W. Tornow, R. T. Braun, W. Glöckle, A. H. Hussein, J. M. Lambert, G. Mertens, C. D. Roper, F. Salinas, I. Slaus, D. E. Gonzalez Trotter, B. Vlahovic, R. L. Walter and H. Witała, Phys. Lett. B.

8. Determinations of the Neutron-Neutron Scattering Length a_{nn} from Kinematically Incomplete Neutron-Deuteron Breakup Data Revisited, W. Tornow, H. Witała and R. T. Braun, Few-Body Systems.

9. Polarization Studies with a Pulsed Beam, J. N. Knudson, J. D. Bowman, B. E. Crawford, P. P. J. Delheij, C. M. Frankle, C. R. Gould, D. G. Haase, M. Iinuma, L. Y. Lowie, A. Masaike, Y. Masuda, Y. Matsuda, G. E. Mitchell, S. Penttila, H. Postma, N. R. Roberson, S. J. Seestrom, E. I Sharapov, H. Shimizu, S. L. Stephenson, Yi-Fen Yen and V. W. Yuan, Proceedings of the Workshop New Tools for Neutron Instrumentation.

10. Critical Comparison of Experimental Data and Theoretical Predictions for N-d Scattering Below the Breakup Threshold, A. Kievsky, S. Rosati, W. Tornow and M. Viviani, Nucl. Phys. A.

11. Study of Parity and Time-Reversal Violation in Neutron-Nucleus Interactions, J. D. Bowman, Yi-Fen Yen, B. E. Crawford, P. P. J. Delheij, C. M. Frankle, K. Fufuda, C. R. Gould, A. A. Green, D. G. Haase, M. Iinuma, J. N. Knutson, L. Y. Lowie, A. Masaike, Y. Masuda, Y. Matsuda, G. E. Mitchell, S. Penttila, H. Postma, N. R. Roberson, S. J. Seestrom, E. I. Sharapov, H. Shimizu, S. L. Stephenson and V. W. Yuan, Proceedings of the International Symposium on Weak and Electromagnetic Interactions in Nuclei.

12. Likelihood Analysis of Parity Violating Asymmetries Measured for Compound Nuclear Resonances, J. D. Bowman, L. Y. Lowie and E. I. Sharapov, Phys. Part. Nucl.

13. Multiple Scattering Effects in (n,γ) Resonances in ^{108}Pd, S. L. Stephenson, J. D. Bowman, H. Postma, S. J. Seestrom and E. I. Sharapov, Proceedings of the Fourth International Seminar on Neutron-Nucleus Interactions.

14. Development of Apparatus for Capture-γ Studies of Parity Violation at Los Alamos, B. E. Crawford, J. D. Bowman, C. M. Frankle, T. Haseyama, A. Masaike, Y. Matsuda, S. I. Penttila, N. R. Roberson, S. J. Seestrom, E. I. Sharapov and S. L. Stephenson, Proceedings of the Fourth International Seminar on Neutron-Nucleus Interactions.

15. Some Aspects of the Analysis of Parity Violation Effects Observed at p-Wave Resonances, H. Postma, J. D. Bowman, B. E. Crawford, F. Corvi, P. P J. Delheij, F. Gunsing, T. Haseyama, J. N. Knudson, L. Y. Lowie, A. Masaike, Y. Masuda, Y. Matsuda, G. E. Mitchell, S. Penttila, N. R. Roberson, S. J. Seestrom, E. I. Sharapov, H. M. Shimizu, S. L. Stephenson, Yi-Fen Yen and V. W. Yuan, Proceedings of Nuclear Dynamics at Long and Short Distances.

16. Experiment II: Parity Violation, G. E. Mitchell, Proceedings of the Workshop on Parity and Time Reversal Violation in Compound Nuclear States.

17. The Fourier Transform as a Signature for Chaos in Nuclear Energy Levels, C. R. Bybee, G. E. Mitchell and J. F. Shriner, Z. Phys. A.

18. Installation of an On-Line Lamb-Shift Spin-Filter Polarimeter in the Triangle Universities Nuclear Laboratory Atomic Beam Polarized Ion Source, A. J. Mendez, C. D. Roper, J. D. Dunham and T. B. Clegg, Rev. of Sci. Instr.

Articles submitted

1. On The Production of ^{26}Al in the Early Solar System by Low Energy Cosmic Rays, N. P. T. Bateman, P. D. Parker and A. E. Champagne, Ap. J. Letters.

2. A Determination of the Asymptotic D- to S-State Ratio for ^{3}He from the Reaction ^{1}H(d,γ)^{3}He at $E_{\mathrm{d,lab}}$=80-0 keV, B. J. Rice and H. R. Weller, Phys. Rev. C.

3. Determination of the Neutron Detection Efficiency of an NE213 Scintillator from 2.5 to 16 MeV using the ^{2}H(d,n)^{3}He Reaction, M. A. Al-Ohali, A. Aksoy, A. Coban, J. M. Hanly, P. D. Felsher, C. R. Howell, W. Tornow, F. Salinas, H. R. Setze and R. L. Walter, Nucl. Instr. and Method in Phys. Res. B.

4. Analyzing Power Measurements for ^{209}Bi(n,n) at 6 and 9 MeV and Consistent Dispersive Optical-Model Analyses for n+^{209}Bi and n+^{208}Pb from -20 to 80 MeV, G. J. Weisel, W. Tornow, C. R. Howell, F. D. Felsher, M. Al-Ohali, M. L. Roberts, R. K. Das, R. L. Walter and G. Mertens, Phys. Rev. C.

5. Energy and Orientation Dependence of Neutron Depolarization in a Large Single Crystal of Ferromagnetic Holmium, V. P. Alfimenkov, A. N. Chernikov, L. Lason, Yu. D. Mareev, V. V. Novitsky, L. B. Pikelner, V. R. Skoy, M. I. Tsulaya, C. R. Gould, D. G. Haase and N. R. Roberson, Journal of Applied Physics.

6. Differential Lifetime Measurements and Configuration Dependent Quadrupole Moments for Superdeformed Bands in Nuclei near ^{152}Dy, D. Nisius, R. V. F. Janssens, E. F. Moore, P. Fallon, B. Crowell, G. Hackman, I. Ahmad, H. Amro, S. Asztalos, M. P. Carpenter, P. Chowdhury, R. M. Clark, P. J. Daly, M. A. Deleplanque, R. M. Diamond, S. M. Fischer, Z. W. Grabowski, T. L. Khoo, T. Lauritsen, I. Y. Lee, A. O. Macchiavelli, R. H. Mayer, F. S. Stephens, A. Afanasjev and I. Ragnarsson, Phys. Lett. B.

7. Analyzing Power Measurements for the d+d−>d+p+n Breakup Reaction at 12 MeV, P. D. Felsher, C. R. Howell, W. Tornow, M. L. Roberts, J. M. Hanly, G. J. Weisel, M. Al-Ohali, R. L. Walter, I. Slaus, J. M. Lambert, P. A. Treado, G. Mertens, A. C. Fonseca, A. Soldi and B. Vlahovic, Phys. Rev. C.

8. Method for Identifying Neutron Resonances in ^{166}Ho Suitable for the Five- Fold Correlation Test of Time Reversal, P. R. Huffman, C. R. Gould, D. G. Haase and R. R. Roberson, Nucl. Instr. Methods in Phys. Res. A.

9. No Evidence for Large Charge-Symmetry Breaking Effects in the ^{3}P$_{J}$ Nucleon-Nucleon Interactions, A. Kievsky, S. Rosati, M. Viviani and W. Tornow, Phys. Rev. C.

III. Conference Reports

1. A Polarized Proton Target for Investigation of $\Delta\sigma_L$ in n-p Scattering, B. W. Raichle, C. R. Gould, D.G. Haase, M. L. Seely, J.R. Walston, N. R. Roberson, W. Tornow, W. S. Wilburn, G. W. Hoffmann and S. I. Penttilä, Bull. Am. Phys. Soc. **40** 1602 (1995).

2. Measurement of the ^{7}Li(n,γ)^{8}Li Cross Section at En=1-1000 eV, J.C. Blackmon, A. E. Champagne, J. K. Dickens, M. A. Hofstee, D. C. Larson, D. C. Ralston, S. Raman and M. S. Smith, Bull. Am. Phys. Soc. **40** 1612 (1995).

3. The ^{9}Be(p,d)^{8}Be and ^{9}Be(p,α)^{6}Li Reactions at Low Energies, C. R. Brune, H. J. Karwowski and E. J. Ludwig, Bull. Am. Phys. Soc. **40** 1612 (1995).

4. The ^{1}H(d,γ)^{3}He Reaction at 80-0 keV, B. J. Rice, L. L. Kiang, G. C. Kiang, R. M. Chasteler, M. A. Godwin, C. M. Laymon, G. J. Schmid, H. R. Weller and D. R. Tilley, Bull. Am. Phys. Soc. **40** 1613 (1995).

5. A Determination of the Vector and Tensor Analyzing Powers in Low-Energy ^{1}H(d,γ)^{3}He reaction, L. Ma, H. J. Karwowski and E. J. Ludwig, Bull. Am. Phys. Soc. **40** 1613 (1995).

6. Measurements of $\Delta\sigma_L$ for Polarized Neutron-Polarized ^{3}He Scattering, C. D. Keith, C. R. Gould, D. G. Haase, M. L. Seely, P. R. Huffman, N. R. Roberson, W. Tornow and W. S. Wilburn, Bull. Am. Phys. Soc. **40** 1613 (1995).

7. Effective Range Parameters for p-d Elastic Scattering, T. C. Black, Z. Ayer, J. C. Blackmon, H. J. Karwowski and E. J. Ludwig, Bull. Am. Phys. Soc. **40** 1613 (1995).

8. Determination of Low-Energy Proton Polarization via the ^{6}Li(p,^{3}He)^{4}He Reaction, C. R. Brune, H. J. Karwowski, E. J. Ludwig and L. Ma, Bull. Am. Phys. Soc. **40** 1615 (1995).

9. Polarized Neutron Source and Detectors for the TUNL Parity-Even Test of Time Reversal Invariance, P. R. Huffman, N. R. Roberson, W. S. Wilburn, C. R. Gould, D. G. Haase, C. D. Keith, B. W. Raichle and M. L. Seely, Bull. Am. Phys. Soc. **40** 1619 (1995).

10. A Stripper Bias Amplifier for Improving the Energy Resolution of Polarized Proton Beams for Parity Violation Measurements at TUNL, W. S. Wilburn, N. R. Roberson and C. Y. Scarlett, Bull. Am. Phys. Soc. **40** 1619 (1995).

11. Thin Solid Deuterated and Hydrogenated Targets for Use in Low-Energy Elastic Scattering Reactions, T. C. Black, E. J. Ludwig and H. J. Karwowski, Bull. Am. Phys. Soc. **40** 1620 (1995).

12. Lifetime Measurements for SD Bands in ^{151}Dy, D. Nisius, R. V. F. Janssens, B. Crowell, I. Ahmad, D. Blumenthal, M. P. Carpenter, D. Gassmann, S. Fischer, T. L. Khoo, T. Lauritsen, P. Fallon, S. Asztalos, B. Cederwall, R. Clark, M. A. Deleplanque-Stephens, I. Y. Lee, R. M. Diamond, A. O. Macchiavelli, F. S. Stephens, R. Mayer, E. F. Moore, H. Amro, P. J. Daly and Z. W. Grabowski, Bull. Am. Phys. Soc. **40** 1624 (1995).

13. Neutron Resonances in ^{165}Ho and the Five-Fold Correlation Test of Time Reversal, P. R. Huffman, N. R. Roberson, C. R. Gould, D. G. Haase, C. M. Frankle and J. A. Harvey, Bull. Am. Phys. Soc. **40** 1625 (1995).

14. The Neutron-Neutron Scattering Length Using ^{2}H(π^-,nnγ) Reaction: LAMPF E1286, T. S. Carman, Q. Chen, C. R. Howell, C. D. Roper, F. Salinas, I. Slaus, W. Tornow, R. L. Walter, A. Hussein, C. Morris, A. Obst, S. Sterbenz, C. F. Moore, C. Whiteley, G. Mertens and E. Pasyuk, Bull. Am. Phys. Soc. **40** 1629 (1995).

15. Polarization Measurements of the D(d,d)D Elastic Scattering at E_d=3 MeV E. J. Ludwig, K. D. Veal and K. A. Fletcher, Bull. Am. Phys. Soc. **40** 1629 (1995).

16. Possible Test of Parity Violation with Charged Particle Resonances, J. F. Shriner, Jr. and G. E. Mitchell, Bull. Am. Phys. Soc. **40** 1634 (1995).

17. Monte Carlo Markov Chain Method for Analyzing Nuclear Reaction Spectra, T. C. Black and W. J. Thompson, Bull. Am. Phys. Soc. **40** 1635 (1995).

18. Superdeformation Studies in ^{191}Hg: Probing the Neutron Single-Particle Levels near N=112, M. P. Carpenter, R. V. F. Janssens, B. Cromwell, I. Ahmad, S. Fischer, D. Gassmann, R. G. Henry, T. L. Khoo, T. Lauritsen, D. Nisius, B. Cederwall, M. A. Deleplanque, R. M. Diamond, P. Fallon, I. Y. Lee, R. M. Diamond, A. O. Macchiavelli, F. S. Stephens, J. A. Becker, M. J. Brinkman, L. P. Farris, E. A. Henry, J. R. Hughes, U. Garg and E. F. Moore, Bull. Am. Phys. Soc. **40** 1636 (1995).

19. The Use of Symmetry Concepts in Atomic, Nuclear, and Particle Physics, E. Merzbacher, Bull. Am. Phys. Soc. **40** 2056 (1995).

20. Parity Violation in Neutron Resonances, G. E. Mitchell, Bull. Am. Phys. Soc. **40** 2056 (1995).

21. Analyzing Powers of the ^{58}Ni(^{6}Li,d)^{62}Zn Reaction at E(^{6}Li)=34 MeV, K. D. Veal, C. R. Brune, H. J. Karwowski, E. J. Ludwig, A. J. Mendez, B. Koslowska, K. W. Kemper, E. E. Bartosz, P. D. Cathers, T. L. Drummer and A. M. Eiro, Bull. Am. Phys. Soc. **40** 2064 (1995).

22. Nuclear Probes of Stellar Evolution, A. E. Champagne, Bull. Am. Phys. Soc. **40** 2066 (1995).

23. A Planned Polarized Deuteron Target for Investigation of $\Delta\sigma_{\rm L}$ and $\Delta\sigma_{\rm T}$ in n-d Scattering, J. R. Walston, C. R. Gould, D. G. Haase, B. W. Raichle, M. L. Seely, N. R. Roberson, W. Tornow, W. S. Wilburn, G. W. Hoffmann and S. I. Pentillä, Bull. Am. Phys. Soc. **40** 2063 (1995).

24. Lifetime Measurements of Identical Superdeformed Bands in ^{151,152}Dy, E. F. Moore, D. Nisius, R. V. F. Janssens, M. P. Carpenter, I. Ahmad, D. Blumen- thal, B. Crowell, T. Dossing, D. Gassmann, T. L. Khoo, T. Lauritsen, P. J. Daly, Z. W. Grabowski, R. H. Mayer, P. Fallon, S. Asztalos, B. Cederwall, M. A. Deleplanque, R. M. Diamond, I. Y. Lee, A. Macchiavelli and F. S. Stephens, Bull. Am. Phys. Soc. **40** 2073 (1995).

25. New Test of P-Even Time Reversal Invariance in Neutron Transmission, C. R. Gould, Bull. Am. Phys. Soc. **40** 1627 (1996).

26. Spin-Filter Polarimeter: On-line Proton and Deuteron Polarimetry in Real Time, C. D. Roper, A. J. Mendez, J. D. Dunham and T. B. Clegg, Bull. Am. Phys. Soc. **41** 862 (1996).

27. A Formalism for γ-Ray Polarization in Radiative Capture Reactions Using Polarized Particle Beams, J. F. Guillemette, H. R. Weller and R. G. Seyler, Bull. Am. Phys. Soc. **41** 896 (1996).

28. Identification of g Transitions in $^{176-179}$Hg Using the Recoil Decay Tagging Method, M. P. Carpenter, D. Ackermann, D. Blumenthal, C. Davids, S. M. Fischer, G. Hackman, R. V. F. Janssens, T. L. Khoo, T. Lauritsen, C. J. Lister, D. Nisius, D. Seweryniak, P. J. Woods, H. Amro, T. Brown, J. H. Hamilton, A. V. Ramayya, W. Reviol, J. Schwarz and J. Simpson, Bull. Am. Phys. Soc. **41** 900 (1996).

29. Lifetime Measurements in ^{180,182,184}Pt Beyond the Backbends, S. S. Ghugre, U. Garg, B. Kharraja, G. Smith, B. Prause, I. Ahmad, M. P. Carpenter, B. Crowell, R. V. F. Janssens, T. L. Khoo, T. Lauritsen, W. Mueller, W. Reviol, L. L. Riedinger, E. F. Moore, R. Kaczarowski and I. M. Govil, Bull. Am. Phys. Soc. **41** 900 (1996).

30. Observation of a Large Longitudinal Analyzing Power in Neutron Transmission through Xe, J. J. Szymanski, W. M. Snow, B. Cain, R. D. Hartman, C. D. Keith, A. Komives,

M. Leuschner, D. Rich, J. D. Bowman, J. Knutson, S. Penttila, S. J. Seestrom, Y. F. Yen, V. W. Yuan, B. Crawford, N. R. Roberson, L. Lowie, G.E. Mitchell, S. Stephenson, T. Haseyama, A. Masaike, Y. Matsuda, P. P. J. Delheij, H. Postma and E. Sharapov, Bull. Am. Phys. Soc. **41** 913 (1996).

31. Parity Violation in Charged Particle Resonances, W. S. Wilburn, N. R. Roberson, G. E. Mitchell and J. F. Shriner, Bull. Am. Phys. Soc. **41** 914 (1996).

32. Parity Violation in the Excited States of ^{4}He, C. D. Keith, C. R. Gould, N. R. Roberson, W. Tornow and W. S. Wilburn, Bull. Am. Phys. Soc. **41** 914 (1996).

33. Kinematically Complete Cross-Section Measurements in Neutron-Deuteron Breakup at 13 MeV, H. R. Setze, C. R. Howell, W. Tornow, R. T. Braun, C. D. Roper, F. Salinas, I. Slaus, D. E. Gonzalez Trotter, R. L. Walter, G. Mertens, H. Witała and J. M. Lambert, Bull. Am. Phys. Soc. **41** 942 (1996).

34. A Test of Time-Reversal Invariance Using MeV Neutrons and Aligned Holmium, P. R. Huffman, N. R. Roberson, W. S. Wilburn, C. R. Gould, D. G. Haase, C. D. Keith, B. W. Raichle, M. L. Seely and J. R. Walston, Bull. Am. Phys. Soc. **41** 964 (1996).

35. A High-Resolution Study of ^{30}P, P. M. Wallace, E. G. Bilpuch, C. R. Westerfeldt, G. E. Mitchell, E. F. Moore, G. A. Vavrina and J. F. Shriner, Bull. Am. Phys. Soc. **41** 984 (1996).

36. In-Beam Spectroscopy of the ^{238}U(n,xn)$^{239-x}$U Reaction at LANSCE, J. A. Becker, L. A. Bernstein, M. A. Stoyer, R. O. Nelson, S. Wender and N. R. Roberson, Bull. Am. Phys. Soc. **41** 985 (1996).

37. Measurements of 2-34 MeV Polarized Neutron Transmission through a Polarized Proton Target, B. W. Raichle, C. R. Gould, D. G. Haase, M. L. Seely, J. R. Walston, B. E. Crawford, W. Tornow, W. S. Wilburn, D. S. Junkin, G. W. Hoffmann and S. I. Penttilä, Bull. Am. Phys. Soc. **41** 1022 (1996).

38. The ^{3}He(d,p)^{4}He Reaction at Low Energies, W. H. Geist, E. J. Ludwig, H. J. Karwowski, C. R. Brune, K. D. Veal and G. M. Hale, Bull. Am. Phys. Soc. **41** 1024 (1996).

39. The ^{12}C(^{6}Li,d)^{16}O Reaction at 34 MeV, A. J. Mendez, C. R. Brune, H. J. Karwowski, E. J. Ludwig, K. D. Veal, E. E. Bartosz, P. D. Cathers, T. L. Drummer, K. W. Kemper and B. Koslowska, Bull. Am. Phys. Soc. **41** 1025 (1996).

40. The TUNL-FELL Inverse Compton γ-Ray Source as a Nuclear Physics Facility, H. R. Weller, N. R. Roberson, E. C. Schreiber, V. Litvinenko, J. M. J. Madey, P. G. O'Shea, T. S. Carman and B. E. Norum, Bull. Am. Phys. Soc. **41** 1039 (1996).

41. Polarized Radiative Capture Reactions Below 100 keV -A New Laboratory for Nuclear Physics, H. R. Weller, Bull. Am. Phys. Soc. **41** 994 (1996).

42. Determination of the Concentration of SF_6 in an Accelerator Gas Mixture by Measuring the Velocity of Sound, W. S. Wilburn, to appear in the Proceedings of the Symposium of Northeastern Accelerator Personnel, Durham NC (1995).

43. The TUNL Low-Energy Beam Facility, C. R. Brune, to appear in the Proceedings of the Symposium of Northeastern Accelerator Personnel, Durham NC (1995).

44. Status of the TUNL ABPIS and Future Developments, T. B. Clegg, to appear in the Proceedings of the Symposium of Northeastern Accelerator Personnel, Durham NC (1995).

45. An Improved Corona Probe Feedthrough and Needle Holder Assembly, E. P. Carter, to appear in the Proceedings of the Symposium of Northeastern Accelerator Personnel, Durham NC (1995).

46. The Origins of TUNL, E. G. Bilpuch, to appear in the Proceedings of the Symposium of Northwestern Accelerator Personnel, Durham NC (1995).

47. Non-Explosive Hydrogen Burning: Where Do We Stand? M. Arnould, N. Mowlavi and A. E. Champagne, to appear in the Proceedings of the 32nd Liege Astrophysics Conference, Liege, Belgium (1995).

48. Parity Violation Effects Observed at Neutron p-Wave Resonances, Their Interpretation and Analysis, H. Postma, J. D. Bowman, B. E. Crawford, P. P. J. Delheij, T. Haseyama, J. N. Knudson, L. Y. Lowie, A. Masaike, Y. Masuda, G. E. Mitchell, S. Penttila, N. R. Roberson, S. J. Seestrom, E. I. Sharapov, H, M. Shimizu, S. L. Stephenson, Yi-Fen Yen and V. W. Yuan, North-West European Nuclear Physics Conference, Amsterdam (1996).

49. Calibrating Target Polarization in a Polarized Neutron-Proton Scattering Experiment, M. L. Seely, C. R. Gould, D. G. Haase, B. W. Raichle, J. R. Walston, N. R. Roberson, W. Tornow, W. S. Wilburn, D. S. Junkin, S. I. Penttila and G. W. Hoffmann, 8th Int. Workshop on Polarized Target Materials and Techniques, Vancouver, Canada (1996).

50. Installation of an On-Line Lamb-Shift Spin-Filter Polarimeter in the Triangle Universities Nuclear Laboratory Atomic Beam Polarized Ion Source, A. J. Mendez, C. D. Roper, J. D. Dunham and T. B. Clegg, ICIS95, Rev. Sci. Instr. **67** 1419 (1996).

51. Static Orientation of Nuclear Targets, D. G. Haase, C. R. Gould, C. D. Keith, M. L. Seely, P. R. Huffman, N. R. Roberson, W. Tornow and W. S. Wilburn, 8th Int. Workshop on Polarized Target Materials and Techniques, Vancouver, Canada (1996).

52. Questions Regarding Microwave Induced Optical Nuclear Polarization, M. L. Seely, C. R. Gould, D. G. Haase, B. W. Raichle, J. R. Walston, N. R. Roberson, W. Tornow and W. S. Wilburn, 8th Int. Workshop on Polarized Target Materials and Techniques, Vancouver, Canada (1996).

53. Roundtable Discussion on Optically Pumped Polarized Ion Sources and Related Topics, T. Clegg, M. Tanaka and A. Zelenski, International Workshop on Polarized Beams and Polarized Targets, World Scientific, p. 151 (1996).

IV. Invited Talks

1. Charged Particle Resonance Tests of Parity and Time Reversal Invariance, G. E. Mitchell, Int. Workshop Parity and Time Reversal Violation in Compound Nuclear States, European Theory Center, Trento, Italy (1995).

2. Statistical Analyses of Neutron Parity Violation Experiments, L. Y. Lowie, Int. Workshop Parity and Time Reversal Violation in Compound Nuclear States, European Theory Center, Trento, Italy (1995).

3. New Test of P-Even Time Reversal Invariance in Neutron Transmission, C. R. Gould, Fall Meeting of the Division of Nuclear Physics, Bloomington, IN (1995).

4. Parity Violation in Neutron Resonances, G. E. Mitchell, Southeastern Section of the American Physical Society, Tallahassee, FL (1995).

5. The Use of Symmetry Concepts in Atomic, Nuclear, and Particle Physics, E. Merzbacher, Southeastern Section of the American Physical Society, Tallahassee, FL (1995).

6. Nuclear Probes of Stellar Evolution, A. E. Champagne, Southeastern Section of the American Physical Society, Tallahassee, FL (1995).

7. Test of Parity and Time Reversal Invariance with Charged Particle Resonances, G. E. Mitchell, Technische Hochschule Darmstadt, Germany (1995).

8. Status of Parity Violation Experiments on Neutron Resonances, G. E. Mitchell, Joint Research Center, Geel, Belgium (1995).

9. Lifetime Measurements and the Issue of Identical Superdeformed Bands, E. F. Moore, Dedication of Gammasphere and Workshop on Gammasphere Physics, Berkeley, CA (1995).

10. Toward a Global Exciton Model for Light Particle Reactions, C. Kalbach, International Symposium on Pre-Equilibrium Reactions, Smolenice Castle, Slovakia (1995).

11. Nuclear Physics at Ultralow Temperatures, David Haase, North Carolina A&T State University (1996).

12. Parity Violation Experiments at TUNL, W. S. Wilburn, Duke University, Durham, NC (1996).

13. The Current Status of Big-Bang Nucleosynthesis, C. R. Brune, University of North Carolina, Chapel Hill, NC (1996).

14. The ^{9}Be(p,d) and ^{9}Be(p,α) Reactions at Low Energies, C. R. Brune, Duke University, Durham, NC (1996).

15. Parity Violation Studies with Epithermal Neutrons, G. E. Mitchell, Int. Conf. Nuclear Dynamics at Long and Short Distances, Angra dos Reis, Brazil (1996).

16. Series of Three Invited Lectures on Statistical Properties and Symmetry Breaking in Nuclei, G. E. Mitchell, Istituto de Fisica, Universidade de Sao Paulo, Brazil (1996).

17. Reaction Rates for Na and Al, A. E. Champagne, Workshop on the Origin of Galactic Radioactivity, Clemson University, Clemson, SC (1996).

18. Multiple Scattering Effects on (n,γ) Resonance in ^{108}Pd, S. L. Stephenson, Fourth Int. Seminar on Neutron-Nucleus Interactions, Dubna, Russia (1996).

19. Polarized Radiative Capture Reactions below 100 keV -A New Laboratory for Nuclear Physics, H. R. Weller, Joint Meeting of The American Physical Society and the American Association of Physics Teachers, Indianapolis, IN (1996).

20. A New Intense Polarized Gamma-Ray Beam for Nuclear Physics, H. R. Weller, Univ. of Ohio, Athens, OH (1996).

21. Searches for Phase Transitions with the GEANIE Array, G. E. Mitchell, Workshop Neutron-Induced Gamma-Ray Physics at LANSCE/WNR, Los Alamos, NM (1996).

22. Remaining Experimental Issues for TRIPLE Parity Violation Measurements, G. E. Mitchell, Workshop Neutron-Induced Gamma-Ray Physics at LANSCE/WNR, Los Alamos, NM (1996).

23. Static Orientation of Nuclear Targets, D. G. Haase, 8th Int. Workshop on Polarized Target Materials and Techniques, Vancouver, Canada (1996).

24. Parity Violation Experiments at TUNL, W. S. Wilburn, Los Alamos National Laboratory, Los Alamos, NM (1996).

25. Nuclear Studies at TUNL Using Polarized Neutron Beams, R. L. Walter, Dept. of Physics, Tsinghua University, Beijing, China (1996).

26. Nuclear Astrophysics, Lecture Series, A. E. Champagne, Institute for Nuclear Theory Summer School, Seattle, WA (1996).

27. Lifetime Measurements and the Decay of Superdeformed Bands in Hg Isotopes: A Matter of Life and Death, E. F. Moore, Int. Conf. Nuclear Structure Around the Turn of the Century, Agia Pelagia, Crete, Greece (1996).

28. Lifetime Measurements and Identical Superdeformed Bands in the A=190 and A=150 Regions, E. F. Moore, Nuclear Structure at the Limits, Argonne National Laboratory (1996).

29. Nuclear Physics Studies Using a Free-Electron Laser Generated Beam, H. R. Weller, The 18th Int. Free Electron Laser Conference, Rome, Italy (1996).

30. Nuclear Science and Society, C. R. Howell, SSRC-Mellon Minority Summer Conference, Stanford University, Stanford, CA (1996).

31. Polarized Targets for Nuclear and Particle Physics, M. L. Seely, North Carolina A&T State University (1996).

32. Polarized Targets through Optical/Microwave Double Resonance, M. L. Seely, North Carolina State University (1996).

V. Seminars at TUNL

1. Gary Mitchell, North Carolina State University (8/31/95)
   Parity Violation in Neutron Resonances

2. Bertrand Desplanques, Grenoble (9/7/95)
   Parity-Non-Conservation in Nuclear Forces at Low Energy: Phenomenology and Questions

3. Rocco Schiavilla, CEBAF (9/14/95)
   Low-Energy Reactions of Astrophysical Interest Involving Few-Nucleon Systems

4. Walter Glöckle, University of Bochum (9/19/95)
   The Hypertriton

5. Joachim Maruhn, University of Frankfurt Germany (9/28/95)
   Inertial Fusion with Heavy Ions

6. M. B. Lewis, Oak Ridge National Laboratory (11/2/95)
   Ion-Track Reaction-Rate Model for Hydrogen Evolution from Polymers

7. Frank Avignone III, University of South Carolina (11/16/95)
   Search for Cold Dark Matter in Southern Argentina via Diurnal Modulation by Scattering in the Earth

8. Peter Herczeg, Los Alamos National Laboratory (11/30/95)
   Time Reversal Violation in Nuclear Processes

9. Robert V. F. Janssens, Argonne National Laboratory (1/11/96)
   Superdeformation Results from Gammasphere

10. S. Raman, Oak Ridge National Laboratory (1/18/96)
    Deformations of Even-Even Nuclei

11. Alan Wuosmaa, Argonne National Laboratory (1/25/96)
    Studying Many-Body Final States in Heavy-Ion Scattering—A New Look at an Old Problem

12. Uwe Greife, Bochum University (2/8/96)
    Direct Approaches to the Nuclear Reactions in the Sun

13. Christian Iliadis, TRIUMF (2/13/96)
    Nuclear Decay Studies of Importance to Stellar Hydrogen and Helium Burning

14. Haiyan Gao, University of Illinois (2/15/96)
    Neutron Magnetic Form Factor Studies Using Polarized ^{3}He *Targets*

15. W. Scott Wilburn, TUNL Duke University (2/20/96)
    Parity-Violation Experiments at TUNL

16. Carl Brune, University of North Carolina (2/22/96)
    The ^{9}Be*(p,d) and* ^{9}Be*(p,*α*) Reactions at Low Energies*

17. Albert Young, Princeton University (2/22/96)
    Probing for Physics Beyond the Standard Model with Nuclear Beta Decay

18. Jeff Templon, MIT (2/27/96)
    "The New Generation of (e,e'p) Experiments"

19. Zhiping Zhao, University of Washington (2/29/96)
    The ^{12}C$(\alpha,\gamma)^{16}$O *Reaction Rates*

20. Ludwig De Braeckeleer, University of Washington (2/29/96)
    The Saga of Neutrinos

21. Lothar Buchmann, TRIUMF (3/14/96)
    The β*-Delayed Particle Decays and Future Experiments in* ^{12}C$(\alpha,\gamma)^{16}$O

22. Ulf Meissner, Bonn, Germany (3/19/96)
    Isospin Symmetry Breaking and the Quark Masses

23. Alejandro Kievsky, Istituto Nazionale di Fisica Nucleare Pisa (3/21/96)
    Variational Calculations for Scattering States in Few-Nucleon Systems

24. Gail Glendinning, Lawrence Livermore National Laboratory (4/2/96)
    Hydrodynamic Instability Experiments on the Nova Laser

25. Calvin Howell, TUNL Duke University (4/18/96)
    The TUNL Computer Upgrade: Progress and Plans

26. Igor Strakovsky, Virginia Polytechnic Institute and State University Blacksburg, VA (5/16/96)
    Updated Resonance Photo-Decay Amplitudes to 2 GeV

27. Ralf Hertenberger, Sektion Physik der Universität München Garching, Germany (5/21/96)
    Construction of a New Atomic Beam Polarized Ion Source for the Munich Tandem Accelerator: A Status Report

28. Randall D. Ledford, Texas Instruments (5/23/96)
    Digital Micromirror Devices (DMD-tm)

29. Michele Viviani, Istituto Nazionale di Fisica Nucleare (5/29/96)
    Theoretical Study of Few-Nucleon Reactions

30. Xunxie Wang, Rutgers University (6/4/96)
    Operation of GeAu Thin Films as Cryogenic Phonon Sensors

31. Thomas B. Clegg, Univ. of NC-CH (7/23/96)
    An Investigation of Paths to Significant Polarized Beam Enhancement at TUNL

TUNL Safety Talks

1. Dr. Carmine Plott, Radiation Safety Office, Duke University (6/3/96)
   Radiation Safety Principles and Regulations

2. Scott Alderman, Environmental Safety Office, Duke University (6/4/96)
   Chemical Safety

3. Chris Westerfeldt, TUNL, Duke University, (6/5/96)
   TUNL Laboratory Safety

4. Paul Carter, TUNL, Duke University, (6/6/96)
   TUNL Emergency Procedures & Tour

TUNL Introduction Lecture Series

1. Mark Mikolajewski, Raleigh Value and Fitting Company (6/10/96)
   Tube and Pipe Connections

2. Paul Carter, TUNL (6/10/96)
   Vacuum Systems in an Accelerator Lab

3. Chris Westerfeldt, TUNL (6/10/96)
   Principles of Accelerator Control Circuits

4. Tom Clegg, Univ. of NC-CH (6/11/96)
   The Physics of the TUNL Polarized Ion Source and Online Beam Polarimetry

5. John Dunham, TUNL (6/11/96)
   Polarized Ion Source Operation and Safety

6. Sidney Edwards, TUNL (6/12/96)
   An Overview of the TUNL Electronic Shop and Computer System

7. Brian Raichle, NC State Univ (6/13/96)
   Experimental Techniques for Detection of Low-Energy Neutrons

8. Bill Geist, Univ. of NC-CH (6/13/96)
   Experimental Techniques for Detection of Low-Energy Gamma-Rays

9. Eric Wulf, Duke Univ. (6/13/96)
   Experimental Techniques for Detection of Low-Energy Charged Particles

10. Vera Hansper, Univ of NC-CH (6/13/96)
    Cross-Section Measurements with the TUNL Enge Splitpole Spectrometer

11. Frank Salinas, TUNL/Duke Univ (6/14/96)
    Data Acquistion and Analysis at TUNL

12. Mikell Seely, NC State University (6/18/96)
    Polarized Target Technology